ASTROPHYSICAL METHODS TO CONSTRAIN AXIONS AND OTHER NOVEL PARTICLE PHENOMENA

Georg G. RAFFELT

Max-Planck-Institut für Physik, Postfach 401212, 8000 München 40, Germany

NORTH-HOLLAND

PHYSICS REPORTS (Review Section of Physics Letters) 198, Nos. 1 & 2 (1990) 1–113. North-Holland

ASTROPHYSICAL METHODS TO CONSTRAIN AXIONS AND OTHER NOVEL PARTICLE PHENOMENA

Georg G. RAFFELT
Max-Planck-Institut für Physik, Postfach 401212, 8000 München 40, Germany

Editor: D.N. Schramm   Received March 1990

Contents:

1. Introduction	3
1.1. Prologue	3
1.2. The stellar energy loss argument	4
1.3. Other methods of stellar particle physics	8
2. Axion phenomenology	10
2.1. Generic features of the Peccei–Quinn mechanism	10
2.2. The most common axion models	15
2.3. Fine points of axion properties	17
3. Axion cosmology	22
3.1. Inflationary scenario	23
3.2. Topological structures	24
3.3. Thermally produced axions	26
3.4. Decaying axions and a glow of the night sky	26
3.5. Experimental search for galactic axions	27
4. Emission rates from stellar plasmas	28
4.1. General discussion of the emission rates	28
4.2. Absorption rates	29
4.3. Many-body effects in stellar plasmas	30
4.4. Compton process	39
4.5. Electron–positron annihilation	41
4.6. Bremsstrahlung by electrons	42
4.7. Axio-recombination and the axio-electric effect	44
4.8. Bremsstrahlung by nucleons	45
4.9. Primakoff effect and axion–photon mixing	49
4.10. Plasmon decay rate	54
5. Energy transfer	55
5.1. Radiative transfer by massive bosons	56
5.2. Opacity contribution of massive pseudoscalars	56
6. Exotic energy loss of low-mass stars; analytic treatment	57
6.1. The equations of stellar structure	57
6.2. Homologous changes	58
7. Axions from the Sun	60
7.1. Energy loss and energy transfer in the Sun; first constraints	60
7.2. Results from a germanium spectrometer	62
7.3. A magnetic conversion experiment	62
7.4. Radiative particle decays and solar γ-rays	63
8. Red giants and horizontal branch stars	63
8.1. The general agenda	64
8.2. The evolution of low-mass stars	65
8.3. Suppression of the helium flash by particle emission	68
8.4. Reduction of the helium burning phase	71
8.5. Core mass at the helium flash	74
9. The white dwarf luminosity function	77
9.1. White dwarfs; theoretical and observed properties	77
9.2. Cooling theory for white dwarfs	79
9.3. Neutrino losses included	81
9.4. Axion bounds	81
10. Cooling of nascent and young neutron stars	82
10.1. Birth and cooling of neutron stars	82
10.2. Supernova explosions and new particle physics	87
10.3. SN 1987A bounds on novel cooling phenomena	89
10.4. Non-detection of new particles from SN 1987A	93
10.5. SN 1987A axion bounds from numerical investigations	93
10.6. Axion trapping	97
10.7. Axion bounds from Einstein observations	97
10.8. What if neutron stars are strange quark stars?	98
11. Summary of axion and neutrino bounds	98
11.1. Neutrinos	98
11.2. Axions	100
References	104

Single orders for this issue

PHYSICS REPORTS (Review Section of Physics Letters) 198, Nos. 1 & 2 (1990) 1–113.

Copies of this issue may be obtained at the price given below. All orders should be sent directly to the Publisher. Orders must be accompanied by check.

Single issue price Dfl. 85.00, postage included.

Abstract:

Various extensions of the standard model of elementary particle interactions predict the existence of new particles such as axions, or "exotic" properties of known particles such as neutrino magnetic moments. If these particles are sufficiently light, they emerge in large numbers from the hot and dense interior of stellar bodies. For appropriate ranges of particle parameters, this "invisible" energy loss would lead to observable changes in the evolution of stars. We review the theoretical methods as well as the observational data that have been employed in order to use stars as "particle physics laboratories" in the spirit of this argument. The resulting constraints on the properties of axions are systematically explored, and the application of the general methods to other cases are mentioned and referenced. Cosmological axion bounds and experiments involving galactic or solar axions are briefly reviewed.

1. Introduction

1.1. Prologue

Fifty years ago, in 1940, Gamow and Schoenberg [1, 2] ushered in the advent of particle astrophysics when they pointed out that neutrinos, the most elusive of all known particles, must play an important role in stellar evolution, particularly in the collapse of evolved stars. However, they considered only nuclear conversions of the type $(A, Z) + e^- \rightarrow (A, Z-1) + \nu_e$ and $(A, Z-1) \rightarrow (A, Z) + e^- + \bar{\nu}_e$, the "urca" reactions which become important only at very high temperatures because of their energy threshold. In 1958, Feynman and Gell-Mann as well as Sudarshan and Marshak proposed the universal V–A interaction law which predicted the existence of a direct neutrino–electron interaction with the strength of the universal Fermi constant. In 1959, Pontecorvo [3] realized almost immediately that this interaction would allow for the bremsstrahlung radiation of neutrino pairs by electrons, and that the absence of a threshold renders this process an important energy loss mechanism for stars. In the same year, Gandel'man and Pinaev [4] calculated the approximate conditions for which neutrino losses would "outshine" the photon luminosity of stars and subsequently the neutrino emissivity of stellar plasmas was calculated by many authors.*) On the basis of astrophysical evidence, Stothers and his collaborators [34–42] established in the late 1960's the existence and approximate magnitude of the direct neutrino–electron interaction which was experimentally measured [43] in 1976.

While neutrino physics today is an integral part of stellar evolution and supernova theory, new concepts of particle physics have emerged that could be equally important despite the relatively low energies available in stellar interiors. In various extensions of the standard model, the spontaneous breakdown of a symmetry of the Lagrangian of the fundamental interactions by some large vacuum expectation value of a new field leads to the prediction of massless particles, the Nambu–Goldstone bosons of the broken symmetry. The most widely discussed example is the axion [44, 45] which arises as the Nambu–Goldstone boson of the Peccei–Quinn symmetry which explains the puzzling absence of a

*) Immediately after Pontecorvo [3] and Gandel'man and Pinaev [4] had calculated the neutrino losses by pair-bremsstrahlung, Chiu and Stabler [5] and Ritus [6] calculated the photoneutrino process, $\gamma + e^- \rightarrow e^- + \nu_e + \bar{\nu}_e$, followed by Adams, Ruderman and Woo [7] who considered the plasmon decay $\gamma_{pl} \rightarrow \nu_e \bar{\nu}_e$. The status of the theory of stellar neutrino emission of the mid-1960's was summarized by Feinberg [8], Ruderman [9] and Chiu [10], and widely used numerical tables were provided by Beaudet, Petrosian and Salpeter [11]. After the discovery of weak neutral currents, the modified emission rates were first calculated by Dicus and his collaborators [12, 13], and the status of the theory of the mid-1970's was reviewed by Barkat [14]. Recently, two groups of authors have provided updated numerical tables [15–17]. A recent discussion of neutrino emission from nuclear matter was provided by Friman and Maxwell [18]. Neutrino emission by electrons in strong magnetic fields (synchrotron radiation of $\nu\bar{\nu}$ pairs) was first discussed by Landstreet [19] – for other processes in the presence of strong magnetic fields see refs. [20–22]. The process $\gamma\gamma \rightarrow \nu\bar{\nu}$ was first discussed by Chiu and Morrison [23] who thought it would substantially contribute to the emission rate, but Gell-Mann [24] showed that it vanishes identically in the V–A theory. The emergence of the intermediate W-boson hypothesis revived this process [25–28], but gauge-invariant calculations, especially in the framework of the standard model, yield negligible rates [29–31], even if one allows for small neutrino masses [32]. This process would be significant if there existed exotic scalar or pseudoscalar weak interactions [33].

neutron electric dipole moment, i.e., it explains *CP*-conservation in strong interactions [46, 47]. The production of axions in stars, like that of neutrinos, is not impeded by threshold effects.

The existence of axions or other Nambu–Goldstone bosons would be a low-energy manifestation of new physics at energy scales much larger than can be probed in the laboratory. Equally, anomalous properties of neutrinos such as electromagnetic dipole moments would point to new physics beyond current laboratory energies. Therefore the physics of neutrinos and Nambu–Goldstone bosons offers a window to high-energy physics, a window to be explored by astrophysical methods in addition to laboratory experiments.

In this review I will summarize the recent discussion of the possible role of axions and other hypothetical particles in astrophysics, and I will review the constraints on the particle properties that have been obtained. There have been a number of recent reviews on the physics of axions [48–53] which mention the astrophysical results. The focus of these papers, however, is the particle-physics aspect of the *CP* problem or the numerical bounds on the Peccei–Quinn scale, and they offer little insight into the methods that have been used to derive these results, leaving unclear their significance and reliability. My review, in contrast, is intended as an overview over the *astrophysical methods* which have been used to derive such constraints. Because "invisible axions" are perhaps the most interesting case of hypothetical low-mass particles, because their properties are particularly well-defined, and because of a personal choice I use their case as a precedent to illustrate these methods. However, for each argument discussed I will summarize the results for other particles, especially neutrinos, that have been derived by the same or similar reasoning.

1.2. The stellar energy loss argument

The main astrophysical method to constrain particle properties that I will explore is the *energy loss argument*: novel, low-mass particles or neutrinos with novel properties would be produced in the interior of stars and, because of their assumed weak interaction with matter and radiation, would escape almost freely, draining the star of energy and thereby changing the course of stellar evolution that would be expected otherwise. While the historical emergence of these ideas in the context of neutrino physics was mentioned above, it should be added that the first application of this argument to other particles was provided by Sato and Sato [54] in 1975 to derive bounds on the coupling strength of light Higgs particles.

Subsequently, the lifetime of the Sun and of horizontal branch stars, the white dwarf luminosity function, bounds on the surface X-ray emission of pulsars, the neutrino signal from SN 1987A, and other arguments were used to constrain the interaction strength of axions [55–100] and other Nambu–Goldstone bosons such as majorons [101–114] and familons [115], of light scalar and vector bosons [116–121], and of light supersymmetric particles [122–129], to constrain anomalous electromagnetic properties of neutrinos [130–146], neutrino right-handed interactions [92, 129, 147, 148], Dirac neutrino masses [92, 149–152], and exotic neutrino–photon couplings [153, 154]. Also, the stellar graviton emission rate was estimated, but naturally it turns out to be too small to have any effect on stellar evolution (for a review see ref. [155] while more recent papers are refs. [156–158]).

Related to the energy loss argument is the *energy transfer argument*: if our low-mass particles interact so strongly that they are produced and reabsorbed or rescattered in the stellar medium, they do not drain the star of energy, rather they contribute to the energy transfer, again changing the standard course of evolution. The energy transfer by neutrinos is an integral part of supernova physics (for a recent review see ref. [159]) while the contribution to the effective opacity in the Sun and horizontal branch stars of hypothetical keV-mass scalars has been used to exclude a large range of parameters [160, 161], see chapter 5 and section 7.1.

In order to establish a connection between astronomical observables and the relevant particle physics model in the framework of the energy loss argument, one generally has to take four distinct steps, each of which involves its own methods and problems.

1.2.1. Step I: phenomenological interaction law

The questions to be addressed by stellar energy loss arguments typically involve new particle physics at large energy scales, while the astrophysical methods lend themselves to probe low-energy phenomena related to these new theories. For invisible axions, the ultimate goal is to identify or constrain the value of the axion decay constant, f_a, which represents the spontaneous breaking of the Peccei–Quinn symmetry, while the astrophysical methods allow one to derive bounds on the stellar axion emission rates and hence on the effective coupling strength of axions to photons, electrons, and nucleons. The Lagrangian for the interaction with photons is*)

$$\mathscr{L}_{a\gamma} = -\tfrac{1}{4} g_{a\gamma} F^{\mu\nu}\tilde{F}_{\mu\nu} a = g_{a\gamma} \boldsymbol{E}\cdot\boldsymbol{B} a\,, \tag{1.1}$$

where $g_{a\gamma}$ is a phenomenological coupling constant of dimension (energy)$^{-1}$, F is the electromagnetic field-strength tensor, $\tilde{F}$ its dual, and a is the pseudoscalar axion field. For the interaction with a fermion species j the Lagrangian is

$$\mathscr{L}_{aj} = -\mathrm{i} g_{aj} \bar{\psi}_j \gamma_5 \psi_j a\,, \tag{1.2}$$

where g_{aj} is a dimensionless Yukawa coupling constant. These phenomenological Lagrangians are the only particle physics ingredients entering the subsequent discussion. In order to establish the precise connection between $g_{a\gamma}$, g_{ae}, g_{aN}, m_a, and f_a I review in chapter 2 the physics of invisible axions which will allow me to establish the connection between the low-energy phenomenology and the fundamental physical theory.

For neutrinos I will discuss constraints on anomalous electromagnetic properties, especially on magnetic and electric dipole and transition moments, μ_{ij} and ε_{ij}. In this case the phenomenological Lagrangian which describes the interaction of the neutrino fields, ψ_i, with the electromagnetic field, F, is

$$\mathscr{L}_{\nu\gamma} = \sum_{i,j=1}^{3} \bar{\psi}_i(\mu_{ij} + \gamma_5 \varepsilon_{ij})\sigma_{\mu\nu}\psi_j F^{\mu\nu}\,. \tag{1.3}$$

*) We always use natural units with $\hbar = c = k_B = 1$. Moreover, we use the rationalized system for the definition of charges and field strengths where the fine structure constant is $\alpha = e^2/4\pi \sim 1/137$ so that the electric charge is $e = 0.30$. The energy density of an electromagnetic field is $(E^2 + B^2)/2$. In the unrationalized system the definitions of charges and field strengths are such that $\alpha = e^2 \sim 1/137$ so that $e = 0.085$ and the energy density of an electromagnetic field is $(E^2 + B^2)/8\pi$. Usually one refers to the two systems as rationalized and unrationalized *units*, although the physical units are the same in both cases – for example, using $\hbar = c = 1$, field strengths can be expressed in eV^2, cm^{-2}, or many other units in both systems. What is different in the two systems is the *definition of what one means with field strength* because only the product of charge times field strength, the force on a test particle, has an operational meaning and is numerically the same in both systems. Still, certain units are always understood to refer to a certain system. Especially the cgs-unit "Gauss" for magnetic fields is understood to refer to an unrationalized system, while the MKSA unit "Tesla" is understood to refer to a rationalized system. Thus, while these units are understood to refer to different definitions of field strength, it is correct to say that a field of 1 T is 10^4 times stronger than one of 1 G, meaning that the Lorentz force on a moving electron would be 10^4 times stronger or that the energy density of the field is 10^8 times larger, even though it has to be evaluated according to different formulae. A given field of 1 G corresponds to a field strength of $1.95 \times 10^{-2}\,\mathrm{eV}^2$ if the latter number is understood in a rationalized system ($\alpha = e^2/4\pi$), used throughout this report, while it corresponds to $6.9 \times 10^{-2}\,\mathrm{eV}^2$ in an unrationalized system ($\alpha = e^2$). Note that in the particle-physics literature rationalized units are always used, while in the plasma-physics literature unrationalized units are generally employed.

However, in this case I do not discuss the connection between the dipole moments and the underlying nonstandard particle-physics models because this would increase the volume of this review beyond reason.

1.2.2. Step II: particle emission rates

Once the phenomenological Lagrangian for the interaction between the new particles and matter and radiation has been established, it may seem like a simple exercise in the evaluation of Feynman graphs to determine the rate of production of these particles from a stellar plasma. However, in the hot and dense stellar medium, many-body effects and the collective behavior of the medium render these calculations much more involved than the corresponding cross-section calculations for laboratory conditions. Indeed, certain processes such as the plasmon decay into neutrinos, $\gamma_{\rm pl} \rightarrow \nu\bar{\nu}$, are possible only in a medium where photons ("plasmons") have an "effective mass", while such decays would not occur in vacuum. Of more relevance to axions, correlation or screening effects substantially reduce the naive interaction rates, in one important case (the Primakoff effect) by two orders of magnitude. In the dense medium of neutron stars, the role of many-body effects for axion emission is not fully understood. The very state of matter at supernuclear densities is not known – the occurrence of new phases such as a pion-condensate or strange quark matter is possible. Even the vacuum transition between axions and photons in external magnetic fields is affected by the magnetically induced photon refractive index. Therefore, naive calculations of emission rates which ignore the presence of the ambient fields or media can be trusted, at best, as order of magnitude estimates. In chapter 4 we will discuss the stellar energy loss rates which are to be expected on the basis of the interactions, eqs. (1.1)–(1.3).

1.2.3. Step III: theoretical path of stellar evolution

Next, one has to discuss the evolutionary pattern of stars that is to be expected if axions or other particles drain energy or contribute to the energy transfer. The effect of energy transfer has been discussed only for some special cases since typically one is interested in very weakly interacting particles where the mean free path far exceeds stellar radii. The energy drain by axions or other particles leads to an acceleration of certain phases of stellar evolution. In order to understand this one has to distinguish carefully between two broad classes of stars – "active" stars which burn nuclear fuel and "dead" stars which do not. A typical example for the former class is our Sun and other main-sequence (MS) stars which burn hydrogen in their center, or horizontal branch (HB) stars which burn helium in their core. These stars support themselves against their own gravity by thermal pressure, resulting in a close interplay between pressure, temperature, energy transfer, and the nuclear burning rates, an interplay which stabilizes the stellar structure: any deviation from equilibrium results in a restoring force.

The energy drain by axions is equivalent to a local energy sink, i.e., at a given density and temperature the effective energy generation rate is the true nuclear burning rate, $\varepsilon_{\rm nuc}$, reduced by neutrino and axion losses, $\varepsilon_{\rm eff} = \varepsilon_{\rm nuc} - \varepsilon_\nu - \varepsilon_{\rm a}$. Because the effective burning rate, $\varepsilon_{\rm eff}$, is fixed by the equilibrium stellar structure, the inclusion of axion losses means that the true burning rate, $\varepsilon_{\rm nuc}$, must be larger than in the absence of axions, requiring an increased temperature because $\varepsilon_{\rm nuc}$ is a steeply rising function of T. Hence a self-consistent stellar structure which includes axion losses is characterized by an increased internal temperature and an increased nuclear burning rate, trends which can be analytically understood (chapter 6). The increase of $\varepsilon_{\rm nuc}$ leads to an increased consumption of nuclear fuel, reducing the duration of the relevant phase: the central hydrogen burning phase for MS stars or the central helium burning phase for HB stars. (The term "axion cooling" which sometimes has been used is somewhat of a misnomer because the temperature in "active" stars actually increases. If axion losses were important in the Sun, the increased central temperature would result in an increased flux of neutrinos, exacerbating the solar neutrino problem.)

When stars run out of nuclear fuel they inevitably must collapse. Depending upon their mass, this collapse leads to one of three possible end states of stellar evolution: white dwarfs, neutron stars, or black holes. White dwarfs arise from progenitor stars of up to several solar masses. They are so compact that the electrons in their interior are degenerate, and it is the electron degeneracy pressure which supports these objects from further collapse. The structural properties of white dwarfs and their thermal properties are largely decoupled, the previous interplay between pressure and temperature is now absent. Moreover, the degenerate electrons transport energy so efficiently that these stars have a practically isothermal core which is insulated from the surrounding space by a surface layer of nondegenerate matter. The cooling rate of the interior is governed by the "thermal resistance" of this skin, and neutrino and axion losses could "shorten out" this insulator. It is now fully justified to speak of "axion cooling" because the energy drain would actually accelerate the speed of white dwarf cooling (chapter 9).

Neutron stars form after the implosion of more massive stars in type II supernovae leading to the ejection of their surface layers. Immediately after the collapse a hot and dense "proto-neutron star" forms in the center of the progenitor. The cooling rate of this object is determined by the diffusion time scale of neutrinos whose mean free path is short compared to the radius of about 50 km of the supernova core. Axions or other particles which interact more weakly than neutrinos would shorten out this "thermal resistance" and accelerate the cooling of a nascent neutron star. The weak interaction cross sections, which keep the neutrinos trapped in a neutron star, scale as E_ν^2 so that, as the temperature drops, the star becomes transparent to neutrinos which dominate the cooling to an age of $\sim 10^5$ yr after formation. Later, photon emission from the surface takes over, and the general picture becomes similar to a white dwarf: a degenerate, almost isothermal interior, insulated by a nondegenerate surface mantle. Bounds from SN 1987A and from late neutron star cooling will be discussed in chapter 10.

There is one special case where axion emission would lead to an extension rather than an acceleration of an evolutionary phase. A red giant is a combination between an "active" and a "dead" star: it consists of a degenerate core, essentially a helium white dwarf, and a nondegenerate extended hydrogen envelope. At the interface between core and envelope, hydrogen burns in a thin shell, with no nuclear burning in the core. However, as the burning front moves out, the core mass grows, its radius shrinks, and it becomes hotter and denser, until helium ignites and the star enters a helium burning phase: it becomes a horizontal branch star. The emission of axions from the red giant core lowers the central temperature and delays the ignition of helium, thereby extending the red giant phase. This argument leads to the most restrictive bound on neutrino dipole moments (section 8.6).

1.2.4. Step IV: comparison with observations

If axion emission significantly changes the standard picture of stellar evolution or the theoretically expected durations of certain evolutionary phases, this result in itself does not provide any insight into axion properties. Only a comparison with observations allows one to arrive at definite conclusions concerning the range of allowed parameters. There are very few cases where we have direct evidence for the time scales of stellar evolution. The age of the Sun, 4.5×10^9 yr, can be inferred from radio-chemical dating of terrestrial, lunar, and meteoritic material. Hence we have direct evidence for the time scale of main-sequence evolution. The measurement of the neutrino burst of SN 1987A gave direct evidence for the cooling rate of nascent neutron stars – their binding energy is radiated away in thermal neutrinos within a few seconds. The historical record of supernova explosions, notably the famous supernova of 1054 A.D. which gave rise to the Crab nebula and pulsar, yields a direct measure for the cooling rates of these individual objects if combined with X-ray measurements of their present-day surface temperature.

Other time scales of evolution such as the white dwarf cooling rate and the helium burning phase of HB stars must be inferred by statistical means using ensembles of stars. Rather than following the evolution of individual stars one considers ensembles which contain stars in various stages of evolution, and from the relative number of stars in different phases one infers their relative duration. Particularly handy ensembles are the globular clusters which are gravitationally bound groups of coeval stars with identical chemical composition. The individual stars mostly differ in their mass and hence in the duration of their hydrogen burning phase. All subsequent phases are so fast that the evolved stars in these clusters have essentially the same mass and are thus practically identical in their properties. Hence these stars as an ensemble map out the evolution of an individual star; we observe "the same star" simultaneously in all advanced stages of evolution such as the red giant and horizontal branch phase. The relative number of stars observed in different phases then gives us a direct measure of the relative duration of these phases for an individual star.

1.3. Other methods of stellar particle physics

While we will mostly review the particle results based on the stellar energy-loss argument, it is worthwhile to briefly mention other methods that can and have been employed to extract useful information for particle physics and cosmology from the observation of stars or using stars as particle sources.

1.3.1. Experimentation with stellar particle fluxes

The photon and neutrino fluxes and the possible fluxes of exotic particles produced in stars can be used for experimentation. The first such discussion was performed by Houtermans and Thirring [162] in 1953 who used the null rate of a Geiger counter to derive a limit on the ionizing power of the calculated solar neutrino flux and thus found a limit of 2×10^{-6} Bohr magnetons on a possible neutrino magnetic moment. Since then, neutrino fluxes have been measured from the Sun [163, 164] and from SN 1987A [165–168]. Especially the SN 1987A neutrino observation was used to investigate the issues of neutrino oscillations in media [169–180] and to constrain radiative [181–185] or other decays [186, 187]. Many of these issues have been reviewed in Bahcall's recent book on neutrino astrophysics [163]. Hypothetical particles such as axions would also emerge from these sources, and the absence of solar γ-rays allows one to rule out the standard axion [188] and to constrain neutrino radiative decays [189, 190]. Also, one may attempt to detect exotic particle fluxes from the Sun such as the flux of invisible axions (section 7.4).

The diffuse neutrino flux from all stars, particularly all supernovae in the universe, in connection with the measured diffuse electromagnetic background spectra, has been used to constrain radiative neutrino decays [183, 189, 191, 192].

Pulsed signals allow one to measure or constrain dispersion effects. The electromagnetic signals from pulsars serve to constrain the photon mass (for reviews see refs. [193, 194]) and the photon interaction with the galactic magnetic field [195]. The absence of "jitter" in the periodic signal of millisecond pulsars constrains distortions of the space–time metric between the earth and these objects, i.e., the method of "pulsar timing" allows one to constrain the cosmic gravitational wave spectrum and thus the existence of possible sources such as cosmic strings (see, for example, ref. [196]). The apparent absence of dispersion of the neutrino burst from SN 1987A has been used to limit the neutrino mass [197–211], its interaction with background magnetic fields [212], "fifth force" long range fields [213, 214], or background matter [215], and to constrain various possible deviations from the equivalence principle [216–221].

1.3.2. Deviation from Coulomb's and Newton's law

There have been many speculations about possible variations from the inverse-square behavior of Coulomb's and Newton's law. With some relevance to "stellar particle physics", the measured spatial variation of Jupiter's magnetic dipole has been used to set important limits on the photon mass (for reviews see refs. [193, 194]). Deviations from Newton's law occur because of general relativistic corrections: the motion of planets, binary stars, light bending by the Sun, and other gravitational lens effects are important tests for general relativity [222, 223]. Also, general relativistic effects must be considered to compute the structure of neutron stars [224]. The existence of other long-range forces ("fifth force") has also been contemplated, forces which are mediated by particles with suitable masses that they produce substantial effects over terrestrial distances without affecting the post-Newtonian approximation at larger scales. The effect of such forces on binary star systems was recently discussed [225], although existing laboratory bounds rule out observable effects.

Of more relevance to this review, non-Newtonian forces could affect stellar structure and solar oscillations [226–229]. It turns out, however, that within existing limits on the strength of such forces, no observable effects on stellar structure or helioseismology can be expected apart from small corrections to stellar lifetimes and oscillation periods. The existence of a fifth force would imply the emission of the relevant field quanta from stars, but within existing laboratory limits on their coupling strength, this energy drain from stars has no observable effect, just as the stellar graviton luminosity is always negligible. If the mass of these particles is so large that the force which they mediate does not reach far enough to affect other tests of general relativity, the energy loss argument provides the best constraint on the relevant coupling strength [116, 117].

Finally, the static, long-range field associated with a new force would change the masses of particles and the values of the fundamental coupling constants in the interior and in the neighborhood of a star [230].

1.3.3. Heavy particles trapped in stars

While light particles such as neutrinos or various Nambu–Goldstone bosons would escape from stellar bodies, other exotic objects such as free quarks, magnetic monopoles, or supersymmetric partners to known particles could be retained and hence could contaminate the normal baryonic material of the celestial bodies. The presence of these particles could affect stars in several ways. Fractionally charged particles could attach themselves to nuclei and would severely alter the nuclear burning rates [231]. Magnetic monopoles in grand unified theories can catalyze baryon decay (Rubakov–Callan effect) and they can annihilate so that MS stars [232], white dwarfs [233], the earth [234, 235], the Jovian planets [235, 236], and particularly old neutron stars [237–241] would possess an efficient new heat source. Also, the high-energy neutrino flux from catalyzed baryon decay in the Sun can be constrained by terrestrial detectors [242–244]. The presence of magnetic fields in various stellar bodies constrains the number of accreted monopoles or severely affects their accretion and annihilation rates [245–248].

Weakly interacting massive particles ("WIMPs") would contribute to the energy transfer in their host star [249–253]. Because of their long mean free path, even a very small contamination is sufficient to provide the dominant form of energy transfer. While such particles probably would not be entrained during star formation [249, 254] they would be accreted if they were the dark matter of the universe [255–261]. Therefore stars can serve as detectors for particle dark matter – the effects on the Sun in the context of the solar neutrino problem [249, 250, 262–266] and helioseismology [267–269], on stellar pulsations [270, 271], on general main sequence stars [272], and on horizontal branch stars [273–280] have been studied. Also, WIMPs trapped in a neutron star could become self-gravitating and form a black hole [281]. While annihilation can substantially reduce the number of WIMPs trapped in a star [282], by the same token it can provide a powerful new energy source if the dark matter background is unusually dense [283], and the high-energy annihilation neutrinos from WIMPs trapped in the Sun will perhaps allow one to detect particle dark matter [284–295].

The effect on the Sun of more exotic trapped particles have also been discussed [296] as well as that of a cosmic string loop [297]. Most recently it was argued that hypothetical charged dark matter particles ("CHAMPs") would build up in neutron stars and form a black hole, destroying the star on a short time scale. This argument excludes a large range of CHAMP masses [298].

1.3.4. New phases of nuclear matter

The interior of neutron stars provides a unique environment where the properties of matter at nuclear and supernuclear densities are of immediate importance. Of particular interest is the possible occurrence of exotic phases of matter such as superfluid and superconducting states, a pion condensate, quark matter, or strange quark matter. Among other consequences, the occurrence of such phases would affect the emission rates of neutrinos or axions. Reviews on the issues of neutron star interiors were provided by Baym and Pethick [299, 300], in the textbook of Shapiro and Teukolsky [301], and by Pines [302] who has stressed the role of neutron stars as "hadron physics laboratories". Many references can be found in the proceedings of the IAU-Symposium No. 125, "The origin and evolution of neutron stars" [303].

2. Axion phenomenology

The experimentally observed absence, or extreme smallness, of a *CP* violating neutron electric dipole moment has been a long standing puzzle of particle physics. The most elegant solution to this problem, proposed by Peccei and Quinn [46, 47], leads to the prediction [44, 45] of a light pseudoscalar particle: the celebrated axion. For very detailed recent reviews see Peccei [48–50], Kim [51] and Cheng [52]. The phenomenological properties of axions are closely related to the properties of neutral pions and are thus well determined. They are essentially characterized by one free model parameter, the Peccei–Quinn scale or axion decay constant, f_a, which may take on any value between $f_{weak} \sim 250$ GeV and the Planck mass of $\sim 10^{19}$ GeV. We introduce the idea of axions and review their phenomenological properties which are of importance for their possible role in astrophysics and cosmology.

2.1. Generic features of the Peccei–Quinn mechanism

2.1.1. The strong CP problem and axions

A number of years ago it was shown [304, 305] that the puzzling discrepancy between the pion masses and the mass of the η meson, the infamous U(1)-problem [306], can be taken as evidence for a nontrivial topological structure of the ground state of quantum chromodynamics (QCD). Apart from the usual color gauge interactions, the effective Lagrangian describing QCD then contains a new term [307, 308],

$$\mathscr{L}_\Theta = \Theta(\alpha_s/8\pi) G_b^{\mu\nu} \tilde{G}_{b\mu\nu} , \tag{2.1}$$

where α_s is the fine structure constant of strong interactions, $G_b^{\mu\nu}$ is the color field strength tensor, $\tilde{G}_{b\mu\nu} = \frac{1}{2}\varepsilon_{\mu\nu\rho\sigma} G_b^{\rho\sigma}$ its dual, and the summation over b refers to the color degrees of freedom. We shall usually write $G\tilde{G} \equiv G_b^{\mu\nu}\tilde{G}_{b\mu\nu}$. The coefficient Θ is a free parameter characterizing the QCD ground state or Θ-vacuum. It can be shown that a transformation $\Theta \to \Theta + 2\pi$ maps the Θ-vacuum onto itself so that *different* ground states are characterized by values in the range $0 \leq \Theta \leq 2\pi$.

Under the combined action of charge conjugation and a parity transformation the Lagrangian eq. (2.1) changes sign. Hence $\mathscr{L}_\Theta$ violates the *CP* invariance of QCD and it can be shown that it leads to a neutron electric dipole moment in the range $|d_n| = |\Theta|(0.04\text{–}2.0) \times 10^{-15}\, e\,\mathrm{cm}$ (see refs. [309–311] and for a review of more recent calculations, ref. [52]). The experimental limit [312, 313], $|d_n| < 5 \times 10^{-25}\, e\,\mathrm{cm}$, indicates that $|\Theta| \lesssim 10^{-9}$, i.e., *CP*-violating effects in QCD are extremely small. This result defies the naive expectation that a dimensionless free parameter of the theory should be of order unity.

The situation becomes even more mysterious if weak interactions are included in the discussion. In the framework of the standard model of weak interactions it is thought that the masses of quarks and leptons arise from their interaction with a scalar Higgs field which assumes a constant vacuum expectation value. This interaction is characterized by a generally complex matrix of Yukawa couplings so that the quark mass matrix, M_q, is generally complex. By suitable transformations of the quark fields it can be made real and diagonal. This procedure, however, involves a global chiral phase transformation which leads to a term in the QCD Lagrangian similar to eq. (2.1) so that the coefficient there actually is $\bar{\Theta} \equiv \Theta + \arg\det M_q$, and the experimental bounds actually refer to $\bar{\Theta}$. Since $\arg\det M_q$ originates in the weak interaction sector which is known to violate *CP* in the K^0–$\bar{K}^0$-meson system, it is difficult to conceive why Θ, arising from a completely different physical origin, should assume a value such as to let $\bar{\Theta}$ so nearly vanish. To amplify this point we note that in the Kobayashi–Maskawa scheme the *CP*-violating amplitude in the K^0–$\bar{K}^0$ system arises from a phase in the quark mass matrix [314], $\delta = 3.3 \times 10^{-3}$. This value sets the scale for the expected value for $\arg\det M_q$ which then has to cancel with Θ to within a precision of about 10^{-6}. Thus a reconciliation of the *CP*-violating effects of weak interactions with the absence of such effects in strong interactions requires an unnatural fine-tuning of the free parameters of the theory.

An elegant solution to this conundrum is provided by a theoretical scheme devised by Peccei and Quinn [46, 47] in which the *CP*-violating term $\mathscr{L}_\Theta$ vanishes dynamically. The Peccei–Quinn mechanism is constructed such that the numerical coefficient $\bar{\Theta}$ can be reinterpreted as a physical field: the axion field. More precisely, in this scheme one introduces a new scalar field, a, which enters eq. (2.1) by

$$\mathscr{L}_\Theta = (\bar{\Theta} - a/f_a)(\alpha_s/8\pi) G\tilde{G} , \tag{2.2}$$

where f_a, having the dimensions of mass or energy, is the *Peccei–Quinn scale* or axion decay constant.*) The complete Lagrangian also contains a kinetic term for the axion field, but no potential, i.e., axions

*) There exist different notations and normalization conventions for f_a in the literature. We use $f_a \equiv (f_a/N)_{\mathrm{Kaplan,\,Sikivie,\,Cheng}} = (F_a/N)_{\mathrm{Kim}} = (v_{\mathrm{PQ}}/N)_{\mathrm{Peccei}} = (f_a/2N)_{\mathrm{Srednicki}}$. We refer to the papers by Kaplan [315], Sikivie [316], Cheng [52], Peccei [48–50], Kim [51] and Srednicki [317]. It was stressed, e.g., by Georgi, Kaplan and Randall [318] that a discussion of the *generic* properties of all axion models does not require the specification of the model-dependent integer N which can be conveniently absorbed in the definition of f_a.

are constructed to be massless. Therefore the total Lagrangian remains invariant under a global shift, $a \rightarrow a + a_0$, apart from changing the interaction term eq. (2.2). This invariance allows one to absorb $\bar{\Theta}$ in the definition of the axion field by the choice $a_0 = \bar{\Theta} f_a$, leading to a complete axion Lagrangian of

$$\mathscr{L}_a = \tfrac{1}{2}(\partial_\mu a)^2 - (\alpha_s/8\pi f_a) a G\tilde{G} . \tag{2.3}$$

For this Lagrangian to be CP invariant, axions must be intrinsically CP-odd, $a \xrightarrow{CP} -a$, because the $G\tilde{G}$ term is odd. Thus by construction, axions are *pseudoscalar* particles, similar to neutral pions. The Lagrangian eq. (2.3) is the minimal ingredient for any axion model: the $aG\tilde{G}$ coupling is the generic feature of axions as opposed to other light pseudoscalar particles such as, for example, majorons [319–321].

The key feature of the Peccei–Quinn mechanism is the observation that axions, although constructed in eq. (2.3) as massless particles, do not remain massless in an effective low-energy theory. The axion–gluon interaction allows for transitions to $q\bar{q}$ states (fig. 2.1). This means physically that there exists a nonvanishing vacuum transition amplitude between axions and neutral pions, i.e., a and π^0 mix with each other. By virtue of this mixing, axions pick up a small mass which is approximately given by [318, 322–324]

$$m_a f_a \sim m_\pi f_\pi . \tag{2.4}$$

Thus the mixing angle between a and π^0 is $\theta_{a\pi} \sim f_\pi/f_a$. The presence of the mass term means that the axion Lagrangian, at low energies, contains a potential $V(a)$ which to lowest order expands as $\frac{1}{2}m_a^2 a^2$. In other words, even if one does not introduce axions, there exists a vacuum energy density $V(\bar{\Theta}) \sim \frac{1}{2}\bar{\Theta}^2 m_\pi^2 f_\pi^2 + O(\bar{\Theta}^4)$. Of course, because of the invariance of $\mathscr{L}_{\Theta}$ with respect to $\bar{\Theta} \rightarrow \bar{\Theta} + 2\pi$, the potential $V(\bar{\Theta})$ is a periodic function with period 2π and consequently $V(a)$ is periodic with $2\pi f_a$. In the Peccei–Quinn scheme, $\bar{\Theta}$ is a physical field so that it will settle in its physical ground state at $\bar{\Theta} = 0$. Hence this "parameter" is driven to its CP-conserving value and the CP-violating term eq. (2.1) vanishes. This *dynamical* realization of CP-conservation in strong interactions is the main feature of the Peccei–Quinn mechanism.

Since axions mix with neutral pions they can interact with photons and nucleons through their pion admixture which fixes the relevant coupling strengths to within factors of order unity. As an example we consider the interaction of axions with the electromagnetic field which is of the general form eq. (1.1). This interaction allows for the two photon decay, $a \rightarrow 2\gamma$, with a decay rate [73, 87]

$$\Gamma(a \rightarrow 2\gamma) = g_{a\gamma}^2 m_a^3 / 64\pi . \tag{2.5}$$

The measured pion radiative width is [325] $\Gamma(\pi^0 \rightarrow 2\gamma) = 7.66\,\mathrm{eV}$, leading to $g_{\pi\gamma} = (40.0\,\mathrm{GeV})^{-1}$. With the mixing angle $\theta_{a\pi} \sim f_\pi/f_a$ we find $g_{a\gamma} \sim 2 \times 10^{-3}/f_a$, yielding the radiative decay time $\tau_{a\rightarrow 2\gamma} \sim (m_\pi/$

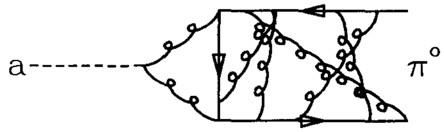

Fig. 2.1. Axion mixing with $\bar{q}q$ states and thus with π^0. The curly lines represent gluons, the solid lines quarks.

$m_a)^5\tau_{\pi^0\to 2\gamma} = 4\times 10^{24}\,\mathrm{s}\,(1\,\mathrm{eV}/m_a)^5$. While in specific axion models this number may vary by factors of order unity, this generic relationship between mass and lifetime singles out *axions* from other hypothetical pseudoscalar particles for which this relationship may be much more arbitrary. The age of the universe is about 5×10^{17} s so that axions with $m_a \lesssim 25$ eV live longer than the universe.

2.1.2. Axions as Nambu–Goldstone bosons of a new chiral symmetry

The invariance of $\mathscr{L}_\Theta$ in eq. (2.1) against transformations of the form $\bar\Theta \to \bar\Theta + 2\pi$, and the corresponding invariance of the axion Lagrangian against transformations $a \to a + 2\pi f_a$, calls for a very simple interpretation of the axion field as the *phase of a new scalar field*. This is seen most easily in an axion model proposed by Kim [326] and independently by Shifman, Vainshtein and Zakharov [327], the KSVZ axion model. While it is not the most economical model in terms of new fields and particles that need to be introduced, it provides the clearest insight into the generic structure of all axion models and allows for a straightforward understanding of the structure of the axion couplings to quarks and leptons.

In the KSVZ-model, one introduces a complex scalar field Φ which does not participate in the weak interactions, i.e., an $\mathrm{SU(2)}\times\mathrm{U(1)}$ singlet. Moreover, one introduces a new fermion field Ψ and considers the following Lagrangian,

$$\mathscr{L} = [(\mathrm{i}/2)\bar\Psi \partial\!\!\!/ \Psi + \mathrm{h.c.}] + \partial_\mu \Phi^\dagger \partial^\mu \Phi - V(|\Phi|) - h[\bar\Psi_L \Psi_R \Phi + \mathrm{h.c.}]\,, \tag{2.6}$$

with the usual kinetic terms, a potential V for the scalar field, and an interaction term, but no explicit mass term for Ψ. The Yukawa coupling h is chosen to be positive, and $\Psi_L \equiv \frac{1}{2}(1-\gamma_5)\Psi$ and $\Psi_R \equiv \frac{1}{2}(1+\gamma_5)\Psi$ are the usual left- and right-handed projections of Ψ. This Lagrangian is invariant under a chiral phase transformation of the form

$$\Phi \to \mathrm{e}^{\mathrm{i}\alpha}\Phi\,, \qquad \Psi_L \to \mathrm{e}^{\mathrm{i}\alpha/2}\Psi_L\,, \qquad \Psi_R \to \mathrm{e}^{-\mathrm{i}\alpha/2}\Psi_R\,, \tag{2.7}$$

where the left- and right-handed fields pick up opposite phases. This chiral symmetry is usually referred to as the Peccei–Quinn symmetry, $\mathrm{U_{PQ}(1)}$.

The potential $V(|\Phi|)$ is chosen such that it has an absolute minimum at $|\Phi| = f_{PQ}/\sqrt{2}$ where f_{PQ} is some large energy scale. One may take the usual Mexican hat potential [328] which arises from suitable self-interactions of Φ. With this choice for V, the ground state of the Lagrangian eq. (2.6) is characterized by a nonvanishing vacuum expectation value $\langle\Phi\rangle = (f_{PQ}/\sqrt{2})\,\mathrm{e}^{\mathrm{i}\varphi}$ where φ is an arbitrary phase. Hence the ground state is neither unique nor invariant under a transformation of the type eq. (2.7); it spontaneously breaks the Peccei–Quinn symmetry. It is then appropriate to express Φ in terms of two real fields, ρ and a, which represent the "radial" and "angular" excitations, respectively,

$$\Phi = (f_{PQ} + \rho)\,\mathrm{e}^{\mathrm{i}a/f_{PQ}}/\sqrt{2}\,. \tag{2.8}$$

The potential V provides a large mass term for ρ, a field which will be of no further interest for our low-energy considerations. Neglecting all terms involving ρ, and introducing the notation $m \equiv h f_{PQ}/\sqrt{2}$, our model Lagrangian is

$$\mathscr{L} = [(\mathrm{i}/2)\bar\Psi \partial\!\!\!/ \Psi + \mathrm{h.c.}] + \tfrac{1}{2}(\partial_\mu a)^2 - m(\bar\Psi_L \Psi_R\, \mathrm{e}^{\mathrm{i}a/f_{PQ}} + \mathrm{h.c.})\,. \tag{2.9}$$

Under a Peccei–Quinn transformation, the fermion fields change as in eq. (2.7) while the a field transforms linearly as $a \to a + \alpha f_{PQ}$. The invariance of the Lagrangian against such shifts is a manifestation of the $U_{PQ}(1)$ symmetry. It implies that a represents a massless particle, the *Nambu–Goldstone boson of the Peccei–Quinn symmetry*.

The last term in eq. (2.9) is identical to $m\bar{\Psi}\,e^{i\gamma_5 a/f_{PQ}}\Psi$. Expanding in powers of a/f_{PQ}, the zeroth order term, $m\bar{\Psi}\Psi$, simply plays the role of a mass term for the fermion field. The remaining contributions describe the interaction of a with Ψ,

$$\mathscr{L}_{int} = -i(m/f_{PQ})a\bar{\Psi}\gamma_5\,\Psi + \cdots . \tag{2.10}$$

The relevant dimensionless Yukawa coupling, $g_a \equiv m/f_{PQ}$, is proportional to the fermion mass. In a theory with several fermion fields, the a field couples most strongly to the heaviest fermion.

In order to identify the a field with the axion one needs a further ingredient, the coupling of the fermion Ψ to gluons. Therefore we take Ψ to be some exotic heavy quark with the usual strong interactions, i.e., it is taken to be an $SU_C(3)$ triplet. The lowest order interaction of the a field with gluons is then given by the triangle graph of fig. 2.2. With the pseudoscalar coupling eq. (2.10) this graph can be directly evaluated, yielding a finite result with no divergences [328]. In the limit where all external momenta in the amplitude fig. (2.2) are small compared with the mass m of the fermion in the triangle loop, one finds an effective coupling to gluons,

$$\mathscr{L}_{aG} = -(g_a/m)(g_s^2/32\pi^2)aG\tilde{G} , \tag{2.11}$$

which is precisely of the required form since $g_a/m = 1/f_{PQ}$.

In more general models, several conventional or exotic quark fields Ψ^j may participate in the Peccei–Quinn scheme. In general, the transformation of each field under a $U_{PQ}(1)$ transformation is characterized by its Peccei–Quinn charge, X_j, according to

$$\Psi_L^j \to e^{iX_j\alpha/2}\Psi_L^j . \tag{2.12}$$

This implies that the Yukawa coupling of each of these fields to a is given by $g_{aj} = X_j m_j/f_{PQ}$, and the $aG\tilde{G}$ coupling arises from a summation over these terms. Introducing the parameter

$$N \equiv \sum_j X_j \tag{2.13}$$

and using $\alpha_s = g_s^2/4\pi$ for the strong fine-structure constant, the $aG\tilde{G}$ coupling is

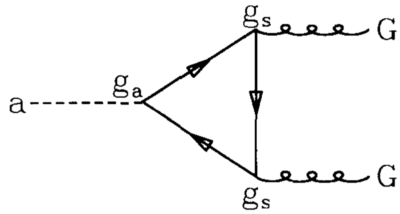

Fig. 2.2. Triangle loop diagram for the interaction of axions with gluons with the strong coupling constant g_s and the Yukawa coupling g_a of axions with the loop fermion. An analogous Feynman graph pertains to the coupling of axions to photons if the fermion is electrically charged (replace g_s with the electric charge).

$$\mathscr{L}_{aG} = -[\alpha_s/(8\pi f_{PQ}/N)]aG\tilde{G} . \tag{2.14}$$

With $f_a \equiv f_{PQ}/N$ we have then found a natural interpretation of the required coupling eq. (2.2) and we are fully entitled to identify a with the axion field.

The potential $V(a)$ for the axion field is by construction periodic with period $2\pi f_a = 2\pi f_{PQ}/N$. However, the interpretation of a as the phase of Φ implies a periodicity with $2\pi f_{PQ}$ so that N must be a nonzero integer. This requirement restricts the possible assignment of Peccei–Quinn charges to the quark fields. It also implies that there remain N different equivalent ground states for the axion field, each of which satisfies $\bar{\Theta} = 0$ and hence solves the CP problem.

2.1.3. Summary

We have now developed a consistent picture of the generic properties of the Peccei–Quinn mechanism to solve the strong CP problem. Further details can be found in the review papers by Peccei [48–50], Kim [51], and Cheng [52]. The Peccei–Quinn mechanism is a very simple and generic extension of the standard theories of strong and electroweak interactions. In summary, it consists of the following generic ingredients:

- The Lagrangian of the fundamental interactions has an extra global chiral symmetry: the Peccei–Quinn symmetry, $U_{PQ}(1)$. This symmetry is spontaneously broken by the vacuum expectation value $f_{PQ}/\sqrt{2}$ of a complex scalar field, Φ. The phase of this field, the Nambu–Goldstone field of $U_{PQ}(1)$, is the *axion field*.
- Through a triangle loop, axions couple to gluons by $(\alpha_s/8\pi f_a)aG\tilde{G}$ where $f_a \equiv f_{PQ}/N$ is the *axion decay constant* and N is a model-dependent integer.
- The $aG\tilde{G}$ coupling breaks the Peccei–Quinn symmetry explicitly because it mixes the axion with the neutral pion, yielding an effective low-energy axion potential (a small axion mass $m_a \sim m_\pi f_\pi/f_a$). This potential forces the axion field into its CP-conserving minimum; CP-conservation in strong interactions is realized *dynamically*. The apparent discrepancy between CP-violating effects in the K^0–$\bar{K}^0$-meson system and the absence of a neutron electric dipole moment vanishes naturally without fine-tuned parameters of the theory.
- The mixing with π^0 generates axion couplings to photons and nucleons, apart from possible direct couplings.
- Axions couple to quarks and leptons, j, through a pseudoscalar (or pseudovector derivative) coupling with an effective Yukawa coupling $(m_j/f_a)(X_j/N)$ with model-dependent Peccei–Quinn charges, X_j.
- The axion mass and all interactions scale with f_a^{-1}, allowing axions to be arbitrarily light and arbitrarily weakly interacting ("invisible" axions).

The most important question to be answered by experiments, astrophysics, and cosmology is: *what is the Peccei–Quinn scale*? While it can take on, in principle, any value between $f_{weak} \sim 250$ GeV scale and the Planck mass of $\sim 10^{19}$ GeV, most of this enormous parameter range can be eliminated by evidence from these different fields.

2.2. The most common axion models

The axion decay constant, f_a, is a free parameter of the models. From a theoretical point of view it is not satisfying, however, to introduce an arbitrary new energy scale so that one will try to relate f_a to other important "milestones" on the long way from f_{weak} to the Planck mass. Since axions appear as the phase of a scalar field Φ, it is natural to relate Φ to the standard Higgs field. In the standard theory, the would-be Nambu–Goldstone boson from the spontaneous breakdown of $SU(2) \times U(1)$ is interpreted as the third component of the neutral gauge boson, Z^0, whence there is no space for the axion. Therefore one needs to introduce two independent Higgs fields, Φ_1 and Φ_2, with vacuum expectation values $f_1/\sqrt{2}$ and $f_2/\sqrt{2}$ which must obey $(f_1^2 + f_2^2)^{1/2} = f_{weak} \equiv (\sqrt{2}G_F)^{-1/2} \sim 250$ GeV. In this *standard axion model* [44–47] Φ_1 gives masses to the charge $\frac{2}{3}$ quarks, while Φ_2 gives masses to the charge $\frac{1}{3}$ quarks and to the charged leptons. Introducing the ratio $x \equiv f_1/f_2$ and the number N_f of families of quarks, the axion decay constant is given by

$$f_a = f_{weak}[N_f(x + 1/x)]^{-1} . \tag{2.15}$$

Since $N_f \geq 3$ one finds $f_a \lesssim 42$ GeV. The standard axion and related "variant" models [329, 330], however, are ruled out by overwhelming experimental and astrophysical evidence (for reviews see refs. [48–52, 331]).

Therefore one is led to introduce an electroweak singlet Higgs field with a vacuum expectation value $f_{PQ}/\sqrt{2}$ which is not related to the weak scale. Taking $f_{PQ} \gg f_{weak}$, the mass of the axion becomes very small, its interactions very weak. Such models are generically referred to as *invisible axion models*. The first of its kind was introduced by Kim [51], and by Shifman, Vainshtein and Zakharov [327] and is usually referred to as the KSVZ model. It corresponds to the model described in the previous section. Its simplicity arises from the fact that the Peccei–Quinn mechanism is totally decoupled from the ordinary particles: at low energies, axions interact with matter and radiation only by virtue of their two-gluon coupling which is generic for the Peccei–Quinn scheme. The KSVZ model in its simplest form is determined by only one free parameter, $f_a = f_{PQ}$, although one is free to introduce N exotic quarks so that $N > 1$ and $f_a = f_{PQ}/N$.

Another commonly discussed model was introduced by Dine, Fischler and Srednicki [332], and independently and previously by Zhitnitskii [333] and is usually referred to as the DFSZ model. It is a hybrid between the standard model and the KSVZ model in that it introduces an electroweak singlet scalar field, Φ, with vacuum expectation value $f_{PQ}/\sqrt{2}$ *and* two electroweak doublet fields, Φ_1 and Φ_2, as above. There is no need, however, for exotic heavy quarks: only the known fermions carry Peccei–Quinn charges. In this model, $f_a = f_{PQ}/N_f$ so that, in the standard picture with three families, the number of degenerate vacua is $N = N_f = 3$. Apart from N_f, the free parameters of this model are f_{PQ} and $x = f_1/f_2$ which determines the relative coupling strength to fundamental fermions. Another common parametrization of this ratio is by an angle, β, which is related to x through $\cos^2\beta = x^2/(x^2 + 1)$ or equivalently by $x = \cot \beta$.

Since $f_{PQ} \gg f_{weak}$ in these models by assumption, it is quite natural to identify f_{PQ} with the grand unification scale [334, 335], $f_{GUT} \approx 10^{16}$ GeV. Such models have quickly fallen into disfavor because the cosmological bounds seemed to indicate that f_a must be much smaller. A careful reconsideration of these arguments reveals, however, that a rigorous cosmological bound exists only in the absence of inflation, while no rigorous bound can be derived in general inflationary universe scenarios (chapter 3).

There exist numerous other axion models, and many attempts to identify the Peccei–Quinn scale with other scales (for a review see ref. [51]). We take the phenomenological approach that the Peccei–Quinn scale is a free parameter to be determined by experimental, astrophysical, and cosmological methods.

Table 2.1
Axion mass and coupling constants. The quark mass ratios z and w were given in eq. (2.16). E and N are the model-dependent coefficients of the electromagnetic and color anomalies. Note that $\xi_0 = 0.75$ corresponds to $E/N = 8/3$, which is characteristic of GUT models. The effective Peccei–Quinn charges c_j are model-dependent numbers of order unity except for hadronic axion models where $c_e \ll 1$. Also, $f_7 \equiv f_a/10^7$ GeV and $m_{eV} \equiv m_a/1$ eV

Axion property	General expression	Numerical expressions in terms of	
		f_a	m_a
Mass	$m_a = \frac{f_\pi m_\pi}{f_a}\left(\frac{z}{(1+z+w)(1+z)}\right)^{1/2}$	$\left(\frac{0.60\times 10^7\ \text{GeV}}{f_a}\right)$ eV	1
Coupling to photons	$g_{a\gamma} = -(\alpha/2\pi f_a)\xi_0$	$-(0.87\times 10^{-3}/f_a)\xi$	$-(1.45\times 10^{-10}/\text{GeV})\xi m_{eV}$
	where $\xi_0 \equiv \frac{E}{N} - \frac{2}{3}\frac{4+z+w}{1+z+w}$ and $\xi \equiv \frac{\xi_0}{0.75} = \frac{E/N - 1.92\pm 0.08}{0.75}$		
Lifetime	$\tau_a = 64\pi/g_{a\gamma}^2 m_a^3$	$8.1\times 10^{25}\ \text{s}\,(f_7^5/\xi^2)$	$6.3\times 10^{24}\ \text{s}/\xi^2 m_{eV}^5$
Coupling to electrons	$g_{ae} = (m_e/f_a)c_e$	$(5.11\times 10^{-4}\ \text{GeV}/f_a)c_e$	$8.5\times 10^{-11} c_e m_{eV}$
Coupling to nucleons	$g_{aN} = (m_N/f_a)c_N$	$(0.939\ \text{GeV}/f_a)c_N$	$1.56\times 10^{-7} c_N m_{eV}$

2.3. Fine points of axion properties

2.3.1. The axion mass at low and high temperatures

The methods of current algebra allow one to derive a more precise expression for the axion mass which arises from its mixing with the neutral pion [317, 318, 322–324], see table 2.1, where the quark mass ratios are [336]

$$z \equiv m_u/m_d = 0.568 \pm 0.042\,, \qquad w \equiv m_u/m_s = 0.0290 \pm 0.0043\,. \tag{2.16}$$

Aside from the uncertainties in z and w, there are higher-order corrections to the current algebra result for m_a which have not been estimated in the literature. Using $m_\pi = 135$ MeV for the pion mass and $f_\pi = 93$ MeV for the pion decay constant we find the numerical results given in table 2.1.

At high temperatures, $T > \Lambda_{QCD}$, where $\Lambda_{QCD} = (100–250)$ MeV characterizes the chiral QCD phase transition, pions do not exist so that axions cannot obtain a mass by a pion admixture. However, instantons, i.e., topologically nontrivial color gauge field configurations, interact with axions through eq. (2.3), leading to a nonvanishing axion mass which has been estimated in the dilute instanton gas approximation to be [337–340]

$$m_a(T) \sim 2\times 10^{-2}\,\frac{(\Lambda_{QCD} m_u m_d m_s)^{1/2}}{f_a}\left(9\ln\frac{\pi T}{\Lambda_{QCD}}\right)\left(\frac{\Lambda_{QCD}}{\pi T}\right)^4\,. \tag{2.17}$$

The light quark masses have been estimated to be [336] $m_u = (5.1\pm 1.5)$ MeV, $m_d = (8.9\pm 2.6)$ MeV, and $m_s = (175\pm 55)$ MeV. At high temperatures the axion mass approaches asymptotically zero. Then, indeed, physics is invariant against arbitrary shifts $a \to a + a_0$ of the axion field.

2.3.2. Axion–photon coupling

By means of their generic coupling to gluons, axions necessarily mix with pions and hence couple to photons. In axion models where the quarks and leptons which carry Peccei–Quinn charges also carry electric charges, there is an additional contribution from a triangle loop diagram as in fig. 2.2, replacing the strong coupling constant, g_s, with the electric charge of the lepton. The total coupling to photons is given by eq. (1.1) where the coupling strength, $g_{a\gamma}$, is given in table 2.1 according to refs. [315, 317]. The coefficient of the electromagnetic anomaly is

$$E = 2 \sum_j X_j Q_j^2 D_j \,, \tag{2.18}$$

where Q_j is the electric charge of the fermion in the loop in units of e, $D_j = 3$ for color triplets (quarks), and $D_j = 1$ for color singlets (charged leptons).

In grand unified models the quarks and leptons of a given family are members of one multiplet which represents the unification group and then one has $E/N = 8/3$. Neglecting w, the GUT axion–photon coupling is

$$g_{a\gamma} = -\frac{\alpha}{2\pi f_a}\,\frac{2z}{1+z}\,. \tag{2.19}$$

However, one may equally consider models where $E/N = 2$ so that

$$g_{a\gamma} = -(\alpha/2\pi f_a)(0.08 \pm 0.08)\,. \tag{2.20}$$

In such models, the axion–photon coupling is strongly suppressed [315], and may actually vanish.

2.3.3. *Pseudoscalar versus derivative interaction*

There has been considerable confusion in the literature concerning the proper structure for the coupling of axions to fermions. We recall that the interpretation of the axion field as the Nambu–Goldstone boson of the Peccei–Quinn symmetry (section 2.1.2) led to the interaction Lagrangian

$$\mathcal{L}_{\rm int} = [(i/2)\bar\Psi \not\partial \Psi + \text{h.c.}] - m[\bar\Psi_L \Psi_R \, e^{ia/f_{PQ}} + \text{h.c.}]\,, \tag{2.21}$$

where Ψ is a fermion field with mass m. Expanding in powers of a/f_{PQ} led to

$$\mathcal{L}_{\rm int} = -i(m/f_{PQ})a\bar\Psi\gamma_5\Psi + (m/2f_{PQ}^2)a^2\bar\Psi\Psi + \cdots\,. \tag{2.22}$$

This Lagrangian contains an infinite series of terms. The complications associated with the higher-order terms can be avoided if one redefines the fermion field by virtue of a local transformation,

$$\psi_L \equiv e^{-ia/2f_{PQ}}\Psi_L\,, \qquad \psi_R \equiv e^{ia/2f_{PQ}}\Psi_R\,. \tag{2.23}$$

The last term in eq. (2.21) is then simply $m\bar\psi\psi$ and plays the role of a mass term. The interaction between ψ and a now arises from the kinetic Ψ term in eq. (2.21),

$$\mathcal{L}_{\rm int} = (1/2f_{PQ})\bar\psi\gamma_\mu\gamma_5\psi\partial^\mu a\,. \tag{2.24}$$

This interaction is of *derivative* nature, and it is linear in a with no higher-order terms.

In order to calculate processes such as the nucleon bremsstrahlung emission of axions, $NN \to NNa$, a pseudoscalar coupling of the type eq. (2.22) was exclusively used in the literature until it became apparent that, in some cases, it leads to incorrect results. The relevant type of error is easiest explained if one considers the scattering process $a + e^- \to e^- + a$. We first calculate the usual scattering matrix element if the interaction is taken to be purely pseudoscalar, i.e., only the first term in eq. (2.22) is used. Taking p_e and p_e' for the electron four-momenta before and after the interaction, u and u' for the electron Dirac spinors, and p_a and p_a' for the axion four momenta, we find

$$\mathcal{M} = \frac{i}{2}\left(\frac{m}{f_{PQ}}\right)^2 \bar{u}'\left(\frac{\not{p}_a}{p_e p_a} + \frac{\not{p}_a'}{p_e p_a'}\right) u \,. \tag{2.25}$$

Then we calculate the same matrix element, using the derivative coupling eq. (2.24),

$$\mathcal{M} = \frac{i}{2}\left(\frac{m}{f_{PQ}}\right)^2 \bar{u}'\left(\frac{\not{p}_a}{p_e p_a} + \frac{\not{p}_a'}{p_e p_a'} - \frac{2}{m}\right) u \,. \tag{2.26}$$

These two expressions differ by a term which arises from the second term in the expansion eq. (2.22). In order to obtain the correct result one either has to use the derivative coupling eq. (2.24), or one has to include this second term as was first emphasized by Raffelt and Seckel [92]. One is fully entitled, of course, to consider hypothetical particles with a purely pseudoscalar coupling, excluding the second term in eq. (2.22). Such particles, however, are not the Nambu–Goldstone bosons of a symmetry and have nothing to do with axions. The Nambu–Goldstone nature of axions is most apparent in the Lagrangian eq. (2.24) where the derivative coupling clearly shows the invariance against transformations of the type $a \to a + a_0$. A purely pseudoscalar Lagrangian does not possess this symmetry.

As an immediate application of this discussion we consider the refractive index for the propagation of axions in a medium. This is of importance, e.g., for the oscillation of the axion field in the early universe. The refractive index in a medium of electrons is computed from the forward scattering amplitude [341] of the process $a + e^- \to e^- + a$. Thus we have to use $p_e' = p_e$, $u' = u$, and $p_a' = p_a$ in the matrix elements above. The purely pseudoscalar case, eq. (2.25), yields $\mathcal{M} = im/f_{PQ}^2$, leading to a refractive index similar to that for photons: apart from a numerical factor, one simply has to replace the electron charge, e, by the axion–electron Yukawa coupling, $g = m/f_{PQ}$. The case of a derivative coupling, eq. (2.26), yields $\mathcal{M} = 0$ so that *axions do not experience refractive effects in a medium*. This is an important difference between Nambu–Goldstone bosons and particles with a purely pseudoscalar coupling. On the basis of more general arguments, Flynn and Randall [342] showed that the derivative nature of the Nambu–Goldstone coupling protects such bosons from developing an effective mass in a medium. Hence, at finite temperature and density, the axion mass is solely given by the expressions in section 2.3.1 above with no additional refractive contributions.

In our discussion of the generic axion properties we have stressed the close relationship between axions and neutral pions. Pions play the role of Nambu–Goldstone bosons of a spontaneously broken $U(2)_{L-R}$ symmetry of QCD so that their interaction with nucleons should be of derivative rather than of pseudoscalar structure. Considering, for example, the scattering process $\pi^0 + p \to p + \pi^0$ would allow one to distinguish between the two cases. Equally, one may consider the bremsstrahlung process $p + p \to p + p + \pi^0$ because the interaction between the protons proceeds predominantly by pion exchange. Choi, K. Kang and Kim [62] pointed out that existing experimental data for this process allow one to distinguish between the pseudoscalar and derivative couplings, and a detailed investigation by Turner, H.-S. Kang and Steigman [98] confirmed that the derivative coupling is appropriate.

Iwamoto [78] also clarified the relationship between the pseudoscalar and the derivative interaction structure.

Following Carena and Peccei [60], the interaction of pions with nucleons is described by the Lagrangian

$$\mathcal{L}_{\mathrm{int}} = g_{\pi\mathrm{N}} \bar{N}\gamma^{\mu}\gamma_5 \boldsymbol{\tau} N \cdot \partial_{\mu} \boldsymbol{\pi} + f_{\pi\mathrm{N}}^2 \bar{N}\gamma^{\mu} \boldsymbol{\tau} N \cdot \partial_{\mu} \boldsymbol{\pi} \times \boldsymbol{\pi} , \tag{2.27}$$

where $g_{\pi\mathrm{N}} \equiv f/m_{\pi} \sim 1/m_{\pi}$ and $f_{\pi\mathrm{N}} \equiv 1/2f_{\pi}$ are the relevant coupling constants with the pion mass, $m_{\pi} = 135$ MeV, and the pion decay constant, $f_{\pi} = 93$ MeV. Also, $\boldsymbol{\tau}$ is a vector of Pauli isospin matrices, and $\boldsymbol{\pi}$ is the isovector of the neutral and charged pion fields, while N is the isodoublet of neutron and proton. Thus there appears an extra six-dimensional term which is not present in our above axion example, eq. (2.24), where only one Nambu–Goldstone boson was present as opposed to the pion isotriplet. As shown by Carena and Peccei, this additional term does not contribute to the bremsstrahlung process in the limit of nonrelativistic nuclei and the analyses of Choi et al. [62] and Turner et al. [98] remain valid.

In order to compute the nucleon bremsstrahlung of axions, $\mathrm{NN} \to \mathrm{NN}a$, one must include axions *and* pions in the discussion. Again, using pseudoscalar couplings for both axions and pions leads to erroneous results, and it is the discrepancy between the original correct result of Iwamoto [77] and the subsequent erroneous result of Pantziris and Kang [86] which led Raffelt and Seckel [92] to discover the practical importance of distinguishing carefully between the pseudoscalar and derivative couplings. Such problems are to be expected in any amplitude where two Nambu–Goldstone bosons are attached to one fermion line. However, when two Nambu–Goldstone bosons are attached to one fermion line, it is sufficient to use a derivative coupling for one of them. For the bremsstrahlung production of axions this means that one may use a pseudoscalar coupling for the axions as long as one uses a derivative coupling for the pions.

We stress that for other bremsstrahlung processes such as $\mathrm{e}^-\mathrm{e}^- \to \mathrm{e}^-\mathrm{e}^-a$, where the particles interact through a virtual photon rather than a virtual pion, no problems arise because only one Nambu–Goldstone boson, the axion, is attached to a fermion line, while the other particle is a photon with the usual gauge coupling. Similarly, for the Compton process, $\gamma\mathrm{e}^- \to \mathrm{e}^-a$, one may use either the pseudoscalar or the derivative axion coupling: both yield the same result.

2.3.4. *Model dependent axion–fermion coupling*

The interpretation of the axion field as the phase of a new scalar field gave, in section 2.1.2, the general exponential interaction Lagrangian of axions with quarks and leptons. To lowest order it is equivalent to the pseudoscalar interaction,

$$\mathcal{L} = -\mathrm{i}(m_j X_j/f_{\mathrm{PQ}}) \bar{\psi}_j \gamma_5 \psi_j a , \tag{2.28}$$

where m_j is the mass of the fermion field ψ_j which carries the Peccei–Quinn charge X_j. The Yukawa coupling constant and the corresponding axionic fine structure constant are given by

$$g_{aj} \equiv m_j X_j/f_{\mathrm{PQ}} , \qquad \alpha_{aj} = g_{aj}^2/4\pi , \tag{2.29}$$

so that we recover eq. (1.2). Various axion models differ in their assignment of Peccei–Quinn charges. However, in all models $N = \Sigma_{\mathrm{quarks}} X_j$ is a nonzero integer. The assignment of Peccei–Quinn charges at high energies is not maintained in the low-energy sector because the spontaneous breakdown of the weak $SU_L(2) \times U_Y(1)$ symmetry at the scale $f_{weak} \sim 250\,GeV$ mixes the axion field with the would-be Nambu–Goldstone boson which becomes the longitudinal component of the Z^0 gauge boson. Hence the Peccei–Quinn charges must be shifted such that the physical axion does not mix with the Z^0, and these shifted values are denoted as X'_j. Also, below the QCD scale of $\Lambda_{QCD} \sim 200\,MeV$, free quarks do not exist, and one needs to consider the effective coupling to nucleons which arises from the direct axion coupling to quarks and from the mixing with π^0 and η. Thus one introduces Peccei–Quinn charges X'_p and X'_n for protons and neutrons. It is useful, moreover, to define effective Peccei–Quinn charges by

$$c_j \equiv X'_j/N . \tag{2.30}$$

Then the Yukawa couplings eq. (2.29) are

$$g_{aj} = (m_j/f_a)c_j . \tag{2.31}$$

Noting that the axion decay constant, f_a, is uniquely related to the axion mass we may write the couplings to electrons and nucleons as given in table 2.1.

In the DFSZ model [332, 333], the low-energy Peccei–Quinn charge for the electron is written as $X'_e = \cos^2\beta$ (conventions of Kaplan [315]), or $X'_e = 2\cos^2\beta$ (conventions of Srednicki [317]) where the parameter β reflects the ratio of the vacuum expectation values of two Higgs fields, $x = f_1/f_2$, through $\cos^2\beta = x^2/(x^2+1)$ or $x = \cot\beta$. Therefore one has

$$\text{DFSZ:}\quad c_e = X'_e/N = \cos^2\beta/N_f , \tag{2.32}$$

where $N_f \gtrsim 3$ is the number of families of quarks. For three families, $N = 3$ and $N = 6$ in Kaplan's and Srednicki's convention, respectively, while always $N_f = 3$. In the KSVZ axion model [326, 327], and in all models where the axions do not couple to light quarks and leptons ("hadronic axions"), $X'_e = 0$ at tree level, although there are radiatively induced, higher-order axion–electron couplings [317].

The nucleon interactions in general axion models were investigated by Kaplan [315] and by Srednicki [317]. Most recently, they were revisited by Mayle et al. [80, 81] whence we find

$$\begin{aligned} c_p &= \left(c_u - \frac{1}{1+z+w}\right)\Delta u + \left(c_d - \frac{z}{1+z+w}\right)\Delta d + \left(c_s - \frac{w}{1+z+w}\right)\Delta s ,\\ c_n &= \left(c_u - \frac{1}{1+z+w}\right)\Delta d + \left(c_d - \frac{z}{1+z+w}\right)\Delta u + \left(c_s - \frac{w}{1+z+w}\right)\Delta s , \end{aligned} \tag{2.33}$$

where the quark mass ratios, z and w, were given in eq. (2.16). For a given quark flavor, $q =$ u, d, or s, the interaction strength with protons depends on the proton spin content carried by this particular quark flavor, $S_\mu\,\Delta q \equiv \langle p|\bar{q}\gamma_\mu\gamma_5 q|p\rangle$ where S_μ is the proton spin. Similar expressions pertain to the coupling with neutrons, and the two sets of expressions are related by isospin invariance. One combination of the parameters is fixed by neutron β-decay, $\Delta u - \Delta d \equiv g_A = 1.25$. Another combination is fixed by hyperon β-decay data and flavor SU(3) symmetry for the baryon octet and leads to $\Delta u + \Delta d - 2\,\Delta s = 0.682$ so that $\Delta u = \Delta s + 0.966$ and $\Delta d = \Delta s - 0.284$. In the DFSZ model, $c_s = c_d = c_e$, $c_u + c_d = 1/N_f$, and $c_u - c_d = -\cos^2\beta/N_f$, leading to $c_u = \sin^2\beta/N_f$ and $c_d = c_s = c_e = \cos^2\beta/N_f$. In the KSVZ model, and in other hadronic axion models, $c_u = c_d = c_s = 0$. Thus, taking $N_f = 3$, we find the results given in table 2.2.

Until recently it was thought that strange quarks would not contribute to the proton or neutron spin,

Table 2.2
Effective Peccei–Quinn charges for protons (c_p) and neutrons (c_n) as discussed in the text

		KSVZ	DFSZ ($N_f = 3$)
General case	c_p	$-0.504 - \Delta s$	$-0.182 - \frac{2}{3}\Delta s + \frac{1}{3}\cos^2\beta\,(\Delta s - 1.25)$
	c_n	$-0.166 - \Delta s$	$-0.261 - \frac{2}{3}\Delta s + \frac{1}{3}\cos^2\beta\,(\Delta s + 1.25)$
NQM ($\Delta s = 0$)	c_p	-0.50	$-0.18 - 0.42\cos^2\beta$
	c_n	-0.17	$-0.26 + 0.42\cos^2\beta$
EMC ($\Delta s = -0.257$)	c_p	-0.25	$-0.01 - 0.50\cos^2\beta$
	c_n	$+0.09$	$-0.09 + 0.33\cos^2\beta$

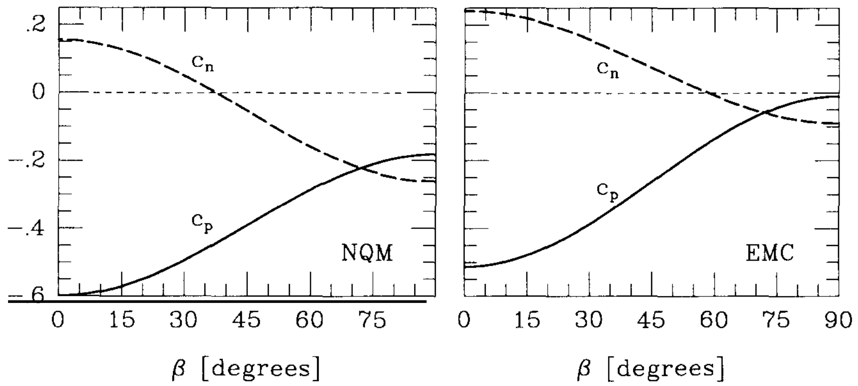

Fig. 2.3. DFSZ-axion coupling to protons, c_p, and neutrons, c_n, for the NQM and EMC cases according to the results given in table 2.2.

$\Delta s = 0$. Mayle et al. [80, 81] refer to this case as the "naive quark model" (NQM) for which one obtains $\Delta u = +0.966$, $\Delta d = -0.284$, and $\Delta s = 0$, yielding the relevant entries in table 2.2. (The results there correspond to Mayle et al.'s values noting that their C_{ap} and C_{an} are given by $12c_p$ and $12c_n$, respectively.) However, recent measurements indicate that $\Delta s \neq 0$, i.e., that a considerable fraction of the proton spin is carried by strange quarks. One result is based on the spin-dependent muo-production structure function, measured by the European Muon Collaboration (EMC) [343]. Ellis, Flores and Ritz found [344] $\Delta s = -0.257$. This result is supported by the analyses of elastic neutrino proton scattering [345, 346], which yield $\Delta s = -0.15 \pm 0.09$. Following Mayle et al. [80, 81] we use the EMC value, i.e., $\Delta u = +0.709$, $\Delta d = -0.541$, and $\Delta s = -0.257$ yielding the EMC entries in table 2.2. It is interesting that the value $\Delta s = -0.15$ of refs. [345, 346] would lead to a near cancellation of the KSVZ axion–neutron coupling. For the DFSZ-model we have plotted, in fig. 2.3, the β-dependence of c_p and c_n for the NQM and the EMC cases.

In the DFSZ-case with $N_f = 3$, the couplings to protons and neutrons are equal for $\cos^2\beta = 0.095$, i.e., $\beta = 72°$, independently of Δs. They would simultaneously vanish for $\Delta s = -0.348$. This value is outside of the range of what is experimentally measured so that in neither class of models do the couplings seem to vanish simultaneously.

3. Axion cosmology

While questions of particle cosmology are not the major focus of this review, we briefly consider the cosmological constraints on axions because the original discussions of this subject [338–340] have recently received severe qualifications. In the framework of a broad class of inflationary scenarios, axions would probably dominate the mass density of the universe, but no rigorous bound on f_a can be derived. In the absence of inflation, or if the universe reheated beyond f_a after inflation, cosmic strings appear which efficiently radiate axions. The resulting mass density in axions is so large that $f_a \lesssim 10^{10}$ GeV according to Davis and Shellard [347, 348] or $f_a \lesssim 10^{12}$ GeV according to Harari and Sikivie [349]. In addition, primordial axions are produced by thermal processes. In a small mass range around a few eV, thermally produced axions may be detectable by their two-photon decay which would produce a characteristic line feature in the "glow of the night sky". If axions are the dark matter, galactic axions with a mass around 10^{-5} eV are detectable in laboratory experiments which already have produced interesting upper limits.

3.1. *Inflationary scenario*

The interpretation of axions as the phase of new scalar field, Φ, allows one to follow the axion field through its cosmic evolution. When the temperature of the universe falls below the Peccei–Quinn scale, the scalar field develops a vacuum expectation value $\langle \Phi \rangle = (f_{PQ}/\sqrt{2})\, e^{ia/f_{PQ}}$ where the value of the phase, a/f_{PQ}, will generally vary with location. Since $T \gg \Lambda_{QCD}$, the potential $V(a)$ is vanishingly small so that there is no energetic difference between regions of the universe with different values of the axion field in the range $0 \le a \le 2\pi f_a$. However, because of the enormous exponential growth factor during inflation which we assume to occur after this epoch, only a small bubble of the initially chaotic universe will become our observable region of space–time [350–353]. Then for us, only one specific initial value $0 \le a_i \le 2\pi f_a$ of the axion field pertains while other regions of the universe, not observable to us, are characterized by other values.

As the universe expands and cools to temperatures near Λ_{QCD}, the potential $V(a)$ begins to develop and the axion field begins to follow the force which drives it toward the equilibrium value at $a = 0$. When the axion mass, $m_a(T)$, becomes larger than the cosmic expansion rate, $H(T)$, the axion field begins to oscillate freely around the minimum of the potential $V(a)$ with a frequency $m_a(T)$. At temperatures below Λ_{QCD}, the axion mass takes on the fixed value given in table 2.1 which then determines the oscillation frequency. Quantum mechanically, these coherent field oscillations are interpreted as highly occupied states with vanishing momentum, i.e., axions are created as a zero-momentum Bose condensate. Thus axions are nonrelativistic from the very moment of their creation which renders them [354] a *cold* dark matter [355] candidate.

A detailed investigation of this mechanism leads to an estimate of the expected cosmic mass density in axions [338–340, 356],

$$\Omega_a = 0.2 \times 10^{\pm 0.5} (f_a/10^{12}\ \mathrm{GeV})^{1.175} \gamma^{-1} h^{-2} (a_i/2\pi f_a)^2 , \tag{3.1}$$

where Ω_a is in units of the critical density, $\rho_{crit} = h^2 \times 1.88 \times 10^{-29}\ \mathrm{g\,cm^{-3}}$, which is necessary to close the universe, h is the present-day Hubble expansion parameter in units of $100\ \mathrm{km\,Mpc^{-1}\,s^{-1}}$, and γ is the ratio of the entropy per comoving volume now to that at the time when the axion field started to oscillate. The uncertainty in the numerical coefficient reflects various theoretical uncertainties. In an inflationary scenario, the universe is flat so that the total energy density equals the critical density, $\Omega = 1$. Since $\Omega_a < \Omega = 1$, the right-hand side of this equation is constrained to be less than unity.

In a flat universe, $\Omega = 1$, the cosmic time and the instantaneous Hubble parameter are related by [357] $t = \frac{2}{3} H^{-1} = 0.65 \times 10^{10}\ \mathrm{yr}\ h^{-1}$. The current age of our universe certainly exceeds 10^{10} yr allowing us to take $h = 0.40$–0.65. If we neglect the possibility of late entropy production, $\gamma = 1$, we find for our universe,

$$\Omega_a = 1.3 \times 10^{\pm 0.6} (f_a/10^{12}\ \mathrm{GeV})^{1.175} (a_i/2\pi f_a)^2 . \tag{3.2}$$

Assuming that axions are the dark matter, $\Omega_a \sim 1$, this equation establishes a relationship between f_a and the value for a_i of that particular primordial domain that evolved into our universe. The parameter $a_i/2\pi f_a$ can take on any value in the interval [0, 1] with equal a priori probability. On the basis of this observation and on the basis of eq. (3.2) it was argued that a constraint on f_a could be derived. For example, with a chance of 99% one has $a_i/2\pi f_a > 0.01$ leading one to argue that $f_a < 3 \times 10^{16}$ GeV at a 99% confidence level.

It was first pointed out by Pi [358] that this type of probabilistic argument is not a rigorous bound since it is possible that we live in a bubble of the universe with a relatively unlikely initial value of the axion field. Moreover, as stressed by Linde [359], proponents of this argument implicitly assume that the a priori probability of a certain value of a_i is identical with the *conditional* probability of us observing such a value. A universe with "forbidden" values of a_i and f_a is still legitimate, only it could not evolve into the universe that we observe. In such a universe, the ratio of axionic dark matter to baryonic material and photons would differ from ours, leading to a different epoch of matter–radiation equality, and it is not assured that all such universes could produce observers. It is well possible that, taking the GUT-scale $f_a \sim 3 \times 10^{16}$ GeV as an example, the probability of producing observers is a function of a_i which sharply peaks around 0.01. Thus we would observe this value in spite of its small a priori probability because values much different from this would not produce anybody to bear witness to this scenario. However, Dowrick and McDougall [360], who have attempted to make this anthropic argument more precise, found no contradiction between the "forbidden" values of f_a and a_i and the existence of possible observers.

All of these arguments are based on treating the Higgs and axion fields on a classical level. Very recently Goldberg [361] has questioned the validity of this approach and has argued that one may not ignore the effects of "second quantization", i.e., the quantum properties of the field amplitudes. He argued that an initial state with a definite value for a_i was a highly unlikely configuration. More typically, the field would be initially "smeared out" around the Mexican hat, and the dependence of Ω_a on the initial value a_i vanishes. Hence, according to Goldberg, the bound $f_a \lesssim 10^{12}$ GeV applies without any dependence on initial conditions. The validity of this line of argument is still being discussed.

3.2. *Topological structures*

If the universe never underwent inflation, or if it reheated after inflation beyond the Peccei–Quinn scale, the evolution of the cosmic axion field differs markedly from the simple picture outlined in the previous section. This was most clearly discussed by Davis and Shellard [348]. At a cosmic temperature around f_{PQ}, the axion field settles somewhere in the "brim" of the Mexican hat potential, with different values $a_i(x)$ in different regions of space. In contrast with the inflationary scenario where only a small domain with approximately constant a_i developed into our universe, these different regions now remain causally connected whence a_i varies over several periods in such a region of space. Since only values in the range $0 \leq a_i \leq 2\pi f_a$ correspond to physically different states, this means that topological defects must form, cosmic strings, around which the axion field varies by one period. The energy per unit length stored in a straight string at rest is given by $\mu \sim 2\pi f_a^2 \ln R/\delta$ where R is some large radius and δ is a lower cutoff from the string core.

Because of the large tension in these strings, they will rapidly oscillate, the major damping mechanism being axionic radiation until one straight string remains per horizon volume. This radiation is the dominant source for cosmic axions as was first pointed out by Davis [347]. String radiation continues until the QCD phase transition occurs when all previously produced axions develop a mass and begin to contribute to the matter density of the universe. Also, at this time the explicit breaking of the Peccei–Quinn symmetry causes the axion field around strings to collapse into domain walls, the strings and walls then colliding among themselves and breaking up [362] although the axions produced in this event alone would not lead to a cosmic energy density problem. However, if there are N different, degenerate ground states as, for example, in the DFSZ model, several domain walls are attached to one string, leading to a more complicated scenario. Indeed, the importance of domain walls in models with $N>1$ was the first instance where the importance of topological defects for the axion cosmology was recognized by Sikivie [363]; in such models the energy density in domain walls would be so large that noninflationary scenarios would require $N=1$.

Following Davis and Shellard [348] we stress that in this noninflationary scenario the axion production by cosmic string radiation is not an additional source for axions beyond the coherent field oscillations discussed above, rather it is the *only* source. Therefore the original discussions of the coherent process [338–340] are meaningless for the noninflationary scenario, and attempts to calculate the cosmic axion density from coherent oscillations with some averaged value for a_i [356] are ill-conceived.

In order to compute the expected energy density in axions, Davis and Shellard [348] modelled the primordial axion string network as a Brownian system with a single step length, $\xi(t)$, where the scaling with cosmic time, t, is taken as $\xi(t)=\bar{\xi}t$ and $\bar{\xi}$ is some dimensionless coefficient of order unity. They found for the axionic density in units of the critical density,

$$\Omega_a = 0.2\times 10^{\pm 0.5}\left(\frac{f_a}{10^{12}\,\mathrm{GeV}}\right)^{1.175}\gamma^{-1}h^{-2}\left(\frac{4\ln(\bar{\xi}\tilde{t}/\delta)}{\bar{\xi}}\sum_n \frac{\varepsilon_n}{n}\right), \tag{3.3}$$

where $\tilde{t}$ is the time near the QCD phase transition when the axion mass is sufficiently large that zero-momentum modes begin to oscillate freely, $\delta\sim 1/f_{PQ}$ is the core radius of axionic strings, and ε_n is the fraction of power which strings radiate into the harmonic of order n. The first part of this result corresponds to the first part of eq. (3.1). Noting that $\Omega_a h^2<1.1$ [356] yields the constraint

$$f_a \lesssim 5\times 10^{10}\,\mathrm{GeV}\left(\frac{1}{\gamma\bar{\xi}}\sum_n \frac{\varepsilon_n}{n}\right)^{-0.85}. \tag{3.4}$$

Davis and Shellard believe that this bound is conservative because it neglects the string kinetic energy, string structure within the horizon such as kinks and loops, and because the effects of the QCD phase transition have been ignored except for giving the previously produced axions a mass.

It is not obvious, however, what one has to choose for the parameters $\bar{\xi}$ and ε_n. While causality limits $\bar{\xi}<1$, Davis and Shellard [348] argue that $\bar{\xi}$ should not be much smaller than unity. They also argue, on the basis of numerical simulations, that most of the energy is radiated into the lowest harmonics. Therefore they claim a bound

$$\text{Davis and Shellard [348]}: \quad m_a \gtrsim 10^{-3}\,\mathrm{eV} \tag{3.5}$$

for the axion mass.

Harari and Sikivie [349], however, claim that the energy spectrum of the radiated axions would not dominantly go into the lowest modes, rather they expect a $1/\omega$ frequency spectrum. This radiation spectrum is also of importance for the possible observation of string radiated "omions" which can oscillate into photons in intergalactic magnetic fields [364]. Harari and Sikivie's treatment implies a bound,

$$\text{Harari and Sikivie [349]:}\quad m_a \gtrsim 10^{-5}\,\text{eV}\,, \tag{3.6}$$

which is about two orders of magnitude less restrictive than Davis and Shellard's bound. A very recent analysis of axion radiation from strings by Dabholkar and Quashnock [365] supports Davis and Shellard's view, while a still unpublished numerical investigation by Hagmann and Sikivie [366] supports Harari and Sikivie's claim. The present author is in no position to decide between these opposing views.

3.3. Thermally produced axions

For sufficiently large values of f_a, axions never were in thermal equilibrium in the early universe and their cosmic abundance is solely determined by the effects discussed in sections 3.1 and 3.2 above. However, axions do interact with the hot and dense primordial plasma so that, for sufficiently small values of f_a, the interaction is so large that axions were in thermal equilibrium at a certain epoch. In this case there are about as many axions in the universe as there are microwave photons, and the axionic mass density is obtained by multiplying this number with m_a. Turner [367] estimated, on the basis of interaction processes such as the Primakoff effect, that this is the case for $f_a \lesssim 10^9\,\text{GeV}\,(m_q/30\,\text{GeV})^{1/2}$ where m_q is the mass of the heaviest quark with which axions interact. In the DFSZ-model this is the mass of the top-quark which is known to exceed ~30 GeV, while in the KSVZ-model m_q may be much larger. Turner [367] found for the density in thermally produced axions,

$$\Omega_a = 8\times 10^{-9}(f_a/10^{12}\,\text{GeV})^{-1}h^{-2}(60/g_*)\,, \tag{3.7}$$

where g_* is the effective number of thermally excited degrees of freedom in the early universe at the time of the axion freeze-out. After this epoch, axions still decay, $a\to\gamma\gamma$, with a rate given in table 2.1 so that Ω_a must be multiplied by e^{-t_U/τ_a} where $t_U = (10\text{–}20)\times 10^9$ yr is the age of the universe.

We illustrate this mass contribution for a typical choice of parameters. We use an intermediate age of the universe, $t_U \sim 5\times 10^{17}$ s, and we take $g_* = 60$. We consider a noninflationary scenario with Davis and Shellard's [348] mass density where we use $\gamma = 1$ and the term in brackets in eq. (3.3) is taken to be 3×10^3, i.e., we use $\Omega_a h^2 = 600\,(f_a/10^{12}\,\text{GeV})^{1.175}$. For the axion lifetime we use the GUT-result eq. (2.20), which is explicitly $\tau_a = 6.3\times 10^{24}\,\text{s}\,(1\,\text{eV}/m_a)^5$. Finally, we also consider the axion–photon coupling for the case $E/N = 2$, see eq. (2.21), which is represented as a dashed line in fig. 3.1 where we show the axion density as a function of m_a.

3.4. Decaying axions and a glow of the night sky

In the previous section we showed that thermally produced axions with masses of a few eV would contribute substantially to the mass density of the universe. In this case, however, the photons from the radiative decay $a\to\gamma\gamma$ may be detectable as a spectral signature in the visible or near-visible (uv) regime, an effect first discussed by Kephart and Weiler [368]. Existing measurements of the brightness of the night sky already require [367]

$$m_a \lesssim 5\ \mathrm{eV}\,, \tag{3.8}$$

a bound which improves to $m_a \lesssim 2$ eV if axions cluster in the haloes of galaxies or in galactic clusters. In this case one would expect a characteristic line feature in the optical spectra of these systems. For masses much larger than these values, all primordial axions would have decayed by today, see fig. 3.1 for the remaining mass density, and the decay photons would contribute to the diffuse electromagnetic background radiations. If axions have masses just below the limit eq. (3.8) they are not rigorously excluded by stellar evolution constraints, and an actual experiment to search for line features in the night sky is under way [369].

3.5. Experimental search for galactic axions

If the early universe never underwent inflation, or if it reheated after inflation beyond the Peccei–Quinn scale, the remaining parameter space for the existence of axions is very narrow if not absent (section 11.2). However, in an inflationary scenario of the early universe, axions could contribute to the dark matter of the universe. Because of their production as a Bose condensate in the zero-momentum mode they would have been nonrelativistic since their creation and thus are a cold dark matter candidate. In this case one would expect that the local galactic dark matter density of about [356] $5 \times 10^{-25}\ \mathrm{g\,cm^{-3}}$ is provided by axions.

Sikivie [370] pointed out that the two-photon coupling of axions allows for transitions between axions and photons in the presence of an external magnetic field (section 4.9.4). For nonrelativistic axions from the galactic halo with a mass $\sim 10^{-5}$ eV the emerging photon has a frequency in the GHz regime. The transition rate can be resonantly enhanced if one uses a high-Q microwave cavity which is placed in an external magnetic field, i.e., one considers the transition between axions and electromagnetic

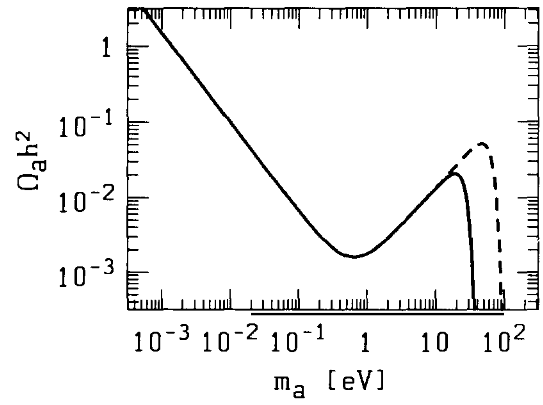

Fig. 3.1. Axionic mass density in a non-inflationary universe, taking thermally produced and string-produced axions into account, and allowing for axion decay. For the string-produced contribution we use Davis and Shellard's [348] value. The dashed line refers to the $E/N = 2$ type photon coupling of eq. (2.20) where we used the face value $g_{a\gamma} = -0.08\alpha/2\pi f_a$.

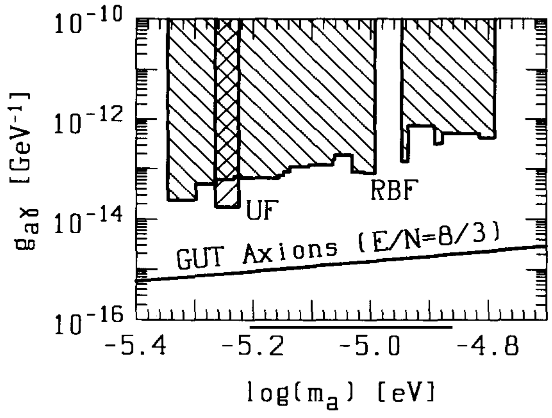

Fig. 3.2. Axion parameters which are excluded, at the 95% CL, by the Rochester–Brookhaven–Fermilab (RBF) Axion Search Experiment [375, 376] and by the University of Florida (UF) Cosmic Axion Search [378], assuming axions are the dark matter in the galactic halo. The local dark matter density is taken to be $5.3 \times 10^{-25}\ \mathrm{g\,cm^{-3}} = 300\ \mathrm{MeV\,cm^{-3}}$. The "axion-line" is for the GUT-case, $E/N = 8/3$.

excitations of the fundamental mode of the cavity. The transition rates have been calculated by a number of authors [370–374]. Of course, in order to search for axions with a given mass, the cavity has to be tuned to the corresponding frequency. Therefore, in a search experiment, one pays for the enhanced transition rate with the need to scan in narrow bins over the interesting interval of masses.

Two experiments of this type have produced first results, the Rochester–Brookhaven–Fermilab (RBF) Axion Search Experiment [375, 376], and the University of Florida (UF) Cosmic Axion Search [377, 378], excluding the cross-hatched regime of m_a and $g_{a\gamma}$ in fig. 3.2 under the assumption that the galactic dark matter halo is made of axions. It is very difficult, but perhaps not impossible, to enhance the experimental sensitivity to a point where, for a given m_a, the excluded regime actually touches the "axion line" in fig. 3.2. Another similar experimental effort is also in progress [379].

4. Emission rates from stellar plasmas

We review the emission rates of axions from stellar plasmas for various conditions and processes. For axions which couple to electrons (DFSZ-type), the dominant emission process in low-mass stars (the Sun, other main-sequence stars, red giants, horizontal branch stars, and white dwarfs) is the Compton-process, $\gamma e^- \to e^- a$, and bremsstrahlung, $e^-(A, Z) \to (A, Z)\, e^- a$. In very low-mass stars, free–bound transitions are also important ("axio-recombination"). For hadronic axions, the only relevant process is the Primakoff effect, $\gamma \xrightarrow{E} a$, which proceeds in the presence of the fluctuating electric field of the plasma by virtue of the $a\gamma\gamma$ coupling. In neutron star matter, the most important emission process is nucleon bremsstrahlung, $NN \to NNa$, for both types of axions. We also discuss plasmon decay into neutrinos, $\gamma_{pl} \to \bar{\nu}\nu$.

4.1. General discussion of the emission rates

When calculating the energy loss of a star by neutrino or axion emission, one is concerned with a system where all particles (nuclei, electrons, photons) are in thermal equilibrium while the neutrinos or axions can freely escape. Hence the production rate of these particles must be computed from detailed microscopic processes and cannot be based on general thermodynamic arguments. A typical example for an emission process is the Compton reaction, $\gamma e^- \to e^- \nu\bar{\nu}$, for neutrino emission or the corresponding process, $\gamma e^- \to e^- a$, for axions. A general expression for the volume emission rate (in $\mathrm{erg\,cm^{-3}\,s^{-1}}$) is,

$$Q = \prod_{j=1}^{N} \int \frac{d^3\boldsymbol{p}_j}{2E_j(2\pi)^3}\, f_j(E_j) \prod_{i=1}^{N'} \int \frac{d^3\boldsymbol{p}'_i}{2E'_i(2\pi)^3}\, [1 \pm f'_i(E'_i)] \int \frac{d^3\boldsymbol{p}_a}{2E_a(2\pi)^3}\, E_a(1+f_a)$$
$$\times \frac{1}{N_{id}!}\, \frac{1}{N'_{id}!} \sum_{\substack{\text{spins}\\ \text{polarizations}}} |\mathcal{M}|^2 (2\pi)^4 \delta^4\Big(\sum_{j=1}^{N} p_j - \sum_{i=1}^{N'} p'_i - p_a\Big)\,, \tag{4.1}$$

where N is the number of initial-state particles, N' that of final-state particles except for the axion whose energy and four-momentum are E_a and p_a, respectively, N_{id} is the number of identical particles of one species in the initial state, and N'_{id} in the final state. There are several such factors if there are several species of identical particles. The phase-space occupation numbers, f_j, are the usual Bose–

Einstein or Fermi–Dirac functions, normalized such that the density of a given particle species is $n_j = \int d^3\boldsymbol{p}_j\, f_j(E_j)/(2\pi)^3$. For the final-state occupation factors, the plus sign applies to bosons (stimulated emission), while the minus sign must be used for fermions (Pauli blocking). The final-state occupation factor for the axions, f_a (not to be confused with the axion decay constant!), is usually neglected because the individual modes have less-than-thermal occupation numbers. The usual energy loss per unit mass is $\varepsilon = Q/\rho$ (in erg g^{-1} s^{-1}).

Besides the stimulation and blocking factors, the presence of the plasma changes the dispersion relation of the participating particles, leading to modified normalizations for initial- and final-state wave functions, to modified propagators for the intermediate states, and to a modified law of energy–momentum conservation. Moreover, excitations ("particles") such as longitudinal plasmons exist which do not occur in vacuum. The presence of the plasma generally also changes the interaction vertices between particles, an effect which is of crucial importance for the plasmon decay, $\gamma_{\rm pl} \to \nu\bar{\nu}$. Finally, every particle simultaneously interacts with many targets. In the Compton process of axion production, for example, the initial photon scatters on many electrons simultaneously, and the total axion production rate arises from the interference of the scattering amplitudes off individual electrons. Since the motion of the electrons is correlated because of their interaction, the interference terms do not average to zero; the emission rates are modified by these correlation effects.

4.2. *Absorption rates*

Axion bounds which are derived on the basis of stellar energy losses are valid only if these particles freely stream out of stars, i.e., if their optical depth is less than ~1. A general expression for the absorption rate of axions, $\Gamma(E_a)$, is analogous to eq. (4.1), summed over all relevant processes. For relativistic particles the absorption rate is identical to the inverse mean free path, $\Gamma(E_a) = \lambda^{-1}(E_a)$. If the absorption rate is so large that axions are in thermal equilibrium with the surrounding heat bath, the principle of detailed balance tells us that

$$\Gamma(E_a) = (dQ_{\rm tot}/dE_a)(d\mathscr{E}_a/dE_a)^{-1}\,, \tag{4.2}$$

where

$$d\mathscr{E}_a/dE_a = (1/2\pi^2)E_a^3/(e^{E_a/T} - 1) \tag{4.3}$$

is the differential energy density of a thermal axion field at temperature T, and $Q_{\rm tot}$ is the volume emission rate, summed over all processes.

If axions are not in thermal equilibrium, the above expression is still a valid order-of-magnitude estimate so that a typical absorption rate is given by

$$\Gamma \sim Q_{\rm tot}/\mathscr{E}_a\,, \tag{4.4}$$

where $\mathscr{E}_a$ is the total energy density of a thermal population of axions. For massless scalars or pseudoscalars,

$$\mathscr{E}_a = (\pi^2/30)T^4\,, \tag{4.5}$$

while for photons an extra factor of 2 appears to count the polarization degrees of freedom. For massive (pseudo-)scalars with $m_a \gg T$, we find

$$\mathscr{E}_a = [T^{3/2} m_a^{5/2}/(2\pi)^{3/2}]\, e^{-m_a/T} . \tag{4.6}$$

If absorption is an important effect, axions contribute to the transfer of energy (chapter 5).

4.3. Many-body effects in stellar plasmas

4.3.1. General remarks on dispersion effects

The propagation of particles is governed by a wave equation which can be expressed in terms of plane-wave components, Ψ, as

$$G^{-1}(\omega, \boldsymbol{p})\Psi(\omega, \boldsymbol{p}) = 0 , \tag{4.7}$$

where ω and $\boldsymbol{p}$ are the frequency and wave vector of the plane wave, respectively, and G is the Green's function or propagator. For scalar or pseudoscalar particles the inverse vacuum propagator is simply the Klein–Gordon operator, $G^{-1}(\omega, \boldsymbol{p}) = \omega^2 - |\boldsymbol{p}|^2 - m^2$. For spin-$\frac{1}{2}$ fermions, Ψ is the relevant Dirac spinor and for photons it is the vector potential, A, so that G is a matrix. The wave equation (4.7) has nonvanishing solutions only if $\det(G^{-1}) = 0$, a condition which relates ω and $\boldsymbol{p}$: the dispersion relation. For isotropic media, it is usually written as*)

$$|\boldsymbol{p}| = n\omega , \tag{4.8}$$

where n is the refractive index. It may also be written as

$$\omega^2 = m_{\rm eff}^2 + |\boldsymbol{p}|^2 , \tag{4.9}$$

although the "effective mass", like the refractive index, is a function of ω and $\boldsymbol{p}$, and $m_{\rm eff}^2$ may even be negative. In vacuum, $m_{\rm eff} = m$, the particle rest mass, so that the vacuum refractive index is $n_{\rm vac} = (1 - m^2/\omega^2)^{1/2}$. The dispersion relation may have several branches, i.e., for a given wave number different frequencies may be allowed.

The procedure of second quantization is such that the energy associated with one quantum of an excitation is $E = \hbar\omega$ so that the thermal phase-space occupation is given by the usual Fermi–Dirac or Bose–Einstein formula. The corresponding wavenumber, $\boldsymbol{p}$, given by the dispersion relation, appears in the law of energy–momentum conservation, although this wavenumber, or "pseudomomentum", should not be confused with the physical momentum of the corresponding excitation.**) The dispersion relation for photons has been discussed, for example, in refs. [382–387], for charged fermions in ref.

*) Alternatively, one sometimes uses $\boldsymbol{p} = n\boldsymbol{p}_{\rm vac}$, a definition which renders the vacuum index equal to unity. Also, in nonisotropic media, n is then a matrix.

**) As a wave propagates through a medium, e.g., a laser beam in water, part of the momentum flow which enters at the surface is carried by the medium. There was a long-standing dispute about the momentum flow carried by the beam, a dispute which was resolved in a paper by Peierls [380] who clarified this question for the case of a classical electromagnetic wave, correcting various errors in the literature, including his own. Experimentally, the question was addressed by sending a powerful laser beam vertically through water and observing the water–air interface. The change in momentum carried by the beam appears as a force on the water surface, causing a visible deformation [381].

[388], and for neutrinos in refs. [389, 390]. The question of the effective nucleon mass in nuclear matter was addressed in refs. [391, 392], and the absence of a medium-induced refractive index for axions in section 2.3.3.

4.3.2. Dispersion relation for plasma modes

The propagation of electromagnetic fields in an isotropic medium is governed by a Green's function which can be written in Feynman gauge as [386]

$$G_{\mu\nu}(q) = -\frac{P_{\mu\nu}}{\varepsilon_{\mathrm{T}}(q)\omega^2 - |\boldsymbol{q}|^2} - \frac{Q_{\mu\nu}}{\varepsilon_{\mathrm{L}}(q)q^2}\,, \tag{4.10}$$

where $q=(\omega, \boldsymbol{q})$ is the energy momentum four-vector of the wave, ε_{T} and ε_{L} are the transverse and longitudinal dielectric permittivities, respectively, and the transverse and longitudinal projection operators are given by

$$P_{\mu\nu} = g_{\mu\nu} - q_\mu q_\nu/q^2 - Q_{\mu\nu}\,; \qquad Q_{\mu\nu} = -\frac{\lambda_\mu\lambda_\nu}{|\boldsymbol{q}|^2 q^2}\,, \quad \lambda = (|\boldsymbol{q}|^2, \omega\boldsymbol{q})\,. \tag{4.11}$$

Propagating modes are characterized by $\det(G^{-1})=0$ or equivalently by the poles of the Green's function. From eq. (4.10) it is clear that the dispersion relation for transverse modes in a plasma is given by $\varepsilon_{\mathrm{T}}(q)\omega^2 - |\boldsymbol{q}|^2 = 0$ and the refractive index for these modes is $n=[\varepsilon_{\mathrm{T}}(q)]^{1/2}$. For longitudinal modes it is given by $\varepsilon_{\mathrm{L}}(q)q^2=0$. These modes exist only in the presence of the plasma, they correspond to oscillations of the negative against the positive charges, and they are characterized by an electric field vector along the direction of propagation with no magnetic field. Transverse plasmons are essentially identical with photons whose dispersion relation is modified by the presence of the plasma.

In order to discuss the plasmon dispersion relation, we introduce a relativistic generalization of the usual plasma frequency [383]

$$\omega_0^2 \equiv 4\pi\alpha n_{\mathrm{e}}/E_{\mathrm{F}} = (4\alpha/3\pi)p_{\mathrm{F}}^3/E_{\mathrm{F}}\,, \tag{4.12}$$

which reduces, in the nonrelativistic limit with $E_{\mathrm{F}} \to m_{\mathrm{e}}$, to the usual result. The dispersion relation for transverse plasmons is given by

$$\omega^2 = \omega_0^2 + |\boldsymbol{q}|^2\,, \tag{4.13}$$

if the electrons are nondegenerate and nonrelativistic, and if the plasmon energy is small compared with the electron mass, $\omega \ll m_{\mathrm{e}}$. For a degenerate electron gas, the dispersion relation is [384, 387]

$$\omega^2 = \begin{cases} \omega_0^2 + (1+\frac{1}{5}v_{\mathrm{F}}^2)|\boldsymbol{q}|^2 & \text{for } |\boldsymbol{q}| \ll \omega_0\,, \\ (1+\frac{1}{5}v_{\mathrm{F}}^2)\omega_0^2 + |\boldsymbol{q}|^2 & \text{for } |\boldsymbol{q}| \gg \omega_0\,, \end{cases} \tag{4.14}$$

where $v_{\mathrm{F}} \equiv p_{\mathrm{F}}/E_{\mathrm{F}}$ is the velocity at the Fermi surface. Finally, if the plasma is relativistic and nondegenerate, i.e., if $T \gg m_{\mathrm{e}}$ and $T \gg E_{\mathrm{F}}$, electrons and positrons contribute equally, and the dispersion relation is [386],

$$\omega^2 = \begin{cases} \frac{4}{9}\pi\alpha T^2 + \frac{6}{5}|\boldsymbol{q}|^2 & \text{for } |\boldsymbol{q}| \ll eT/3\,, \\ \frac{4}{6}\pi\alpha T^2 + |\boldsymbol{q}|^2 & \text{for } |\boldsymbol{q}| \gg eT/3\,. \end{cases} \tag{4.15}$$

For $\omega > 2m_e$, these waves are damped by pair production, otherwise they are not damped at all to this order in α. Damping occurs only by scattering on electrons which introduces an imaginary part to the refractive index of higher order.

The dispersion relation of longitudinal plasmons is given, for a nondegenerate, nonrelativistic plasma by [387]

$$\omega^2 = \omega_0^2 + (3T/m_e)|\boldsymbol{q}|^2\,. \tag{4.16}$$

For these waves the phase velocity, $\omega/|\boldsymbol{q}|$, is less than the speed of light, whence electric charges can "surf" in longitudinal waves, leading to damping to lowest order in α (Landau damping). For $|\boldsymbol{q}| \gtrsim k_D$, this damping is large and longitudinal modes are no longer stable. For degenerate electrons, the dispersion relation is [387],

$$\omega^2 = \omega_0^2 + \tfrac{3}{5}v_F^2|\boldsymbol{q}|^2\,, \tag{4.17}$$

applicable for $v_F|\boldsymbol{q}| \ll \omega_0$. In the opposite limit, $v_F|\boldsymbol{q}| \gg \omega_0$, the spectrum of longitudinal oscillations reduces to two-particle excitations of an electron–hole [387]. For a relativistic, nondegenerate plasma, one has [386]

$$\omega^2 = \begin{cases} \frac{4}{9}\pi\alpha T^2 + \frac{3}{5}|\boldsymbol{q}|^2 & \text{for } |\boldsymbol{q}| \ll eT/3\,, \\ [1 + 4\exp(-6|\boldsymbol{q}|^2/4\pi\alpha T^2)]|\boldsymbol{q}|^2 & \text{for } |\boldsymbol{q}| \gg eT/3\,. \end{cases} \tag{4.18}$$

These oscillations are stable since the phase velocity, again, exceeds the speed of light.

In the presence of magnetic fields, the dispersion relations are, in general, much more complicated. For the axion problem, photon dispersion in the strong magnetic fields near pulsars is of some interest, and can be expressed in simple terms if $\omega \ll m_e$. In the presence of a magnetic field, B, which is transverse to the photon direction of propagation, we consider two linear polarization states with the electric field vector parallel ($\|$) and perpendicular ($\perp$) to the external magnetic field. The indices of refraction for these two modes are [393, 394]

$$n_\perp = 1 + \tfrac{8}{45}\alpha^2B^2/m_e^4\,, \qquad n_\| = 1 + \tfrac{14}{45}\alpha^2B^2/m_e^4\,, \tag{4.19}$$

where we have used a rationalized definition of the field strengths (see footnote in subsection 1.2.1). If the magnetic field is not transverse, only the transverse component enters, and the $\perp$ polarization state is the one with the electric field vector perpendicular to both, $\boldsymbol{k}$ and $\boldsymbol{B}$.

4.3.3. Nucleon dispersion in dense nuclear matter

In a dense nuclear medium, the effective nucleon mass, m_N^*, deviates substantially from the vacuum value, $m_N = 939$ MeV. At several times nuclear density, values which are believed to occur in the core of supernovae, the effective mass may be as low as $m_N^* = 0.5m_N$, strongly affecting the phase-space distribution of the nuclei. A calculation of m_N^* has to rely on an effective theory which describes the interaction of nucleons and mesons. Renormalizable, relativistic theories of this type ("quantum hadron

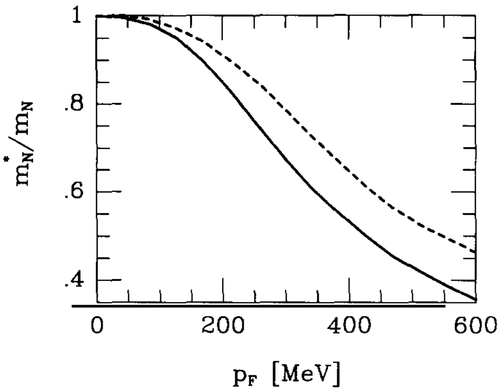

Fig. 4.1. Effective nucleon mass in an extended nuclear medium according to a relativistic Brueckner calculation including vacuum fluctuations [392]. The solid curve is for a nuclear medium with equal numbers of protons and neutrons, the dashed curve is for neutron matter. In both cases p_F is the Fermi momentum of the nucleons: $p_F = 280\,\mathrm{MeV}$ corresponds to nuclear density, and $p_F = 400\,\mathrm{MeV}$ to three times this density.

dynamics", QHD) have only recently been developed. A typical result [391, 392] for the nucleon effective mass from a self-consistent relativistic Brueckner calculation including vacuum fluctuations is shown in fig. 4.1. A relativistic Hartree calculation yields a similar result. The parameters chosen for this calculation yield nuclear saturation at a density which corresponds to a nucleon Fermi momentum of $p_F = 280\,\mathrm{MeV}$, and three times this density corresponds to $p_F = 400\,\mathrm{MeV}$, about the upper limit of what might be expected for a supernova core.

4.3.4. Screening of electric fields

In order to discuss the behavior of static electric fields in a plasma, we begin with the general electromagnetic propagator, eq. (4.10). In the static limit, $\omega = 0$, only the following components contribute,

$$G_{00}(0, \boldsymbol{q}) = -1/\varepsilon_L(0, \boldsymbol{q})|\boldsymbol{q}|^2\,, \qquad G_{ij}(0, \boldsymbol{q}) = (1/|\boldsymbol{q}|^2)(-\delta_{ij} + q_i q_j/|\boldsymbol{q}|^2)\,. \tag{4.20}$$

This means, in particular, that the radial variation of the electrostatic potential of a point charge is given by the Fourier transform of G_{00}. In a sufficiently dilute plasma, the static longitudinal permittivity is of the form

$$\varepsilon_L(0, \boldsymbol{q}) = 1 + k_S^2/|\boldsymbol{q}|^2\,. \tag{4.21}$$

Therefore $G_{00} = -(|\boldsymbol{q}|^2 + k_S^2)^{-1}$ and the electrostatic potential of a point charge varies as $r^{-1}\,\mathrm{e}^{-k_S r}$, rendering k_S a screening wave number and its inverse a screening radius.

In order to derive the screening scale for a neutral plasma we imagine that a point charge is added to the system. The field of this charge will be screened because the plasma will be polarized. We first consider a "one-component plasma" where one species of particles is thought to provide a homogeneous, neutralizing background and only the other species can move and contribute to the polarization. We first take the electrons as the particles which are allowed to move, take them to be degenerate, and use a Thomas–Fermi model in the potential of the extra charge. One finds $k_S = k_{TF}$ where the Thomas–Fermi wavenumber is [395],

$$k_{\mathrm{TF}} = (4\alpha p_{\mathrm{F}} E_{\mathrm{F}}/\pi)^{1/2} . \tag{4.22}$$

The Fermi momentum and Fermi energy are related to the electron density by

$$p_{\mathrm{F}} = (3\pi^2 n_{\mathrm{e}})^{1/3} , \qquad E_{\mathrm{F}} = (p_{\mathrm{F}}^2 + m_{\mathrm{e}}^2)^{1/2} . \tag{4.23}$$

With our relativistic definition of E_{F}, the nonrelativistic case is characterized by $E_{\mathrm{F}} \to m_{\mathrm{e}}$.

If the electrons are nondegenerate, one considers the "law of atmospheres" in the potential of the extra charge, taking a self-consistent, screened potential, i.e., one solves the Boltzmann–Poisson equation to lowest order. This leads to $k_{\mathrm{S}} = k_{\mathrm{D}}$ with the Debye–Hückel wavenumber [396],

$$k_{\mathrm{D}} = (4\pi\alpha n_{\mathrm{e}}/T)^{1/2} . \tag{4.24}$$

The plasma can be viewed as degenerate if $k_{\mathrm{TF}} \ll k_{\mathrm{D}}$ which translates, for the nonrelativistic case, into $(3\pi/2)T \ll p_{\mathrm{F}}^2/2m_{\mathrm{e}}$.

A realistic case of a one-component plasma is a medium where the electrons are degenerate while the nuclei are not as in a red giant core. We take first the hypothetical case of a degenerate hydrogen plasma. The screening scale of the electrons is given by k_{TF}, while that for the protons is given by k_{D}, and since $k_{\mathrm{D}} \gg k_{\mathrm{TF}}$ because of the assumed degeneracy, our test charge will be screened dominantly by the protons. This confirms the naive picture that a degenerate electron gas is much "stiffer" than the nondegenerate nuclei gas. Therefore the degenerate electrons, indeed, provide an approximately homogeneous background of a neutralizing charge distribution. If the nuclei have charge $Z > 1$, their screening length is given by eq. (4.24) with $n_{\mathrm{e}} \to Z^2 n_{\mathrm{nuc}}$. If there are several species of nuclei, the screening contribution of the ions is given by

$$k_{\mathrm{ions}} = \left(\frac{4\pi\alpha}{T} \sum_{\mathrm{ions}} Z_i^2 n_i \right)^{1/2} . \tag{4.25}$$

If the electrons are nondegenerate, the total screening wavenumber is given by

$$k_{\mathrm{S}} = (k_{\mathrm{D}}^2 + k_{\mathrm{ions}}^2)^{1/2} , \tag{4.26}$$

a result which applies for the conditions in the solar interior or in the center of horizontal branch stars.

4.3.5. General remarks on correlation effects

In order to appreciate the importance of correlation effects, we consider as an example the Compton production of a massless scalar particle, $\gamma e^- \to e^- \chi$. In vacuum, the differential cross-section is given by $\mathrm{d}\sigma/\mathrm{d}\Omega = |f(q)|^2$ where q is the energy–momentum transfer between γ and χ, and f is the scattering amplitude to be determined by the usual Feynman rules. For simplicity we consider the electron mass to be large compared to the photon energy, $m_{\mathrm{e}} \gg \omega$, whence the energy of the outgoing scalar is identical to that of the incoming photon, and we consider the electron to be at rest. Taking N electrons at fixed locations with relative separations $\boldsymbol{r}_{ij}$, the total scattering amplitude is the sum of that on the individual electrons. Hence the differential scattering cross-section of the ensemble is

$$\frac{\mathrm{d}\sigma_N}{\mathrm{d}\Omega} = |f(0, \boldsymbol{q})|^2 \sum_{i,j=1}^{N} \cos(\boldsymbol{q} \cdot \boldsymbol{r}_{ij}) . \tag{4.27}$$

In a stellar plasma we are interested in a physical situation where the photons interact with many different random ensembles of electrons, leading to a statistical average of this expression. Then all scattering centers are equivalent, and we may express the average scattering cross section on one electron as

$$\mathrm{d}\sigma/\mathrm{d}\Omega = |f(0, \boldsymbol{q})|^2 S(0, \boldsymbol{q}) ,$$

where $S(0, \boldsymbol{q})$ is the *static structure factor* for the electrons. The average scattering cross section on N electrons is now simply given by $\mathrm{d}\sigma_N/\mathrm{d}\Omega = N\,\mathrm{d}\sigma/\mathrm{d}\Omega$ because the structure factor accounts for the thermal average of the interference terms. Comparing with eq. (4.27) gives

$$S(0, \boldsymbol{q}) \equiv \lim_{N\to\infty} \left\langle N^{-1} \sum_{i,j=1}^{N} \cos(\boldsymbol{q}\cdot\boldsymbol{r}_{ij}) \right\rangle_{\text{thermal}} . \tag{4.28}$$

If the coordinates of the electrons were completely uncorrelated as in an ideal Boltzmann gas, the terms with $i \neq j$ would not contribute, and $S(0, \boldsymbol{q}) = 1$. Physically this means that the interference terms from scattering on different electrons vanish on average, and the total scattering rate is simply the sum of the individual rates.

In a real plasma, however, the mutual interaction between charged particles correlates their motion and locations; if an electron is known to be at position $\boldsymbol{r}$, the probability of finding another electron near the same location is less than average, while the probability of finding a proton is larger than average. Hence the static structure factor is a nontrivial function of the plasma properties. More generally, one must also allow for the motion and recoil effects of the targets so that the scattered particles need not have the same energy as the incoming ones, leading to the definition of a *dynamic structure factor*, $S(q)$. The complete particle emission rate from a stellar plasma requires inclusion of $S(q)$ in the integrand of eq. (4.1). In the context of axion emission where the nonrelativistic scattering amplitude depends on the electron spin coordinates, one also has to consider the spin–spin correlation between electrons.

4.3.6. *Static structure factors*

The screening of electric fields in a plasma is closely related to the correlation of the positions and motions of the charged particles. If an electron is known to be in a certain position, the probability of finding another electron in the immediate neighborhood is less than average, while the probability of finding a nucleus is larger than average. If we consider one particle of a given species to be the origin of a coordinate system, and if the average density of that species is n, the deviation of the actual density from average is

$$S(\boldsymbol{r}) = \delta^3(\boldsymbol{r}) + nh(\boldsymbol{r}) , \tag{4.29}$$

where h measures the correlation between these particles. In an ideal Boltzmann gas, of course, $h = 0$. The Fourier transform,

$$S(\boldsymbol{q}) = \int \mathrm{d}^3\boldsymbol{r}\, S(\boldsymbol{r})\, \mathrm{e}^{-\mathrm{i}\boldsymbol{q}\cdot\boldsymbol{r}} , \tag{4.30}$$

is the *static structure factor*. In the absence of correlations, $h = 0$, we naturally have $S(\boldsymbol{q}) = 1$, and the scattering cross sections remain unchanged. A typical example for the role of the structure factor is Thomson scattering of photons on electrons. If one measures the scattering of radio waves in ionized layers of the atmosphere, the correct cross section is $d\sigma_{\rm plas}(\boldsymbol{q})/d\Omega = S_e(\boldsymbol{q})\, d\sigma_{\rm vac}(\boldsymbol{q})/d\Omega$ where $\boldsymbol{q}$ is the momentum transfer [397]. Also, Thomson scattering on electrons in stellar plasmas is an important contribution to the opacities, and the inclusion of S_e substantially reduces the scattering rate, an effect which was recently revisited [398].

In order to illuminate the relationship between correlations and screening more clearly, we consider a one-component plasma where the mobile particles have charge e. In this case the static structure factor for the mobile particles is related to the longitudinal dielectric permittivity by virtue of the fluctuation dissipation theorem by [387, 399],

$$S(\boldsymbol{q}) = (|\boldsymbol{q}|^2/k_D^2)[1 - 1/\varepsilon_L(\boldsymbol{q})]\,, \tag{4.31}$$

where the Debye screening length was defined in eq. (4.24). For a sufficiently dilute plasma, we have $\varepsilon_L(\boldsymbol{q}) = 1 + k_D^2/|\boldsymbol{q}|^2$, corresponding to a Yukawa form of the screened potential. In this case one finds

$$S_D(\boldsymbol{q}) = |\boldsymbol{q}|^2/(|\boldsymbol{q}|^2 + k_D^2)\,. \tag{4.32}$$

Of course, if the mobile particles have charge Ze, one simply has to replace $n_e \to Z^2 n_{\rm nuc}$ in eq. (4.24).

If the plasma is sufficiently cold, the screening will not be of Yukawa type, and the structure factor will deviate from the simple Debye formula. The plasma can be considered cold if the average Coulomb interaction energy between ions is much larger than typical thermal energies. To quantify this measure, one introduces the ion-sphere radius, a, by virtue of $n = (4\pi a^3/3)^{-1}$ where n is the number density of the mobile particle species. Hence a measure for the Coulomb interaction energy is $Z^2\alpha/a$, assuming the ions have charge Ze. One usually introduces the parameter

$$\Gamma \equiv \alpha Z^2/aT\,, \tag{4.33}$$

as a measure for how strongly the plasma is coupled. For $\Gamma \ll 1$ it is weakly coupled and approaches an ideal Boltzmann gas. Since $k_D^2 a^2 = 3\Gamma$, the weak-coupling structure factor eq. (4.32) can be written as

$$S_D(\boldsymbol{q}) = |a\boldsymbol{q}|^2/(|a\boldsymbol{q}|^2 + 3\Gamma)\,. \tag{4.34}$$

This result applies even for large Γ if $|a\boldsymbol{q}| \ll 1$. For $\Gamma \gg 1$, the plasma is strongly coupled, and for $\Gamma \gtrsim 168$ the ions will arrange themselves in a body-centered cubic lattice [400, 401]. In fig. 4.2 we show S and S_D as functions of $|a\boldsymbol{q}|$ for $\Gamma = 2$, 10, and 100. The emerging periodicity for a strongly coupled plasma is quite apparent. It is also clear that for $\Gamma \lesssim 1$ the Debye formula gives a fair representation of the structure factor while for a strongly coupled plasma it is completely misleading. The interior of white dwarfs is typically in the regime of large Γ, and old white dwarfs are believed to crystallize.

In order to compute emission rates from nondegenerate objects like the Sun or other main sequence stars, we need to consider a two-component plasma where particles of positive and negative charges contribute to screening. The structure factor for a two-component plasma is quite different from the case of only one component. If the electrons are mobile on the background of a uniform positive charge distribution, their structure factor is given by eq. (4.24), assuming weak coupling of the plasma. If the ions are also mobile, it is given by [404]

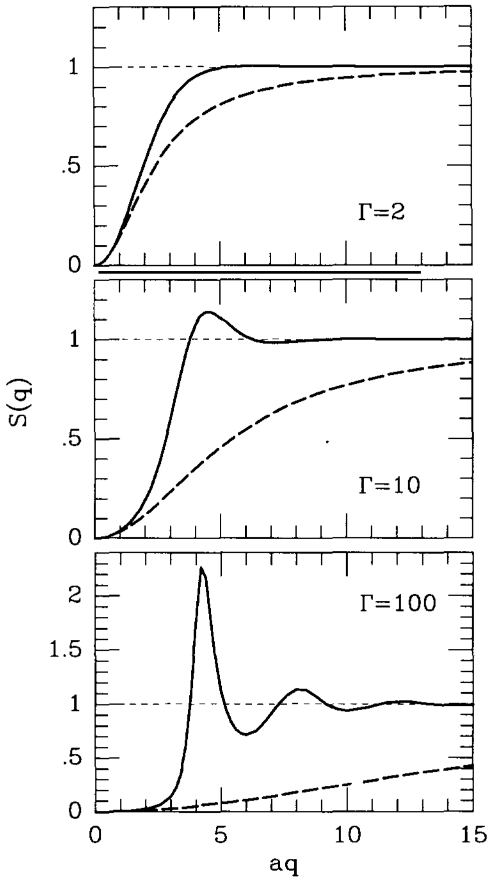

Fig. 4.2. Static structure factor for a one-component plasma according to numerical calculations [402, 403] (solid lines). The dashed lines correspond to the Debye structure factor eq. (4.34).

$$S_e(\boldsymbol{q}) = (|\boldsymbol{q}|^2 + k_{\rm ions}^2)/(|\boldsymbol{q}|^2 + k_{\rm ions}^2 + k_{\rm D}^2)\,, \tag{4.35}$$

where the ionic contribution was defined by eq. (4.25). This structure factor must be used, for example, if one wishes to calculate the emission of some weakly interacting scalar or vector particle, χ, which is produced in the Sun by the Compton process, $\gamma e^- \to e^- \chi$. If there is only one species of ions with charge Ze, the small-$\boldsymbol{q}$-value is $S_e(0) = Z/(1 + Z)$ whence the corrections are always relatively small. In a one-component plasma, $S_e(0) = 0$.

We now consider a scattering process for which the scattering amplitude is proportional to the electric charge of the target. An example is neutrino scattering by virtue of an anomalous magnetic dipole moment, $\nu_L + (A, Z) \to (A, Z) + \nu_R$, and also Primakoff production of axions, $\gamma + (A, Z) \to (A, Z) + a$, by virtue of the $a\gamma\gamma$ vertex. In this case one is not interested in the correlation between the positions of particles of a given species, rather one needs to consider the charge correlation. Given a charge Ze at the origin, the deviation from the average charge distribution is $ZeS(\boldsymbol{r})$ with $S(\boldsymbol{r}) = \delta^3(\boldsymbol{r}) + h(\boldsymbol{r})$ where now h is a function that integrates to -1 because of global charge neutrality of the plasma. With this definition of S, the static structure factor is found to be [87]

$$S(\boldsymbol{q}) = |\boldsymbol{q}|^2/(|\boldsymbol{q}|^2 + k_{\text{ions}}^2 + k_{\mathrm{D}}^2)\,, \tag{4.36}$$

where, of course, weak coupling of the plasma was assumed.

4.3.7. *State of the plasma in stellar interiors*

When calculating the axion emission rates one may consider, in principle, all possible combinations of temperatures and densities. In practice, only very specific conditions are encountered, leading to a much simpler discussion. Also, for any given set of conditions, typically only one process dominates so that one may focus on relatively few cases when embarking on a detailed calculation. In order to briefly discuss the plasma conditions relevant for astrophysical particle bounds it is convenient to introduce the usual chemical composition parameters, X, Y, X_{12}, etc., which characterize the mass fractions of the elements ^{1}H, ^{4}He, ^{12}C, etc. so that the number density of a species with mass fraction X_j, atomic weight A_j, and charge $Z_j e$ is given by

$$n_j = (\rho/m_{\mathrm{u}})X_j/A_j\,, \tag{4.37}$$

where $m_{\mathrm{u}} = 1.66 \times 10^{-24}$ g is the atomic mass unit and ρ is the mass density. The number density of electrons is given by

$$n_{\mathrm{e}} = \sum_j Z_j n_j = \frac{\rho}{m_{\mathrm{u}}} \sum_j \frac{X_j Z_j}{A_j}\,. \tag{4.38}$$

One sometimes uses the "mean molecular weight", μ_{e}, for the electrons, i.e., the atomic mass units of the plasma per electron, so that $n_{\mathrm{e}} = \rho/\mu_{\mathrm{e}} m_{\mathrm{u}}$. Also, $Y_{\mathrm{e}} = \mu_{\mathrm{e}}^{-1}$ is sometimes used for the mean number of electrons per baryon. In table 4.1 we give an overview over the plasma conditions that we are going to encounter when deriving astrophysical particle bounds.

Table 4.1
Plasma characteristics for typical conditions encountered in various astrophysical sites which are important to derive particle constraints

	Center of standard solar model	Core of HB stars	Red giant core just before helium flash	White dwarf	Supernova core
Characteristic	nondegenerate, nonrelativistic	nondegenerate, nonrelativistic	degenerate, weakly coupled	degenerate, strongly coupled	relativistic
Temperature	1.55×10^7 K = 1.3 keV	$\sim 10^8$ K = 8.6 keV	$\sim 10^8$ K = 8.6 keV	$(10^6\text{–}10^7)$ K = (0.09–0.86) keV	(20–60) MeV
Density [g cm^{-3}]	156	$\sim 10^4$	$\sim 10^6$	1.8×10^6 (center for $M = 0.66 M_\odot$)	$\sim 10^{15}$
Composition	$X = 0.35$	^{4}He, ^{12}C, ^{16}O ($\mu_{\mathrm{e}} = 2$)	^{4}He ($\mu_{\mathrm{e}} = 2$)	^{12}C, ^{16}O ($\mu_{\mathrm{e}} = 2$)	$Y_{\mathrm{e}} \sim 0.30$
Electron density [cm^{-3}]	6.3×10^{25}	3.0×10^{27}	3.0×10^{29}	5.3×10^{29}	1.8×10^{38}
Fermi momentum	24.3 keV	88 keV	409 keV	495 keV	345 MeV
Fermi energy $(p_{\mathrm{F}}^2 + m_{\mathrm{e}}^2)^{1/2} - m_{\mathrm{e}}$	0.58 keV	7.6 keV	144 keV	200 keV	344 MeV
Plasma coupling	$\Gamma = 0.07$	0.12	0.57	433–43.3	
Plasma frequency	0.3 keV	2.0 keV	18 keV	23 keV	19 MeV
Screening	Debye $k_{\mathrm{S}} = (k_{\mathrm{D}}^2 + k_{\text{ions}}^2)^{1/2}$ = 9.1 keV	Debye $k_{\mathrm{S}} = (k_{\mathrm{D}}^2 + k_{\text{ions}}^2)^{1/2}$ = 27 keV	Debye k_{ions} = 222 keV	strong	

4.4. Compton process

We begin our detailed investigation of the axion emission rates with Compton production, $\gamma e^- \to e^- a$, see fig. 4.3. This process was first considered by Sato and Sato for the emission of scalar Higgs particles from stars. The most general discussion of the matrix element and cross section was provided in refs. [61, 405]. A detailed discussion of the emission rates was provided in refs. [74, 86]. Electron spin correlation, which is important in a degenerate plasma, was never taken into account, and the effect of a finite plasmon mass has only been estimated.

For our discussion of the Compton effect we use the pseudoscalar interaction Lagrangian eq. (1.2) with a Yukawa coupling, g_a, for the electrons, and with the corresponding axionic fine structure constant, $\alpha_a = g_a^2/4\pi$. The invariant matrix element is found to be [74]

$$\sum_{\substack{\text{spins}\\ \text{polarizations}}} |\mathcal{M}|^2 = \frac{m_e^2 - u}{s - m_e^2} + \frac{s - m_e^2}{m_e^2 - u} - 2\,, \tag{4.39}$$

where the axion mass and the plasma frequency have been neglected, and the Mandelstam variables are $s = (p_e + k_\gamma)^2$ and $u = (p_e - k_a)^2$ with p_e the four-momentum of the initial-state electron, and k_γ and k_a the four-momenta of the photon and axion, respectively. The full expression with nonvanishing m_a and ω_0 was derived in ref. [61] – it is extremely complicated and not needed for our purposes. The total scattering cross-section for massless photons and axions is found to be

$$\sigma_C = \pi\alpha\alpha_a\left(\frac{\log(s/m_e^2)}{s - m_e^2} - \frac{3s - m_e^2}{2s^2}\right), \tag{4.40}$$

a result shown in fig. 4.4. For scalar or vector particle production, the cross section is not suppressed at low CM energies. This suppression is an effect of the derivative nature of the pseudoscalar coupling (section 2.3.3).

We are mostly interested in a nonrelativistic plasma where $p_e \sim (m_e, 0)$ and the photon energy

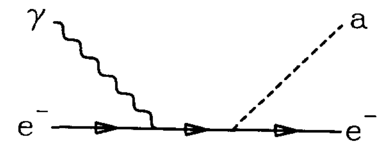

Fig. 4.3. Feynman graph for the Compton production of axions, or for the Compton absorption, if read in the reverse direction. The second graph with the axion and photon vertex interchanged is not shown.

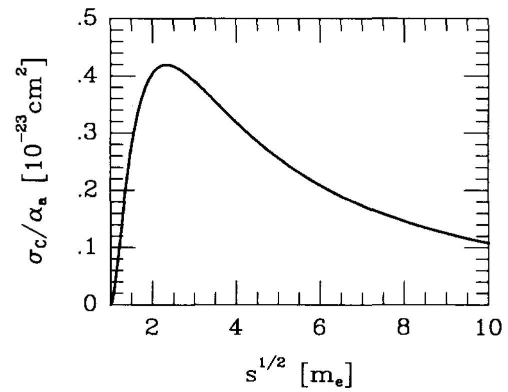

Fig. 4.4. Cross section for the Compton production of massless axions as a function of the CM energy, $s = (p_e + k_\gamma)^2$. The suppression at low energies arises from the derivative coupling of axions and would be absent for scalar (as opposed to pseudoscalar) particles.

$\omega \ll m_e$. In this case one readily finds [87]

$$\sigma_C = \tfrac{4}{3}\pi(\alpha\alpha_a/m_e^2)\omega^2/m_e^2 . \tag{4.41}$$

In this limit, the energy of the outgoing axion is identical with that of the incoming photon, and the energy loss rate is simply found by folding σ_C with the electron density, n_e, and the black-body photon flux at temperature T,

$$\mathrm{d}n/\mathrm{d}\omega = (1/\pi^2)\omega^2/(e^{\omega/T} - 1) . \tag{4.42}$$

In the non-degenerate limit, the lowest-order relativistic correction was analytically calculated by Fukugita, Watamura and Yoshimura [74], yielding a volume energy loss rate

$$Q_C = \frac{160\zeta(6)\alpha\alpha_a}{\pi}\,\frac{n_e T^6}{m_e^4}\left(1 - \frac{36\zeta(7) - 14\zeta(6)}{\zeta(6)}\,\frac{T}{m_e} + O(T^2/m_e^2)\right) , \tag{4.43}$$

where ζ is the Riemann zeta function. Fukugita et al. have numerically calculated correction factors to the lowest-order result, taking into account relativistic and degeneracy effects. It is worth noting that the effect of degeneracy is to *enhance* the emission rate: for a fixed temperature and increasing density, the emission rate increases slightly *faster* than the trivial n_e factor of eq. (4.43). This occurs because with increasing degeneracy, electrons occupy states of larger momentum, increasing the CM scattering cross-section which is suppressed for low energies (fig. 4.3). This increased cross-section slightly overcomes the effect of Pauli blocking of final states.

Fukugita et al.'s [74] correction factors, however, do not take into account the finite value of the plasmon frequency, which should be a small correction for $\omega_0 \lesssim T$, but is important in the cores of red giant stars. They also ignore the correlation between the electron targets. From our discussion in section 4.1.3 we conclude that, if axions were scalar (as opposed to pseudoscalar) particles, one would have to include the structure factor S_e, similar to the case of Thomson scattering. Axions, however, couple to the electron spin and the structure of the scattering amplitude implies that its sign depends on the spin of the initial electron. If we consider scattering from an ensemble, the interference between the amplitudes of two given electrons will be destructive or constructive, depending on the relative spin orientation of the electrons. Therefore, in an ensemble with no correlation between the spins, the interference terms average to zero. Therefore we believe that for the Compton production of *pseudoscalars* from a nondegenerate plasma, the structure factor S_e, which expresses the correlation between locations but not spins, should not appear and the result eq. (4.43) remains valid. For degenerate electrons, the spins are correlated; the Pauli exclusion principle states that it is less likely than average to find an electron with the same spin near a given electron that one of opposite spin. Hence for degenerate electrons, a spin correlation factor should appear in eq. (4.43).

Compton production is important for axion emission from the Sun and from horizontal branch stars, environments which are essentially nondegenerate, allowing one to use eq. (4.43). In horizontal branch stars with $T \sim 10^8\,\mathrm{K} = 8.6\,\mathrm{keV}$, the relativistic correction in eq. (4.43) is a reduction by ~40%. An important axion constraint, however, was derived using red giants before the helium flash [63, 93] where axion emission occurs from a degenerate plasma. While in this context the spin correlation of electrons and the finite value of the plasma frequency are of crucial importance, the Compton effect is less important than bremsstrahlung in this environment so that there is no need for a precise Compton rate.

Compton emission from a very degenerate and relativistic plasma was also considered in the context of axion emission from SN 1987A in ref. [75], correcting previous results in ref. [70]. A crude estimate yields

$$Q_C \sim (2\alpha\alpha_a/3\pi)T^5 \ln(2E_F T/m_e^2)\,. \tag{4.44}$$

Numerical details were given in ref. [75], but for these conditions nucleon bremsstrahlung by far dominates so that a detailed knowledge of the Compton rates is not warranted.

The emission of pseudoscalars with a large mass, $m_a \gg T$, from a nondegenerate, nonrelativistic plasma is of some interest. The axion energy is then very close to threshold, $E_a \sim m_a$, and one may consider the Compton production of nonrelativistic axions from electrons at rest, yielding [161]

$$Q_C = (2^{5/2}\alpha\alpha_a/\pi)n_e(m_a^{9/2}T^{3/2}/m_e^4)\,e^{-m_a/T} \tag{4.45}$$

to lowest order.

4.5. Electron–positron annihilation

The process $e^+e^- \to \gamma a$ (fig. 4.5) is never of practical importance because positrons are only present in sufficient numbers at high temperatures, conditions for which other processes such as nucleon bremsstrahlung become more important. For completeness we quote the result for the emission rate, valid for nondegenerate, nonrelativistic conditions where $T \ll m_e$ [74, 86],

$$Q_{ann} = (\alpha\alpha_a/\pi^2)m_e^2T^3\,e^{-2m_e/T}\,. \tag{4.46}$$

This result does not depend on the electron density because the electron and positron distributions are characterized by equal but opposite chemical potentials which cancel each other. For very relativistic and degenerate conditions as are encountered in supernova explosions, we have estimated the rate to be

$$Q_{ann} \sim (\alpha\alpha_a/6\pi^3)E_F^3T^2\,e^{-E_F/T}\ln(9E_F T/2m_e^2)\,. \tag{4.47}$$

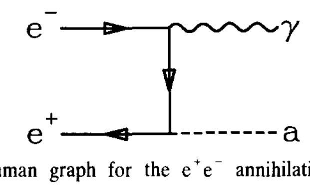

Fig. 4.5. Feynman graph for the e^+e^- annihilation process. The second graph with the axion and photon vertex interchanged is not shown.

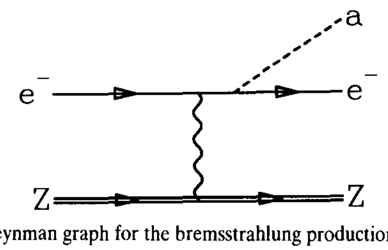

Fig. 4.6. Feynman graph for the bremsstrahlung production of axions, or for the absorption by inverse bremsstrahlung, if read in the reverse direction. The double line represents either a nucleus of charge Ze, or another electron. The outgoing axion may also be attached to the incoming electron line, and if the double line represents an electron, also to the incoming and outgoing double line. Thus there are two Feynman amplitudes for the electron–nucleus process, and eight amplitudes for the e^-e^- process, because the axion can be attached to four different fermion "legs", and each such graph has an exchange graph with the outgoing (or incoming) electron labels interchanged.

4.6. Bremsstrahlung by electrons

4.6.1. Nondegenerate plasma

In stellar interiors, three-body processes frequently are more important than two-body reactions. If one replaces the photon in the Compton process, fig. 4.3, by a virtual photon, i.e., if this photon is replaced by the Coulomb field of a charged particle, one arrives at the corresponding three-body process: bremsstrahlung emission, fig. 4.6. Simply put, this process competes with the Compton reaction because there are more charged particles in a stellar plasma than free photons. In the solar center, for example, the electron density is $n_e = 6 \times 10^{25}\ \mathrm{cm}^{-3}$, while the density of black-body photons at a temperature $T = 1.3$ keV is $n_\gamma = 2\zeta(3)T^3/\pi^2 = 6 \times 10^{22}\ \mathrm{cm}^{-3}$. More rigorously speaking, the electron which radiates an axion must interact with the ambient electromagnetic field in order to conserve energy and momentum. Compton emission corresponds to the interaction with the transverse modes of the electromagnetic field, while bremsstrahlung corresponds to the interaction with the longitudinal modes. The relative importance of these processes depends on the relative power in transverse and longitudinal electromagnetic field fluctuations.

The process $e^-(A, Z) \rightarrow (A, Z)\, e^- a$ was first discussed by Krauss, Moody and Wilczek [79], while Raffelt [87] included the process $e^-e^- \rightarrow e^-e^- a$ and corrected a minor algebraic error of the previous calculation. The bremsstrahlung of *photons* by electrons, $e^-e^- \rightarrow e^-e^-\gamma$ is suppressed to lowest order because two particles of equal mass as they move under the influence of their Coulomb interaction do not produce a time-varying electric dipole moment; this reaction is suppressed because of the E1 structure of the photon emission. Axion radiation, on the contrary, compares to M1 transitions because of its "spin-flip" nature so that the e^-e^- process is not suppressed relative to the e^-p process. Moreover, the relevant nuclei in stars are of low charge so that the coherent Z^2 enhancement is of little importance, allowing the e^-e^- process to compete.

The calculation of the emission rate in a nondegenerate, nonrelativistic plasma is straightforward. In order to estimate the importance of screening, the Coulomb propagator, $|\boldsymbol{q}|^{-2}$, is replaced by $(|\boldsymbol{q}|^2 + \kappa^2)^{-1}$ where κ is a screening scale, approximately given by the Debye scale. A rigorous treatment of screening has not been performed; it would involve specifying the appropriate ion structure factor for the combined system of electrons and nuclei in a situation where this structure is probed by an electron. Our previous discussion of these structure factors does not rigorously apply because of the identity of the probing electrons with the electrons of the plasma. For all situations of practical interest, screening turns out to be a relatively minor correction. To lowest order in κ, the volume emissivity ($\mathrm{erg\, cm^{-3}\, s^{-1}}$) was found to be [87]

$$Q_{\mathrm{brems}} = \tfrac{128}{45}(2/\pi)^{1/2}(\alpha^2\alpha_a/m_e)(T/m_e)^{5/2} n_e \sum_j n_j \left[Z_j^2\left(1 - \frac{5}{4}\frac{\kappa^2}{m_e T}\right) + \frac{Z_j}{2^{1/2}}\left(1 - \frac{5}{2}\frac{\kappa^2}{m_e T}\right)\right], \quad (4.48)$$

where the sum is extended over all nuclear species. The quadratic term in Z_j corresponds to electron–nucleon bremsstrahlung, while the linear term represents the e^-e^- process (note that the electron density is given by $n_e = \Sigma_j Z_j n_j$). For later comparison it is also instructive to derive the specific emissivity, $\varepsilon = Q/\rho$, if there is only one species of nuclei with charge Z and atomic weight A, neglecting the effect of screening and the contribution of the electron targets,

$$\varepsilon_{\mathrm{ND}} = \frac{128}{135\pi^2}\left(\frac{2}{\pi}\right)^{1/2} \frac{Z^2\alpha^2\alpha_a}{Am_u} \frac{T^{5/2}p_E^3}{m_e^{7/2}}, \quad (4.49)$$

where we have expressed the electron density in terms of the Fermi momentum, $n_e = p_F^3/3\pi^2$, and the atomic mass unit is $m_u = 1.661 \times 10^{-24}$ g.

4.6.2. Degenerate plasma

Bremsstrahlung is a particularly important effect in white dwarfs and the cores of red giants before the helium flash, i.e., under conditions of degeneracy. In this case we neglect completely the e^-e^- process which is more strongly suppressed by degeneracy than the electron–nucleus process. For the latter we take the target nuclei to be static and heavy. Then one finds for the volume emissivity [93]

$$Q_D = \frac{4\alpha^2\alpha_a}{\pi^2} \sum_j Z_j^2 n_j \int_{m_e}^{\infty} dE_1\, f(T, E_1) \int_{m_e}^{E_1} dE_2\, [1 - f(T, E_2)]$$

$$\times \int \frac{d\Omega_2}{4\pi} \int \frac{d\Omega_a}{4\pi} \frac{|\boldsymbol{p}_1||\boldsymbol{p}_2|E_a^2}{|\boldsymbol{q}|^4} \left(2E_a^2 \frac{p_1p_2 - m_e^2 + p_a(p_2 - p_1)}{(p_1p_a)(p_2p_a)} + 2 - \frac{p_1p_a}{p_2p_a} - \frac{p_2p_a}{p_1p_a} \right), \tag{4.50}$$

where the index 1 refers to the incoming, 2 to the outgoing electron, $f(T, E)$ is the electron phase space distribution, $f = (e^{(E-E_F)/T} + 1)^{-1}$ for the degenerate case, $\boldsymbol{q} \equiv \boldsymbol{p}_1 - \boldsymbol{p}_2 - \boldsymbol{p}_a$ is the momentum transfer to the nucleus, and the axion energy is $E_a = E_1 - E_2$. If the electrons are very degenerate, the energy integrals can be done analytically. Moreover, all electron momenta are close to the Fermi surface, $|\boldsymbol{p}_1| \sim |\boldsymbol{p}_2| \sim p_F$. Using the notation $\beta_F \equiv p_F/E_F$ and c_{12} for the cosine of the angle between $\boldsymbol{p}_1$ and $\boldsymbol{p}_2$, etc., and considering only one nuclear species, one finds for the specific emissivity, $\varepsilon_D = Q_D/\rho$ [84, 85, 88, 93],

$$\varepsilon_D = \frac{\pi^2}{15} \frac{Z^2\alpha^2\alpha_a}{A} \frac{T^4}{m_e^2 m_u} F, \tag{4.51}$$

$$F = \frac{m_e^2}{m_e^2 + p_F^2} \int \frac{d\Omega_2}{4\pi} \int \frac{d\Omega_a}{4\pi} \frac{2(1 - c_{12}) - (c_{1a} - c_{2a})^2}{(1 - \beta_F c_{1a})(1 - \beta_F c_{2a})} \frac{4p_F^4}{|\boldsymbol{q}|^4}. \tag{4.52}$$

In a degenerate plasma, the electric fields of the nuclei are screened because of the polarizability of the degenerate electron gas. Hence the Coulomb propagator, $|\boldsymbol{q}|^{-2}$, must be replaced by $(|\boldsymbol{q}|^2 + k_{TF}^2)^{-1}$, appropriate for an exponentially screened electric field with the Thomas–Fermi screening scale, $k_{TF} = (4\alpha p_F E_F/\pi)^{1/2}$. Moreover, the scattering amplitudes from different nuclei interfere, and one must include the static ion structure factor, $S_{ions}(\boldsymbol{q})$, leading to

$$1/|\boldsymbol{q}|^4 \rightarrow S_{ions}(\boldsymbol{q})/(|\boldsymbol{q}|^2 + k_{TF}^2)^2. \tag{4.53}$$

The correction factor, F, must be separately determined for various conditions.

We begin with a nonrelativistic, weakly coupled plasma as appropriate for the cores of red giant stars before the helium flash. In this case the structure factor is given by the Debye formula, eq. (4.32). To simplify further we note that the forward divergence of the Coulomb denominator is mostly cut off by the ion correlation effect because the Debye screening scale, $k_{ions}^2 = 4\pi Z^2\alpha n_{nuc}/T$, far exceeds k_{TF}^2 so that we may neglect k_{TF} entirely. Also, the momentum transfer can be approximated by $|\boldsymbol{q}|^2 \sim |\boldsymbol{p}_1 - \boldsymbol{p}_2|^2 \sim 2p_F^2(1 - c_{12})$. Finally we consider a nonrelativistic approximation where we may use $\beta_F = 0$

in eq. (4.52), leading to [93]

$$F = [m_e^2/(m_e^2 + p_F^2)]^{\frac{2}{3}} \ln[(8p_F^2 + k_{\rm ions}^2)/k_{\rm ions}^2] \,. \tag{4.54}$$

An exact calculation would only slightly change the argument of the logarithm. For a helium plasma with $\rho = 10^6\,{\rm g\,cm^{-3}}$ and $T = 10^8$ K, we find $p_F = 409$ keV and $k_{\rm ions} = 222$ keV so that $F = 1.4$.

It is instructive to compare the degenerate result with that for nondegenerate conditions, eq. (4.49),

$$\frac{\varepsilon_D}{\varepsilon_{ND}} = \frac{9\pi^4}{128}\left(\frac{\pi}{2}\right)^{1/2}\left(\frac{Tm_e}{p_F^2}\right)^{3/2} F = \left(\frac{4.19\,Tm_e}{p_F^2}\right)^{3/2} F \,. \tag{4.55}$$

For the plasma conditions of a red giant core, $\rho = 10^6\,{\rm g\,cm^{-3}}$ and $T = 10^8$ K, this ratio is 0.05, revealing that the nondegenerate rates would overestimate the true emission rate by a factor of ~20.

For a strongly coupled, degenerate plasma typical for white dwarfs the factor F was calculated numerically by Nakagawa et al. [84, 85] for a ^{12}C plasma. For densities in the range $(10^4$–$10^6)\,{\rm g\,cm^{-3}}$ and temperatures of $(10^6$–$10^7)$ K, it is found that $F = 1.0$ within ~20% so that for practical calculations this value is a satisfactory approximation.

Iwamoto [77] considered the emission from the crust of a neutron star where the electrons are very relativistic. According to Nakagawa et al. [84], Iwamoto's analytic result is slightly in error. In contrast with the nonrelativistic conditions of white dwarfs, ion correlations are now an important effect, suppressing Iwamoto's result by 1–2 orders of magnitude. In refs. [84, 85], numerical results for F in neutron star matter were given for a wide range of densities.

4.7. Axio-recombination and the axio-electric effect

Another possible source for stellar axions arises from free–bound transitions where a bare nucleus captures an electron to form an ion with a K-shell electron: "axio-recombination" [66]. In the Sun, this process contributes about 4% of the total axion flux which is mostly due to bremsstrahlung. The energy loss rate is $\propto T^{3/2}$, while bremsstrahlung is $\propto T^{5/2}$, and the Compton effect is $\propto T^6$. In other words, axio-recombination is of importance mostly in low-mass stars which have much lower internal temperatures than the Sun; it would dominate in main sequence stars with $M \lesssim 0.2M_\odot$ [66]. Because stars with such low masses live much longer than the age of the universe, all such stars presently observed are far from the end of their main-sequence evolution. Therefore, even if axion emission was to be important in these objects, no *observable* effect has been proposed in the literature that would allow one to identify these axion losses or to derive interesting bounds.

Of more practical interest is the inverse process where an axion incident on an atom unbinds an electron; the "axio-electric effect" [67, 68]. Because of the M1 nature of the axion coupling to nonrelativistic electrons, the axio-electric cross section is obtained from the photo-electric one by multiplication with the usual spin-flip factor, apart from a reduced coupling strength,

$$\sigma_{\rm axio} = (\alpha_a/\alpha)(|\boldsymbol{p}_a|/2m_e)^2\sigma_{\rm photo} \,. \tag{4.56}$$

Thus one can obtain this cross section by a simple scaling of tabulated values. This effect serves to constrain the solar axion flux which could produce keV electrons in a Ge spectrometer designed to search for double-β decay (section 7.2).

4.8. Bremsstrahlung by nucleons

4.8.1. The matrix element

The axion coupling to nucleons allows for processes similar to those involving electrons, an example being the proton Compton process, $\gamma p \to pa$. Generically, the Yukawa coupling to a fermion is given by $g_a = m/f_a$, apart from a factor of order unity, so that axions couple about 2000 times stronger to protons than to electrons. However, the Compton cross section is proportional to g_a^2/m^4 so that it varies with the fermion mass as m^{-2}, and the proton Compton effect is still much weaker than the electron effect in the nonrelativistic regime. This is not necessarily the case in supernovae with temperatures as high as 50 MeV where the electron Compton cross section is on the "right side" of the maximum in fig. 4.4 while the proton cross section is on the "left side". However, under such conditions the bremsstrahlung emission of axions by nucleons is more efficient than two-body reactions involving photons.

Bremsstrahlung emission by nucleons (fig. 4.7), $NN \to NNa$, was first calculated by Iwamoto [77] on the basis of Friman and Maxwell's [18] results for the corresponding bremsstrahlung process emitting neutrino pairs. It is interesting to note that for nonrelativistic nucleons only the axial coupling of the neutrino current to the nucleon current contributes so that the relevant Lagrangian has the Dirac structure $\bar{N}\gamma_5\gamma_\mu N J^\mu_{\text{neutrino}}$. The derivative form of the axion coupling has the structure $\bar{N}\gamma_5\gamma_\mu N\partial^\mu a$ so that the nuclear matrix elements for both processes are the same, while the emission rate is different because of the different final-state phase space. We stress that the derivative structure of the axion interaction is the more fundamental form (section 2.3.3) so that the results of Pantziris and Kang [86], based on a naive application of the pseudoscalar coupling, are incorrect. Another problem relates to the use of the one-pion exchange approximation to model the nuclear forces, a method which was the major advance of the work of Friman and Maxwell over previous calculations of the neutrino emission rates. As discussed in section 2.3.3, the one-pion exchange approximation accounts well for the cross section of the related process, $NN \to NN\pi^0$, which has been experimentally studied so that we trust it gives a good estimate of the emission rates.

The matrix element for the $nn \to nna$ process was first calculated by Iwamoto [77] assuming degenerate nucleons, while Brinkmann and Turner [57] provided a detailed discussion of all processes and degeneracy conditions. Taking the nucleons to be nonrelativistic, the squared matrix element is always of the form*)

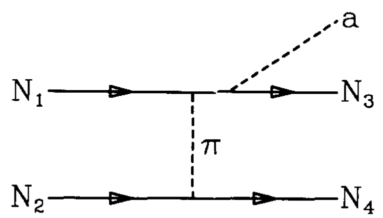

Fig. 4.7. Feynman graph for the nucleon bremsstrahlung production of axions, or for the absorption by inverse bremsstrahlung, if read in the reverse direction. The outgoing axion may also be attached to any of the other nucleon lines. Thus there are eight Feynman amplitudes because of the exchange of the outgoing (or incoming) nucleon labels. The exchange graphs of the np process involve intermediate *charged* pions.

*) In the axion literature, the pion–nucleon coupling was generally expressed in terms of f/m_π with $f \sim 1$ so that even in expressions where the pion mass had been neglected in intermediate states, it appeared explicitly in the final result. Moreover, the dependence of the emission rates on the value of the effective nucleon mass was obscured. Therefore we prefer to express the coupling in terms of the "pion fine-structure constant", $\alpha_\pi \sim 15$, which is related to f by $(f/m_\pi)^2 = 4\pi\alpha_\pi/(2m_N)^2$.

$$\sum_{\text{spins}} |\mathcal{M}|^2 = \frac{16(4\pi)^3}{3} \frac{\alpha_\pi^2 \alpha_a}{m_N^2} \left(\frac{|\boldsymbol{k}|^4}{(|\boldsymbol{k}|^2 + m_\pi^2)^2} + \text{similar terms} \right), \tag{4.57}$$

where $\alpha_\pi \sim 15$ is the "pion–nucleon fine-structure constant", and $\boldsymbol{k}$ is the momentum transfer carried by the intermediate pion. The expression in brackets is generally very complicated, in particular for the np process where various interference terms between direct and exchange graphs appear. (An expression for the complete matrix element was given in the appendix of ref. [98].) Moreover, in a dense nuclear medium correlation and polarization effects further complicate this expression [71]. Therefore we begin our discussion by taking the expression in brackets to be a constant (3 for the degenerate nn or pp process), and lump all other effects into a set of unknown "form factors", F_j.

4.8.2. Degenerate and nondegenerate emission rates

In order to express the emission rates in a compact form, it is convenient to define a number of "fine-structure constants" in terms of the Yukawa couplings, g_{an} and g_{ap}, to neutrons and protons, respectively,

$$\begin{aligned} &\alpha_n \equiv g_{an}^2/4\pi\,, \qquad \alpha_p \equiv g_{ap}^2/4\pi\,, \\ &\alpha_1 \equiv (g_{an} + g_{ap})^2/16\pi\,, \qquad \alpha_2 \equiv (g_{an}^2 + g_{ap}^2)/8\pi\,. \end{aligned} \tag{4.58}$$

For equal couplings, $g_a \equiv g_{an} = g_{ap}$, all of these terms are the same and equal to $\alpha_a \equiv g_a^2/4\pi$. The volume emissivity for degenerate nucleons is [57, 77]

$$Q_D = \frac{31\pi^2}{945} \frac{\alpha_\pi^2}{m_N^2} T^6 \left[\alpha_n p_n F_n + \alpha_p p_p F_p + (\tfrac{8}{3}\alpha_1 F_1 + \tfrac{20}{3}\alpha_2 F_2) \left(\frac{p_n^2 + p_p^2}{2} \right)^{1/2} \left(1 - \frac{|p_n^2 - p_p^2|}{2(p_n^2 + p_p^2)} \right) \right], \tag{4.59}$$

where p_n and p_p are the Fermi momenta of the nucleons. If the matrix element is taken to be a constant, $F_n = F_p = F_1 = F_2 = 1$, while in general these factors depend on the Fermi momenta. If in addition $g_a \equiv g_{an} = g_{ap}$ and $p_F \equiv p_n = p_p$, the term in square brackets is $34\alpha_a p_F/3 = 11.33\alpha_a p_F$. For nondegenerate and nonrelativistic conditions one finds the corresponding result [57]

$$Q_{ND} = \frac{128}{315\pi^{9/2}} \frac{\alpha_\pi^2}{m_N^2} \frac{T^{7/2}}{m_N^{5/2}} [\alpha_n p_n^6 F_n + \alpha_p p_p^6 F_p + (\tfrac{8}{3}\alpha_1 F_1 + \tfrac{20}{3}\alpha_2 F_2) p_n^3 p_p^3]\,. \tag{4.60}$$

Taking equal Fermi momenta and couplings, and taking all $F_j = 1$, the ratio between the degenerate and nondegenerate emission rates is

$$\xi \equiv Q_D/Q_{ND} = \tfrac{31}{384}\pi^{13/2}(m_N T/p_F^2)^{5/2}\,. \tag{4.61}$$

The "crossover temperature" between degenerate and nondegenerate conditions, defined as the temperature at which $\xi = 1$, is

$$T_{\text{cross}} = 0.140 p_F^2/m_N\,. \tag{4.62}$$

Taking the vacuum nucleon mass, $m_N = 939$ MeV, and a typical Fermi momentum for a supernova core, $p_F = 380$ MeV, this is $T_{cross} = 22$ MeV [57, 58]. This result would indicate that generally the nondegenerate rates were more appropriate [57]. However, in all of the emission rates one should use the *effective nucleon mass*, m_N^*, rather than the vacuum value. A typical value relevant for supernova conditions is $m_N^* = 0.5 m_N$ (fig. 4.1). Hence the borderline between the emission rates is shifted to much larger temperatures so that in a supernova core with $T = (20\text{–}60)$ MeV neither asymptotic expression for the emission rate is a good approximation. Hence, in a numerical investigation of a supernova collapse including axion emission, one should use the analytic approximations of Brinkmann and Turner [57] which are valid for all degrees of degeneracy (see below), in conjunction with an appropriate value for the effective nucleon mass (see section 4.8.4 below). Of course, in order to discuss the cooling of old neutron stars by axion emission, the degenerate emission rates are a good approximation.

4.8.3. Analytic approximation for the intermediate regime

Brinkmann and Turner [57] have provided a convenient analytic approximation for the emission rates,

$$Q = (256\pi^3\alpha_\pi^2 T^{13/2}/m_N^{*3/2})[\alpha_n F_n I(y_n, y_n) + \alpha_p F_p I(y_p, y_p) + (\tfrac{8}{3}\alpha_1 F_1 + \tfrac{20}{3}\alpha_2 F_2) I(y_n, y_p)]\,. \tag{4.63}$$

The integral expression $I(y_i, y_j)$ is analytically approximated

$$I_{fit}(y_i, y_j) = \left[2.39\times10^5\left(e^{-y_i-y_j} + \frac{e^{-y_i}+e^{-y_j}}{4}\right) + \frac{1.73\times10^4}{y_*^{1/2}} + \frac{6.92\times10^4}{y_*^{3/2}} + \frac{1.73\times10^4}{y_*^{5/2}}\right]^{-1}, \tag{4.64}$$

where $y_* \equiv 1 + \frac{1}{2}|y_i + y_j|$. The quantities y_i ($i =$ n or p) are defined to be μ_i/T where μ_i is the nonrelativistic chemical potential; for extreme degeneracy, $\mu = E_F - m_N \sim p_F^2/2m_N$. The Fermi momentum, number density, and chemical potential for a given species are related by

$$n = p_F^3/3\pi^2 = (2^{1/2}/\pi)(m_N T)^{3/2} g(y)\,, \tag{4.65}$$

$$g(y) \equiv \int_0^\infty du\, \frac{u^{1/2}}{e^{u-y}+1} = \begin{cases} \frac{1}{2}\pi^{1/2} e^y & \text{for } y \ll -1 \text{ (nondegenerate)}\,, \\ \frac{2}{3} y^{3/2} & \text{for } y \gg +1 \text{ (degenerate)}\,. \end{cases} \tag{4.66}$$

For intermediate values, a good fit is provided by the Taylor expansion

$$g_{fit}(y) = 0.678 + 0.536y + 0.1685y^2 + 0.0175y^3 - 3.24\times10^{-3}y^4\,, \tag{4.67}$$

which is good to better than 1% for $-1 < y < 5$.

4.8.4. The factors F_j and many-body effects

The main uncertainty in all of these expressions is the actual value of the factors F_j which are complicated functions of the nucleon Fermi momenta and such parameters as the pion mass. If one models the nucleon–nucleon interaction by a one-pion exchange potential, and if one neglects the pion mass, $m_\pi = 0$, explicit results for various degrees of degeneracy are given in table 4.2 according to ref.

Table 4.2
Form factors F_j according to ref. [57] if the pion mass is neglected, $m_\pi = 0$, for varying degrees of degeneracy, characterized by β as defined in the text

	General expression	Degenerate ($\beta = 0$)	Nondegenerate ($\beta = 1.0845$)
F_n, F_p	$1 - \frac{1}{3}\beta$	1	0.639
F_1	$1 - \frac{2}{3}\beta$	1	0.277
F_2	$1 - \frac{2}{15}\beta$	1	0.855

[57]. The remaining parameter is $\beta \equiv 3\langle(\hat{\boldsymbol{k}} \cdot \hat{\boldsymbol{l}})^2\rangle$ where $\boldsymbol{k}$ and $\boldsymbol{l}$ are the momentum transfers in the direct and exchange graphs, respectively, and the average is with regard to the directions of the axion emission. For degenerate conditions and a nonvanishing pion mass some of the form factors were evaluated by Ishizuka and Yoshimura [76], yielding exceedingly complicated results.

More importantly, many-body effects have not been rigorously taken into account although undoubtedly they would change the matrix element. The most detailed discussion of this issue was performed by Ericson and Mathiot [71] who claimed that correlation and polarization effects would reduce the emission rates by an additional factor of about 1/2. These authors also claimed that ρ exchange would lead to a further reduction by a factor of about 1/6. However, this effect would also appear in nucleon–nucleon bremsstrahlung emission of pions in laboratory experiments for which the one-pion approximation was found to be a good approximation [98, 62] if a pseudovector pion interaction is used (section 2.3.3), and we shall ignore this factor.

We now collect the following effects that reduce the F_j factors from their initially assumed unit values. Nondegeneracy reduces them by a few tens of percent. (F_1 is reduced much more, see table 4.2. However, it has a much smaller overall coefficient than the dominant F_2 term, and may be even less important because of destructive interference between the neutron and proton coupling. Hence the precise treatment of this term will never make much of a difference.) The effect of a finite pion mass also reduces F_j by a similar amount so that, taken together, a reduction by $\sim 1/2$ seems realistic. Correlation effects probably reduce the rates by a further factor of $\sim 1/2$. This effect, however, may not yet be fully understood, and it may be prudent to allow also for the possibility of an enhancement by a similar amount. Hence it appears realistic to adopt

$$F_j = (1/2)^{1\pm 1} \tag{4.68}$$

as a choice for F_j, including a crude estimate of the uncertainty, a choice to be used in the intermediate regime between degeneracy and nondegeneracy relevant for supernova cores.

Next, the effective coupling constants also change. However, Turner et al. argue [98], on the basis of the nonlinear sigma model, that the combination of parameters, $\alpha_\pi^2 \alpha_a / m_N^2$, should remain approximately constant at high densities. Mayle et al. [81] similarly find that, at three times nuclear density,

$$(\alpha_\pi^2 \alpha_a / m_N^2)^* (\alpha_\pi^2 \alpha_a / m_N^2)^{-1} \sim 0.3\text{–}1.5\,. \tag{4.69}$$

Therefore it appears realistic to multiply the emission rates with a further factor $0.7 \times (1/2)^{\pm 1}$ to account for this effect.

If $\alpha_\pi^2 \alpha_a / m_N^2$ stays approximately constant at varying density, the changes caused by using the effective nucleon mass are best understood by considering the quantity $m_N^2 Q(m_N, p_F, T)$ for "nuclear

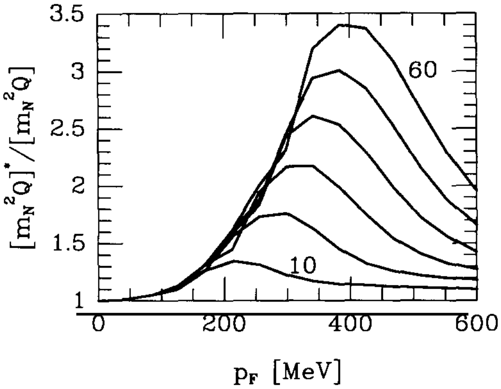

Fig. 4.8. Change of the axion emission rate when using the effective nucleon mass, assuming that $\alpha_\pi^2\alpha_a/m_N^2$ remains constant, taking equal numbers of protons and neutrons with identical Fermi momentum, p_F, and equal axion couplings to n and p. We used the effective nucleon mass given by the solid line in fig. 4.1, and the Brinkmann–Turner rates, eq. (4.63), with unit form factors. The curves are for $T = (10–60)$ MeV in steps of 10 MeV.

matter", i.e., for equal numbers of protons and neutrons, and with equal axion couplings. We have calculated this quantity on the basis of the Brinkmann–Turner expression eq. (4.63) with unit form factors, using the effective nucleon mass, $m_N^*(p_F)$, corresponding to the solid line in fig. 4.1, and have divided it by the same quantity, taken with the vacuum nucleon mass. This ratio, $[m_N^2 Q(m_N, p_F, T)]^*/[m_N^2 Q(m_N, p_F, T)]$, is shown in fig. 4.8 as a function of p_F for several temperatures. For large p_F, this ratio is unity because for the degenerate rates $m_N^2\, Q$ is independent of the nucleon mass. For very low p_F, it is unity because the effective and vacuum nucleon masses approach each other. In the intermediate regime, relevant for SN cores, the emission rate *increases* by as much as a factor of ~3 if one uses the effective nucleon mass.

In summary, the emission rates of the previous section, taking $F_j = 1$, must be multiplied by an overall factor

$$f_{\text{corr}} \sim 0.3 \times (1/2)^{\pm 2} \tag{4.70}$$

to account for the finite value of the pion mass, correlation effects, and the density variation of the coupling constants. Moreover, the effective nucleon mass must be used in all expressions except in the term $\alpha_\pi^2\alpha_a/m_N^2$ which should be kept fixed.

4.9. Primakoff effect and axion–photon mixing

4.9.1. Primakoff effect versus Compton scattering

If a pseudoscalar particle couples to electrons with a Yukawa coupling, g_{ae}, it necessarily also couples to photons by virtue of a triangle-loop amplitude analogous to that shown in fig. 2.2. So long as all the energies of the external particles (axion and photons) are far below the electron mass, the loop can be integrated [328] to give an effective Lagrangian for the coupling of axions to photons of the form eq. (1.1) with $g_{a\gamma} = -\alpha g_{ae}/\pi m_e$. Of course, if the axion couples to other charged leptons or to quarks, this expression will change, and even destructive interference between different amplitudes is possible, a fact which constitutes the major uncertainty of axion bounds based on the photon coupling. For now we assume that the electron coupling is the only axion interaction.

We may now consider the production of axions in the electromagnetic field of a charged particle (fig.

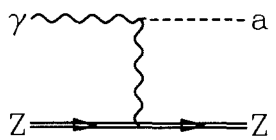

Fig. 4.9. Feynman graph for the Primakoff effect where a photon transforms into an axion in the electromagnetic field of a nucleus with charge Ze.

4.9), a process usually called the "Primakoff effect" after the analogous reaction involving neutral pions which was originally used to measure the pion–photon interaction strength. One readily finds for the differential cross-section on a particle with charge Ze and "infinite" mass,

$$\mathrm{d}\sigma_{\mathrm{P}}/\mathrm{d}\Omega = (g_{\mathrm{a}\gamma}^2 Z^2 \alpha/8\pi)|\boldsymbol{k}\times\boldsymbol{p}|^2/|\boldsymbol{k}-\boldsymbol{p}|^4\,, \tag{4.71}$$

where $\boldsymbol{k}$ is the initial-state photon momentum, and $\boldsymbol{p}$ is the final-state axion momentum. Taking massless axions, assuming that the photon coupling arises solely from an electron triangle loop, and taking a singly charged target, $Z=1$, this is

$$\mathrm{d}\sigma_{\mathrm{P}}/\mathrm{d}\Omega = (\alpha^3\alpha_{\mathrm{ae}}/8\pi^2 m_{\mathrm{e}}^2)(1+\cos\vartheta)/(1-\cos\vartheta)\,, \tag{4.72}$$

where ϑ is the scattering angle, and $\alpha_{\mathrm{ae}} = g_{\mathrm{ae}}^2/4\pi$. In order to understand why one would want to consider this higher-order process, we quote the corresponding low-energy Compton scattering cross section (fig. 4.3),

$$\mathrm{d}\sigma_{\mathrm{C}}/\mathrm{d}\Omega = (\alpha\alpha_{\mathrm{ae}}/4m_{\mathrm{e}}^2)(\omega/m_{\mathrm{e}})^2(1-\cos\vartheta)^2\,, \tag{4.73}$$

where ω is the photon (or axion) energy. If the target for both reactions consists of electrons, there is, in principle, an interference term. However, because the Compton effect involves a spin flip of the electron, while the Primakoff effect does not, the low-energy amplitudes do not interfere. The Compton effect, because of its spin-flip nature, is suppressed by a $(\omega/m_{\mathrm{e}})^2$ factor, while the Primakoff effect, being of higher order, is suppressed by α^2. In the solar interior, typical energies are of the order $\omega \sim T = 1.3\,\mathrm{keV}$ so that $\omega/m_{\mathrm{e}} \sim 1/400$, somewhat smaller than $\alpha = 1/137$ so that one may reasonably expect that the Primakoff effect, in spite of being higher-order, is of great importance for axion emission in stars.

However, apart from axion models where the direct coupling to electrons vanishes (and the coupling to photons is due to the axion–pion mixing), the Primakoff effect turns out to be negligible compared to the Compton effect if one properly takes account of the correlation effects in the presence of a stellar plasma which strongly modify the vacuum cross section. This must be expected because the total vacuum Primakoff cross-section diverges logarithmically, and this Coulomb logarithm is cut off, in a plasma, by screening effects. For massive axions or pions, even the vacuum Primakoff cross-section is finite because the particle mass provides a cutoff as one can easily derive from the general expression eq. (4.71). However, for invisible axions with masses much smaller than the temperatures in a typical stellar plasma, the screening or correlation effects are the dominant effect to moderate the Coulomb divergence.

4.9.2. Primakoff emission rate

The Primakoff effect as an axion emission process in stellar plasmas was first considered by Dicus et al. [64] for the case of standard axions where the dominant cutoff of the Coulomb divergence is provided by the axion mass of ~100 keV. A subsequent calculation by Fukugita et al. [74] for invisible axions incorrectly used the "plasma mass" of the photons as the dominant cutoff. Later, Raffelt [87] gave a correct derivation, using the appropriate ion structure factor, and subsequently gave a second derivation, considering the fluctuating $\boldsymbol{B}\cdot\boldsymbol{E}$ term in the plasma as a random source for the axion field [91]. Later, the Primakoff effect was calculated again by Pantziris and Kang [86], producing the previous incorrect result with the plasma frequency as a cutoff. Similarly, Chanda, Nieves and Pal [61], apparently not being aware of the previous work, calculated the emission rate on the basis of a sophisticated but erroneous analysis, again finding the plasma frequency as the relevant cutoff scale. The correct cutoff scale, of course, is the Debye screening length. This is physically obvious because it is the finite reach of the Coulomb field of a given charge in a plasma which cuts off far-field effects.

Formally, the Primakoff cross section on a target Ze in a plasma is found by including the structure factor, eq. (4.36), so that $(\mathrm{d}\sigma_\mathrm{P}/\mathrm{d}\Omega)_\mathrm{plasma} = (\mathrm{d}\sigma_\mathrm{P}/\mathrm{d}\Omega)_\mathrm{vacuum} S(\boldsymbol{k}-\boldsymbol{p})$, leading to

$$(\mathrm{d}\sigma_\mathrm{P}/\mathrm{d}\Omega)_\mathrm{plasma} = (g_{a\gamma}^2 Z^2\alpha/8\pi)|\boldsymbol{k}\times\boldsymbol{p}|^2/|\boldsymbol{k}-\boldsymbol{p}|^2(|\boldsymbol{k}-\boldsymbol{p}|^2+\kappa^2)\,, \tag{4.74}$$

an expression which does not diverge in the forward direction. The screening scale is

$$\kappa^2 \equiv k_\mathrm{ions}^2 + k_\mathrm{D}^2 = \frac{4\pi\alpha}{T}\sum_{\substack{\text{ions}\\\text{electrons}}} Z_j^2 n_j\,. \tag{4.75}$$

The differential transition rate is found by summing over all targets so that

$$\frac{\mathrm{d}\Gamma_\mathrm{P}}{\mathrm{d}\Omega} = \sum_{\substack{\text{ions}\\\text{electrons}}} n_j\left(\frac{\mathrm{d}\sigma_\mathrm{P}}{\mathrm{d}\Omega}\right)_\mathrm{plasma} = \frac{g_{a\gamma}^2 T\kappa^2}{32\pi^2}\,\frac{|\boldsymbol{k}\times\boldsymbol{p}|^2}{|\boldsymbol{k}-\boldsymbol{p}|^2(|\boldsymbol{k}-\boldsymbol{p}|^2+\kappa^2)}\,. \tag{4.76}$$

Therefore the ratio of the differential transition rate with screening over that without screening is simply $|\boldsymbol{k}-\boldsymbol{p}|^2/(|\boldsymbol{k}-\boldsymbol{p}|^2+\kappa^2)$. Taking the solar interior as an example, a typical momentum transfer is characterized by the temperature, $T = 1.3$ keV, while $\kappa \sim 9$ keV, leading to a substantial suppression of the emission rate. Without screening, the total rate diverges logarithmically, while our expression can be integrated to yield the transition rate of a photon of energy ω into axions,

$$\Gamma_\mathrm{P}(\omega) = (g_{a\gamma}^2 T\kappa^2/32\pi)[(1+\kappa^2/4\omega^2)\ln(1+4\omega^2/\kappa^2)-1]\,. \tag{4.77}$$

This expression was averaged over photon polarizations so that the axion absorption rate in the same medium is twice as large. In the limit of small frequencies, $\omega \ll \kappa$, the transition rate expands as $\Gamma_\mathrm{P} = g_{a\gamma}^2\omega^2 T/16\pi$, completely independently of κ and the density. However, while $T \ll \kappa$ in the Sun or red giants, the major contribution of the emission rate comes from a region of the photon black-body spectrum where $\kappa \sim \omega$ and we may not use this approximation.

The actual emission rate is obtained by folding $\Gamma_\mathrm{P}(\omega)$ with the black-body photon spectrum. Assuming that the plasma frequency can be neglected, $\omega_0 \ll T$, one finds for the volume emissivity [87]

$$Q_\mathrm{P} = (g_{a\gamma}^2/4\pi^2)T^7\xi^2 f(\xi^2)\,,\quad \xi \equiv \kappa/2T\,, \tag{4.78}$$

$$f(\xi^2) = \frac{1}{2\pi}\int_0^\infty \mathrm{d}x\,[(x^2+\xi^2)\ln(1+x^2/\xi^2)-x^2]\,\frac{x}{e^x-1}\,. \tag{4.79}$$

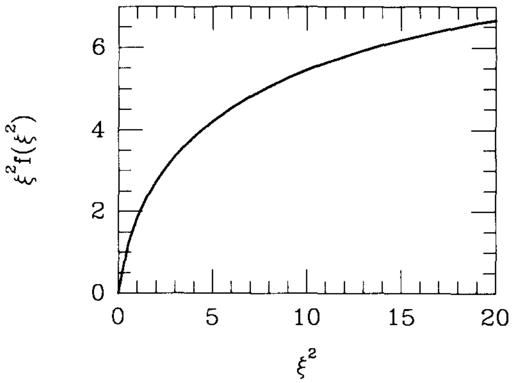

Fig. 4.10. Function $\xi^2 f(\xi^2)$ as defined in eq. (4.79).

We show $\xi^2 f(\xi^2)$ in fig. 4.10. In the entire Sun, $\xi^2 = 12$ with a variation of at most ~15%. For a pure helium red giant with $\rho = 10^4\ \mathrm{g\,cm^{-3}}$ and $T = 10^8$ K it is $\xi^2 = 2.5$. For a degenerate configuration with arbitrary plasma frequency, the emission rate was calculated in ref. [89] where a tabulated form for the relevant parameter range was given. In fig. 8.6 we show $\varepsilon_P = Q_P/\rho$ at $T = 10^8$ K as a function of density.

4.9.3. *Primakoff effect versus plasmon decay*

There has been considerable confusion in the literature about the possibility of a plasmon decay process [74, 82, 86], $\gamma_{pl} \to a\gamma$. In ref. [91] it was pointed out that one must carefully specify the nature of the participating excitations, i.e., whether they are transverse plasmons, γ_t, or longitudinal ones, γ_ℓ. In a nonrelativistic, nondegenerate plasma, transverse plasmons propagate like massive particles with a mass equivalent to the plasma frequency, ω_0, so that energy–momentum conservation prohibits such processes as $\gamma_t \to a\gamma_t$, $2\gamma_t \to a$, or $a \to 2\gamma_t$. However, the plasmon decay and plasmon coalescence processes, $\gamma_t \to a\gamma_\ell$ and $\gamma_t\gamma_\ell \to a$, are permitted because of the peculiar form of the longitudinal dispersion relation.

We recall, however, that longitudinal plasmons are the result of coherent fluctuations of the electric charge density. If $\omega_0 \ll T$, these modes are highly occupied and can be viewed as classical electric field configurations so that the process $\gamma_t \to a$ with γ_ℓ in the initial or final state can be viewed as a transition $\gamma_t \xrightarrow{E} a$ where E represents a classical electric field configuration. In other words, the electric field of a longitudinal plasmon is but a specific superposition of the Coulomb fields of the charged particles in the plasma. Hence these plasma processes are to be viewed as the Primakoff effect on a specific subset of all possible charge configurations in the plasma. In the static limit, all electric field fluctuations are contained in the static structure factor, $S(\boldsymbol{q})$, which we used to derive the Primakoff emission rate which thus already includes the plasma decay and coalescence process. This was discussed in detail in ref. [91] where the Primakoff emission rate was rederived by considering the fluctuating, classical $\boldsymbol{E}\cdot\boldsymbol{B}$ term in the plasma as a source for the axion field.

4.9.4. *Axio-electrodynamics and axion–photon mixing*

This discussion of the Primakoff effect and plasma processes indicates that one can get substantial insight into the question of axion–photon transitions by considering the classical field equations for the combined system of electromagnetism and axions ("axio-electrodynamics"). The Lagrangian density is

$$\mathscr{L}_{\gamma,a} = -\tfrac{1}{4}F_{\mu\nu}F^{\mu\nu} + \tfrac{1}{2}(\partial_\mu a \partial^\mu a - m_a^2 a^2) - \tfrac{1}{4}g_{a\gamma}F_{\mu\nu}\tilde{F}^{\mu\nu}a\,, \tag{4.80}$$

leading to the vacuum equations of motion [370, 406]

$$\begin{aligned} &\nabla\cdot \boldsymbol{E} = -g_{a\gamma}\boldsymbol{B}\cdot\nabla a\,, \qquad \nabla\times\boldsymbol{E} = -\partial_t \boldsymbol{B}\,, \qquad \nabla\cdot\boldsymbol{B} = 0\,, \\ &\nabla\times\boldsymbol{B} = \partial_t\boldsymbol{E} + g_{a\gamma}(\boldsymbol{B}\partial_t a + \nabla a\times\boldsymbol{E})\,, \qquad (-\partial_t^2 + \nabla^2)a = m_a^2 a + g_{a\gamma}\boldsymbol{E}\cdot\boldsymbol{B}\,. \end{aligned} \tag{4.81}$$

Thus the time-varying, random $\boldsymbol{E}\cdot\boldsymbol{B}$ term in a plasma is a source for the axion field. Also, a laser beam propagating in an external static magnetic field is an axion source [407–413], axions propagating in external fields are a photon source [83, 370, 414], and photons interacting with static axion field configurations experience a nontrivial refractive effect [415, 416].

It is interesting that the transitions between axions and photons in an external field can be viewed as a mixing phenomenon. While this applies to all such transitions including the galactic axion search experiments (section 3.5) where one considers transitions between plane wave axion states and the electromagnetic excitations of a microwave cavity, the mixing formalism is particularly illuminating for transitions between plane wave states as, for example, in the propagation of a laser beam or solar axions in an external magnetic field. Raffelt and Stodolsky [411] have derived a linearized wave equation for the propagation of a plane wave in the z-direction with a frequency ω in the presence of a transverse magnetic field, B,

$$\left[\omega + \frac{1}{2}\begin{pmatrix} 4\xi\omega & 0 & 0 \\ 0 & 7\xi\omega & g_{a\gamma}B \\ 0 & g_{a\gamma}B & -m_a^2/\omega \end{pmatrix} - \mathrm{i}\partial_z\right]\begin{pmatrix} A_\perp \\ A_\parallel \\ a \end{pmatrix} = 0\,, \tag{4.82}$$

where $A_\perp$ represents the electromagnetic vector potential for the photon component with an electric field vector perpendicular to the direction of propagation and the external B field, $A_\parallel$ represents the orthogonal polarization state, and a is the axion component. The linearized equation is valid if all entries in the mixing matrix are $\ll\omega$. The photon birefringence in external fields was derived from the Euler–Heisenberg Lagrangian, not contained in eq. (4.80), and leads to the refractive indices eq. (4.19), i.e., $\xi = (4\alpha^2/45)(B^2/m_e^4)$. Equation (4.82) allows one to discuss axion–photon transitions entirely along the lines of neutrino-mixing phenomena. In particular, if the magnetic field is as strong as those believed to exist near pulsars, the photon terms in the mixing matrix exceed the axion term and axion–photon transitions are strongly suppressed (section 10.7).

In a medium, the photon entries must be replaced by $4\xi\omega \to 2\omega(n_\perp - 1)$ and $7\xi\omega \to 2\omega(n_\parallel - 1)$, representing the total refractive indices. If photon refraction is dominated by the plasma mass, ω_0, as for X-rays in a low-Z gas such as hydrogen or helium, the mixing equation is

$$\left[\omega + \frac{1}{2\omega}\begin{pmatrix} -\omega_0^2 & g_{a\gamma}B\omega \\ g_{a\gamma}B\omega & -m_a^2 \end{pmatrix} - \mathrm{i}\partial_z\right]\begin{pmatrix} A_\parallel \\ a \end{pmatrix} = 0\,. \tag{4.83}$$

One can choose the plasma frequency by adjusting the gas pressure such that $\omega_0 = m_a$, allowing for strongly enhanced transition rates in a solar axion detector [414]. Also, if the gas density varies in space or time so that an adiabatic crossover between the axion mass and the plasma frequency occurs, one may expect resonant transitions in the spirit of the MSW effect [411–413].

4.10. Plasmon decay rate

We will discuss astrophysical bounds on neutrino magnetic and electric dipole and transition moments in some detail. These moments μ_{ij} and ε_{ij}, respectively, couple neutrinos directly to the electromagnetic field by means of the effective Lagrangian eq. (1.3). This interaction allows for the radiative decay, $\nu_i \rightarrow \nu_j \gamma$, if $m_j < m_i$ with a rate [417]

$$\Gamma(\nu_i \rightarrow \nu_j \gamma) = (1/8\pi)(|\mu_{ij}|^2 + |\varepsilon_{ij}|^2) m_i^3 [1 - (m_j/m_i)^2]^3 . \tag{4.84}$$

More importantly for our purposes, it allows for the "photon decay", $\gamma_{\mathrm{pl}} \rightarrow \bar{\nu}_i \nu_j$ (fig. 4.11), if the photon dispersion relation in the ambient medium is such that this decay is kinematically allowed. We will only use stars where the plasma is nonrelativistic and either nondegenerate (HB stars) or degenerate (core of red giants before the helium flash, white dwarfs) so that the relevant dispersion relations are given by eqs. (4.14)–(4.17). We will only consider the decay of transverse plasmons because the contribution of longitudinal excitations is typically smaller, and at most of the same order as that of transverse excitations [11]. Hence, neglecting longitudinal plasmons will render our bounds slightly more conservative without introducing a large error. For transverse plasmons we will always use the dispersion relation

$$\omega^2 = \omega_0^2 + |\boldsymbol{q}|^2 \tag{4.85}$$

with the plasma frequency eq. (4.12). This relation is a fair approximation to eqs. (4.13) and (4.14) if we note that in white dwarfs and red giant cores $v_{\mathrm{F}}/5 \sim 0.13$ where we have used the data given in table 4.1. With this simplification we can treat transverse plasmons kinematically like particles of mass ω_0, allowing for a simple analytic result for the plasmon decay rate [130, 132]

$$\Gamma(\gamma_{\mathrm{pl}} \rightarrow \bar{\nu}\nu) = (\mu_\nu^2/24\pi)\omega_0^3 , \tag{4.86}$$

$$\mu_\nu^2 \equiv \sum_{i,j=1}^{3} (|\mu_{ij}|^2 + |\varepsilon_{ij}|^2) , \tag{4.87}$$

assuming that all neutrinos are sufficiently light. If neutrinos are Majorana particles, this summation double-counts final states and a factor 1/2 must appear on the rhs. Also, for Majorana neutrinos, the diagonal components vanish identically, $\mu_{ii} = \varepsilon_{ii} = 0$.

The resulting energy loss rate because of plasmon decay is

$$Q_\mu = (\mu_\nu^2/24\pi)\omega_0^4 N_\gamma , \tag{4.88}$$

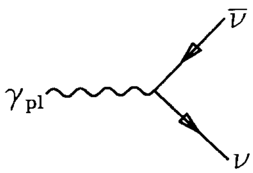

Fig. 4.11. Feynman graph for plasmon decay into a neutrino pair.

where

$$N_\gamma = \frac{1}{\pi^2} \int_{\omega_0}^{\infty} \frac{\omega(\omega^2 - \omega_0^2)^{1/2}}{e^{\omega/T} - 1} \, d\omega \tag{4.89}$$

is the number density of thermal photons, or rather of transverse plasmons.

Even in the absence of anomalous dipole moments neutrinos couple to photons in the presence of a plasma because of an amplitude involving real electrons in the intermediate state. The energy loss rate from the decay of transverse plasmons is found to be [11]

$$Q_{\text{standard}} = F_\nu (G_F^2/48\pi^2\alpha)\omega_0^6 N_\gamma \,. \tag{4.90}$$

The overall factor is

$$F_\nu = \tfrac{1}{4}[(1 + 4\sin^2\Theta_w)^2 + n(1 - 4\sin^2\Theta_w)^2]\,, \tag{4.91}$$

where n is the number of neutrino families other than ν_e which are light enough to be emitted. For ν_e the rate is so large (the first term above) because charged and neutral currents contribute. If the weak mixing angle were exactly $\sin^2\Theta_w = 1/4$, only $\bar\nu_e\nu_e$ pairs would be emitted and $F_\nu = 1$. Taking $\sin^2\Theta_w = 0.23$ and $n = 2$ we find $F_\nu = 0.925$.

The ratio between the rates is

$$Q_\mu / Q_{\text{standard}} = 0.30\mu_{12}^2 F_\nu^{-1}(10\,\text{keV}/\omega_0)^2\,, \tag{4.92}$$

where $\mu_{12} = \mu_\nu/10^{-12}\mu_B$ with the Bohr magneton, $\mu_B = e/2m_e$. Hence, in a red giant, these rates are about equal for $\mu_\nu \sim 2\times 10^{-12}\mu_B$.

For completeness we also give the total electromagnetic scattering cross section of ultrarelativistic neutrinos, $\nu_i + (Ze) \to (Ze) + \nu_j$ on a particle with charge Ze which is found to be [418, 419]

$$\sigma_{ij} = |\mu_{ij} \mp \varepsilon_{ij}|^2 Z^2\alpha[\ln(t_{\max}/t_{\min}) - (s - m_{\text{target}}^2)/s]\,, \tag{4.93}$$

where s and t are the usual Mandelstam variables. The minus sign applies if the initial-state neutrino was left-handed (implying that the final-state is right-handed), and the plus sign in the opposite case [420]. If neutrinos are Dirac particles, and if the CP-symmetry is conserved, there is no relative phase between μ_{ij} and ε_{ij}, allowing for destructive interference in some experiments [420]. If neutrinos are Dirac particles, the flipped states are noninteracting with respect to weak interactions, allowing one to use the SN 1987A cooling argument (section 10.3).

5. Energy transfer

If axions or other particles interact so strongly that they cannot freely stream out of stars, they contribute to the radiative transfer of energy. We review the general expression for the radiative opacity of massive bosons, and give explicit expressions focussing on the Compton scattering process for axions.

5.1. Radiative transfer by massive bosons

Following closely refs. [160, 161] we begin this discussion by deriving a general expression for the radiative transfer by massive bosons. For a sufficiently short mean free path, l, of these particles in the stellar medium, the radiation field can be taken to be approximately isotropic locally. The local energy flux density is then given by $F_\omega = -(\beta_\omega/3) l_\omega \nabla\varepsilon_\omega$, where the index ω indicates that this equation refers to specific quantities; the total flux is obtained by integrating over energies. The velocity is $\beta_\omega = [1-(m_a/\omega)^2]^{1/2}$. As before, we use natural units with $\hbar = c = k_B = 1$. Writing the mean free path at frequency ω as $l_\omega = (\kappa_\omega \rho)^{-1}$ (mass density ρ) defines the opacity, κ_ω, usually expressed in units of $cm^2\,g^{-1}$. In local thermal equilibrium the specific energy density for massive bosons is

$$\varepsilon_\omega = g_{spin}\,\omega^2(\omega^2 - m_a^2)^{1/2}/2\pi^2(e^{\omega/T}-1)\,, \tag{5.1}$$

where g_{spin} is the number of polarization degrees of freedom. The total energy flux carried by our particles is found by integrating over all frequencies,

$$F = -\frac{\nabla T}{3\rho}\int_{m_a}^{\infty} d\omega\,\frac{\beta_\omega \varepsilon'_\omega}{\kappa_\omega}\,, \tag{5.2}$$

where we have used $\nabla\varepsilon_\omega = (\partial\varepsilon_\omega/\partial T)\nabla T \equiv \varepsilon'_\omega \nabla T$. For photons, one usually writes $F = -\nabla a T^4/3\kappa_\gamma\rho$ where aT^4 is the total energy density in photons ($a = \pi^2/15$). This equation defines the Rosseland mean opacity, κ_γ. For other bosons we define a corresponding quantity,

$$\kappa_a \equiv 4aT^3\left(\int_{m_a}^{\infty} d\omega\,\frac{\beta_\omega\varepsilon'_\omega}{\kappa_\omega}\right)^{-1}. \tag{5.3}$$

In the stellar evolution equations one must substitute

$$\kappa_\gamma \to (\kappa_\gamma^{-1} + \kappa_a^{-1})^{-1}\,, \tag{5.4}$$

in order to obtain the total magnitude of radiative transfer. In the large-mass limit, $m_a \gg T$, one finds to lowest order,

$$\kappa_a = \frac{4\pi^4}{15}\left(\frac{T}{m_a}\right)^3 e^{m_a/T}\left(\int_0^{\infty} dy\,\frac{y\,e^{-y}}{\kappa_\omega(y)}\right)^{-1}, \tag{5.5}$$

where we have used $y \equiv \beta_\omega^2 m_a/2T$ so that the energy of nonrelativistic bosons is given by $\omega = m_a + yT$.

5.2. Opacity contribution of massive pseudoscalars

The radiative transfer by massive particles has been discussed in detail only for pseudoscalars which couple to electrons with a Yukawa coupling, g_a, corresponding to a fine-structure constant $\alpha_a = g_a^2/4\pi$. While the mean free path for these particles is determined by various processes such as inverse bremsstrahlung, Compton absorption, Primakoff effect, and decay, a rough estimate for the conditions in a main-sequence star is obtained by focussing on the Compton effect. The Compton absorption rate, $ae^- \to e^-\gamma$, for massive pseudoscalars is found to be, if $T \ll m_a \ll m_e$,

$$\Gamma_C = \frac{4\pi\alpha\alpha_a m_a^2}{m_e^4} n_e = 9.5 \times 10^6\ \mathrm{s}^{-1}\ \alpha_a \left(\frac{m_a}{1\ \mathrm{keV}}\right)^2 \frac{\rho\mu_e^{-1}}{1\ \mathrm{g\ cm}^{-3}}, \tag{5.6}$$

where μ_e is the "mean molecular weight for the electrons", defined such that $n_e = \rho/\mu_e m_u$ with the atomic mass unit $m_u = 1.661 \times 10^{-24}$ g. With the mass fraction of hydrogen, X, this is $\mu_e^{-1} = (1 + X)/2$. With $(\kappa_\omega \rho)^{-1} = l_\omega = \beta_\omega/\Gamma_\omega$ this leads to an explicit expression

$$\kappa_a \rho = [(2\pi)^{7/2}/45](T/m_a)^{5/2}\, e^{m_a/T}\Gamma_C\,. \tag{5.7}$$

Numerically, this is

$$\kappa_a = 4.4 \times 10^{-3}\ \mathrm{cm}^2\ \mathrm{g}^{-1} \alpha_a \mu_e^{-1} (m_a/1\ \mathrm{keV})^{-0.5} (T/1\ \mathrm{keV})^{2.5}\, e^{m_a/T}, \tag{5.8}$$

to be compared with the standard Rosseland photon opacity, for example at the solar center of $\kappa_\gamma = 1.1\ \mathrm{cm}^2\ \mathrm{g}^{-1}$.

6. Exotic energy loss of low-mass stars; analytic treatment

An analytic treatment of the effect of exotic energy losses (e.g., axion losses) on low-mass stars yields several general resuts. The nuclear burning rate increases, shortening the stellar lifetime. If the energy transfer in the star proceeds by radiation, the surface photon luminosity increases compared with a standard star. For a convective structure, the surface luminosity decreases.

6.1. The equations of stellar structure

In chapter 1 we gave a general overview of how stars react to the energy drain imposed by the emission of light particles such as axions or neutrinos. Compact stars such as white dwarfs or neutron stars have no nuclear energy sources and are supported by the pressure of degenerate fermions. They have a limited amount of thermal energy so that axions simply shorten the duration of the star's cooling phase. For "active" stars such as our Sun which support themselves by thermal pressure, essentially being in virial equilibrium, this equilibrium is maintained by the self-regulation between pressure, temperature, nuclear burning, and energy loss. The particle emission perturbs this intricate but stable interplay, and the nonlinearity of the stellar structure equations requires a more subtle treatment to understand the effect of energy losses. Simply put, such stars react by contraction, increasing the depth of the average gravitational potential. By the virial theorem this corresponds to raising the average kinetic energy of the nuclei, thus the temperature, and hence the nuclear burning rate, so that the axion losses are compensated for. Assuming that the temperature and density dependence of the nuclear burning rates is steeper than that of the axion losses, the structure of the star changes very little to accommodate axion losses, even if these losses have a magnitude of the overall photon luminosity.

These qualitative considerations have been cast into a rigorous analytic treatment by Frieman, Dimopoulos and Turner [72], whose line of argument we shall closely follow. The structure and evolution of a star is governed by the condition of hydrostatic equilibrium,

$$\mathrm{d}p/\mathrm{d}r = -G_{\mathrm{N}} M_r \rho / r^2 , \tag{6.1}$$

where p is the local pressure, G_{N} is Newton's constant, ρ the local mass density, and M_r is the total mass interior to the radius r. The main assumption entering this equation is that of spherical symmetry, neglecting such effects as rotation of the star, binary motion, or magnetic field contributions to the pressure. Secondly, one invokes the principle of thermal equilibrium,

$$\mathrm{d}L_r/\mathrm{d}r = 4\pi r^2 \varepsilon\rho , \tag{6.2}$$

where L_r is the net flux of energy through a spherical surface at radius r, and ε is the effective nuclear burning rate, in $\mathrm{erg\,g^{-1}\,s^{-1}}$, so that $\varepsilon\rho$ is the volume energy generation rate in $\mathrm{erg\,cm^{-3}\,s^{-1}}$. The effective burning rate, i.e., the actual energy deposition to the local thermal heat bath is given by

$$\varepsilon = \varepsilon_{\mathrm{nuc}} - \varepsilon_{\nu} - \varepsilon_{\mathrm{x}} , \tag{6.3}$$

where $\varepsilon_{\mathrm{nuc}}$ is the actual energy liberated in nuclear reactions, ε_{ν} is the standard neutrino emission rate, and ε_{x} represents a nonstandard energy drain such as axion losses or anomalous electromagnetic neutrino production. The energy flux, L_r, is driven by the large temperature gradient from the center to the stellar surface. The relationship between L_r and $\mathrm{d}T/\mathrm{d}r$ is generally nonlinear, especially if convection is the dominant form of transfer. However, for low-mass stars like the Sun it is believed that the transfer of energy proceeds by radiation and conduction, in which case we have a linear equation of energy transfer,

$$L_r = -4\pi r^2 (1/3\kappa\rho)\, \mathrm{d}(aT^4)/\mathrm{d}r , \tag{6.4}$$

where aT^4 is the energy density stored in the radiation field (in natural units $a = \pi^2/15$) and κ is the opacity. It is generally given by

$$1/\kappa = 1/\kappa_{\gamma} + 1/\kappa_{\mathrm{c}} + 1/\kappa_{\mathrm{x}} , \tag{6.5}$$

where κ_{γ} is the radiative opacity, κ_{c} arises from electron conduction which dominates, e.g., in white dwarfs, and κ_{x} accounts for exotic contributions such as that from "strongly" interacting bosons discussed in chapter 5, or the conductive transfer of WIMPs or cosmions mentioned in chapter 1. Note that $(\kappa_{\gamma}\rho)^{-1}$, having the dimension of length, is the Rosseland average of the photon mean free path.

6.2. Homologous changes

In order to study the effect of exotic energy losses on stellar evolution, we begin with the standard case where $\varepsilon_{\mathrm{x}} = 0$ and $1/\kappa_{\mathrm{x}} = 0$, and assume that a star of given mass and chemical composition has established an equilibrium configuration. Then we imagine that axion losses are slowly "switched on" and we ask how the previous equilibrium structure changes in reaction to these losses. In order to study the new structure perturbatively, Frieman et al. [72] assumed that the new "axionic configuration" arises from the standard configuration by virtue of a homology transformation, i.e., "the distance between any two points is altered in the same way as the radius of the configuration". Thus, if the new radius of the star is given by $R' = yR$ with a dimensionless scaling factor y, then every point in the star is mapped to a new position $r' = yr$. The mass interior to the new radius is identical with that interior to the old location, $M'(r') = M(r)$, and the chemical composition at r' is the same as that at r. The density is transformed by $\rho'(r') = y^{-3}\rho(r)$, and from eq. (6.1) one finds that the pressure scales as $p'(r') = y^{-4}p(r)$. The equation of state for a nondegenerate, low-mass star is with good approximation given by the ideal-gas law, $p = R_g \rho T/\mu$, where μ is the average molecular weight of the electrons and nuclei and R_g is the ideal-gas constant. Since $\mu'(r') = \mu(r)$ by assumption, the temperature is found to scale as $T'(r') = y^{-1}T(r)$, and the temperature gradient as $\mathrm{d}T'(r')/\mathrm{d}r' = y^{-2}\,\mathrm{d}T(r)/\mathrm{d}r$. Thus, under a homology transformation, the density, pressure, and temperature profiles are unchanged aside from a global rescaling.

The assumption that the star reacts to axion emission by a homologous contraction imposes restrictions on the constitutive relations for the effective energy generation rate and the opacity. In particular, for a chemically homogeneous star it implies that

$$\varepsilon \propto \rho^n T^\nu , \qquad \kappa \propto \rho^s T^p . \tag{6.6}$$

For the opacity, Frieman et al. [72] took the Kramers law with $s = 1$ and $p = -3.5$, which is found to be an accurate interpolation formula throughout most lower main-sequence interiors. Hence the local energy flux scales as

$$L'(r') = y^{-1/2}L(r) . \tag{6.7}$$

The hydrogen burning rate, $\varepsilon_{\mathrm{nuc}}$, also has the required form with $n = 1$, and for the pp-chain $\nu = 4$–6. For now we shall assume that the energy loss rate, ε_{x}, follows the same proportionality, and we shall ignore the standard neutrino losses, ε_ν, which are small on the lower main sequence*) so that

$$\varepsilon = (1 - \delta_{\mathrm{x}})\varepsilon_{\mathrm{nuc}} , \tag{6.8}$$

where $\delta_{\mathrm{x}} < 1$ is a number which depends on the interaction strength of the new particles. From eq. (6.2) we conclude that

$$L'(r') = y^{-(3+\nu)}(1 - \delta_{\mathrm{x}})L(r) , \tag{6.9}$$

leading to

$$y = (1 - \delta_{\mathrm{x}})^{1/(\nu + 5/2)} . \tag{6.10}$$

Assuming $\delta_{\mathrm{x}} \ll 1$, Frieman et al. [72] then found for the fractional changes of the stellar radius, luminosity, and interior temperature,

$$\delta R/R = -\delta_{\mathrm{x}}/(\nu + 5/2) , \qquad \delta L/L = +\delta_{\mathrm{x}}/(2\nu + 5) , \qquad \delta T/T = +\delta_{\mathrm{x}}/(\nu + 5/2) . \tag{6.11}$$

*) Following general conventions we may equally imagine that the standard neutrino losses are included in $\varepsilon_{\mathrm{nuc}}$ so that $\varepsilon = \varepsilon_{\mathrm{nuc}} - \varepsilon_{\mathrm{x}}$.

In other words, the star contracts, becomes hotter, and the surface photon luminosity increases, i.e., the star "overcompensates" for the new losses. Moreover, even if axion losses are as large as the surface photon luminosity, $\delta_x = 1/2$, the overall changes in the stellar structure remain moderate. Hence, the predominant effect is an increased consumption of nuclear fuel at almost unchanged stellar structure, leading to a decrease of the duration of the main-sequence burning phase of

$$\delta\tau/\tau \sim -\delta_x \,. \tag{6.12}$$

The "standard Sun" is halfway through its main-sequence evolution so that a conservative constraint is $\delta_x < 1/2$.

In general, the exotic losses do not have the same temperature and density dependence as the nuclear burning rate, implying a breakdown of the homology condition. However, to lowest order these results will remain valid if we interpret δ_x as a suitable average, i.e., $\delta_x = \langle \varepsilon_x/\varepsilon_{\rm nuc} \rangle_{\rm star}$. For the pp-chain, the temperature dependence of $\varepsilon_{\rm nuc}$ is not very steep, and since the stellar structure changes only very little, δ_x can be computed from the unperturbed stellar model.

For a convective structure as is appropriate for main sequence stars with masses $M \lesssim 0.3 M_\odot$ or for the cores of helium burning stars, a similar treatment leads to

$$\delta R/R = -\delta_x/(\nu + 11/2) \,, \qquad \delta L/L = -5\delta_x/(2\nu + 11) \,, \qquad \delta T/T = +\delta_x/(\nu + 11/2) \,. \tag{6.13}$$

These stars also contract, and the internal temperature increases, but the surface luminosity decreases.

7. Axions from the Sun

The age of the Sun is directly established from radiochemical dating of terrestrial, lunar, and meteoritic material, allowing one to derive first constraints on light particle emission. Its radius and luminosity constrain the efficiency of any new contribution to the transfer of energy. The Sun may serve as a source for terrestrial axion experiments which look for the appearance of X-rays in a strong magnetic field. An existing germanium spectrometer, built to search for double-β decay, sets limits on the solar axion flux. The absence of solar γ-rays constrains the decay rate of particles produced in the Sun.

7.1. Energy loss and energy transfer in the Sun; first constraints

The observed properties of the Sun allow one to constrain the interaction strength of axions and other light particles [74, 87, 160, 161]. We stress that the constraints from other arguments that will be discussed in the following chapters are generally much more restrictive so that the solar bounds are of little practical interest. Still, in order to illustrate the general methods it is worthwhile to consider particle emission from the Sun. We focus on the simple case of pseudoscalar particles with a mass, m_a, which couple only to electrons with an "axionic" fine-structure constant, $\alpha_a = g_a^2/4\pi$, where g_a is the Yukawa coupling for the pseudoscalar interaction. These particles can be produced by the Compton process, $\gamma e^- \rightarrow e^- a$, by bremsstrahlung emission, $e^-(Z, A) \rightarrow (Z, A) e^- a$, and through a triangle loop diagram by the Primakoff process (section 4.9). They can be absorbed by the inverse of these processes and by their decay, $a \rightarrow \gamma\gamma$. However, since we are only interested in a simple estimate and an illustration of the arguments, we follow Carlson and Salati [160] and Raffelt and Starkman [161], and focus on the Compton process and its inverse.

If these particles can freely escape, they drain the Sun of energy and cause its radius to shrink and its surface luminosity to rise. However, these effects can be compensated for by a small change of the initial helium abundance, a quantity which is not known and rather must be inferred from solar evolution calculations. Hence, the observed luminosity and radius cannot serve to constrain solar axion losses. In principle, a measurement of the solar neutrino flux would show any discrepancy between the effective nuclear burning rate, $\varepsilon_{\rm eff}$, which is related to the surface photon luminosity, and the actual nuclear burning rate, $\varepsilon_{\rm nuc}$. However, existing and future experiments are sensitive mostly to electron neutrinos which can oscillate into other flavor states on their way from the solar center to the earth [163] so that the measured $\nu_{\rm e}$-flux is not a reliable measure of $\varepsilon_{\rm nuc}$.

The only remaining criterion is the solar age of 4.5×10^9 yr which was established by radiochemical dating of terrestrial, lunar, and meteoritic material (for a summary see refs. [421, 422]). This age is about half the standard main-sequence lifetime of the Sun, and following chapter 6 we conclude that the nuclear fuel consumption cannot exceed twice its standard value, i.e., an approximate constraint is $\varepsilon_{\rm a}\lesssim\varepsilon$ where the effective burning rate in the solar center is $\varepsilon\sim10\,{\rm erg\,g^{-1}\,s^{-1}}$. The Compton volume emission rate was given in eq. (4.43) for massless axions. The physical parameters of the solar core were given in table 4.1 and one easily finds that the condition $\varepsilon_{\rm a}\lesssim\varepsilon$ leads to $\alpha_{\rm a}\lesssim10^{-21}$. Including bremsstrahlung emission and integrating over a standard solar model yields the axion luminosity [87]

$$L_{\rm a}=6.0\times10^{21}L_\odot\alpha_{\rm a}\,. \tag{7.1}$$

Demanding $L_{\rm a}<L_\odot$ leads to a more restrictive constraint, $\alpha_{\rm a}<1.7\times10^{-22}$. For particle masses much in excess of the internal temperature of ~1 keV, the emission rate eq. (4.45) applies, and our simple criterion yields [160, 161]

$$\log\alpha_{\rm a}\lesssim-19-4.5\log(m_{\rm a}/{\rm keV})+0.32(m_{\rm a}/{\rm keV})\,. \tag{7.2}$$

These results are shown as the lower solid line in fig. 7.1.

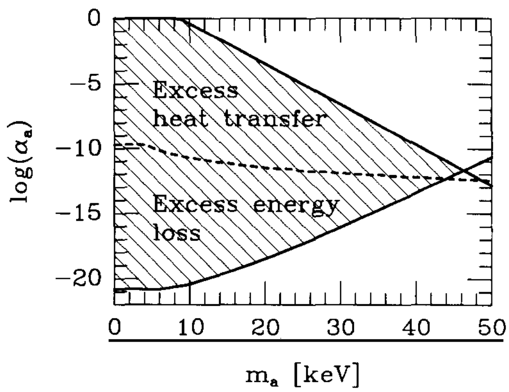

Fig. 7.1. Effects of massive, pseudoscalar particles on the Sun, taking only the Compton effect into account. Above the dashed line, the particles would contribute to the radiative energy transfer, below they would freely escape and drain the Sun of energy. The cross-hatched region of parameters is excluded by this simple argument. (Adapted from ref. [161].)

If the particles are so "strongly" interacting that they do not freely escape, they contribute to the radiative transfer of energy as discussed in chapter 5. In particular, the opacity contribution due to the Compton process was given in eq. (5.8). The observed radius and luminosity of the Sun confirm the standard value of the opacities at least to within a factor of a few $\mathrm{cm^2/g}$ so that a nominal criterion to constrain axions is $\kappa_a^{-1} < \kappa_\gamma^{-1}$. A typical value for the radiative opacities is $\kappa_\gamma \sim 1.1\ \mathrm{cm^2/g}$, leading to the constraint [160, 161]

$$\log \alpha_a \gtrsim 2.3 - 0.32(m_a/\mathrm{keV}) + 0.5 \log(m_a/\mathrm{keV}) . \tag{7.3}$$

This line is the upper solid curve in fig. 7.1. The division line between the regime of free escape and the "trapped" regime is also easily obtained and is shown as a dashed line. Of course, for parameters near the dashed line, neither the concept of energy transfer nor that of free escape do rigorously apply. Of course, this part of the parameter range is in the middle of the excluded regime and thus of no further interest.

7.2. Results from a germanium spectrometer

The sun can also serve as a source for axions or other pseudoscalars which one can attempt to measure in a terrestrial detector. If axions couple to electrons as in our above example, they would interact with the electrons in a germanium spectrometer which was designed to detect neutrinoless double-β decays [423]. On the basis of our discussion section 4.6.1 one can easily calculate the axion spectrum from bremsstrahlung emission, which is the dominant process, and on the basis of section 4.4 the Compton contribution. The absorption in the detector is due to the axio-electric effect (bound–free absorption) discussed in section 4.7. Assuming that axion emission is only a minor perturbation of the Sun one can compute the solar axion flux at the earth on the basis of a standard solar model. From the absence of a signal in their germanium spectrometer, Avignone et al. [423] found a bound on the axionic fine-structure constant of $\alpha_a < 0.8 \times 10^{-21}$. Of course, if axions would saturate this bound, axion emission would be a major energy drain of the Sun, excluding this parameter range (section 7.1). Moreover, the axion bounds to be discussed in the following chapters are much more restrictive: $\alpha_a \lesssim 0.7 \times 10^{-26}$. In other words, the possibility of detecting solar axions by this method is excluded by many orders of magnitude.

7.3. A magnetic conversion experiment

If axions or other (pseudo-) scalar particles do not couple to electrons such as hadronic axions, the bounds on the electron coupling do not apply. In this case axions are produced in the Sun only by the Primakoff process (section 4.9), i.e., the axion–photon coupling eq. (1.1) allows photons to transform into axions in the fluctuating electric fields of the solar plasma. The transition rate was given in eq. (4.77). The lifetime of helium burning stars (horizontal branch stars) sets a bound $g_{a\gamma} \lesssim 10^{-10}\ \mathrm{GeV}^{-1}$ on the axion–photon coupling (chapter 8), leading us to define $g_{10} \equiv g_{a\gamma} \times 10^{10}$ GeV. The axionic energy drain of the Sun is found to be [87] $L_a = 1.7 \times 10^{-3} L_\odot g_{10}^2$ so that axion emission is known to be only a small perturbation of the Sun. An analytic approximation to the differential axion flux at the earth, obtained from integrating over a standard solar model, is found to be [414]

$$\frac{\mathrm{d}\Phi}{\mathrm{d}E_a} = g_{10}^2\, \frac{4.02 \times 10^{10}}{\mathrm{cm^2\ s\ keV}}\, \frac{(E_a/\mathrm{keV})^3}{\mathrm{e}^{E_a/1.08\ \mathrm{keV}} - 1} . \tag{7.4}$$

The total number flux at the earth is $\Phi_a = g_{10}^2\, 3.54 \times 10^{11}\,\mathrm{cm}^{-2}\,\mathrm{s}^{-1}$, with an average energy $\langle E_a \rangle = 4.2\,\mathrm{keV}$.

Following the original work of Sikivie who discussed the possibility of detecting solar axions by conversion into X-rays in the presence of a strong magnetic field, i.e., the inverse of the Primakoff production process in the Sun, Van Bibber et al. [414] proposed a practical design for such a detector, involving a large superconducting magnet such as that of the decommissioned Fermilab bubble chamber. The most important feature of that proposal is to fill the conversion volume with a low-Z gas such as H_2 or He which causes the photons to propagate like massive particles. If one adjusts the gas pressure such as to match the effective photon and axion masses, the conversion probability can be resonantly enhanced (section 4.9.4). In refs. [411, 414], photon–axion oscillations in the presence of a medium, with or without absorption, were discussed in detail. According to ref. [414], the solar axion flux would be detectable over about a decade in $g_{a\gamma}$ values above the HB star bound. While this experiment is not currently pursued in the U.S., there appears to be a new effort to perform this kind of experiment in the Soviet Union [424].

It is interesting that the range of parameters that can be probed with this experiment is not excluded, at least not rigorously excluded, by any other method. Especially the range of parameters excluded by SN 1987A (chapter 10) does not seem to reach to such low values of the Peccei–Quinn scale because of axion trapping (section 10.6), i.e., there appears to be a window of allowed values for the axion mass or Peccei–Quinn scale between the HB star bound (chapter 8) and the SN 1987A bound. Of course, such a window can only exist for hadronic axions which do not couple to electrons.

7.4. *Radiative particle decays and solar γ-rays*

If elementary particles produced in the Sun are radiatively unstable, their decay photons will contribute to the solar X- and γ-ray spectrum. This argument allows one, for example, to derive a bound on the radiative decay time of electron neutrinos of $\tau_{\nu_e}/m_{\nu_e} > 7 \times 10^9\,\mathrm{s/eV}$ [189, 190], about eight orders of magnitude more restrictive than direct laboratory bounds. Equally, one can constrain the radiative decays of axions produced in the Sun. Of course, the decay width of very light axions is so small that no useful results can be extracted. For axion masses above ~10 keV the plasma production processes are seriously suppressed, but axions are still produced by nuclear reactions. A particularly useful case is $d + p \to {}^3\mathrm{He} + \gamma(5.5\,\mathrm{MeV})$ which is part of the standard pp reaction chain in the Sun and is therefore known to occur at a total rate of $1.7 \times 10^{38}\,\mathrm{s}^{-1}$ in the Sun. The final-state photon can be replaced by an axion or other boson in a certain fraction of all cases. This method among others was used to rule out the standard axion [188].

8. Red giants and horizontal branch stars

The evolutionary pattern of low-mass stars is well understood, and supported by detailed observational data, notably by the color–magnitude diagrams of open and globular clusters. Excessive energy losses by particle emission from red giants could suppress helium ignition, contrary to the observed existence of horizontal branch (HB) stars. Even if helium ignites, the helium burning lifetime would be shortened, a quantity that is measured by the observed number of HB stars in open and globular clusters relative to stars in other phases of evolution. Also, a delay of helium ignition would lead to an increased luminosity at the tip of the red giant branch (RGB), a quantity that can be directly measured.

These considerations lead to some of the most powerful bounds on axion couplings and neutrino electromagnetic properties.

8.1. The general agenda

One of the most sensitive tests of stellar evolution theory is provided by the color–magnitude diagrams of stellar clusters, notably of globular clusters, an example of which is shown in fig. 8.1. In our galaxy, 131 globular clusters are known [425], each of which consists of many stars, in some cases tens of thousands, providing a rich sample of coeval stars with approximately equal chemical composition. Globular clusters are the oldest objects in the galaxy and hence formed at least 10 Gyr ago, with age estimates derived from their intrinsic properties varying between about 12 and 18 Gyr. The lifetime of stars depends mostly on their mass with lower-mass stars living longer, a crude scaling being $t_{\rm life} \propto M^{-3}$ [426]. Therefore the stars in globular clusters which are still actively burning have masses $M \lesssim 0.80 M_\odot$ where $M_\odot = 2\times 10^{33}$ g is the solar mass unit. In other words, we have detailed and statistically significant information on the evolution of low-mass stars, which are therefore ideal to test variations of stellar evolution theory that would be caused by "exotic" particle emission.

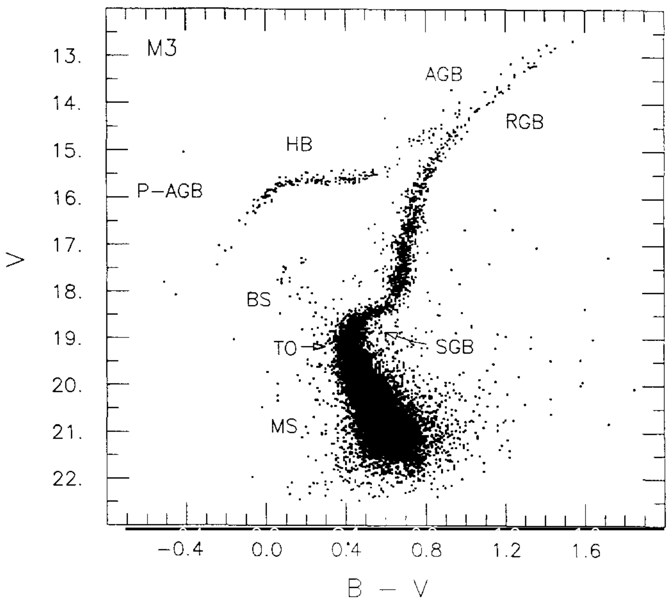

Fig. 8.1. Color–magnitude diagram of the globular cluster M3 according to ref. [460], based on the photometric data of 10 637 stars. According to ref. [427], the following classification has been adopted for the various evolutionary stages. MS (main sequence): core hydrogen burning. BS (blue stragglers). TO (main sequence turn-off): central hydrogen is exhausted. SGB (subgiant branch): hydrogen burning in a thick shell. RGB (red giant branch): hydrogen burning in a thin shell with a growing core until helium ignites. HB (horizontal branch): helium burning in the core and hydrogen burning in a shell. AGB (asymptotic giant branch): helium and hydrogen shell burning. P-AGB (post-asymptotic giant branch): final evolution from the AGB to the white dwarf stage. Note that on the horizontal axis, the color, the surface temperature increases to the left. The brightness measure on the vertical axis are "visual magnitudes", i.e., they measure the logarithmic luminosity in the visual spectrum. The HB bends down toward the left, i.e., towards hotter stars. This decrease in visual brightness of hotter HB stars reflects that more and more energy is emitted in the ultraviolet spectrum. In "bolometric magnitudes", i.e., after correcting for the finite window of the photographically observed spectrum, the HB turns out to be truly horizontal: all stars have the same total luminosity within a narrow range. (I thank A. Renzini for providing me with an original for this figure.)

The neutrino, axion, and other particle emission rates are generally steeply rising functions of temperature and density so that one may think that their effect would be much more pronounced in stellar objects with hotter and denser interiors than the relatively modest conditions encountered in low-mass stars. Under more extreme conditions, however, the standard neutrino luminosity is important which, at high temperatures and densities, typically is an even steeper function of these parameters so that it is more difficult, e.g., for axions to compete. Evolved low-mass stars, i.e., red giants, horizontal branch stars, and white dwarfs, are objects which emit most of their energy in photons, but are at the borderline where standard neutrino emission becomes important. For example, standard neutrino losses are thought to delay the helium flash, but only by an amount on the borderline of being detectable in the color–magnitude diagrams of globular clusters. In other words, evolved low-mass stars are objects where axion emission is most likely to make an *observable* difference relative to the standard evolution picture.

This reasoning breaks down when the conditions are so extreme as in the core of a collapsing star where neutrinos are actually trapped. In this case, again, axion emission can make a difference precisely if axions are more weakly interacting than neutrinos, and very useful constraints were derived from SN 1987A (chapter 10). In summary, the most interesting cases are not the conditions where axion emission is largest, the most interesting cases are where axion emission makes the largest difference in astronomical observables.

8.2. The evolution of low-mass stars

The evolution of low-mass stars [427, 428] consists of several physically distinct phases with characteristic surface properties (luminosity, temperature, and radius). When these stars form, they contract until their interior is so hot that hydrogen burning ignites, replenishing the thermal energy which the star constantly loses because of its surface radiation. At this point, the star reaches an equilibrium state which is largely governed by the virial theorem. This means that further contraction would lead to further heating, increased nuclear burning, further heating and pressure increase, and hence expansion. Expansion away from the equilibrium position would lead to cooling, a drop in the burning rates, a further loss in temperature and pressure and hence to contraction. This subtle interplay is described by the stellar structure equations discussed in chapter 7. It is clear that stars with a larger mass have a larger average gravitational potential, hence a larger internal temperature because of the virial theorem and hence larger burning rates and a larger luminosity. A crude scaling is given by $L \propto M^4$ [426].

It is customary to discuss the surface properties of stars by means of the Hertzsprung–Russell diagram, or its observational counterpart, the color–magnitude diagram. On the vertical axis one shows luminosity (or brightness), on the horizontal axis surface temperature (color) with the temperature decreasing to the right. In such a diagram, the hydrogen burning stars occupy a diagonal band, the main-sequence (MS) shown in fig. 8.1. Different loci on the main-sequence are occupied by stars with different mass. In fig. 8.2 we show the evolutionary track of a low-mass star ($M = 0.8 M_\odot$) as well as its luminosity evolution. During the MS evolution, the luminosity and surface temperature stay approximately constant, so that a star of fixed mass will approximately stay at its location on the MS for the entire hydrogen burning phase. The inner structure of the Sun as an example for a MS star is shown in fig. 8.3a.

Once the hydrogen in the center is exhausted, a helium core begins to form which is supported by electron degeneracy pressure, while hydrogen burns in a shell. This development is accompanied by

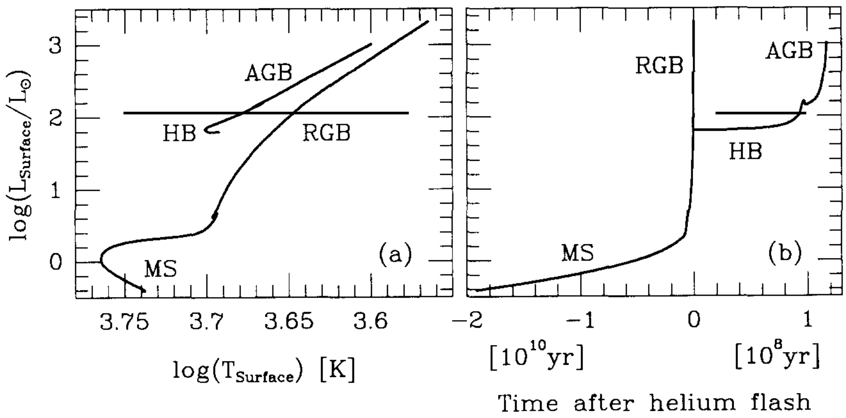

Fig. 8.2. Evolutionary track of a $0.8M_{\odot}$ star ($Z = 0.004$) from zero-age to the asymptotic giant branch. The acronyms for the evolutionary phases are: MS (main sequence), RGB (red giant branch), HB (horizontal branch), AGB (asymptotic giant branch). a, Hertzsprung–Russell diagram. b, luminosity versus time. (Track calculated with Dearborn's evolution code.)

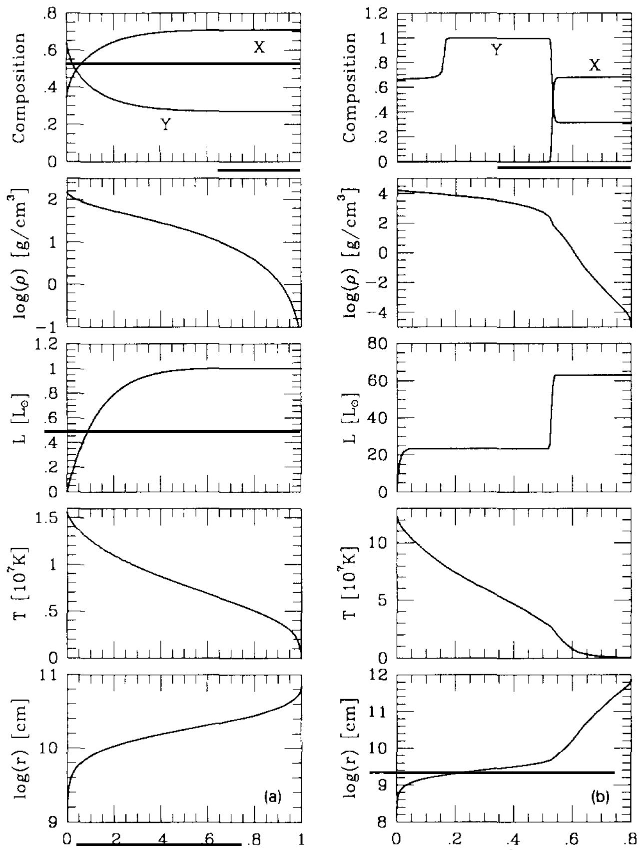

Fig. 8.3. a. Inner structure of the Sun as an example for a low-mass, main-sequence (MS) star which is about half-way through its hydrogen burning phase. (Solar model taken from Bahcall [163].) b. Inner structure of a horizontal branch (HB) star with metallicity $Z = 0.004$ after about 2.5×10^7 yr which is about a quarter of the HB lifetime. (Model taken from ref. [279].)

expansion of the surface layers, leading to a reduced surface temperature at approximately the same luminosity, i.e., the evolutionary track turns right (fig. 8.2). Stars in this phase are known as subgiants (SG). Such stars are characterized by two opposing trends: a contracting inner core which becomes more and more degenerate, and an expanding envelope.

As the degenerate helium core grows in mass (which means that its radius actually shrinks), the gravitational potential at its surface will be dominated by *its* mass, not by the total mass of the star; the contribution of the extended envelope becomes less and less important. Above the degenerate helium core, however, the medium still supports itself by thermal pressure against the gravity of the core which thus determines the temperature and hence the hydrogen burning rate. Thus, as the core mass grows, the core temperature and hydrogen luminosity increase while the envelope further expands with decreasing surface temperature; the star moves up the red giant branch (RGB), see figs. 8.1 and 8.2. Thus, while the conditions at the center of a MS star are determined by the global properties (the total mass) of the star, the red giant properties are determined by the *core mass*, so that different loci on the RGB are determined by the core mass while being largely independent of the total mass. Different stars along the RGB in fig. 8.1 are stars with slightly different total mass which determined their MS lifetime and hence the starting time of their red giant evolution, but because their properties are mostly determined by their core mass, they can be viewed as tracing out the evolutionary track of a single star, yielding a close correspondence with the single-star evolutionary track in fig. 8.2.

Eventually, when the core mass has reached a value $\sim 0.5 M_\odot$, the density and temperature are so high ($\rho \sim 10^6\ \mathrm{g\,cm^{-3}}$ and $T \sim 10^8\ \mathrm{K}$) that the triple alpha reaction, $3\,{}^4\mathrm{He} \to {}^{12}\mathrm{C}$, becomes more and more important. The rate for this reaction is extremely sensitive to density and temperature, approximately $\varepsilon_{3\alpha} \propto \rho^2 T^{40}$, so that one may actually speak of a very specific "ignition" point. The pressure, however, is still dominated by degenerate electrons so that the energy produced by helium burning does not, at first, lead to cooling as the core begins to expand; the nuclear reactions run away, an event called the "helium flash".

A self-regulating equilibrium is achieved only after the core has expanded to a density of $\sim 10^4\ \mathrm{g\,cm^{-3}}$, although it remains essentially at the same temperature, $10^8\ \mathrm{K}$. The core is now very similar to a MS star, except that helium burns in its center rather than hydrogen, and that the burning rate is governed by the core mass which plays the role of the total mass in a MS star. Hydrogen still burns in a shell, and the envelope is still expanded, so that the luminosity of the shell source is still determined by the core mass. Because of the core expansion during the helium flash, the gravitational potential is smaller, and hydrogen burning correspondingly smaller, although it still dominates the total luminosity of a helium burning star (fig. 8.3b). Helium ignition, therefore, leads to a dramatic *reduction* of the total luminosity and hence to a sudden break of the RGB which is thus characterized by a fixed maximum luminosity at its tip. We note that a helium flash occurs only for stars with $M \lesssim 2.2 M_\odot$ because more massive stars never develop a fully degenerate helium core.

The ability of the envelope to transport energy depends on its opacity, which in turn is a sensitive function of the "metallicity", i.e., the abundance by mass, Z, of all elements heavier than helium. For the Sun, $Z = 0.02$, while for typical globular clusters, which belong to an older generation of stars (population II), $Z \sim 10^{-2.5}$–10^{-4}. Moreover, stars lose mass along the RGB so that typical total masses of globular cluster stars after the helium flash are $\sim(0.65$–$0.70) M_\odot$. For such conditions the radius of the envelope of helium burning stars and hence their surface temperature is extremely sensitive to the total mass of the envelope, its metallicity, and the luminosity which it has to carry. These stars, therefore, occupy a horizontal band in the Hertzsprung–Russell diagram, called the horizontal branch (HB), see fig. 8.1. For stars in open clusters which are of a more contemporary generation (population

I) like our Sun, the helium burning stars do not spread out in surface temperature and are thus all contained in a "clump" in the Hertzsprung–Russell diagram. Apart from a higher metallicity and larger total mass, these "clump giants" are physically equivalent to HB stars.

During the HB evolution, the hydrogen burning shell moves further out, and the core grows. However, because it is not degenerate, its radius also grows, and the hydrogen source actually decreases with time. Conversely, the central helium source increases, and the total luminosity remains almost fixed during the HB evolution (fig. 8.2). In the core, energy is transported by convection. This entails that nuclear fuel is dredged to the center of the core, substantially increasing the amount of helium available for burning. This can be appreciated by comparing the composition profile in fig. 8.3b with the luminosity profile. The central burning source is characterized by the small region where the luminosity rises from 0 to about $25 L_\odot$, while the convective region is where the helium abundance, Y, has been depleted. The observed lifetime of HB stars cannot be understood without this convective supply of fuel.

When helium in the center is exhausted, the star makes a transition to a double-shell configuration with helium and hydrogen burning in a shell each, leaving behind a carbon–oxygen core. This development is accompanied by a second luminosity ascent along the asymptotic giant branch (AGB). The further evolution is fast and complicated, with the two shells interacting and thermal pulses occurring. Eventually, these stars become white dwarfs, i.e., completely degenerate stars with no nuclear fuel left to burn.

The physical characteristics of these different evolutionary phases of low-mass stars are summarized in table 8.1.

8.3. Suppression of the helium flash by particle emission

8.3.1. General argument

If the core of a red giant near the helium flash produces a large flux of neutrinos or other particles, the resulting cooling will prevent helium from igniting until larger densities have been achieved, i.e.,

Table 8.1
Physical characteristics of the main evolutionary phases of low-mass stars. The properties of red giants are understood to be near the helium flash

	Main sequence (MS)	Red giant branch (RGB)	Horizontal branch (HB) and "clump giants"
Energy source	central hydrogen	shell hydrogen	shell hydrogen (dominates) central helium
Duration	$\sim 10^{10}$ yr	$\sim 10^8$ yr	$\sim 10^8$ yr
Luminosity	$1 L_\odot$ (our Sun)	$\sim 2000 L_\odot$ (at helium flash)	$\sim 50 L_\odot$ ($M \sim 0.65 M_\odot$, $Z = 0.001$)
Luminosity determined by	total mass	core mass (grows along RGB)	core mass at helium flash (universal apart from weak dependence on metallicity)
Core mass	–	$\sim 0.5 M_\odot$ (at helium flash)	$\gtrsim 0.5 M_\odot$
Central density	$\sim 10^2\ \mathrm{g\,cm^{-3}}$	$\sim 10^6\ \mathrm{g\,cm^{-3}}$	$\sim 10^4\ \mathrm{g\,cm^{-3}}$
Central temperature	$\sim 10^7$ K	$\sim 10^8$ K	$\sim 10^8$ K
Conditions near center	nondegenerate	degenerate	nondegenerate
Energy transfer near center	radiation	electron conduction	convection

until the core has grown to a larger mass. The standard neutrino losses, for example, cause an increase of the core mass of $\sim 0.03 M_\odot$ [429]. Since electron conduction is efficient at transporting heat from the hydrogen burning shell into the center, and since the core also heats by the release of gravitational energy because of its contraction due to growth, the energy loss rate must be efficient enough to compete with these heating mechanisms. For a sufficiently large energy loss rate the helium flash will be delayed so much that the hydrogen burning front reaches the stellar surface, i.e., the helium flash would never occur and the star would directly become a helium white dwarf after ascending the RGB, contrary to the observation of HB stars and "clump giants".

8.3.2. A specific case: the electron coupling of pseudoscalars

This argument was first advanced by Dearborn, Schramm and Steigman [63], who followed the evolution of red giants numerically, incorporating axion emission in Dearborn's stellar evolution code. They gave bounds on the axion–electron coupling and on the axion–photon coupling, which were required to be so small that helium would ignite in their calculations. Unfortunately, the correct emission rates had not been calculated at the time, and the Primakoff rate, relevant for the axion–photon coupling, was overestimated by a large factor, invalidating the bound on the axion–photon coupling. Later, the red-giant evolution calculations were repeated with the correct Primakoff emission rates by Raffelt and Dearborn [89] who found that the helium flash was never suppressed. However, they derived a new bound on the axion–photon coupling because axion emission would decrease the HB lifetime (section 8.5).

In order to constrain the coupling of axions or other pseudoscalars to electrons, Dearborn et al. [63] used the following expression for the bremsstrahlung emission rate, $e^- + (Z, A) \rightarrow (Z, A) + e^- + a$,

$$\varepsilon = 3.34 \times 10^{27}\ \mathrm{erg\,g^{-1}\,s^{-1}}\ g_a^2 \rho_6 T_8^{2.5}\, e^{-\omega_0/T}\,, \tag{8.1}$$

where g_a is the axion–electron Yukawa coupling, ρ_6 is the density in $10^6\ \mathrm{g\,cm^{-3}}$, and T_8 is the temperature in 10^8 K, ω_0 is the plasma frequency, and we have assumed a pure helium plasma, appropriate for the core of a red giant before the helium flash. They also gave an expression for the Compton emission rate, but it is negligible in a red giant core compared to bremsstrahlung. On the basis of this rate they found that the helium flash was suppressed unless $g_a < 1.4 \times 10^{-13}$.

The correct emission rate was discussed in section 4.6.2, and using eqs. (4.51) and (4.54) we find

$$\varepsilon = 1.21 \times 10^{26}\ \mathrm{erg\,g^{-1}\,s^{-1}}\ g_a^2 T_8^4\,, \tag{8.2}$$

with a different temperature and density dependence. Therefore it is not obvious what one would find if one would incorporate the correct emission rate into a stellar evolution code. However, in order to derive an estimate of the parameter space that is likely to be excluded by the helium ignition argument, we note that $\omega_0/T \sim 2$ near the center of a red giant, and taking $\rho_6 = 1$ and $T_8 = 1$, Dearborn et al.'s emission rate is a factor of ~ 4 larger than the correct rate. Hence their bound on g_a must probably be relaxed by a factor of 2 so that helium ignites if $g_a \lesssim 3 \times 10^{-13}$.

However, for this bound to apply one must assume that axions or other pseudoscalars freely escape from the red giant core. On the basis of eqs. (4.4) and (4.51) and noting that the volume emission rate is $Q = \varepsilon\rho$ we can easily estimate the inverse mean free path to be

$$l^{-1} \sim 2\alpha^2 \alpha_a Z^2 F \rho / m_e^2 m_u A\,, \tag{8.3}$$

with the axionic fine-structure constant, $\alpha_a = g_a^2/4\pi$. Taking a density of $10^6\,\mathrm{g\,cm^{-3}}$ a core radius of $R_{core} = 10^9$ cm, and using $R_{core}/l < 1$ as a criterion for axions to escape freely leads to the requirement $g_a < 6 \times 10^{-7}$. Therefore the range

$$3 \times 10^{-13} \lesssim g_a \lesssim 6 \times 10^{-7}\,, \tag{8.4}$$

is excluded by the helium ignition argument. For values smaller than the lower bound, axions would not suppress the helium flash, for values larger than the upper bound, they would not freely escape and contribute to the transfer of energy, possibly even helping helium to ignite.

It is also of interest to consider pseudoscalars with a nonvanishing mass, m_a. These particles can be considered massless for the purpose of this argument if $m_a \lesssim T \sim 8.6$ keV. For larger masses, the emission rate will be suppressed by a Boltzmann factor, $e^{-m_a/T}$, whence the "effective coupling constant" is estimated to be $g_a\,e^{-m_a/2T}$. Similarly, the mean free path is reduced by the nonrelativistic velocity so that, for the purpose of reabsorption, we have to substitute $\alpha_a \to \alpha_a(m_a/T)^{1/2}$. Thus the excluded regime is estimated to be

$$-12.5 + 0.025 m_{keV} \lesssim \log(g_a) \lesssim -6.2 - 0.25\log(1 + 0.12 m_{keV})\,, \tag{8.5}$$

where $m_{keV} = m_a/\mathrm{keV}$. This excluded parameter range is shown in fig. 8.4.

Considering specifically DFSZ-axions with three families of quarks, the interaction strength with electrons and the axion mass are related by [see table 2.1 and eq. (2.32)]

$$g_a = 2.8 \times 10^{-11} m_{eV} \cos^2\beta\,, \tag{8.6}$$

where $m_{eV} = m_a/\mathrm{eV}$ and $0 \le \beta \le 90°$ is a free parameter of the model. For $\beta = 0$ we show this relationship as a short-dashed line in fig. 8.4. The excluded range in terms of m_{eV} and β is shown in fig. 8.5.

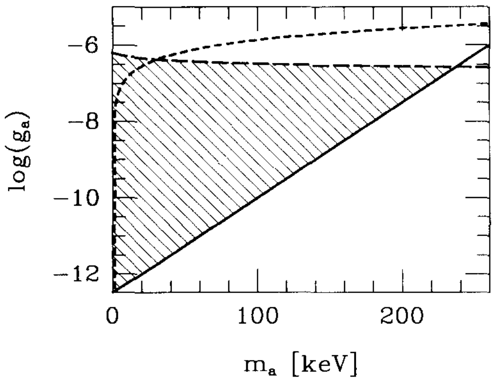

Fig. 8.4. We estimate that the hatched area of parameter space is excluded by the helium ignition argument. Above the long-dashed line, the pseudoscalars would not escape from the red giant core, below the solid line, they would not drain enough energy. The short-dashed line is the locus of parameters for DFSZ-axions with $\cos^2\beta = 1$.

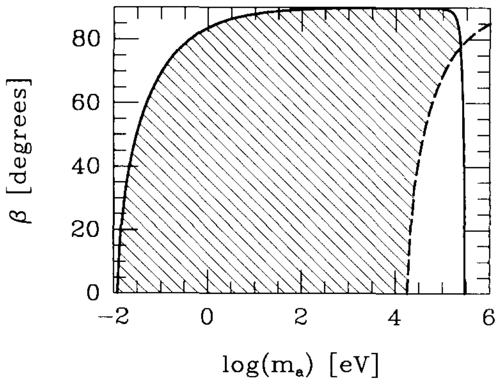

Fig. 8.5. The hatched area of DFSZ-axion parameters is excluded by the helium ignition argument. As in fig. 8.4, the long-dashed line marks the borderline beyond which axions would not escape from the red giant core, while beyond the solid line the energy drain is too small to prevent the helium flash.

8.4. Reduction of the helium burning phase

8.4.1. General argument and its applications

If the helium flash occurs in spite of particle emission, the further evolutionary path can still change substantially. When the star has found its new equilibrium structure with a helium-burning core it will still emit particles. This emission may be larger or smaller compared to the red giant before the flash. For example, the plasmon-decay emissivity of neutrinos, $\gamma_{pl} \to \nu_e \bar{\nu}_e$, is essentially proportional to $\omega_0^4 e^{-\omega_0/T}$, and since the plasma frequency, ω_0, is much smaller after the helium flash than before, the neutrino losses drop by several orders of magnitude. Conversely, the emission of hadronic axions by the Primakoff effect is strongly suppressed by screening effects which are much more severe in the red giant before the flash than in the core of a helium-burning star afterwards so that axion emission rises substantially (fig. 8.6). In either case, the energy drained by the particle losses must be supplied by the nuclear reactions.

According to the analytic treatment of Frieman et al. [72] (chapter 6), a star adjusted to axion or neutrino losses has a very similar structure compared with a no-loss model because it takes only a small contraction to increase the temperature and thus the nuclear burning rates enough to provide for the particle flux. Hence the dominant effect of the drain will be an increased nuclear fuel consumption, reducing the helium burning lifetime, t_{He}, by a factor $L_{3\alpha}(L_x + L_{3\alpha})$ where L_x is the exotic particle luminosity while $L_{3\alpha}$ is the total energy production of the core if there were no particle losses, $L_{3\alpha} \sim 15 L_\odot$. The actual reduction will be even larger if particle emission has delayed the helium flash so that the core of the helium burning configuration is larger than standard, further shortening t_{He}.

Observationally, the helium-burning lifetime of population I stars, i.e., stars of the most recent generation like our Sun, was determined by Cannon [430], comparing the number of "clump giants" (helium burning stars) in the open cluster M67 with the number of stars per luminosity interval near the MS turnoff. He found $t_{He} = 150 \times 10^6$ yr, with a large statistical uncertainty, however, because of the small total number of clump giants, $N = 5$. Tinsley and Gunn [431] derived $t_{He} = (127 \pm 29) \times 10^6$ yr from low-mass giants of the old galactic disk population. This is in full agreement with the evolutionary

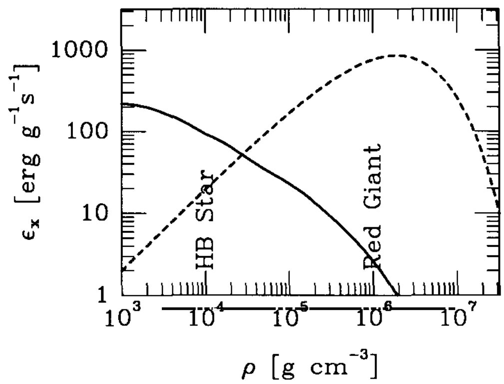

Fig. 8.6. Energy loss rates per unit mass for a pure helium plasma at $T = 10^8$ K as a function of density. The solid line is the Primakoff axion luminosity for $g_{a\gamma} = 10^{-10}\ \mathrm{GeV}^{-1}$, the dashed line is the anomalous neutrino plasmon decay luminosity for a neutrino dipole moment of $10^{-11}\mu_B$. If multiplied with $M_c \sim 0.5 M_\odot$, these curves yield the particle luminosity of the core of a red giant before the helium flash ($\rho \sim 10^6\ \mathrm{g\,cm^{-3}}$) or of a helium burning star (HB star or clump giant, $\rho \sim 10^4\ \mathrm{g\,cm^{-3}}$). Therefore the Primakoff axion luminosity of the core increases during the helium flash, neutrino emission decreases.

calculations of Sweigart and Gross [432] who found $t_{\mathrm{He}} \sim 10^8$ yr, the precise value depending on the core mass, total mass, metallicity, and helium content of the envelope.

This agreement led Raffelt and Dearborn [90] to point out that a reduction of t_{He} by a factor of ~2 was conservatively excluded on the basis of these observations. In other words, the core luminosity of exotic particles, L_x, must not exceed the standard nuclear energy production rate of the core, $L_{3\alpha}$. Taking a typical core density of $10^4\ \mathrm{g\,cm^{-3}}$ and a temperature of 10^8 K, the particle emission rate at these conditions is thus constrained by

$$\varepsilon_x \lesssim 100\ \mathrm{erg\,g^{-1}\,s^{-1}}\,. \tag{8.7}$$

This is a universal criterion that can be applied to a large variety of cases. Indeed, this argument was considered to be a standard result even before it had been put on a firm observational basis, and it was used to constrain the properties of neutrinos [69, 90, 132, 134, 135], axions [56, 64, 65, 73, 74, 86, 89], majorons [101], light supersymmetric particles [69, 122, 123], and of light scalar and vector bosons [116, 117, 119]. Some of these results are summarized in table 8.2. The bound on the Yukawa coupling of pseudoscalars thus derived is somewhat less restrictive than the above result based on the helium ignition argument.

It is important to recall that our general argument was based on a comparison between number counts (i.e., the evolutionary speed) of stars during the helium burning phase versus the MS near its turnoff. Hence we assumed implicitly that the MS evolution remains unaffected for particle parameters which substantially affect the helium burning configuration. This assumption is justified as long as the emission rates are steeply rising functions of temperature and density.

The duration of helium burning can also be constrained by the "R-method" where one compares the number of HB stars in a globular cluster with the number of red giants with luminosities exceeding the HB luminosity [433]. While this method allows for a more precise determination of t_{He}, it is a much more complicated argument because particle emission effects both quantities that are being compared,

Table 8.2
Constraints on the properties of light particles based on the observed duration of helium burning in low-mass stars, i.e., based on eq. (8.7)

Particle property	Dominant process	Constraint	References
Yukawa coupling, g_s (g_v), of scalar (vector) boson, ϕ, to electrons	bremsstrahlung $e^- + \alpha \to \alpha + e^- + \phi$	$g_s < 3 \times 10^{-14}$ $g_v < 2 \times 10^{-14}$	[116, 117]
Yukawa coupling, g_s (g_v), of scalar (vector) boson, ϕ, to baryons	Compton $\gamma + \alpha \to \alpha + \phi$	$g_s < 1.1 \times 10^{-10}$ $g_v < 0.8 \times 10^{-10}$	[116, 117]
Photoproduction cross section of Van der Velde's [118] X^0 boson	photoproduction $\gamma + \alpha \to \alpha + X^0$	$\sigma_{\mathrm{tot}} < 3 \times 10^{-50}\ \mathrm{cm}^2$	[119]
Yukawa coupling, g_p, of pseudoscalar boson, ϕ, to electrons	Compton $\gamma + e^- \to e^- + \phi$	$g_p < 0.8 \times 10^{-12}$	[56, 64, 65, 73] [74, 86, 87]
Effective coupling, $g_{p\gamma}$, of pseudoscalar boson, ϕ, to photons	Primakoff $\gamma + (\alpha, e^-) \to (\alpha, e^-) + \phi$	$g_{p\gamma} < 1 \times 10^{-10}\ \mathrm{GeV}^{-1}$	[87, 89]
Neutrino dipole moment	plasmon decay $\gamma_{\mathrm{pl}} \to \nu\bar{\nu}$	$\mu_\nu < 1 \times 10^{-11}\mu_B$	[90, 132, 134, 135]

although by different amounts. This method, therefore, does not allow one to derive a simple and general argument.

8.4.2. A numerical result: bounds on the axion–photon coupling

The general argument presented in the previous section was used by Raffelt and Dearborn [89] to derive a bound on the axion–photon coupling. Starting with the Lagrangian eq. (1.1) they derived the Primakoff emission rates for all conditions relevant during the evolution of a low-mass star from the MS to the AGB, and they included this rate in Dearborn's stellar evolution code. They followed the evolution of a $1.3M_\odot$ star with an initial helium abundance, $Y = 0.25$, and a metallicity, $Z = 0.02$, parameters that were motivated by the properties of the stars in the open cluster M67, a case that had been considered by Cannon [430] to derive an observational result for the helium burning lifetime (see section 8.4.1). The results of this numerical calculation are summarized in table 8.3 where we list the luminosity at the helium flash, $L_{\rm fl}$, the core mass at the flash, $M_{\rm c}$, identical with the core mass used for the following helium burning phase, the time it took to reach the helium flash from the zero-age MS, $t_{\rm fl}$, and the duration of helium burning, $t_{\rm He}$. Also, in fig. 8.7 we show the internal structure of this star on the RGB near the helium flash in the absence of axions, and with axions for $g_{a\gamma} = 10^{-9}\,\mathrm{GeV}^{-1}$.

It is important to note that the helium flash always occurred; it could not be suppressed even by unreasonably large values of $g_{a\gamma}$. This is understood because the Primakoff emission rates are strongly suppressed in the dense core because of correlation effects. For $g_{a\gamma} = 1 \times 10^{-10}\,\mathrm{GeV}^{-1}$, the core mass increased only by about $0.014M_\odot$, while $t_{\rm He}$ was reduced by almost a factor of 1/2. This behavior is understood because the core expands during the helium flash, its density dropping by 2 orders of magnitude until it reaches its helium burning equilibrium. At this reduced density at almost the same temperature the Primakoff emissivity is much larger, explaining why the helium burning phase is much more affected than the red giant phase. To illustrate this point we show, in fig. 8.6, the Primakoff emission rate from a pure helium plasma at $T = 10^8$ K as a function of density. Because the core mass before and after the helium flash is the same, this emission rate per unit mass is a direct measure of the total luminosity of the core.

In summary, the work of ref. [89] establishes a bound

$$g_{a\gamma} < 1 \times 10^{-10}\,\mathrm{GeV}^{-1}\,, \tag{8.8}$$

on the basis of the observed duration of helium burning, superseding refs. [61, 63, 65, 73, 74, 86] where incorrect emission rates had been used.

Table 8.3
Properties of a $1.3M_\odot$ star ($Y = 0.25$, $Z = 0.02$) at the helium flash (tip of the RGB), and helium burning lifetime after the flash, $t_{\rm He}$, for several values of the axion–photon coupling strength (taken from ref. [89]). $t_{\rm fl}$ is the time of the flash after formation of the star

$g_{a\gamma}$ $[10^{-9}\,\mathrm{GeV}^{-1}]$	$\log L_{\rm fl}$ $[L_\odot]$	$M_{\rm c}$ $[M_\odot]$	$t_{\rm fl}$ $[10^9\,\mathrm{yr}]$	$t_{\rm He}$ $[10^6\,\mathrm{yr}]$
0.00	3.34	0.477	5.4	120
0.10	3.42	0.491	5.3	69
0.30	3.68	0.546	5.3	16
1.00	4.00	0.648	4.5	
2.50	4.18	0.744	2.1	

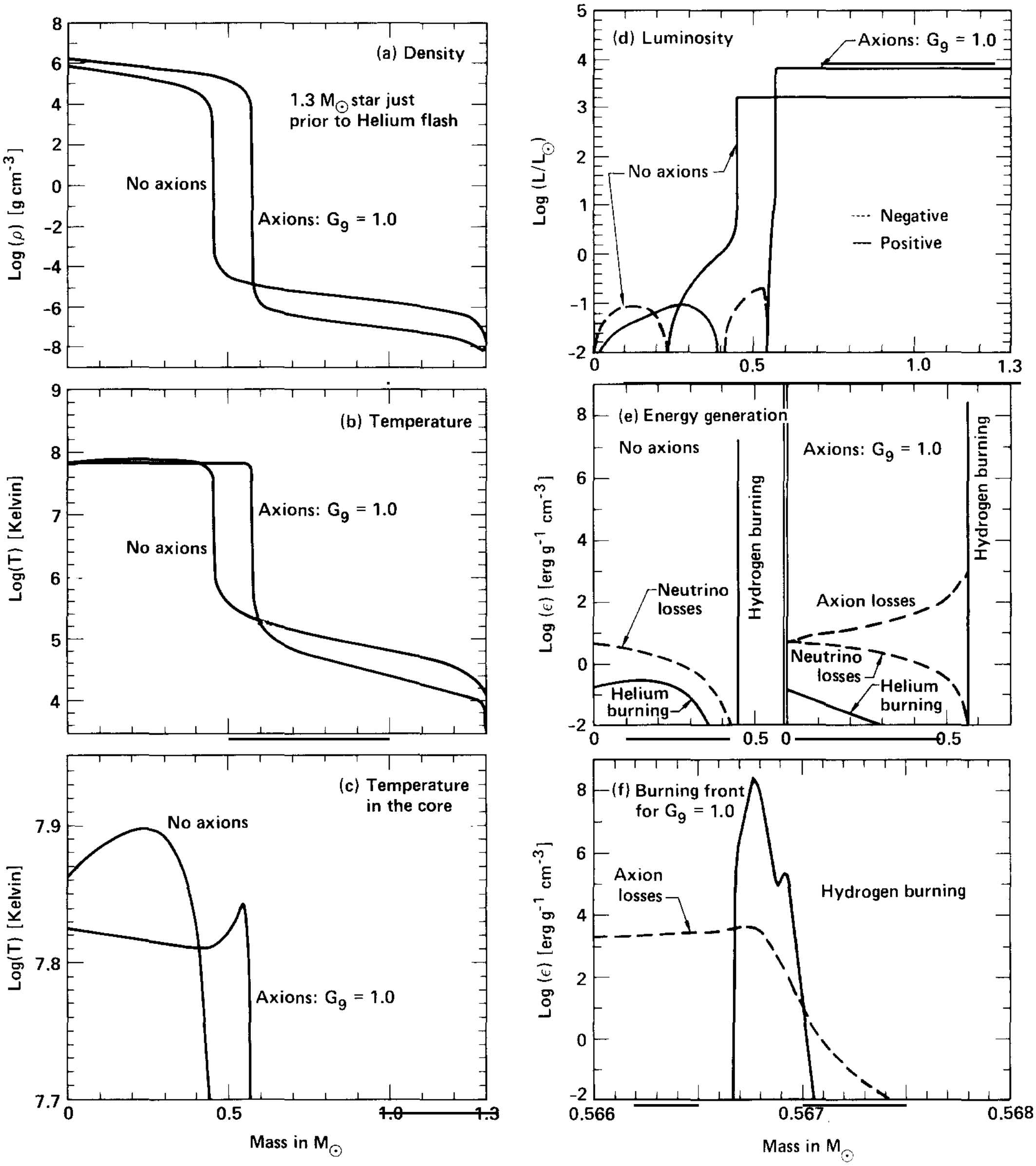

Fig. 8.7. Inner structure of a $1.3M_\odot$ star ($Y = 0.25$, $Z = 0.02$) near the helium flash, without axion emission and with Primakoff emission at the level $g_{a\gamma} = 10^{-9}\ \mathrm{GeV}^{-1}$. d. The dashed parts of the curves refer to negative values of L, i.e. to an inward heat flow. e, f. The dashed lines refer to energy losses (neutrinos, axions), while the solid lines refer to nuclear energy generation rates. (Taken from ref. [89].)

8.5. Core mass at the helium flash

8.5.1. General argument

The Primakoff emission of axions decreases with increasing density and thus, as shown in fig. 8.6, this emission rate sharply rises during the helium flash when the core of a red giant expands. In this case the helium burning lifetime was dramatically shortened although the core mass at the helium flash was hardly affected by axion emission, see table 8.3. In most cases, however, the situation will be reversed; the emission rate will be a rising function of density at a fixed temperature. As an example we show, in fig. 8.6 as a dashed line, the energy loss rate by plasmon decay (section 4.10), $\gamma_{pl} \to \nu\bar{\nu}$, for neutrinos with an anomalous magnetic dipole moment, μ_ν. In such cases the dominant effect of particle emission will be a delay of the helium flash, i.e., an increase of the core mass, δM_c, when helium finally ignites. The helium burning lifetime, t_{He}, will be shortened, but mostly because the core mass is larger, leading to an acceleration of the evolution that is familiar from hydrogen burning stars on the MS; more massive stars evolve faster. Also, the luminosity at the tip of the RGB will be larger, i.e., the observable break of the RGB will occur at an increased luminosity which, in turn, depends only on the increased core mass because hydrogen burning in a shell in red giants is mostly regulated by the core mass. In other words, the effect of particle emission in such cases can be discussed entirely in terms of an anomalous core mass increase, δM_c, which, in turn, can be related to the particle emission rates near the helium flash.

A discussion along these lines was recently performed by Raffelt [146] who considered the effect of δM_c on three independent observables of the color–magnitude diagrams of globular clusters. The first observable is the luminosity or rather absolute bolometric magnitude*) of RR Lyrae stars, M_{RR}. These stars are HB stars with a surface temperature near $10^{3.85}\,\mathrm{K} = 7080\,\mathrm{K}$, the "instability strip" where their surface layers exhibit a dynamic instability, leading to a pulsating luminosity. Their average bolometric magnitude is calculated to be [146]

$$M_{RR} = 0.59 - 3.5(Y_e - 0.25) + 0.16(3 + \log Z) - \Delta_{RR} - 7.3\,\delta M_c\,, \tag{8.9}$$

where Y_e is the envelope helium abundance, Z the metallicity, and Δ_{RR} the average brightness excess of RR Lyrae stars over zero-age HB models which are constructed such that their surface temperature falls into the RR Lyrae strip. δM_c is understood in units of the solar mass, $M_\odot$.

The second observable is the brightness at the tip of the RGB, i.e., at the helium flash, or rather, the brightness difference between this break of the RGB and the RR Lyrae stars. It is predicted to be [146]

$$\Delta M_{RR}^{tip} = 4.13 - 4.4(Y_e - 0.25) + 0.39(3 + \log Z) - \Delta_{RR} + 4.0\,\delta M_c\,. \tag{8.10}$$

Thus, an increased core mass causes the luminosity of HB stars to increase, and also causes the luminosity at the tip of the RGB to increase, but by different amounts so that the difference between the two is also predicted to increase. Clearly, the brightness difference between stars in the same cluster is observationally much better determined than the absolute magnitude of either RR Lyrae stars or the tip of the RGB which depend on an independent distance determination.

The third observable is the ratio, R, between the duration of helium burning over the duration of the red giant evolution, where in this context the RGB is understood to encompass only those red giants with luminosities exceeding RR Lyrae stars. This ratio is identical with the number ratio of stars on the HB versus the RGB in globular clusters. It is predicted to be [146]

$$\log R = 0.151 + 2.3(Y_e - 0.25) + 0.029(3 + \log Z) + 0.33\Delta_{RR} - 0.7\,\delta M_c\,. \tag{8.11}$$

*) We recall that the absolute bolometric magnitude is given in terms of the surface luminosity by $M_{bol} = 4.72 - 2.5\log(L/L_\odot)$. While this is a dimensionless number it is usually given in "magnitudes" or "mag" which is formally equivalent to 1, similar to the angular unit "rad".

From observations of the intrinsic properties of globular clusters one obtains the following results [146]:

$$\begin{aligned} \Delta M_{\mathrm{RR}}^{\mathrm{tip}} &= (4.19 \pm 0.03) + (0.41 \pm 0.06)(3 + \log Z)\,, \\ \log R &= (0.162 \pm 0.016) + (0.065 \pm 0.032)(3 + \log Z)\,, \end{aligned} \tag{8.12}$$

where the errors reflect 1σ statistical uncertainties of the observations. The predicted and observed metallicity dependences agree well with each other, allowing one to eliminate the terms in $\log Z$. Moreover, by statistical parallax determinations of field RR Lyrae stars one finds

$$\langle M_{\mathrm{RR}} \rangle = 0.62 \pm 0.14\,, \tag{8.13}$$

where the sample has an average metallicity of $\log Z \sim -2.7$. Combining these results leads to three expressions for the envelope helium abundance,

$$\begin{aligned} \Delta M_{\mathrm{RR}}^{\mathrm{tip}}: &\quad Y_{\mathrm{e}} = (0.237 \pm 0.007) - 0.23\Delta_{\mathrm{RR}} + 0.91\,\delta M_{\mathrm{c}}\,, \\ M_{\mathrm{RR}}: &\quad Y_{\mathrm{e}} = (0.237 \pm 0.040) - 0.29\Delta_{\mathrm{RR}} - 2.09\,\delta M_{\mathrm{c}}\,, \\ R: &\quad Y_{\mathrm{e}} = (0.251 \pm 0.008) - 0.14\,\Delta_{\mathrm{RR}} + 0.31\,\delta M_{\mathrm{c}}\,. \end{aligned} \tag{8.14}$$

One may then use either the first and third or the second and third equations to eliminate the helium abundance, leading to

$$\delta M_{\mathrm{c}} = +0.023 \pm 0.018 + 0.15\Delta_{\mathrm{RR}}\,, \qquad \delta M_{\mathrm{c}} = -0.006 \pm 0.017 - 0.06\Delta_{\mathrm{RR}}\,. \tag{8.15}$$

Combining these results one may safely neglect the Δ_{RR} term since this quantity will be $\lesssim 0.2$ mag so that one finds an allowed regime [146]

$$\delta M_{\mathrm{c}} = 0.009 \pm 0.012\,. \tag{8.16}$$

In order to appreciate the tightness of this constraint we mention that "switching off" the standard neutrino losses would lead to $\delta M_{\mathrm{c}} \sim -0.030 M_{\odot}$, i.e., the observations are marginally sensitive to the standard neutrino losses at the helium flash, leaving little if any room for exotic particle losses.

8.5.2. A specific constraint: neutrino dipole moments

If neutrinos had anomalous magnetic or electric dipole moments, the enhanced plasmon decay rate (section 4.10) would lead to an increased core mass of [146]

$$\delta M_{\mathrm{c}} = 0.015 M_{\odot} \times \mu_\nu / 10^{-12} \mu_{\mathrm{B}} \tag{8.17}$$

[Bohr magneton $\mu_{\mathrm{B}} = e/2m_{\mathrm{e}}$; for the definition of μ_ν see eq. (4.87)]. In conjunction with eq. (8.16) this yields

$$\mu_\nu < 3 \times 10^{-12} \mu_B \,. \tag{8.18}$$

This is the most restrictive constraint on anomalous neutrino dipole moments.

9. The white dwarf luminosity function

The number of white dwarfs per luminosity interval in the solar neighborhood provides a direct measure of the cooling speed of these stars, constraining the efficiency of any energy loss mechanism other than the standard neutrino volume emission (young white dwarfs) and photon surface radiation. One finds a constraint of $\alpha_a \lesssim 10^{-26}$ for the "fine-structure constant" of light pseudoscalar particles to electrons. An anomalous neutrino magnetic dipole moment has also been constrained, $\mu_\nu \lesssim 10^{-11} \mu_B$ (Bohr magnetons).

9.1. White dwarfs; theoretical and observed properties

White dwarfs (WDs) represent the final state of the evolution of stars with initial masses of up to a few $M_\odot$. For reviews see refs. [301, 434, 435]. They are compact objects which are supported by electron degeneracy pressure and thus are in hydrostatic equilibrium without need for nuclear burning; the hydrostatic and thermal properties are largely decoupled. The radius of a WD decreases with increasing mass because, in order to support the extra weight, the electrons must be squeezed into higher momentum states. As long as they remain nonrelativistic, one finds from a polytropic approximation of the WD structure [301],

$$R = 8880\,\mathrm{km}\,(M_\odot/M)^{1/3}(2/\mu_e)^{5/3} \,. \tag{9.1}$$

The pressure is provided mostly by the degenerate electrons, while the self-gravity is mostly due to the nucleons which is why the "mean molecular weight of the electrons", μ_e, appears. WDs typically do not contain any hydrogen so that $\mu_e = 2$. However, if the mass becomes so large and the radius so small that the electrons become relativistic, there exists no stable configuration, i.e., the masses of WDs must be below the Chandrasekhar limit [301],

$$M_{\mathrm{Ch}} = 1.457 M_\odot (2/\mu_e)^2 \,. \tag{9.2}$$

Observationally it turns out, however, that the WD mass distribution is strongly peaked near $M = 0.6 M_\odot$ [436] so that in observed WDs a nonrelativistic treatment of the electrons is appropriate. In a polytropic approximation, the central density of WDs is given by [301]

$$\rho_c = 1.46 \times 10^6\,\mathrm{g\,cm^{-3}}\,(M/0.6 M_\odot)^2 (\mu_e/2)^5 \,. \tag{9.3}$$

Since stars of masses up to a few $M_\odot$ are believed to become WDs, the excess mass is lost before reaching the WD stage. In particular, a large fraction of the mass is ejected when the star ascends the asymptotic giant branch, just prior to collapsing to a WD. The ejected material forms a "planetary nebula" so that the central stars of planetary nebulae are identified with nascent WDs. The rate of WD formation as inferred from the luminosity function discussed below is in good agreement with the observed formation rate of planetary nebulae within the statistical and systematic uncertainties of a factor of ~2 [437]. A theoretical evolutionary path for a $3M_{\odot}$ star from the main-sequence to the WD stage was performed, e.g., in ref. [438].

The hottest and brightest WDs have a luminosity of $L \sim 10^{-1} L_{\odot}$ while for the faintest ones $L \sim 4 \times 10^{-5} L_{\odot}$. Thus, in spite of being hot, WDs are generically faint because of their small surface area. This implies that they can be observed only in the immediate solar neighborhood, typically out to ~100 pc for bright WDs. Since the vertical scale height of the galactic disk of ~250 pc [439] is much larger, the observed WDs essentially fill a spherical volume around the Sun and it is customary to express the observations in terms of a volume density. The total density of degenerates is on the order of $10^{-2}\,\mathrm{pc}^{-3}$. The observed luminosity function, i.e., the density of WDs per brightness interval, is shown in fig. 9.1 and listed in table 9.1 according to refs. [437, 439]. The luminosity function is characterized by three important features: its slope, which characterizes the form of the cooling law, its amplitude, which characterizes the cooling time and WD birthrate, and its sudden break at $\log(L/L_{\odot}) \sim -4.7$, which characterizes the beginning of WD formation, i.e., the oldest WDs have not yet reached lower luminosities. From this break one can derive an age for the galactic disk of (9.3 ± 2.0) Gyr where 1 Gyr = 10^9 yr [440]. All of these features can be used to constrain the operation of a novel cooling mechanism.

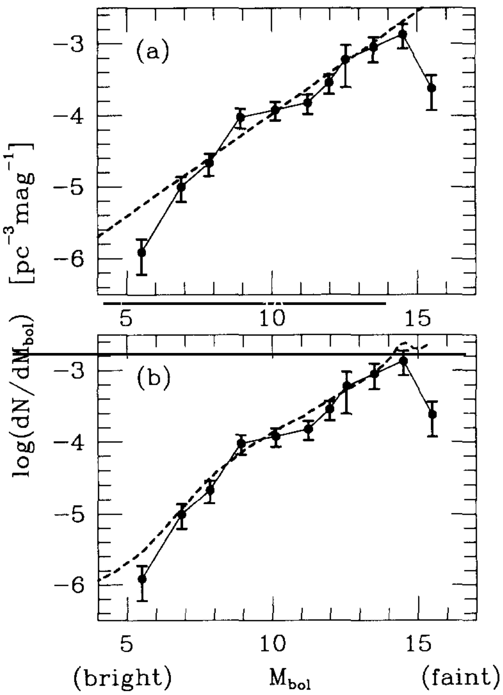

Fig. 9.1. Observed luminosity function of white dwarfs as listed in table 9.1. a. The dashed line represents Mestel's cooling law with an assumed constant white dwarf birthrate of $B = 10^{-3}\,\mathrm{pc}^{-3}\,\mathrm{Gyr}^{-1}$. b. The dashed line was obtained from the numerical cooling curve of ref. [444] for a $0.6M_{\odot}$ white dwarf, assuming the same constant birthrate. Standard neutrino cooling was included in this calculation.

Table 9.1
Observed luminosity function for white dwarfs. The data were taken from refs. [437, 439]. For the hot and bright degenerates (upper part of the table) a large fraction of their spectrum lies in the ultraviolet regime, causing a large discrepancy between the absolute visual magnitude, M_V, and the absolute bolometric magnitude, M_{bol}. For the hot dwarfs, the bins originally had been chosen on the M_V-scale with a width of 0.5 mag, centered on the half-magnitudes, and the listed M_{bol} is the mean in these intervals. Note that $\log(L/L_\odot) = (4.72 - M_{bol})/2.5$

M_V	Mean M_{bol}	Mean $\log_{10}(L/L_\odot)$	dN/dM_{bol} [$pc^{-3}\,mag^{-1}$]	$\log_{10}(dN/dM_{bol})$
9.5	5.50	−0.31	1.22×10^{-6}	−5.91 (+0.18, −0.31)
10.0	6.88	−0.86	1.01×10^{-5}	−5.00 (+0.14, −0.21)
10.5	7.84	−1.25	2.16×10^{-5}	−4.67 (+0.13, −0.18)
11.0	8.92	−1.68	9.56×10^{-5}	−4.02 (+0.12, −0.16)
11.5	10.12	−2.16	1.21×10^{-4}	−3.92 (+0.11, −0.15)
12.0	11.24	−2.61	1.51×10^{-4}	−3.82 (+0.11, −0.16)
12.5	11.98	−2.90	2.92×10^{-4}	−3.54 (+0.11, −0.16)
13.0	12.55	−3.13	6.07×10^{-4}	−3.22 (+0.20, −0.39)
	13.50	−3.51	0.89×10^{-3}	−3.05 (+0.14, −0.21)
	14.50	−3.91	1.34×10^{-3}	−2.87 (+0.14, −0.20)
	15.50	−4.31	0.24×10^{-3}	−3.62 (+0.18, −0.31)

9.2. Cooling theory for white dwarfs

A low-mass star becomes a WD when its nuclear energy resources have been exhausted; it shines its residual thermal energy. Therefore the evolution of a WD must be viewed as a cooling process as was first pointed out by Mestel [441]. Because electron conduction is an efficient mechanism of energy transfer, the interior can be viewed, in a first approximation, as an isothermal heat bath with a total amount of thermal energy, U. The nondegenerate surface layers have a large "thermal resistance" and efficiently isolate the hot interior from the cold surrounding space, throttling the energy loss by photon radiation, L_γ. Of course, WDs can also lose energy by neutrino volume emission, L_ν, and by other particle emission, L_x. Hence WD cooling is governed by the equation

$$dU/dt = -(L_\gamma + L_\nu + L_x)\,. \tag{9.4}$$

This simple picture ignores the possibility of residual nuclear burning near the surface, a possibly important luminosity source for faint WDs [442]. In order to translate this equation into the observable luminosity function, we assume a constant WD birthrate, B, so that the total number density of degenerates is $N = Bt_{gal}$. Taking the above values of $N \sim 10^{-2}\,pc^{-3}$ and $t_{gal} = 9.3$ Gyr for the age of the galactic disk, one has $B \sim 10^{-3}\,pc^{-3}\,Gyr^{-1}$. Since the number density of WDs in a given magnitude interval, dM_{bol}, is proportional to the time interval, dt, it takes to cool through this magnitude range, one readily obtains

$$\frac{dN}{dM_{bol}} = B\,\frac{dt}{dM_{bol}} = -B\,\frac{dU/dM_{bol}}{L_\gamma + L_\nu + L_x}\,. \tag{9.5}$$

The photon luminosity is related to the bolometric magnitude by

$$L_\gamma = 77.3 L_\odot 10^{-2M_{bol}/5}\,. \tag{9.6}$$

This definition is equivalent to $\log(L_\gamma/L_\odot) = (4.72 - M_{\rm bol})/2.5$. L_γ is related to the internal temperature, T, by the thermal conductance of the surface layers, while U, L_ν, and $L_{\rm x}$ are given in terms of T, so that one can express these quantities in terms of L_γ and hence $M_{\rm bol}$. In this simple treatment we have assumed identical properties for all WDs, and especially a fixed mass, M.

For hot WDs, the thermal energy is largely stored in the nondegenerate nuclei. Treating the nuclei as an ideal gas, the internal energy is

$$U = \frac{3}{2}\, T\, \frac{M}{m_{\rm u}} \sum_j \frac{X_j}{A_j} \equiv CT\,, \tag{9.7}$$

where X_j is the mass fraction of the element j with the atomic mass A_j, $m_{\rm u} = 1.661 \times 10^{-24}$ g is the atomic mass unit. Numerically,

$$C = 3.95 \times 10^{-2}\, \frac{L_\odot\, {\rm Gyr}}{10^7\,{\rm K}}\, \frac{M}{M_\odot} \sum_j \frac{X_j}{A_j}\,. \tag{9.8}$$

At sufficiently low temperatures, the ideal-gas law breaks down, and eventually the nuclei arrange themselves in a crystal lattice. In these phases, the internal energy is a more complicated function of temperature. The heat capacity per nucleon, which is 3/2 for the ideal-gas law, rises to 3 near the Debye temperature, $\Theta_{\rm D}$, and then drops to zero approximately as $(16\pi^4/5)(T/\Theta_{\rm D})^3$ [301]. However, since the observed WD masses are around $0.6M_\odot$, the densities of these stars are small enough that even the oldest WDs have not had enough time to reach the crystallization phase. Hence the ideal-gas law is a reasonable first approximation.

The thermal conductance of the surface layers is more difficult to calculate. In order to estimate the energy flux, one has to solve the stellar structure equations (6.1) and (6.4) for these layers. Assuming a Kramer's opacity law, $\kappa = \kappa_0 \rho T^{-7.2}$, one finds approximately [301, 443]

$$L = 1.7 \times 10^{-3} L_\odot (M/M_\odot)(T/10^7\,{\rm K})^{7/2} \equiv KT^{7/2}\,, \tag{9.9}$$

where T is the internal temperature.

With these results the luminosity function is found to be

$$\frac{{\rm d}N}{{\rm d}M_{\rm bol}} = \frac{4\ln(10)}{35}\, B\, \frac{C(L_\gamma/K)^{2/7}}{L_\gamma + L_\nu + L_{\rm x}}\,. \tag{9.10}$$

With $B_{-3} \equiv B/10^{-3}\,{\rm pc}^{-3}\,{\rm Gyr}^{-1}$, this is numerically

$$\frac{{\rm d}N}{{\rm d}M_{\rm bol}} = B_{-3} \cdot 2.2 \times 10^{-4}\,{\rm pc}^{-3}\,{\rm mag}^{-1}\, \frac{10^{-4M_{\rm bol}/35}}{77.3 \times 10^{-2M_{\rm bol}/5} + L_\nu/L_\odot + L_{\rm x}/L_\odot} \left(\frac{M}{M_\odot}\right)^{5/7} \sum_j \frac{X_j}{A_j}\,. \tag{9.11}$$

If we ignore L_ν and $L_{\rm x}$, this is

$$\frac{{\rm d}N}{{\rm d}M_{\rm bol}} = B_{-3} \cdot 2.9 \times 10^{-6}\,{\rm pc}^{-3}\,{\rm mag}^{-1}\, 10^{2M_{\rm bol}/7} \left(\frac{M}{M_\odot}\right)^{5/7} \sum_j \frac{X_j}{A_j}\,. \tag{9.12}$$

Taking now $M = 0.6M_\odot$ and an equal mixture of ^{12}C and ^{16}O we find

$$\log(\mathrm{d}N/\mathrm{d}M_{\mathrm{bol}}) = \tfrac{2}{7}M_{\mathrm{bol}} - 6.84 + \log(B_{-3}) , \tag{9.13}$$

a behavior known as Mestel's cooling law. For $B_{-3} = 1$ this function is shown as a dashed line in fig. 9.1a. Detailed cooling curves and luminosity functions have been calculated, for example, in refs. [440, 442, 444–447] while the elementary treatment is described in Mestel's original paper [441] and in refs. [301, 443].

9.3. Neutrino losses included

In numerical calculations it is easy to include standard neutrino losses. The dominant emission process at the relevant conditions is the plasma process, $\gamma_{\mathrm{pl}} \rightarrow \nu_e\bar{\nu}_e$. In fig. 9.1b we show a luminosity function which we have derived from a numerical cooling curve published in ref. [444] for a $0.6M_\odot$ white dwarf, assuming a constant WD birthrate of $10^{-3}\ \mathrm{pc}^{-3}\ \mathrm{Gyr}^{-1}$ as above. From fig. 9.1b and from the theoretical luminosity functions of other authors, e.g. ref. [440], it appears that the dip in the luminosity function for bright WDs should be associated with neutrino losses.

If the neutrino emission rate were much stronger than standard, the dip would be much deeper. The observation of several bright WDs in the Hyades cluster was used by Stothers [41] to constrain the efficiency of neutrino cooling. He found that an emission rate 300 times stronger than standard could be conservatively excluded. If neutrinos had anomalous electric or magnetic dipole moments the standard plasmon decay rate would be enhanced – the ratio between the "exotic" and the standard rate were given in eq. (4.92). Hence Stother's result implies $\mu_\nu \lesssim 3\times 10^{-11}\mu_{\mathrm{B}}$.

Recently, Blinnikov [131] has considered the WD luminosity function, including nonstandard neutrino losses. He found that the "neutrino dip" at the bright side of the luminosity function was too deep unless

$$\mu_\nu < 10^{-11}\mu_{\mathrm{B}} , \tag{9.14}$$

when comparing his theoretical cooling times with the empirical luminosity function of field WDs, shown in fig. 9.1. [For a discussion of the plasma decay rate see section 4.10 and especially for the definition of μ_ν see eq. (4.87).]

9.4. Axion bounds

It is now very simple to derive conservative bounds on the coupling of axions or other pseudoscalar particles to electrons, results which were first discussed in ref. [88] and corrected for ion correlation effects in refs. [84, 85]. The emission rate for the relevant conditions of a degenerate, strongly coupled plasma were given in eq. (4.51), and we use a "correlation factor", $F = 1.0$, as discussed at the end of section 4.6. We assume an equal mixture of carbon and oxygen. Then we find for the axion luminosity as a function of the interior temperature,

$$L_{\mathrm{a}} = \alpha_{\mathrm{a}}\cdot 2.0\times 10^{23} L_\odot (M/M_\odot)(T/10^7\ \mathrm{K})^4 , \tag{9.15}$$

where α_{a} is the "axionic fine-structure constant". This expression enters eq. (9.11) in place of L_x. It is interesting that the temperature variation of this expression is almost identical to that of the photon luminosity, eq. (9.9), so that the shape of the cooling curve would remain essentially unchanged, even if axion cooling dominated the WD energy loss, in contrast with neutrino cooling, which changes the shape of the luminosity function. Also, if we were to consider scalar as opposed to pseudoscalar particles, the bremsstrahlung emission rate would be proportional to T^2 rather than T^4, the extra factor of T^2 for pseudoscalars arising from the spin-flip nature of the emission process. Thus, if scalars dominated WD cooling, the shape of the luminosity function would be altered.

If axion emission dominated WD cooling, the overall amplitude of the luminosity curve would be reduced correspondingly, and since the shape remains approximately unchanged, the empirically inferred birthrate of WDs would be increased by a factor $1 + L_a/L_\gamma$. Since the birthrate inferred from the luminosity function corresponds within a factor ~2 to the observed birthrate of planetary nebulae, it is justified to use $L_a \lesssim L_\gamma$ as a constraint on the axion luminosity. Moreover, the overall time scale of cooling would be reduced by a factor $(1 + L_a/L_\gamma)^{-1}$. The sharp drop in the luminosity function at the faint end is interpreted as the beginning of WD formation, implying an age of the galactic disk of ~9 Gyr. Any contribution of axion cooling would reduce this number. Recalling that the age of the solar system is known to be 4.5 Gyr, a reduction of the age of the galactic disk by a factor of 2 appears to be an extremely generous allowance, i.e., $L_a < L_\gamma$ is a very conservative constraint. Taking a WD mass of $0.6 M_\odot$, the internal temperature for faint dwarfs ($M_{\rm bol} = 14$) is $\sim 6 \times 10^6$ K, leading to $L_a/L_\gamma = \alpha_a \cdot 1.17 \times 10^{26} (T/10^7\ \mathrm{K})^{1/2} = \alpha_a \cdot 0.91 \times 10^{26}$. Hence the requirement $L_a < L_\gamma$ leads to the constraint

$$\alpha_a < 1.1 \times 10^{-26}\,, \tag{9.16}$$

valid for all pseudoscalars with masses $m_a \lesssim 1$ keV. A corresponding constraint for scalars or other light particles has not been derived in the literature.

10. Cooling of nascent and young neutron stars

The observation of a neutrino pulse from SN 1987A confirmed the theoretically expected cooling speed of nascent neutron stars to be a few seconds. This result excludes excessive cooling by axions, right-handed neutrinos, or other novel low-mass particles, allowing one to derive bounds on the axion–nucleon coupling, right-handed neutrino coupling, masses as well as electromagnetic dipole moments of Dirac neutrinos, and other particle properties. The cooling speed of young neutron stars ($t \sim 10^3$ and 10^4 yr) can be established by the observation of thermal surface radiation (X-rays) from pulsars of known age, and measurements of the Einstein Observatory allow one to set tentative constraints on exotic cooling agents.

10.1. Birth and cooling of neutron stars

10.1.1. Stellar collapse

While in chapters 8 and 9 we have discussed how time scales of stellar evolution can be determined statistically from ensembles of stars and can then be used to constrain novel forms of energy loss, we now consider neutron stars, objects which evolve so fast that we have direct evidence for individual cooling time scales. Neutron stars are born in type II supernova explosions which occur when stars of masses exceeding $\sim 10 M_\odot$ have developed a large iron core which no longer can produce energy by nuclear burning (for recent reviews see refs. [159, 448]). At the time of collapse, such a star consists of an iron core of $\sim 1.3 M_\odot$ at a density of $\sim 10^{10}\,\mathrm{g\,cm^{-3}}$ and a temperature of $\sim 7.6\times 10^9\,\mathrm{K} = 0.66\,\mathrm{MeV}$, of a mantle of $\sim 3 M_\odot$ with nuclear burning in several shells, and an envelope of unprocessed hydrogen and helium. At this point the medium becomes unstable to two reactions, the photodissociation of iron, $\gamma + {}^{56}\mathrm{Fe} \to 13\alpha + 4\mathrm{n}$, and electron capture, $\mathrm{e}^- + \mathrm{p} \to \mathrm{n} + \nu_\mathrm{e}$. The former reaction is endothermic and thus absorbs energy, while the neutrinos produced in the latter reaction at first escape freely, also draining the star of energy. Therefore, further compression fails to increase the pressure enough to support the core, resulting in a run-away of these reactions and an almost free-fall collapse.

As the core becomes hotter and denser, neutrinos become trapped at a density of $\sim 3\times 10^{11}\,\mathrm{g\,cm^{-3}}$, i.e., their mean free path becomes smaller than the core radius, and from then on they are entrained by the collapsing material. The infall is halted only when the medium reaches nuclear densities where the equation of state stiffens. The sudden interception of the collapse leads to a "bounce", i.e., the formation of a shock wave at a mass shell around $(0.8\text{–}0.9) M_\odot$, well inside the iron core. This shock wave moves outward, depositing energy and thus dissociating the nuclei of the medium as it passes. When it reaches the neutrino-sphere, i.e., the shell inside of which neutrinos are trapped, the dissociation of the nuclei leads to a sudden decrease of the coherent neutrino cross-sections and thus to a break-out of the neutrino luminosity (fig. 10.1). When the shock reaches the edge of the iron core after ~ 1 s, a "proto-neutron star" or "nascent neutron star" has formed, and about half of its binding energy, $E_\mathrm{b} \sim (2\text{–}3)\times 10^{53}$ erg, has already been emitted. The further evolution must be viewed as a cooling phenomenon, not unlike the cooling of a white dwarf. This means that the star is now essentially supported by degeneracy pressure so that its further thermal evolution (cooling) does no longer change its structure in any dramatic way.

10.1.2. SN 1987A neutrino observations

While the emission of neutrinos from a fixed neutrino sphere over the next several seconds with a thermal spectrum is an oversimplification, such a cooling model is sufficiently detailed to allow for a comparison with the sparse data from the neutrino observations of SN 1987A (tables 10.1 and 10.2).

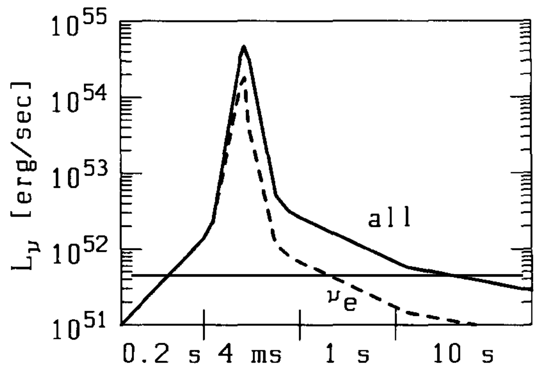

Fig. 10.1. Schematic view of the neutrino luminosity expected from a type II supernova (adapted from Cooperstein in ref. [159]). There are several breaks of scale in the horizontal axis, separating the following periods: first ~ 0.2 s, infall from core density, $\sim 10^{10}\,\mathrm{g\,cm^{-3}}$, to maximum scrunch, $\sim 10^{15}\,\mathrm{g\,cm^{-3}}$; next ~ 0.004 s, from bounce to shock breakout at the neutrino sphere; further ~ 1 s until shock reaches edge of iron core; in the following ~ 10 s, most of the remaining binding energy is radiated from the neutrino sphere.

Table 10.1
Neutrino burst from SN 1987A in the IMB detector [166]. The event time is relative to the first event which occurred on 23 February 1987, 7:35:41.374 (UT), with an uncertainty of ± 0.05 s. The angle is the polar angle with respect to the direction away from the SN. The energy is the measured energy of the electron or positron. If the events were due to $\bar{\nu} + p \to n + e^+$ on free protons, $E_{\bar{\nu}}$ was typically ~2 MeV larger than the measured e^- energy

Event	Time [s]	Angle [deg]	Energy [MeV]
1	0.00	80 ± 10	38 ± 7
2	0.41	44 ± 15	37 ± 7
3	0.65	56 ± 20	28 ± 6
4	1.14	65 ± 20	39 ± 7
5	1.56	33 ± 15	36 ± 9
6	2.68	52 ± 10	36 ± 6
7	5.01	42 ± 20	19 ± 5
8	5.58	104 ± 20	22 ± 5

Table 10.2
Neutrino burst from SN 1987A in the Kamiokande-II detector [168]. The event time is relative to the first event which occurred on 23 February 1987, 7:35:35 (UT), with an uncertainty of $\pm 1{:}00$ min. The angle is the polar angle with respect to the direction away from the SN. The energy is the measured energy of the electron or positron

Event	Time [s]	Angle [deg]	Energy [MeV]
1	0.00	18 ± 18	20.0 ± 2.9
2	0.11	40 ± 27	13.5 ± 3.2
3	0.30	108 ± 32	7.5 ± 2.0
4	0.32	70 ± 30	9.2 ± 2.7
5	0.51	135 ± 23	12.8 ± 2.9
6	0.69	68 ± 77	6.3 ± 1.7
7	1.54	32 ± 16	35.4 ± 8.0
8	1.73	30 ± 18	21.0 ± 4.2
9	1.92	38 ± 22	19.8 ± 3.2
10	9.22	122 ± 30	8.6 ± 2.7
11	10.43	49 ± 26	13.0 ± 2.6
12	12.44	91 ± 39	8.9 ± 1.9

The most detailed analysis along these lines was performed by Loredo and Lamb [211] who were the first authors to include the detector background events in their analysis. They investigated a variety of cooling models and found that an exponential cooling model was preferred with a constant radius of the neutrino sphere, $R_{\rm obs}$, and a time-varying temperature,

$$T(t) = T_0\, e^{-t/4\tau}\,, \tag{10.1}$$

so that τ is the luminosity decay time scale. Moreover, they used the parameter

$$\alpha \equiv (R_{\rm obs}/10\,{\rm km})(50\,{\rm kpc}/D) g^{1/2}\,, \tag{10.2}$$

where D is the distance to SN 1987A and g is a weight factor which is unity if only left-handed, massless neutrinos of any given flavor are being emitted (three flavors are assumed to exist). They also took the mass of the electron neutrino as a free parameter in order to allow for signal dispersion, and they introduced two separate offset times for the IMB and Kamiokande II detectors between the arrival of the first neutrinos and the first detected event. Hence they allowed the following six parameters to vary in order to achieve a maximum likelihood result: T_0, τ, α, m_{ν_e}, $t_{\rm off}$(IMB), and $t_{\rm off}$(KII). The best-fit values are given in table 10.3, first column, where we also show the inferred values for the neutron star proper radius, R, the total amount of binding energy, and the number of expected neutrino detections in each detector. In fig. 10.2 we show the projection of the 68% and 95% confidence volume on the T_0–τ-plane. The neutrino mass is found to be limited by 23 eV at the 95% CL, and taking this value as a fixed choice, the best-fit values for the remaining five parameters are given in table 10.3, second column.

These results confirm beautifully the standard picture of neutron star formation, and in particular confirm the expected values for the temperature at the neutrino sphere, the time scale of cooling, and the total amount of energy which was radiated in neutrinos. This latter result directly excludes the possible existence of more than two or three extra neutrino flavors, a result which is, of course, obsolete

Table 10.3
Maximum likelihood results inferred from the observed neutrino pulse of SN 1987A, using an exponential cooling model, and including detector background events in the analysis (Loredo and Lamb [211]). If the neutrino mass is taken to be a free parameter, the best-fit result is $m_{\nu_e} = 0$, with all other parameters having the best-fit values shown in the first column. In the second column, we show the results if m_{ν_e} is assumed to be 23 eV, a value which is an upper limit at the 95% CL

Fitted parameters			Inferred parameters		
m_{ν_e}	0	23 eV	m_{ν_e}	0	23 eV
T_0	4.47 MeV	4.84 MeV	E_b	2.86×10^{53} erg	2.33×10^{53} erg
τ	4.15 s	2.96 s	R	22.6 km	20.6 km
α	2.26	2.06	N_{det} (KII)	12.5	11.5
t_{off} (KII)	0	3.57 s	N_{det} (IMB)	5.51	6.14
t_{off} (IMB)	0	0.85 s			

in view of the recent precision measurements of the Z^0 width at SLAC [449] and CERN [450–453]. Most important for our purposes is the confirmation of the cooling time scale which was not excessively shortened by novel effects. This conclusion remains valid even if one allows for signal dispersion, i.e., the inferred time scale of neutrino emission at the source is not very sensitive even to an extreme choice of an assumed neutrino mass.

10.1.3. Late-time cooling and Einstein observations

After a few seconds, the temperature at the neutrino sphere has dropped so much that the IMB and Kamiokande II detectors are no longer sensitive to the neutrino flux, but the star continues to cool by surface neutrino emission. When the inner temperature has reached $\sim 10^9\,\mathrm{K} \sim 100\,\mathrm{keV}$ after (10–100) yr, the neutron star becomes transparent to neutrinos, and continues to cool by neutrino volume

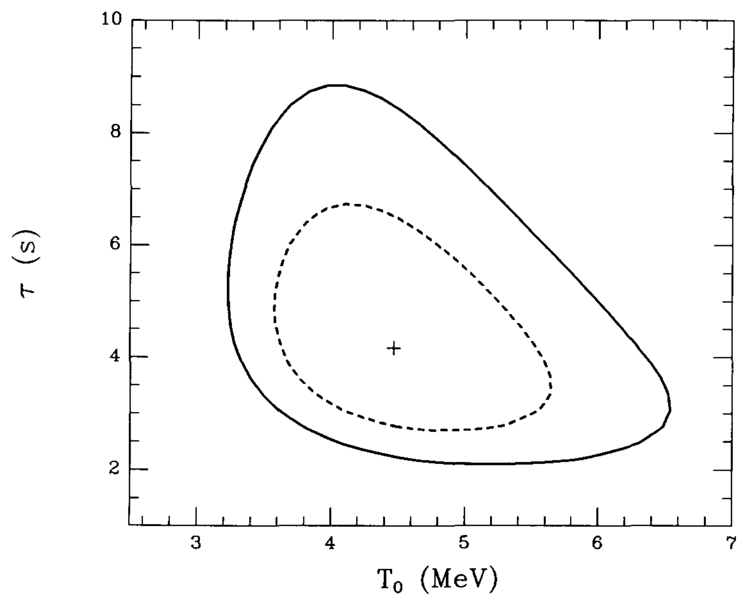

Fig. 10.2. Projection of the 68% (dashed line) and 95% (solid line) confidence volume for the exponential cooling model (Loredo and Lamb [211]). The cross marks the best-fit values (see first column in table 10.3). (I thank T. Loredo for providing an original for this figure.)

emission. After $\sim 10^5$ yr it reaches an inner temperature of $\sim 2\times 10^8$ K, a point at which photon emission from the surface becomes the dominant form of cooling. In fig. 10.3 we show the central temperature, surface temperature, neutrino luminosity, and photon luminosity as functions of age, taken from a numerical calculation of Nomoto and Tsuruta [454], their case "FP" which corresponds to a phenomenological equation of state of intermediate stiffness.

Such calculations can be confronted with observations by using data of the Einstein Observatory, the X-ray satellite HEAO-2 that was launched in 1979. In several supernova remnants, X-ray emission from a compact source was discovered, while in most cases the non-observation of such a source allows one to set an upper limit (see table 10.4). In these cases it is not even certain whether there is a neutron star in the SN remnant. The absence of a neutron star can be understood since type I supernovae are thought to occur when a white dwarf accretes enough material to ignite carbon, leading to a nuclear run-away and likely to the disruption of the star. Hence type I supernovae are physically completely distinct from type II. The absence of a neutron star can also be understood if black holes form in some type II supernovae.

Therefore, the most crucial test consists of a comparison of the four X-ray sources in SN remnants listed in table 10.4, 3C 58, the Crab pulsar, RCW-103, and the Vela pulsar, where the effective surface temperatures were quantitatively established. Given the large uncertainties in the observations and in the theoretical predictions, we may group the first three cases together at an age of $\sim 10^3$ yr where they yield a surface temperature of $(2.0–2.4)\times 10^6$ K, while the Vela pulsar yields $(0.8–1.1)\times 10^6$ K at $t\sim 10^4$ yr (see table 10.5). Standard cooling calculations, notably of Nomoto and Tsuruta [454, 456], using a variety of plausible equations of state, and including such effects as nucleon superfluidity and

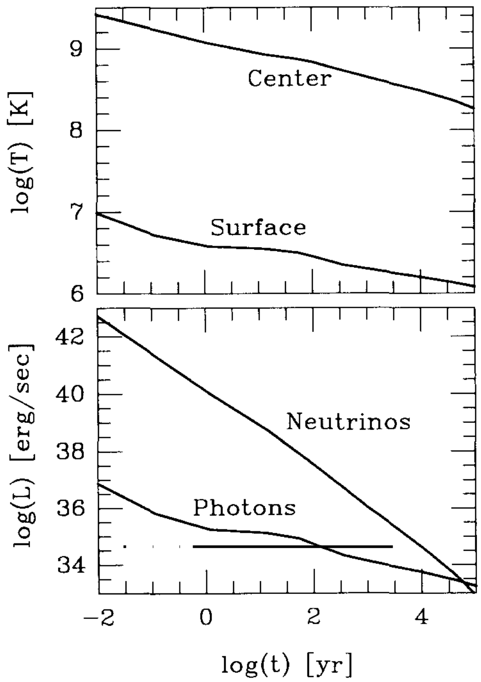

Fig. 10.3. Cooling of a neutron star with an equation of state of intermediate stiffness, ignoring such effects as nucleon superfluidity or a pion condensate (after Nomoto and Tsuruta [454], case FP).

Table 10.4
Einstein observations of supernova remnants, adapted from Tsuruta [455]. An h in the age column refers to a historical supernova. The uncertainty of the observations is mostly due to the uncertain amount of interstellar absorption

Name	Age [yr]	Pulsar detected	T_{eff} of compact source [10^6 K]	
			detection	upper limit
Cas A	300 (h)	–		1.5 ± 0.1
Kepler	375 (h)	–		2.0 ± 0.2
Tycho	407 (h)	–		1.1 ± 0.1
3C 58	(800) (h)	–	2.2 ± 0.2	
Crab	925 (h)	radio, optical, X-rays	2.2 ± 0.2	
SN 1006	973 (h)	–		0.68 ± 0.06
0540-693	1660	optical, X-rays	detected	
RCW-103	1500 ± 500	–	2.15 ± 0.15	
RCW-86	1794 (h)	–		1.5 ± 0.1
MSH15-52	1850 ± 250	radio, X-rays	detected	
W-28	3400	–		1.6 ± 0.1
G350.0-18	~8000	–		1.6 ± 0.1
G22.7-0.2	~10000	–		2.0 ± 0.2
Vela X	~12000	radio, optical	0.95 ± 0.15	

Table 10.5
Confronting neutron star cooling calculations with observations. (Data from table 10.4, predictions from Nomoto and Tsuruta [456].)

Objects	Age [yr]	Surface temperature [10^6 K]	
		observed	predicted
3C 58, Crab, RCW-103	$\sim 10^3$	2.0–2.4	1.6–2.3
Vela X	$\sim 10^4$	0.8–1.1	1.2–1.7

magnetic fields, yield surface temperatures at these ages as given in table 10.5. The observations at 10^3 yr are in agreement with the predictions, while the Vela result at 10^4 yr is, at best, in marginal agreement, and probably too low. This led Nomoto and Tsuruta [456] to speculate that a novel form of input physics may be needed to bring theory and observations into agreement. Conversely, the agreement at 10^3 yr may not be significant because it is not certain that HEAO-2 actually observed thermal surface radiation because of the lack of spectral sensitivity of that instrument. Since X-rays conceivably can be produced by other mechanisms in the environment of a young neutron star, the agreement at the younger age may be fortuitous. Therefore the most serious limitation to the significance of any bounds of exotic cooling processes derived from these cases is the uncertainty of the measured X-ray spectrum.

10.2. Supernova explosions and new particle physics

While the birth of a neutron star in type II supernova explosions must be considered a well understood phenomenon, the actual explosion which ejects the mantle and envelope of the progenitor star is more difficult to account for. The problem is that most of the energy liberated in the collapse of the iron core, (2–3) $\times 10^{53}$ erg, is emitted in neutrinos, while only ~1% is transferred to the mantle and envelope. In other words, coupling the implosion of the core to an explosion of the mantle and envelope is a difficult theoretical problem. The general view is that these layers are pushed out by the shock wave that forms at the core bounce. However, the energy of this shock is severely depleted as it passes through the outer layers of the iron core so that is is very difficult to obtain SN explosions on the computer, and it may be impossible unless the iron core of the progenitor star is smaller than had been thought possible until recently. A variation on this theme is Wilson's delayed shock scenario where the shock wave stalls, but neutrinos from the cooling core transfer enough energy to revive the shock and cause the SN to explode.

This difficulty is sometimes called the "supernova problem" and has stimulated some speculations about the role of new particle physics to obtain an explosion. Falk and Schramm [139] discussed radiatively decaying neutrinos and, from the requirement that such decays would not transfer *too much* energy to the mantle and envelope, derived a bound on the radiative decay width. Conversely, for a narrow range of decay parameters, such effects could help trigger the explosion, a possibility first advanced by Sato and Kobayashi [457], and further elaborated by Takahara and Sato [458]. Schramm and Wilson [459] obtained numerical SN explosions by energy transfer through radiatively decaying standard axions, particles which are now excluded but which at the time had reportedly been detected.

If neutrinos have magnetic or electric dipole moments, the electromagnetic scattering of trapped left-handed neutrinos in the SN core on charged particles will flip their helicity, and if the helicity-flipped states are right-handed, i.e., sterile with respect to weak interactions (implying that neutrinos are of Dirac type), they can escape from the core. This leads to a new mechanism of cooling and thus to constraints on neutrino dipole moments (section 10.3 below). However, once the right-handed neutrinos have left the core, they can be rotated back into interacting states by the strong magnetic fields that are thought to exist near the core surface, and that are observed at pulsars. Therefore, again, neutrinos would transfer energy to the mantle and envelope and trigger the explosion. This scenario was first proposed by Dar (1987), but never published because of heavy criticism. More recent discussions are those of Voloshin [144] and of Blinnikov and Okun [138] who included in their discussion the problem of magnetic spin oscillations in the presence of a dense medium where the left- and right-handed neutrinos follow different dispersion relations, leading to the possibility of strong suppression or resonant enhancement of the oscillations.

One may take the opposite point of view and look at situations where new particles would deprive the shock of even more energy than in SN models with standard physics. The observed occurrence of SN explosions then leads to constraints on certain particle properties. Nötzold [142] derived a bound on (Dirac) neutrino dipole moments of $\mu_\nu \lesssim 6 \times 10^{-12} \mu_\mathrm{B}$ (Bohr magneton $\mu_\mathrm{B} = e/2m_\mathrm{e}$) on the basis of such reasoning.

In the following section we will discuss bounds on particle properties that were derived by the requirement that the observed neutrino signal from the cooling proto-neutron star after collapse was not unduly shortened. It must be stressed, however, that particles with properties that remain allowed by that argument may still have an important impact during the infall phase and on the formation and propagation of the shock wave. This point was stressed by Fuller, Mayle and Wilson [109] who investigated numerically the effect of the triplet majoron model on SN physics during the infall and core bounce phase.*)

*) The triplet majoron model, however, is now obsolete because the recent precision measurements of the Z^0 decay width at SLAC [449] and CERN [450–453] exclude the existence of triplet majorons which would contribute the equivalent of two neutrino flavors (see the last paragraph of ref. [101]).

10.3. SN 1987A bounds on novel cooling phenomena

10.3.1. General argument

In section 10.1.2 we have shown that the IMB and Kamiokande II neutrino observations are in good agreement with the standard picture of the formation and early cooling by neutrinos of a neutron star after a SN collapse. Now assume the existence of some new particle, X, light enough to be thermally produced in the SN core, $m_x \lesssim 10\,\mathrm{MeV}$, and more weakly interacting than neutrinos. If the interaction of these X-particles, e.g., axions or right-handed neutrinos, is strong enough for them to be trapped, they will be thermally emitted from an "X-sphere" at a radius $R_x < R_\nu$ (neutrino sphere radius R_ν). By the Stefan–Boltzmann law, the total flux, L_x, from this black-body emission scales as $R_x^2 T^4(R_x)$. For a nascent neutron star, $R^2 T^4(R)$ is a rapidly decreasing function of radius so that $L_x > L_\nu$, i.e., L_x *increases* with a *decreasing* coupling strength, g_x, of these particles. This behavior is schematically illustrated in fig. 10.4. Of course, if g_x is so small that the X mean free path exceeds the neutron star radius, these particles will be emitted from the entire volume of the star. In this case L_x will be dominated by some specific emission process, e.g., axion bremsstrahlung from nucleons , $\mathrm{n} + \mathrm{p} \rightarrow \mathrm{n} + \mathrm{p} + a$, and thus will be proportional to g_x^2, see fig. 10.4, so that L_x now decreases with decreasing interaction strength. This leaves a range of coupling strengths where the new particles would dominate the cooling of the nascent neutron star, a general argument first raised by Ellis and Olive [69] who also showed a figure similar to fig. 10.4.

Observationally this means that the total energy emitted in neutrinos will be reduced, and the cooling time scale will be shortened. It turns out, however, that the total amount of energy emitted in neutrinos, E_ν, is relatively insensitive to the X coupling strength. This is so because about half of E_ν is emitted immediately after the shock wave has broken through the neutrino sphere (fig. 10.1) when the dissociation of large nuclei leads to a sudden jump in the neutrino mean free path. The (volume) emission of X-particles, however, will typically be dominated by the inner core where the densities are highest. This part of the core, however, is at first at relatively low temperatures, see fig. 10.5 where we show snapshots of the temperature profile of a newly born neutron star for the first 20 seconds. Hence

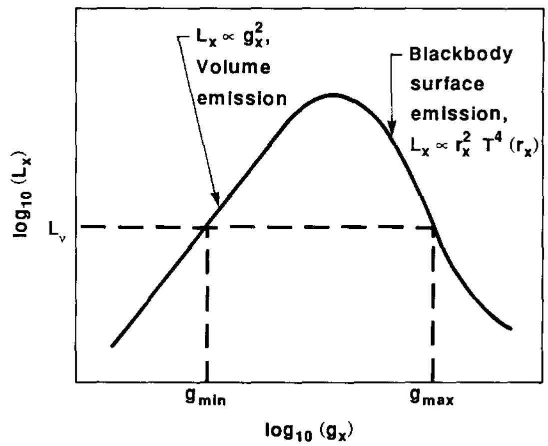

Fig. 10.4. Schematic dependence of the "exotic" luminosity, L_x, on the coupling strength of the new particles, g_x, which could be, for example, the Yukawa coupling of axions to nucleons or a "right-handed Fermi constant". In the range $g_{min} < g_x < g_{max}$, the novel energy loss would exceed the neutrino luminosity, L_ν. (Taken from Raffelt and Seckel [92].)

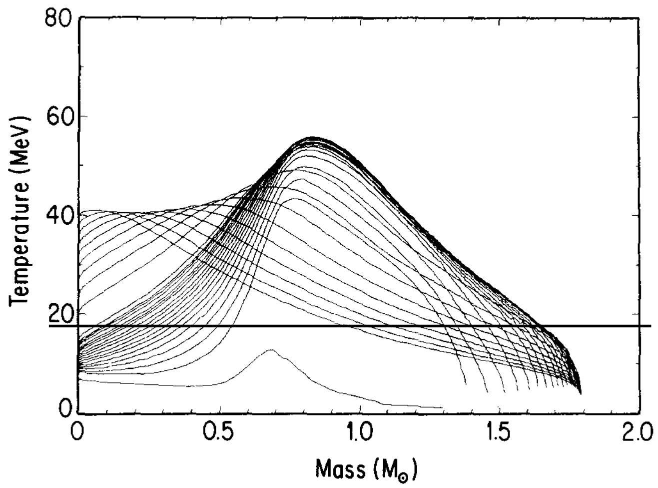

Fig. 10.5. Snapshots of the matter temperature versus the enclosed baryon mass of the case A standard collapse calculation of Burrows et al. [58]. The initial model ($t = 0$) is the bottom curve. The snapshots are every 0.1 s for the first two seconds, and then every 2 s until the end at $t = 20$ s. (I thank A. Burrows for providing an original for this figure.)

the (volume) emission of X-particles will start slowly as energy diffuses into the inner core, and thus will be important mostly during the exponential cooling phase after the first neutrino burst.

Therefore novel forms of energy loss will mostly compete with neutrino cooling after the first burst, and thus will mostly shorten the "cooling tail" of the signal [92]. Here the main observable to constrain particle parameters is the duration of the neutrino signal, not the total amount of binding energy inferred from this signal. The duration of the neutrino signal as a function of particle parameters is illustrated in fig. 10.6 for the case of invisible axions where we show the duration as a function of the axion–nucleon coupling strength, g_a. For details see sections 10.5 and 10.6 below; here we only note that if axions are very weakly interacting they do not affect the neutrino signal (free streaming side in fig. 10.6), and if they are very strongly interacting they also have no effect (trapping side of fig. 10.6). For a certain range of coupling strengths they shorten the signal substantially.

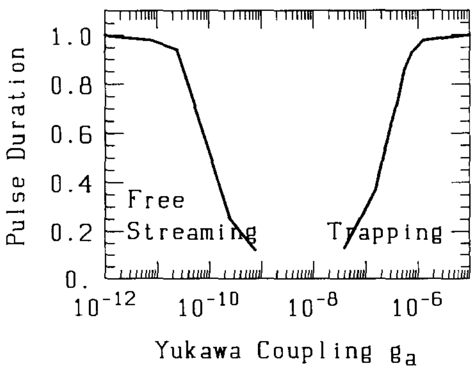

Fig. 10.6. Duration of the neutrino pulse from a supernova, taking axion emission into account, assuming identical Yukawa couplings to protons and neutrons, g_a. For a very small or very large coupling strength the duration is normalized to unity, reflecting the standard value where axion cooling is irrelevant. This figure is based on the numerical investigations of Burrows et al. [58, 59], case B. We show an average of the results relevant for the IMB and Kamiokande detectors. No numerical results are available in the intermediate regime between free streaming and trapping, partly because there is no simple numerical procedure to treat that regime.

In general, the observed duration of neutrino emission (see table 10.3) precludes L_x to exceed L_ν by much, and because $L_\nu \sim 3\times10^{52}$ erg/s during the exponential cooling phase, and because the core mass is $\sim 1 M_\odot$, a crude bound on new particle properties is set by the requirement

$$\varepsilon_x \lesssim 10^{19}\,\mathrm{erg\,g^{-1}\,s^{-1}}\,, \tag{10.3}$$

where the novel energy loss rate is to be calculated at the core conditions, $\rho \sim 0.8\times10^{15}\,\mathrm{g\,cm^{-3}}$ and $T\sim(30\text{–}60)$ MeV. This simple criterion applies to the free streaming case while no simple argument appears to exist for the trapping regime.

10.3.2. *Application to specific cases*

Detailed numerical investigations in the framework of this method are available only for axions, see sections 10.5 and 10.6 below. For many other cases, variations of the general argument in a simple analytic form were applied, and we may now go through a list of cases other than axions. A summary of the results is given in table 10.6.

A class of particles other than axions that could drain the SN core of energy are right-handed (RH) neutrinos, i.e., noninteracting states. These particles could be an entire new class of sterile neutrinos, particularly if the known neutrinos are of Majorana type. If the known neutrinos are Dirac particles, they could simply be the helicity-flipped states. The simplest way to produce RH neutrinos is by the

Table 10.6
Constraints on the properties of light particles based on the observed duration of the SN 1987A neutrino pulse. The quoted results are "middle of the road" values, ignoring possible reductions by many-body effects and by various uncertainties. These numbers, therefore, are uncertain by at least a factor of ~3 in either direction. The issue of Nambu–Goldstone bosons coupled to neutrinos was motivated by the triplet majoron model. Because of the lepton-number violating properties of that model, SN physics may be more complicated, and the quoted bounds have been questioned [107]. See also refs. [105, 106, 109]. However, the triplet majoron model is now excluded (see footnote in subsection 10.3.1) so that this discussion has become obsolete. Bounds on singlet majorons were provided in refs. [112–114], but they cannot be represented in a simple way in this table

Particle property	Dominant process	Constraint	References
Dirac neutrino, mass	helicity flip of trapped ν_L $\nu_L + N \to N + \nu_R$	$m_\nu < 20$ keV	[92, 149–151]
Dirac neutrino, dipole moment	helicity flip of trapped ν_L $\nu_L + (p, e^-) \to (p, e^-) + \nu_R$	$\mu_\nu < 0.5\times10^{-12}\mu_B$ $\mu_\nu < 8\times10^{-12}\mu_B$	[141] [136]
Right-handed Fermi constant (charged currents)	modified urca processes $n + n \to n + p + e^- + \bar\nu_{eR}$ $n + p + e^- \to n + n + \nu_{eR}$	$G_{RH} < 0.3\times10^{-4} G_F$	[92, 147]
Right-handed Fermi constant (neutral currents)	pair bremsstrahlung: $n + p \to n + p + \nu_R + \bar\nu_R$	$G_{RH} < 10^{-4} G_F$	[92]
Squark mass	pair bremsstrahlung $n + p \to n + p + \tilde\gamma + \tilde\gamma$	$m_{\tilde q} > 1$ TeV	[127–129]
Yukawa coupling, g_a, of pseudoscalar boson, ϕ, to nucleons	nucleon bremsstrahlung $n + p \to n + p + \phi$	$g_a < 10^{-10}$	[58, 80, 81, 92, 97] (see also section 10.5.)
Yukawa coupling, g_ν, of pseudoscalar boson, ϕ, to neutrinos	neutrino annihilation $\nu\bar\nu \to 2\phi$	$g_\nu < 0.3\times10^{-5}$ $g_\nu < 2\times10^{-5}$	[111] [108]

same processes which produce LH states, assuming there exist RH weak interactions on some level. Assuming further that these RH interactions have the same structure as the LH interactions, one may easily derive bounds on a RH Fermi constant, G_{RH}. On the basis of the modified urca processes, $\mathrm{n}+\mathrm{n}\to\mathrm{n}+\mathrm{p}+\mathrm{e}^-+\bar{\nu}_{\mathrm{eR}}$ and $\mathrm{e}^-+\mathrm{n}+\mathrm{p}\to\mathrm{n}+\mathrm{n}+\nu_{\mathrm{eR}}$, which involve charged currents, one finds in the free streaming regime [92] $G_{\mathrm{RH}}\lesssim 3\times 10^{-5}\,G_{\mathrm{F}}$. The trapping regime is of much less interest because it overlaps with a regime excluded by laboratory data. On the basis of another emission process, $\mathrm{e}^-+\mathrm{p}\to\mathrm{n}+\nu_{\mathrm{R}}$ one finds a similar constraint [147]. In the standard left–right symmetric models, this result can be translated into a bound on the mass of RH gauge bosons, $m_{\mathrm{W_R}}$, and the standard $\mathrm{W_R}$–$\mathrm{W_L}$-mixing angle, ζ [147],

$$[\zeta^2+(m_{\mathrm{W_L}}/m_{\mathrm{W_R}})^4]^{1/2}\lesssim 3\times 10^{-5}\,. \tag{10.4}$$

Similarly, one may constrain RH neutral currents on the basis of bremsstrahlung processes, $\mathrm{N}+\mathrm{N}\to\mathrm{N}+\mathrm{N}+\bar{\nu}_{\mathrm{R}}\nu_{\mathrm{R}}$, yielding [92] $G_{\mathrm{RH}}\lesssim 10^{-4}$, although a somewhat weaker bound was reported by other authors [129, 147, 148]. Moreover, in standard left–right symmetric models, the RH neutral current has vector structure and thus does not contribute to nucleon bremsstrahlung [129], leaving us with a much less efficient emission process, $\mathrm{e}^+\mathrm{e}^-\to\bar{\nu}_{\mathrm{R}}\nu_{\mathrm{R}}$. For E_6 models, where RH neutrino masses can be expected to be naturally small, the neutral-current bremsstrahlung rates are not suppressed, and a detailed analysis and interpretation of the constraints is available [129, 148]. A constraint on a neutrino charge radius [145], we believe, should be discussed in a unified picture with RH neutral current interactions since in the framework of electroweak gauge theories a neutrino charge radius is a problematic concept.

In the previous cases one had to assume that the mass of the RH neutrinos was small enough for them to be thermally emitted from the SN. The following arguments rely on various processes of flipping the helicity of Dirac neutrinos, thereby transforming an interacting (LH) state into a sterile (RH) state of the same mass. For ν_{e} and ν_μ the following constraints are thus valid without restriction, while for ν_τ with a laboratory limit on its mass of 35 MeV most likely there exists a mass range near this limit where the following bounds can be evaded. The simplest way to flip the helicity is by a mass term, i.e., the neutrinos trapped in the SN core will develop RH components if they have a Dirac mass. The resulting neutrino luminosity will be so large that one can infer a bound [92, 149–151] $m_\nu\lesssim 20\,\mathrm{keV}$. It was claimed that the excluded mass range reaches up to ~35 MeV, with a substantial uncertainty, however, so that τ neutrinos with masses near their laboratory limit are still allowed by this argument. If neutrinos had a magnetic or electric dipole moment, interactions with charged particles in the SN core would also flip the helicity, yielding a bound [136, 140, 141] of $\mu_\nu\lesssim 10^{-12}\mu_{\mathrm{B}}$ where $\mu_{\mathrm{B}}=e/2m_{\mathrm{e}}$ is the Bohr magneton. Finally, the helicity flip in the gravitational field of the nascent neutron star in the context of novel gravitational interactions was also discussed, allowing one to constrain the parameters of such models [152].

In supersymmetric models with light photinos, these particles would be emitted by nucleon bremsstrahlung processes. The cross section is $\propto m_{\tilde{\mathrm{q}}}^{-4}$, leading to a constraint on the squark mass of [127–129] $m_{\tilde{\mathrm{q}}}\gtrsim 1\,\mathrm{TeV}$.

Many authors [101–114] have discussed the effect of majorons on supernovae, although most of them concentrated on the triplet majoron model which is now excluded on the basis of the measured Z^0 width (see footnote in section 10.3.1). However, the most recent investigation [114] is a detailed account of bounds on the singlet majoron model, excluding a large range of neutrino masses and vacuum expectation values.

10.4. Non-detection of new particles from SN 1987A

It is still possible that the SN core emitted a large pulse of new particles and one may wonder whether they could have been detected in the IMB and Kamiokande II detectors. One interesting case is that of right-handed neutrinos which were produced by helicity flips from electromagnetic interactions with charged particles. These neutrinos could oscillate back into left-handed, interacting states on their way from the SN core to Earth. Indeed, this possibility was raised as a mechanism to cause the SN mantle to explode (section 10.2). The angle of rotation of the expectation value of the neutrino spin is proportional to $\int \mu_\nu B_t \, dl$ where B_t is the transverse magnetic field along the line of sight with the SN. Of course, in the mantle and envelope, the relevant expression is more complicated because the two helicity states follow different dispersion relations. However, even the galactic magnetic field of $\sim 3\times 10^{-6}$ G with a coherence scale of $\sim$300 pc is enough to reflip neutrinos from SN 1987A if $\mu_\nu \gtrsim 3\times 10^{-14}\mu_B$. The reflipped neutrinos could be detected, and would cause a different signal from that observed because their energies would be characteristic of core temperatures rather than characteristic for the temperature at the neutrino sphere [136, 142]. This argument is especially powerful for those neutrinos that were emitted from behind the neutrino sphere, before the shock reached this point, i.e., the right-handed neutrinos that would be emitted before the deleptonization burst. The electron neutrinos in this region are degenerate and have large Fermi energies and would thus cause a very prominent signal. The absence of such detections led Nötzold [142] to infer

$$\mu_{\nu_e} < 1.5\times 10^{-12}\mu_B \,, \tag{10.5}$$

a bound which applies to the diagonal magnetic (or electric) dipole moment of Dirac electron neutrinos. It is conditional on the assumption that the Earth was not coincidentally located at a "node" of the spin oscillation pattern of the neutrino pulse.

Another interesting case is that of axions which are on the trapping side of the regime excluded by the cooling argument. Engel, Seckel and Hayes [96] argued that axions which interact so strongly that they are trapped could also be detected in the water Čerenkov detectors. Especially the reaction $a + {}^{16}\mathrm{O} \rightarrow {}^{16}\mathrm{O}^*$ could serve to absorb axions in the detector. The nuclear de-excitation often includes γ-rays with energies of 5–10 MeV which trigger the Kamiokande detector with an efficiency similar to that of electrons in the same energy range. Taking a common Yukawa coupling to protons and neutrons, g_a, these authors find that in the range $6\times 10^{-7} \lesssim g_a \lesssim 1\times 10^{-3}$ the axion flux should have produced more than 5 (and up to 200) observable events at Kamiokande, and so this range is excluded.

10.5. SN 1987A axion bounds from numerical investigations

While the "cooling argument" of the nascent neutron star in SN 1987A has yielded many interesting constraints, notably on neutrino properties (see table 10.6), only the cases of invisible axions [58, 80, 81] and that of triplet majorons [109] have been investigated numerically. We do not consider the triplet majoron model any further because it is now excluded (footnote in section 10.3.1). When the numerical works for the axion case were performed, the understanding of the relevant emission rates was in a state of flux, and none of the groups used the appropriate rates described in section 4.8. Burrows, Turner and Brinkmann (BTB) [58] used the "exact" rates of Brinkmann and Turner [57], but with the vacuum nucleon mass, thereby underestimating the axion luminosity. Mayle, Wilson, Ellis, Olive, Schramm and Steigman in their first paper (MI) [80] used the degenerate rates with the vacuum nucleon mass, while in their second paper (MII) [81] they used the nondegenerate rates, again with the vacuum nucleon mass, although they mentioned that one should use an effective nucleon mass of $\sim 0.5m_N$. Moreover, BTB considered a "generic axion case" with equal couplings to protons and neutrons while MI and MII used specifically the DFSZ model, and stated their results as a function of the free parameter, β, of this model. We will attempt to reduce these results to a common and correct set of assumptions.

We begin with pseudoscalar particles which couple to protons and neutrons with equal Yukawa strengths, g_a. This is the case considered by BTB who included the rates eq. (4.63) in Burrows' supernova code, using fixed form factors corresponding to $\beta = 1/2$ (table 4.2), i.e., $F_n = F_p = 5/6$, $F_1 = 2/3$, and $F_2 = 14/15$, and using the vacuum nucleon mass. For several values of g_a they calculated the number of neutrino events to be expected in the IMB and Kamiokande II detectors, N_{det}, and the duration of the neutrino pulses in each detector. In their work, this quantity is defined to be the time, $\Delta t(90\%)$, which is required to accumulate 90% of the expected counts in each detector. They also calculated the total amount of energy in neutrinos, E_ν, and axions, E_a, to be emitted in each case. They performed this calculation for three different equations of state. In fig 10.7 we show these results for their "case B" (cases A and C yield similar results). As predicted in our general discussion in section

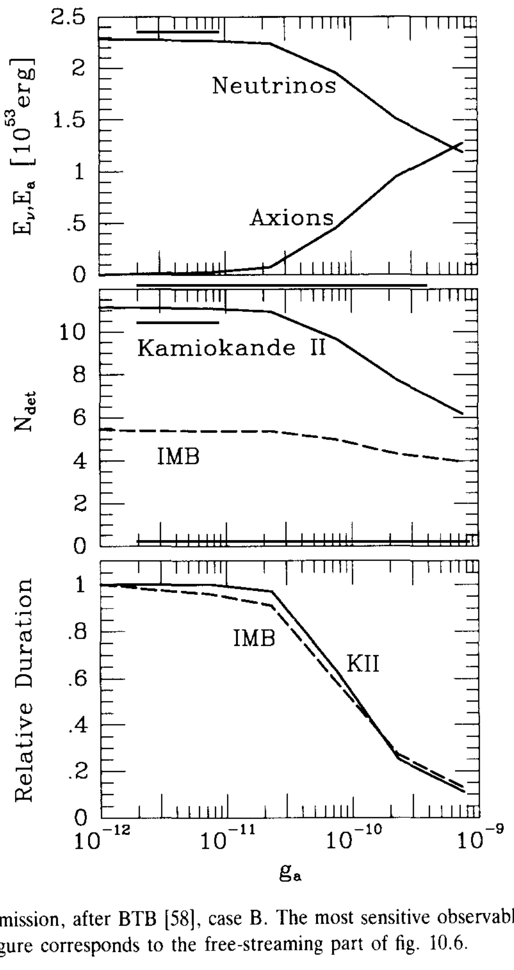

Fig. 10.7. Core collapse including axion emission, after BTB [58], case B. The most sensitive observable quantity is the duration of the measured neutrino pulse. The lower panel of this figure corresponds to the free-streaming part of fig. 10.6.

10.3, it is the duration of the neutrino pulse which is the observable most sensitive to axion losses, while the total amount of energy radiated in axions as well as the total number of neutrinos detected remain almost unchanged for values of g_a where the duration of the pulse drops substantially. (See also fig. 10.6 for the variation of the pulse duration.)

No precise statistical reasoning was offered in the numerical works that would allow one to state a confidence level at which the expected pulse duration for a given value of g_a is in agreement or disagreement with the observed data. Nevertheless, the quantity $g_{1/2}$, i.e., the coupling strength g_a at which the pulse duration is shortened by a factor 1/2 appears to be a reasonable albeit arbitrary choice. From the calculations of BTB one infers $g_{1/2} \sim 1 \times 10^{-10}$. However, these authors used the vacuum nucleon mass in their calculations. From fig. 10.5 we conclude that typical temperatures relevant for axion emission were in the range (20–40) MeV, at densities corresponding to Fermi-momenta ~380 MeV. Hence, from fig. 4.8 we conclude that they underestimated axion emission by a factor of ~1/2. With eq. (4.70) we conclude that BTB's emission rates should be multiplied by $\sim 2 \times 0.3 \times 2^{\pm 2}$. Since the emission rates are proportional to g_a^2, we estimate

$$g_{1/2} \sim 1.3 \times 10^{-10} \times 2^{\pm 1} . \tag{10.6}$$

Next, we turn to MI and MII who also considered the duration of the neutrino pulse as their main criterion. They used the DFSZ model, but for $\beta = 72°$ the neutron and photon couplings are equal, and we can extract their results that would correspond to BTB's "generic case". From MI, where they used the degenerate emission rates, we infer $g_{\rm lim} = 0.5 \times 10^{-11}$ for their limiting value after correcting for an erroneous factor of 2 in their emission rate (see MII). From MII, where they used the nondegenerate rates throughout, we infer $g_{\rm lim} = 1.3 \times 10^{-11}$. However, they used the vacuum nucleon mass, and following their discussion, a value of $m_N^* \sim 0.5 m_N$ would have been appropriate, leading to a correction factor of $0.5^{2.5/2}$. Hence we infer from MI and MII an identical result of $g_{\rm lim} \sim 0.5 \times 10^{-11}$.

While the agreement between these two results confirms our earlier conclusion that the conditions pertaining to axion bounds are intermediate between degeneracy and nondegeneracy, this agreement also means that both results equally overestimate the actual bound. The asymptotic expressions overestimate the emission rates in the region of crossover by as much as a factor of 5, see Brinkmann and Turner [57]. Also, we must apply the factor eq. (4.70) so that we infer $g_{\rm lim} \sim 0.2 \times 10^{-10} \times 2^{\pm 1}$. Finally we note from their display of the $\bar\nu_e$ luminosity, that their curve marked "$f_a = 0.08 \times 10^{12}$ GeV" corresponds to a reduction of the time constant of the neutrino pulse a factor of ~2, while they actually used a value $f_a = 0.2 \times 10^{12}$ GeV to derive their limiting case. Hence we infer

$$g_{1/2} \sim 0.5 \times 10^{-10} \times 2^{\pm 1} , \tag{10.7}$$

on the basis of MI and MII.

The discrepancy of about a factor of 3 between the two groups probably may be ascribed to different input physics. Mayle and Wilson's models are characterized by higher temperatures, leading to larger emission rates and hence more restrictive axion bounds. It thus appears reasonable to combine the two results to infer

$$g_{1/2} \sim (0.3\text{–}2.6) \times 10^{-10} , \tag{10.8}$$

for the axion coupling constant where the neutrino pulse would be shortened by a factor of 1/2.

If the axion couplings to protons and neutrons are not equal, we may estimate the dependence of the emission rates on the individual couplings by taking specific values for the mass fractions of neutrons and protons, respectively. While BTB do not state specific values, MI and MII give $X_n = 0.88$ and $X_p = 0.12$ as a typical case. Of course, these values change with time and radius so that our following estimate is very crude. With these mass fractions and using the F_j values listed in table 4.2, we infer that the degenerate emission rates, eq. (4.59), are proportional to $0.15\alpha_n + 0.08\alpha_p + 0.22\alpha_1 + 0.56\alpha_2$, while the nondegenerate rates, eq. (4.60), are proportional to $0.42\alpha_n + 0.01\alpha_p + 0.07\alpha_1 + 0.51\alpha_2$. Taking an average, we find that the neutrino signal will be shortened by a factor 1/2 if

$$[0.55g_{an}^2 + 0.31g_{ap}^2 + 0.14(g_{an} + g_{ap})^2/4]^{1/2} \sim (0.3\text{–}2.6) \times 10^{-10}\,.$$

Finally, using table 2.1 (bottom line) we find

$$m_{1/2} \sim (0.2\text{–}1.7) \times 10^{-3}\ \mathrm{eV} \times [0.55c_n^2 + 0.31c_p^2 + 0.14(c_n + c_p)^2/4]^{-1/2} \tag{10.9}$$

for the axion mass which shortens the neutrino signal by a factor 1/2.

We now discuss this result in the framework of two typical axion models. Beginning with KSVZ-type axions, we use the couplings of table 2.2, keeping the amount of proton spin carried by strange quarks, Δs, a free parameter. In fig. 10.8 we show $m_{1/2}$ as a function of Δs where the hatched band reflects the uncertainty of this result. We also show m_{trap} (see below): axion masses between $m_{1/2}$ and m_{trap} are excluded by the SN 1987A neutrino observations. Clearly, the boundary of the excluded range is very uncertain, and even axion masses as large as 10^{-2} eV may be tolerable. The variation of the results with Δs is a relatively minor uncertainty compared with the uncertainty resulting from SN physics and the uncertainty of the emission rates. In fig. 10.9 we show similar results for DFSZ-axions, taking two specific values, $\Delta s = 0.0$ (NQM) and -0.26 (EMC).

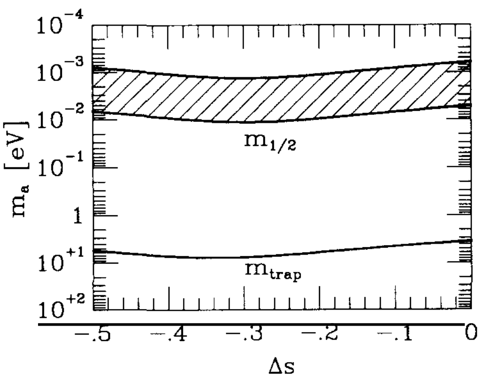

Fig. 10.8. SN 1987A axion bounds for KSVZ-axions, using the couplings of table 2.2. The hatched band is the range for $m_{1/2}$, the axion mass for which the duration of the neutrino signal would be shortened by a factor 1/2, inferred from the numerical works [58, 80, 81]. The "trapping mass" was inferred from ref. [97], but no estimate for its uncertainty is available.

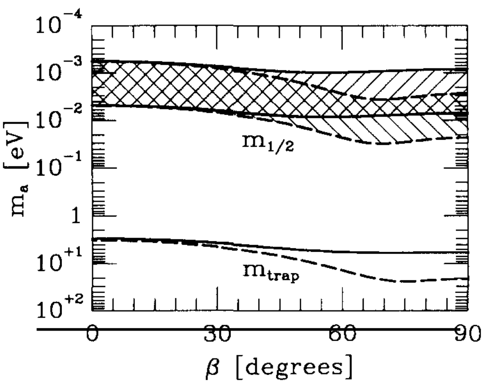

Fig. 10.9. SN 1987A axion bounds for DFSZ-axions, using the couplings of table 2.2, analogous to fig. 10.8. The NQM case corresponds to $\Delta s = 0$ (solid line) while the EMC case has $\Delta s = -0.26$ (dashed line).

10.6. Axion trapping

If axions interact too strongly, they do not freely stream out of the SN core, but rather will be radiated from an "axio-sphere" similar to the neutrino sphere. Turner [97] has investigated this question quantitatively, and he finds that axions which couple more strongly than $g_{\mathrm{trap}} = 1.7 \times 10^{-7}$ are not excluded on the basis of the SN 1987A neutrino observations. However, Turner's interaction rate is too small by a factor of ~2, relaxing this boundary to $\sim 1.1 \times 10^{-7}$. The conditions most relevant for axion trapping are those near the neutrino sphere with temperatures of (5–10) MeV, and a density of $\sim 10^{11}\,\mathrm{g\,cm^{-3}}$, more than three orders of magnitude less than in the inner core. Therefore the nondegenerate interaction rates are fully justified, the nucleon mass is at its vacuum value, and all interactions can be viewed as taking place in vacuum. However, neglecting the pion mass in the matrix element is a rather bad approximation. The form factors, F_j, in the emission rates, and similar factors in the absorption rate, arise from terms such as $A(\boldsymbol{k}) \equiv |\boldsymbol{k}|^4/(|\boldsymbol{k}|^2 + m_\pi^2)^2$ in the squared matrix element where $\boldsymbol{k}$ is the momentum transfer carried by the intermediate pion. Taking $T = 8\,\mathrm{MeV}$ as a temperature corresponding to the axio-sphere leads to a typical momentum transfer of $|\boldsymbol{k}| \sim (3m_{\mathrm{N}}T)^{1/2} \sim 150\,\mathrm{MeV}$, hence $F_j \sim 0.3$. Taking equal numbers of protons and neutrons near the neutrino sphere yields the trapping condition $2.0 \times 10^{-7} \sim (0.5g_{\mathrm{an}}^2 + 0.5g_{\mathrm{ap}}^2)^{1/2}$, or

$$m_{\mathrm{trap}} \sim 1.3\,\mathrm{eV} \times (0.5c_{\mathrm{n}}^2 + 0.5c_{\mathrm{p}}^2)^{-1/2}\,. \tag{10.10}$$

It is not quantitatively clear, however, how this value relates to the shortening of the observed neutrino pulse and thus it is only a crude upper limit for the axion masses that can be excluded. We show m_{trap} for KSVZ- and DFSZ-axions in figs. 10.8 and 10.9.

Very recently a numerical investigation of the trapping regime was conducted by Burrows, Ressell and Turner [59] who implemented radiative energy transfer by axions in their supernova code. This work for the first time allows one to relate quantitatively the duration of the neutrino signal to a particle coupling constant in the trapping regime. In fig. 10.6 we show the duration of the neutrino signal in the trapping regime, assuming equal coupling strengths to neutrons and protons. To prepare this figure we have taken an average between the results relevant for the IMB and Kamiokande detectors. From fig. 10.6 we conclude that the neutrino signal in the axion trapping regime is reduced by a factor 1/2 for $g_{\mathrm{a}} = 2 \times 10^{-7}$ which fortuitously coincides with our above corrected version of Turner's [97] analytic result. Hence eq. (10.10) remains valid and, moreover, can be interpreted as giving the value for $m_{1/2}$ in the trapping regime.

10.7. Axion bounds from Einstein observations

Iwamoto [77] showed that in young neutron stars axion emission would dominate neutrino emission for a large range of parameters not excluded by other arguments, except for the SN 1987A neutrino observations which were not available at the time. Later Tsuruta and Nomoto [99] incorporated the nn bremsstrahlung rates into their numerical evolution code and calculated cooling curves for several values of the axion–neutron coupling. Assuming that the Einstein data actually establish the surface temperature of young neutron stars at $t \sim 10^3$ yr (table 10.5), they found an axion constraint of

$$g_{\mathrm{an}} \lesssim 10^{-10}\,. \tag{10.11}$$

It is not clear, however, how this result would vary if one also considered the axion–proton coupling, and if one would allow these couplings to vary independently. Nevertheless, this result is comparable to the SN 1987A results.

Finally, it was proposed that the axions emerging from a neutron star could convert into X-rays in the strong magnetic fields near the pulsar surface, leading to a detectable signal [83]. However, these transitions are strongly suppressed by photon refractive effects caused by the magnetic fields (section 4.9.4) so that the arguments of ref. [83] do not apply as was shown in ref. [411].

10.8. What if neutron stars are strange quark stars?

It has sometimes been speculated that the ground state of nuclear matter would be a medium of free quarks and gluons, i.e., that at sufficiently high densities nuclear matter makes a phase transition to a quark–gluon plasma. This means that "neutron stars" could consist of free quarks and gluons rather than of nucleons, and a supernova core after collapse could contain a region of a quark–gluon plasma. Most recently a number of authors [55, 55a, 94] have investigated the issue of axion emission from a quark–gluon plasma and how it would affect bounds on the axion mass from SN 1987A.

The SN 1987A bounds are mostly of importance for hadronic axion models for which bounds based on the axion–electron coupling do not apply. Hadronic axions by definition do not couple to leptons at tree level and also typically do not couple to normal quarks. Hence for conditions of a quark–gluon plasma such axions only couple to exotic heavy colored objects (which would not be present in a SN core) and to free gluons by virtue of the Lagrangian eq. (2.3) which is the most generic ingredient of all axion models so that the axion–gluon interaction is completely model-independent. Therefore, in a quark–gluon plasma hadronic axions can be produced only by processes involving their coupling to gluons while there is no equivalent to the nucleon bremsstrahlung processes which dominate in the nuclear matter phase.

Salati and Ellis [94] have discussed axion emission from the gluonic plasmon decay process, $g_t \to g_\ell + a$, where g_t and g_ℓ refer to transverse and longitudinal gluonic modes, respectively. The emission rate from this process alone is much less than that for nucleon bremsstrahlung at the same density and temperature so that these authors conclude that the axion bounds will be substantially weakened if SN cores actually consist of a quark–gluon plasma. However, Altherr [55a] pointed out that the gluonic Primakoff effect, $g + q \to q + a$, would be more important. This process is analogous to fig. 4.9 if the double line is interpreted as representing a quark and the wavy lines as representing gluons. Altherr found that the bound on the Peccei–Quinn scale and thus on the axion mass would remain essentially unchanged, i.e., that the emission rate would be about the same as that from nuclear matter at similar densities and temperatures.

11. Summary of axion and neutrino bounds

We summarize the astrophysical bounds on axions and neutrinos that were discussed in this report.

11.1. Neutrinos

11.1.1. Masses

From the absence of dispersion of the neutrino pulse of SN 1987A one infers a mass bound for the electron neutrino of

$$m_{\nu_e} < 23\,\mathrm{eV} \tag{11.1}$$

at the 95% CL (section 10.1.2 and ref. [211]). If neutrinos are Dirac particles so that flipping their helicity causes them to be sterile with respect to standard weak interactions, the cooling argument of the SN 1987A neutron star (section 10.3) yields a bound [92, 149–151]

$$m_{\nu_{\mu,\tau}} \lesssim 25\,\mathrm{keV}\,, \tag{11.2}$$

with an uncertainty of at least a factor of 3 in either direction. The laboratory bounds are $m_{\nu_\mu} < 250\,\mathrm{keV}$ at 90% CL and $m_{\nu_\tau} < 35\,\mathrm{MeV}$ at 95% CL [325]. There exists a range of allowed mass values for ν_τ near this experimental bound because of trapping.

11.1.2. Right-handed interactions

If right-handed neutrinos exist they would have been produced in the core of SN 1987A, escaped freely, and thus the cooling argument applies (section 10.3). If the right-handed interactions are described by an effective current–current Lagrangian in analogy with the left-handed currents, the right-handed Fermi constant is constrained by $G_{\mathrm{RH}} \lesssim 0.3 \times 10^{-4} G_{\mathrm{F}}$ (charged currents) and $G_{\mathrm{RH}} \lesssim 10^{-4} G_{\mathrm{F}}$ (neutral currents), see section 10.6 and table 10.6. The best laboratory bound is $G_{\mathrm{RH}} \lesssim 0.17 \times 10^{-2} G_{\mathrm{F}}$ (charged currents).

11.1.3. Magnetic and electric dipole moments

It is now known that there exist exactly three light neutrino flavors [449–453], all of which could have anomalous magnetic dipole and transition moments, μ_{ij}, as well as electric dipole and transition moments, ε_{ij}, where $i, j = 1, 2, 3$, denoting the mass eigenstates. These properties would allow for radiative neutrino decays, $\nu_i \to \nu_j + \gamma$, plasmon decay in stars, $\gamma_{\mathrm{pl}} \to \nu_i \bar{\nu}_j$, and electromagnetic scatterings, $\nu_i + (Ze) \to (Ze) + \nu_j$, provided that the appropriate kinematic constraints are observed. (See section 4.10 for the rates and cross sections.) All of these processes have been used to constrain various entries of the magnetic and electric dipole matrices.

During the time of the neutrino observations, the solar maximum mission (SMM) satellite was operational and registered a normal background flux of γ-rays [182]. The absence of a γ burst in association with the neutrino burst allows one to constrain radiative neutrino decays [181–183], $\tau_{\nu_e}/m_{\nu_e} \gtrsim 2 \times 10^{15}\,\mathrm{s/eV}$, where τ is the *radiative* lifetime only. A similar bound pertains to μ and τ neutrinos if they are lighter than about 20 eV while for larger masses the bound is less restrictive because the photon spectrum would be spread out in time. A general bound, valid for all families, is [183]

$$\frac{\tau_\nu}{1\,\mathrm{s}} \gtrsim \begin{cases} 2 \times 10^{15} (m_\nu/1\,\mathrm{eV}) & \text{if } m_\nu \lesssim 20\,\mathrm{eV}\,, \\ 3 \times 10^{16} & \text{if } 20\,\mathrm{eV} \lesssim m_\nu \lesssim 100\,\mathrm{eV}\,, \\ 8 \times 10^{17} (1\,\mathrm{eV}/m_\nu) & \text{if } 100\,\mathrm{eV} \lesssim m_\nu \lesssim 1\,\mathrm{MeV}\,. \end{cases} \tag{11.3}$$

More interestingly, these results can be expressed in terms of the electric or magnetic transition moments. Considering specifically the decay $\nu_i \to \nu_j + \gamma$ we find

$$\frac{(|\mu_{ij}|^2+|\varepsilon_{ij}|^2)^{1/2}}{\mu_B} \lesssim \begin{cases} 1\times 10^{-8}(1\ \mathrm{eV}/m_\nu)^2 & \text{if } m_\nu \lesssim 20\ \mathrm{eV}\,, \\ 5\times 10^{-10}(1\ \mathrm{eV}/m_\nu) & \text{if } m_\nu \gtrsim 100\ \mathrm{eV}\,, \end{cases} \tag{11.4}$$

where $\mu_B = e/2m_e$ is the Bohr magneton.

The SN 1987A cooling argument (section 10.3) can be used because the electromagnetic moments would lead to helicity flips in the electromagnetic scattering of trapped, left-handed neutrinos on charged particles. This argument [136, 141], as well as the absence of high-energy events in the detectors [142] leads to the constraint

$$\left(\sum_{i,j=1}^{3}(|\mu_{ij}|^2+|\varepsilon_{ij}|^2)\right)^{1/2} < (0.5\text{–}5)\times 10^{-12}\mu_B\,, \tag{11.5}$$

where the sum is to be extended over all neutrinos with $m_i \lesssim 1$ MeV.

Finally, the plasmon-decay width for $\gamma_{pl}\rightarrow \nu_i\bar{\nu}_j$ would lead to the cooling of the core of red giants before the helium flash, increasing the core mass of red giants and horizontal branch stars (section 8.5), and leading to a constraint [146]

$$\left(\sum_{i,j=1}^{3}(|\mu_{ij}|^2+|\varepsilon_{ij}|^2)\right)^{1/2} < 2\times 10^{-12}\mu_B\,. \tag{11.6}$$

A constraint of $1\times 10^{-11}\mu_B$ arises from the white dwarf luminosity function (section 9.3) and from the duration of helium burning in low-mass stars (section 8.4). This result applies to Dirac neutrinos, while for Majorana neutrinos the final states must not be counted twice, i.e., the bounds are less restrictive by a factor $2^{1/2}$.

11.2. Axions

11.2.1. Pseudoscalar couplings to fermions and photons

We begin with the bounds on the couplings of (pseudoscalar) Nambu–Goldstone bosons to fermions. The most restrictive lower bound on the Yukawa coupling to electrons, g_{ae}, arises from the "helium ignition argument" (section 8.3.2). It was first presented in ref. [63], and a slightly revised result (section 8.3.2) is

$$g_{ae} < 3\times 10^{-13}\,, \tag{11.7}$$

valid for $m_a \lesssim 30$ keV. This bound is conservative because even if the helium flash occurred, the increased core mass would make itself known by an increased luminosity at the tip of the giant branch and a shortened helium burning lifetime (section 8.4). A bound which is only slightly less restrictive arises from the white dwarf luminosity function (section 9.4 and refs. [84, 85, 88]). If the interaction is too strong, our bosons would not escape from red giant cores or white dwarfs, but then they would contribute to the energy transfer in stars (chapter 5), and the known properties of the Sun preclude such strong interactions (section 7.1 and refs. [160, 161]), leaving no room for a window below the bound eq. (11.7).

The most restrictive bounds on the Yukawa coupling to nucleons, g_{an} and g_{ap}, arise from the observed duration of the SN 1987A neutrino signal (section 10.5 and refs. [58, 59, 80, 81, 92, 97]). Neglecting a small term proportional to $(g_{an}+g_{ap})^2$, the bound is

$$(0.6g_{an}^2+0.4g_{ap}^2)^{1/2} \lesssim 3^{\pm 1}\times 10^{-10}\,. \tag{11.8}$$

The large uncertainty arises from variations between different numerical SN codes, unknown correction factors due to many-body effects, and the sparse data (few observed neutrinos from SN 1987A). The criterion in deriving this bound was a shortening of the observed neutrino pulse by a factor of 1/2. If the pseudoscalars interact too strongly they are trapped, and it was estimated that for $(0.5g_{\mathrm{an}}^2 + 0.5g_{\mathrm{ap}}^2)^{1/2} \gtrsim 2\times 10^{-7}$ the neutrino signal would also be shortened by a factor of 1/2 (section 10.6 and refs. [59, 97]).

A bound similar to eq. (11.8) arises from the observed cooling time scale of neutron stars at an age of $\sim 10^3$ yr (section 10.7 and refs. [77, 99]), but these arguments have to rely on the assumption that the observed X-ray emission of compact sources in SN remnants actually represents thermal surface radiation.

The photon coupling was constrained by considering the helium burning lifetimes of low-mass stars (section 8.4 and ref. [89]), leading to a bound, for $m_{\mathrm{a}} \lesssim 30$ keV,

$$g_{\mathrm{a}\gamma} < 1\times 10^{-10}\ \mathrm{GeV}^{-1}\,, \tag{11.9}$$

assuming that the lifetime is not shortened by more than a factor of 1/2. In this case many-body effects can be treated with high accuracy so that the major uncertainty lies in the observational determination of the helium burning lifetime which is thought to be known to at least within a factor of two from number counts in open clusters and the old galactic disk population. Conceivably, this bound could be enhanced by a detailed comparison of number counts in globular clusters with numerical evolutionary sequences.

11.2.2. Axion mass bounds and axion windows

We may now translate the bounds on the various coupling constants into axion mass bounds. Taking the generic relationship between fermion couplings and the axion mass eq. (2.31), the bound on the electron coupling eq. (11.7) yields

$$m_{\mathrm{a}} < 0.35\times 10^{-2}\ \mathrm{eV}\ c_{\mathrm{e}}^{-1}\,. \tag{11.10}$$

In the DFSZ-model, specifically, we have $c_{\mathrm{e}} = \cos^2\beta/N_{\mathrm{f}}$ according to eq. (2.32) so that

$$m_{\mathrm{a}} < 1.1\times 10^{-2}\ \mathrm{eV}/\cos^2\beta\,, \tag{11.11}$$

where we have taken the number of families to be $N_{\mathrm{f}} = 3$. Similar, the SN 1987A bound yields a bound of

$$m_{\mathrm{a}} \lesssim 0.6\times 10^{-3\pm 0.5}\ \mathrm{eV}\ (0.6c_{\mathrm{n}}^2 + 0.4c_{\mathrm{p}}^2)^{-1/2}\,. \tag{11.12}$$

For the KSVZ-model this is $m_{\mathrm{a}} \lesssim 3\times 10^{-3\pm 0.5}$ (fig. 10.8) while for DFSZ-axions the excluded regime was shown as a function of the free parameter β in fig. 10.9.

Finally, the constraint eq. (11.9) on the photon coupling, together with table 2.1, yields

$$m_{\mathrm{a}} < 0.7\ \mathrm{eV}\left|\frac{0.75}{E/N - 1.92}\right|. \tag{11.13}$$

For DFSZ-axions or any GUT axion model ($E/N = 8/3$) the correction factor equals 1, while for models with $E/N = 2$ this bound is strongly suppressed.

The axion bounds are best summarized by fig. 11.1 where we show the excluded mass range. For

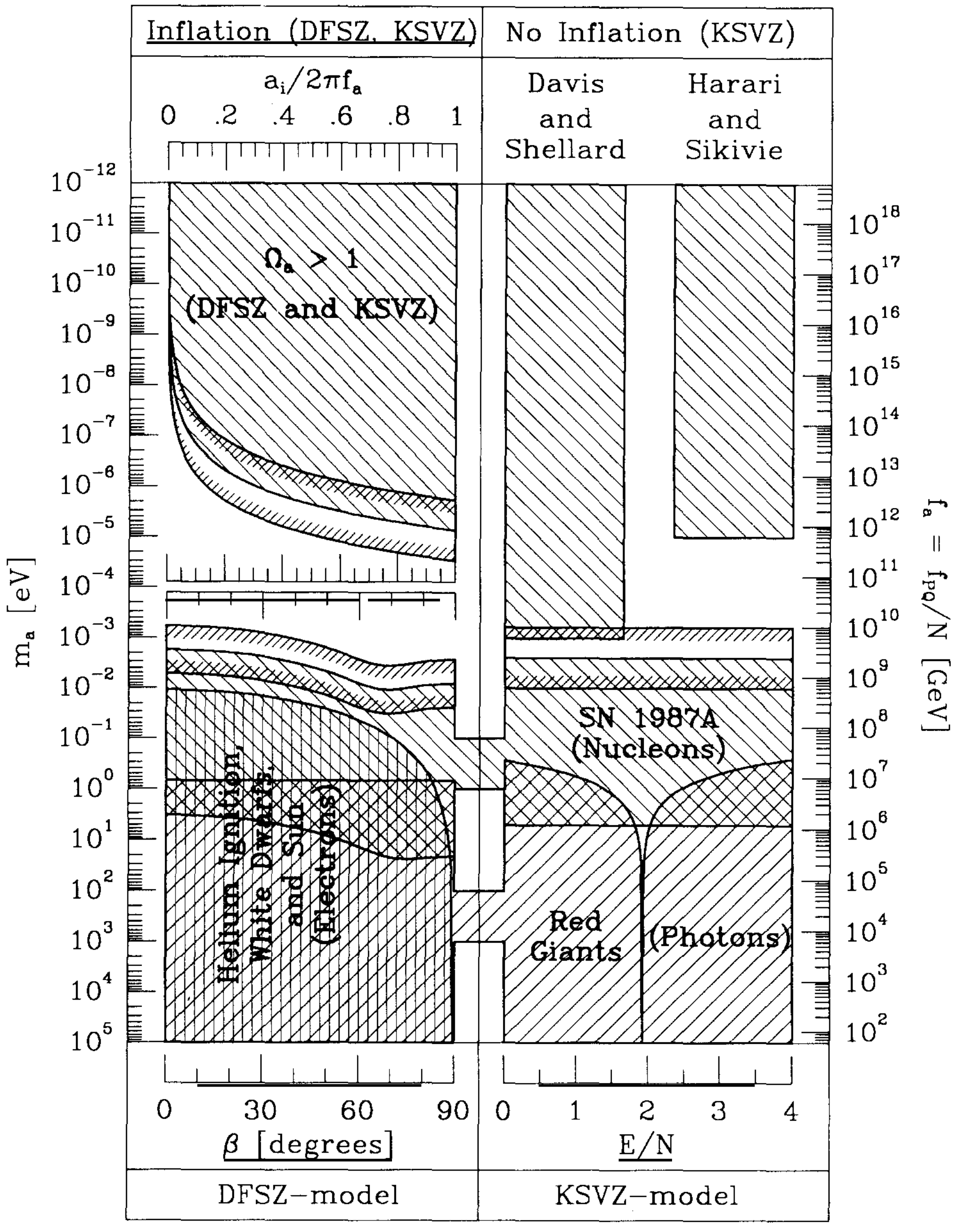

Fig. 11.1. Synopsis of astrophysical and cosmological bounds on the axion mass. For KSVZ-axions, the only free parameter is E/N, the coefficient of the electromagnetic anomaly, while for DFSZ-axions it is the angle β which measures the ratio of the vacuum expectation values of two low-energy Higgs fields which give masses to up and down quarks, respectively. The SN 1987A bounds for DFSZ-axions are shown for the EMC case with $\Delta s = -0.26$. The parameter E/N is not a continuous variable, rather it is the ratio of small integers. For $E/N = 2$, there is a window of allowed masses between the SN 1987A and the red giant bound. "No Inflation" means either that there is no inflation, or that the universe was reheated beyond the Peccei–Quinn scale after inflation, allowing for the formation of cosmic strings and domain walls, effects which exclude models with $N > 1$ such as the DFSZ-model. In the presence of inflation, the initial "misalignment value" of the axion field, $a_i/2\pi f_a$, can take on any value in the interval [0, 1]. It is disputed whether or not all of these values have equal conditional probabilities to produce possible observers, and according to Goldberg [361], there is no dependence on a_i. We also indicate the uncertainty of the SN 1987A bound and of the inflationary axion bound. It is not clear whether or not there is a window between the Davis–Shellard bound and the SN 1987A bound. If there is no window, axions need inflation.

KSVZ-type axions it is shown as a function of the electromagnetic anomaly coefficient, E/N, which affects the coupling strength to photons, while all other couplings are uniquely fixed, barring the uncertainty of the amount of proton spin carried by strange quarks. However, the results are rather insensitive to this value within the experimentally allowed range. While E/N in any realistic axion model must be the ratio of small integers, the graphical display is facilitated by treating it as a continuous variable. The dip in the constraints from the photon coupling at $E/N = 1.92$ could equally occur at $E/N = 2$ because the number 1.92 is uncertain within ± 0.08 (see section 2.3.2). However, the dip would be filled in somewhat by higher-order interactions. For DFSZ-axions the constraints are shown as a function of β which affects somewhat the coupling to nucleons, affects drastically the coupling to electrons, and leaves the photon coupling entirely untouched: $E/N = 8/3$.

Because of axion trapping in the supernova for m_a exceeding a few eV there exists a small window of allowed axion masses for hadronic axions between the red giant and SN 1987A bound, a range sometimes referred to as "Turner's window". The magnitude of this window, and whether or not one has to appeal to $E/N = 2$ for its existence, depends critically on the SN 1987A axion bounds in the trapping regime. Moreover, for most parameters in this window axions could trigger the Kamiokande detector so efficiently that most of the relevant parameter range is excluded (see sections 10.6 and ref. [96]).

We also show the cosmological constraints that were discussed in chapter 3. If the universe never underwent inflation, or if it inflated before the Peccei–Quinn symmetry breaking, we have to focus on $N = 1$ models to avoid overclosing the universe by the energy associated with domain walls. Even for $N = 1$ models there is only a narrow range of axion masses which possibly remains allowed. If Davis and Shellard's [348] treatment of the string radiated axion density is correct, axions are necessarily a large fraction of the cosmic mass density, and most likely affect supernova physics. A more rigorous treatment of string radiation and of supernova physics with axions might reveal that this entire window is closed.

If the universe inflated after the Peccei–Quinn symmetry breaking there remains a large range of masses where axions are allowed, and for specific combinations of m_a and the initial "misalignment" they would be the dark matter of the universe. In the mass range around 10^{-5} eV galactic axions can be detected, in principle, in laboratory experiments.

11.2.3. Summary and outlook

In summary, the astrophysical and cosmological axion constraints leave a number of interesting windows for the possible existence of axions that should be further explored. A better understanding of many-body effects in the core of supernovae and a truly self-consistent calculation taking these effects into account is of great interest. "Turner's window" between the red giant and SN 1987A bounds for hadronic axion models can be explored, in principle, by laboratory experiments searching for solar axions (section 7.3), and the same window is accessible to searches for a spectral line from axion decay in the "glow of the night sky" (section 3.4). The cosmic mass density from axionic string decay should be treated in more detail so that, perhaps, the SN 1987A and the cosmological bounds can be brought to overlap, allowing one to conclude that axions need inflation, unless they lie in Turner's window.

The most important question, however, is whether axions are the dark matter of the universe. Searches for galactic axions (section 3.5) are therefore of paramount importance. While a negative search result cannot rule out the existence of axions, the parameter range accessible to microwave cavity searches covers a well-motivated range of parameters for one of the few serious cold dark matter candidates.

Acknowledgements

There are many friends and colleagues to whom I am directly and indirectly indebted for having made possible the writing of this report, especially to my collaborators in this field, Dave Dearborn, Andy Gould, Pierre Salati, Dave Seckel, Joe Silk, Glenn Starkman, and Leo Stodolsky. I appreciate that Adam Burrows, Tom Loredo and Alvio Renzini provided me with originals for several figures, and that Michael Turner provided me with preliminary results of ongoing research as well as a number of helpful comments on the manuscript. My special thanks go to Joe Silk and Dave Dearborn who opened up the opportunity for me to do astro–particle physics research in Berkeley where most of this report was written, and to John Bahcall for the same opportunity in Princeton where this work was begun. David Schramm originally solicited this work as an editor of Physics Reports, and provided a lot of much-needed encouragement on the way. I acknowledge financial support by the Institute for Advanced Study in Princeton (U.S.A.), by the Max-Planck-Society (West Germany) through their Otto-Hahn-Fellowship program, and in Berkeley (U.S.A.) by grants from NSF, NASA, DOE, and the Institute for Geophysics and Planetary Physics, Livermore.

References

[1] G. Gamow and M. Schoenberg, Phys. Rev. 58 (1940) 1117.
[2] G. Gamow and M. Schoenberg, Phys. Rev. 59 (1941) 539.
[3] B. Pontecorvo, Zh. Eksp. Teor. Fiz. 36 (1959) 1615 [Sov. Phys. – JETP 9 (1959) 1148].
[4] G.M. Gandel'man and V.S. Pinaev, Zh. Eksp. Teor. Fiz. 37 (1959) 1072 [Sov. Phys. – JETP 10 (1959) 764].
[5] H.-Y. Chiu and R.C. Stabler, Phys. Rev. 122 (1961) 1317.
[6] V.I. Ritus, Zh. Eksp. Teor. Fiz. 41 (1961) 1285 [Sov. Phys. – JETP 14 (1962) 915].
[7] J.B. Adams, M.A. Ruderman and C.-H. Woo, Phys. Rev. 129 (1963) 1383.
[8] G. Feinberg, Proc. R. Soc. London A 285 (1965) 257.
[9] M.A. Ruderman, Rep. Prog. Phys. 28 (1965) 411.
[10] H.-Y. Chiu, Annu. Rev. Nucl. Sci. 16 (1966) 591.
[11] G. Beaudet, V. Petrosian and E.E. Salpeter, Astrophys. J. 150 (1967) 979.
[12] D.A. Dicus, Phys. Rev. D 6 (1972) 941.
[13] D.A. Dicus, E.W. Kolb, D.N. Schramm and D.L. Tubbs, Astrophys. J. 210 (1976) 481.
[14] S. Barkat, Annu. Rev. Astron. Astrophys. 13 (1975) 45.
[15] H. Munakata, Y. Kohyama and N. Itoh, Astrophys. J. 296 (1985) 197; 304 (1986) 580 (E).
[16] P.J. Schinder, D.N. Schramm, P.A. Wiita, S.H. Margolis and D.L. Tubbs, Astrophys. J. 313 (1987) 531.
[17] N. Itoh, T. Adachi, M. Nakagawa, Y. Kohyama and H. Munakata, Astrophys. J. 339 (1989) 354; Erratum to be published.
[18] B.L. Friman and O.V. Maxwell, Astrophys. J. 232 (1979) 541.
[19] J.D. Landstreet, Phys. Rev. 153 (1967) 1372.
[20] V. Canuto and L. Fassio-Canuto, Phys. Rev. D 7 (1973) 1593.
[21] V. Canuto and L. Fassio-Canuto, Phys. Rev. D 7 (1973) 1601.
[22] C.K. Chou, L. Fassio-Canuto and V. Canuto, Astrophys. J. 227 (1979) 974.
[23] H.-Y. Chiu and P. Morrison, Phys. Rev. Lett. 5 (1960) 573.
[24] M. Gell-Mann, Phys. Rev. Lett. 6 (1961) 70.
[25] D. Boccaletti, V. de Sabbata and C. Gualdi, Nuovo Cimento 33 (1964) 520.
[26] D. Boccaletti, V. de Sabbata and C. Gualdi, Nuovo Cimento 40A (1965) 705.
[27] J.A. Campbell, Austr. J. Phys. 21 (1968) 139.
[28] S.G. Matinyan and N.N. Tsilosuni, Zh. Eksp. Teor. Fiz. 41 (1961) 1681 [Sov. Phys. – JETP 14 (1962) 1195].
[29] L. Rosenberg, Phys. Rev. 129 (1963) 2786.
[30] M.J. Levine, Nuovo Cimento 48 (1967) 67.
[31] V.K. Cung and M. Yoshimura, Nuovo Cimento 29A (1975) 557.
[32] A. Halprin, Phys. Rev. D 11 (1975) 147.
[33] A.A. Natale, V. Pleitez and A. Tacla, Phys. Rev. D 36 (1987) 3278.

[34] R. Stothers and H.-Y. Chiu, Astrophys. J. 135 (1962) 963.
[35] R. Stothers, Astrophys. J. 138 (1963) 1085.
[36] C.-W. Chin, H.-Y. Chiu and R. Stothers, Ann. Phys. (NY) 39 (1966) 280.
[37] R. Stothers, Astron. J. 71 (1966) 943.
[38] R. Stothers, Astrophys. J. 155 (1969) 935.
[39] R. Stothers and C.-W. Chin, Astrophys. J. 158 (1969) 1039.
[40] R. Stothers, Astrophys. Lett. 4 (1969) 187.
[41] R. Stothers, Phys. Rev. Lett. 24 (1970) 538.
[42] R. Stothers, Astrophys. J. 175 (1972) 717.
[43] F. Reines, H.S. Gurr and W.H. Sobel, Phys. Rev. Lett. 37 (1976) 315.
[44] S. Weinberg, Phys. Rev. Lett. 40 (1978) 223.
[45] F. Wilczek, Phys. Rev. Lett. 40 (1978) 279.
[46] R.D. Peccei and H.R. Quinn, Phys. Rev. Lett. 38 (1977) 1440.
[47] R.D. Peccei and H.R. Quinn, Phys. Rev. D 16 (1977) 1791.
[48] R.D. Peccei, in: Neutrino '81, eds R.J. Cence et al. (Univ. of Hawaii, Honolulu, 1981).
[49] R.D. Peccei, in: Proc. Fourth Kyoto Summer Institute on Grand Unified Theories and Related Topics 1981, eds M. Konuma and T. Maskawa (World Scientific, Singapore, 1981).
[50] R.D. Peccei, in: *CP* Violation, ed. C. Jarlskog (World Scientific, Singapore, 1989).
[51] J.E. Kim, Phys. Rep. 150 (1987) 1.
[52] H.-Y. Cheng, Phys. Rep. 158 (1988) 1.
[53] H.-Y. Cheng, Phys. Rev. D 36 (1987) 1649.
[54] K. Sato and H. Sato, Prog. Theor. Phys. 54 (1975) 1564.
[55] T. Altherr, Z. Phys. C 47 (1990) 559.
[55a] T. Altherr, Report HU-TFT-90-36 (June 1990), to be published in Ann. Phys. (NY).
[56] A. Barroso and G.C. Branco, Phys. Lett. B 116 (1982) 247.
[57] R.P. Brinkmann and M.S. Turner, Phys. Rev. D 38 (1988) 2338.
[58] A. Burrows, M.S. Turner and R.P. Brinkmann, Phys. Rev. D 39 (1989) 1020.
[59] A. Burrows, T. Ressell and M.S. Turner, to be published in Phys. Rev. D.
[60] M. Carena and R.D. Peccei, Phys. Rev. D 40 (1989) 652.
[61] R. Chanda, J.F. Nieves and P.B. Pal, Phys. Rev. D 37 (1988) 2714.
[62] K. Choi, K. Kang and J.E. Kim, Phys. Rev. Lett. 62 (1989) 849.
[63] D.S.P. Dearborn, D.N. Schramm and G. Steigman, Phys. Rev. Lett. 56 (1986) 26.
[64] D.A. Dicus, E.W. Kolb, V.L. Teplitz and R.V. Wagoner, Phys. Rev. D 18 (1978) 1829.
[65] D.A. Dicus, E.W. Kolb, V.L. Teplitz and R.V. Wagoner, Phys. Rev. D 22 (1980) 839.
[66] S. Dimopoulos, J. Frieman, B.W. Lynn and G.D. Starkman, Phys. Lett. B 179 (1986) 223.
[67] S. Dimopoulos, G.D. Starkman and B.W. Lynn, Phys. Lett. B 167 (1986) 145.
[68] S. Dimopoulos, G.D. Starkman and B.W. Lynn, Mod. Phys. Lett. A 8 (1986) 491.
[69] J. Ellis and K.A. Olive, Nucl. Phys. B 233 (1983) 252.
[70] J. Ellis and K.A. Olive, Phys. Lett. B 193 (1987) 525.
[71] T.E.O. Ericson and J.-F. Mathiot, Phys. Lett. B 219 (1989) 507.
[72] J.A. Frieman, S. Dimopoulos and M.S. Turner, Phys. Rev. D 36 (1987) 2201.
[73] M. Fukugita, S. Watamura and M. Yoshimura, Phys. Rev. Lett. 48 (1982) 1522.
[74] M. Fukugita, S. Watamura and M. Yoshimura, Phys. Rev. D 26 (1982) 1840.
[75] T. Hatsuda and M. Yoshimura, Phys. Lett. B 203 (1988) 469.
[76] N. Ishizuka and M. Yoshimura, Prog. Theor. Phys. 84 (1990) 233.
[77] N. Iwamoto, Phys. Rev. Lett. 53 (1984) 1198.
[78] N. Iwamoto, Phys. Rev. D 39 (1989) 2120.
[79] L.M. Krauss, J.E. Moody and F. Wilczek, Phys. Lett. B 144 (1984) 391.
[80] R. Mayle, J.R. Wilson, J. Ellis, K. Olive, D.N. Schramm and G. Steigman, Phys. Lett. B 203 (1988) 188.
[81] R. Mayle, J.R. Wilson, J. Ellis, K. Olive, D.N. Schramm and G. Steigman, Phys. Lett. B 219 (1989) 515.
[82] K.O. Mikaelian, Phys. Rev. D 18 (1978) 3605.
[83] D.E. Morris, Phys. Rev. D 34 (1986) 843.
[84] M. Nakagawa, Y. Kohyama and N. Itoh, Astrophys. J. 322 (1987) 291.
[85] M. Nakagawa, T. Adachi, Y. Kohyama and N. Itoh, Astrophys. J. 326 (1988) 241.
[86] A. Pantziris and K. Kang, Phys. Rev. D 33 (1986) 3509.
[87] G. Raffelt, Phys. Rev. D 33 (1986) 897.
[88] G. Raffelt, Phys. Lett. B 166 (1986) 402.
[89] G. Raffelt and D. Dearborn, Phys. Rev. D 36 (1987) 2211.

[90] G. Raffelt and D. Dearborn, Phys. Rev. D 37 (1988) 549.
[91] G. Raffelt, Phys. Rev. D 37 (1988) 1356.
[92] G. Raffelt and D. Seckel, Phys. Rev. Lett. 60 (1988) 1793.
[93] G. Raffelt, Phys. Rev. D 41 (1990) 1324.
[94] P. Salati and J. Ellis, report CERN-TH-5693 (1990), to be published.
[95] K. Sato, Prog. Theor. Phys. 60 (1978) 1942.
[96] J. Engel, D. Seckel and A.C. Hayes, Phys. Rev. Lett. 65 (1990) 960.
[97] M.S. Turner, Phys. Rev. Lett. 60 (1988) 1797.
[98] M.S. Turner, H.-S. Kang and G. Steigman, Phys. Rev. D 40 (1989) 299.
[99] S. Tsuruta and K. Nomoto in: Proc. IAU Symp. No. 124, Observational Cosmology, 1986.
[100] M.I. Vysotskii, Ya.B. Zel'dovich, M.Yu. Khlopov and V.M Chechetkin, Pis'ma Zh. Eksp. Teor. Fiz. 27 (1978) 533 [JETP Lett. 27 (1978) 502].
[101] H.M. Georgi, S.L. Glashow and S. Nussinov, Nucl. Phys. B 193 (1981) 297.
[102] G.B. Gelmini, S. Nussinov and M. Roncadelli, Nucl. Phys. B 209 (1982) 157.
[103] E.W. Kolb, D.L. Tubbs and D.A. Dicus, Astrophys. J. 255 (1982) L57.
[104] D.A. Dicus, E.W. Kolb and D.L. Tubbs, Nucl. Phys. B 223 (1983) 532.
[105] Y. Aharonov, F.T. Avignone III and S. Nussinov, Phys. Lett. B 200 (1988) 122.
[106] Y. Aharonov, F.T. Avignone III and S. Nussinov, Phys. Rev. D 37 (1988) 1360.
[107] Y. Aharonov, F.T. Avignone III and S. Nussinov, Phys. Rev. D 39 (1989) 985.
[108] K. Choi, C.W. Kim, J. Kim and W.P. Lam, Phys. Rev. D 37 (1988) 3225.
[109] G. Fuller, R. Mayle and J.R. Wilson, Astrophys. J. 332 (1988) 826.
[110] R.V. Konoplich and M.Yu. Khlopov, Sov. J. Nucl. Phys. 47 (1988) 565 [Yad. Fiz. 47 (1986) 891].
[111] J.A. Grifols, E. Massó and S. Peris, Phys. Lett. B 215 (1988) 593.
[112] S. Bertolini and A. Santamaria, Phys. Lett. B 220 (1989) 597.
[113] Z.G. Berezhiani and A.Yu. Smirnov, Phys. Lett. B 220 (1989) 279.
[114] K. Choi and A. Santamaria, Phys. Rev. D 42 (1990) 293.
[115] A.V. Averin, A.V. Borisov and A.I. Studenikin, Phys. Lett. B 231 (1989) 280.
[116] J.A. Grifols and E. Massó, Phys. Lett. B 173 (1986) 237.
[117] J.A. Grifols, E. Massó and S. Peris, Mod. Phys. Lett. A 4 (1989) 311.
[118] J.C. van der Velde, Phys. Rev. D 39 (1989) 1492
[119] G. Raffelt, Phys. Rev. D 38 (1988) 3811.
[120] S. Hoffmann, Phys. Lett. B 193 (1987) 117.
[121] A.A. Ansel'm and M.V. Polyakov, Sov. J. Nucl. Phys. 47 (1988) 1150 [Yad. Fiz. 47 (1988) 1818].
[122] M. Fukugita and N. Sakai, Phys. Lett. B 114 (1982) 23.
[123] A. Bouquet and C.E. Vayonakis, Phys. Lett. B 116 (1982) 219.
[124] J.D. Anand, S.N. Biswas, A. Goyal and J.N. Passi, Phys. Rev. D 29 (1984) 1270.
[125] A. Halprin, Phys. Rev. D 32 (1985) 3081.
[126] K. Hikasa, M. Kobayashi and M. Yoshimura, Prog. Theor. Phys. 78 (1987) 180.
[127] J. Ellis, K.A. Olive, S. Sarkar and D.W. Sciama, Phys. Lett. B 215 (1988) 404.
[128] J.A. Grifols, E. Massó and S. Peris, Phys. Lett. B 220 (1989) 591.
[129] J.A. Grifols and E. Massó, Nucl. Phys. B 331 (1990) 244.
[130] J. Bernstein, M. Ruderman and G. Feinberg, Phys. Rev. 132 (1963) 1227.
[131] S.I. Blinnikov, ITEP-Preprint No. 19 (1988), unpublished.
[132] P. Sutherland, J.N. Ng, E. Flowers, M. Ruderman and C. Inman, Phys. Rev. D 13 (1976) 2700.
[133] S. Nussinov and Y. Rephaeli, Phys. Rev. D 36 (1987) 2278.
[134] M. Fukugita and S. Yazaki, Phys. Rev. D 36 (1987) 3817.
[135] G. Raffelt, D. Dearborn and J. Silk, Astrophys. J. 336 (1989) 64.
[136] R. Barbieri and R.N. Mohapatra, Phys. Rev. Lett. 61 (1988) 27.
[137] R. Barbieri, R.N. Mohapatra and T. Yanagida, Phys. Lett. B 213 (1988) 69.
[138] S.I. Blinnikov and L.B. Okun, Pis'ma Astron. Zh. 14 (1988) 867.
[139] S.W. Falk and D.N. Schramm, Phys. Lett. B 79 (1978) 511.
[140] I. Goldman, Y. Aharonov, G. Alexander and S. Nussinov, Phys. Rev. Lett. 60 (1988) 1789.
[141] J.M. Lattimer and J. Cooperstein, Phys. Rev. Lett. 61 (1988) 23.
[142] D. Nötzold, Phys. Rev. D 38 (1988) 1658.
[143] L.B. Okun, Sov. J. Nucl. Phys. 48 (1988) 967 [Yad. Fiz. 48 (1988) 1519].
[144] M.B. Voloshin, Phys. Lett. B 209 (1988) 360.
[145] J.A. Grifols and E. Massó, Phys. Rev. D 40 (1989) 3819.
[146] G. Raffelt, Report CfPA-TH-89-017, Astrophys. J. (1990), to be published.

[147] R. Barbieri and R.N. Mohapatra, Phys. Rev. D 39 (1989) 1229.
[148] J.A. Grifols, E. Massó and T.G. Rizzo, Report MAD/PH/549 (December 1989).
[149] K.J.F. Gaemers, R. Gandhi and J.M. Lattimer, Phys. Rev. D 40 (1989) 309.
[150] J.A. Grifols and E. Massó, Phys. Lett. B 242 (1990) 77.
[151] A. Pérez and R. Gandhi, Phys. Rev. D 41 (1990) 2374.
[152] D. Choudhury, N.D. Hari Dass and M.V.N. Murthy, Classical Quantum Gravity 6 (1989) L167.
[153] R. Stothers, Phys. Rev. D 2 (1970) 1417.
[154] R. Stothers, Phys. Lett. A 36 (1971) 5.
[155] G. Papini and S.R. Valluri, Phys. Rep. 33 (1977) 51.
[156] G. Schäfer and H. Dehnen, Phys. Rev. D 27 (1983) 2864.
[157] R.J. Gould, Astrophys. J. 288 (1985) 789.
[158] S. del Campo and L.H. Ford, Phys. Rev. D 38 (1988) 3657.
[159] G.E. Brown, ed., Phys. Rep. 163 (1988) 1.
[160] E.D. Carlson and P. Salati, Phys. Lett. B 218 (1989) 79.
[161] G. Raffelt and G. Starkman, Phys. Rev. D 40 (1989) 942.
[162] F.G. Houtermans and W. Thirring, Helv. Phys. Acta 27 (1954) 81.
[163] J.N. Bahcall, Neutrino Astrophysics (Cambridge Univ. Press, Cambridge, 1989).
[164] K.S. Hirata et al., Phys. Rev. Lett. 63 (1989) 16.
[165] R.M. Bionta et al., Phys. Rev. Lett. 58 (1987) 1494.
[166] C.B. Bratton et al., Phys. Rev. D 37 (1988) 3361.
[167] K.S. Hirata et al., Phys. Rev. Lett. 58 (1987) 1490.
[168] K.S. Hirata et al., Phys. Rev. D 38 (1988) 448.
[169] J. Arafune, M. Fukugita, T. Yanagida and M. Yoshimura, Phys. Lett. B 194 (1987) 477.
[170] J. Arafune and M. Fukugita, Phys. Rev. Lett. 59 (1987) 367.
[171] J. Arafune, M. Fukugita, T. Yanagida and M. Yoshimura, Phys. Rev. Lett. 59 (1987) 1864.
[172] T.K. Kuo and J. Pantaleone, Phys. Rev. D 37 (1988) 298.
[173] P.O. Lagage, M. Cribier, J. Rich and D. Vignaud, Phys. Lett. B 193 (1987) 127.
[174] H. Minakata, H. Nunokawa, K. Shiraishi and H. Suzuki, Mod. Phys. Lett. A 2 (1987) 827.
[175] H. Minakata and H. Nunokawa, Phys. Rev. D 38 (1988) 3605.
[176] H. Minakata and H. Nunokawa, TMUP-HEL-8913 (1989).
[177] S.P. Mikheev and A.Yu. Smirnov, Sov. Phys. - JETP 64 (1986) 4 [Zh. Eksp. Teor. Fiz. 91 (1986) 7].
[178] D. Nötzold, Phys. Lett. B 196 (1987) 315.
[179] S.P. Rosen, Phys. Rev. D 37 (1988) 1682.
[180] T.P. Walker and D.N. Schramm, Phys. Lett. B 195 (1987) 331.
[181] F. von Feilizsch and L. Oberauer, Phys. Lett. B 200 (1988) 580.
[182] E.L. Chupp, W.T. Vestrand and C. Reppin, Phys. Rev. Lett. 62 (1989) 505.
[183] E.W. Kolb and M.S. Turner, Phys. Rev. Lett. 62 (1989) 509.
[184] T. Hatsuda, C.S. Lim and M. Yoshimura, Phys. Lett. B 203 (1988) 462.
[185] M. Takahara and K. Sato, Mod. Phys. Lett. A 2 (1987) 293.
[186] J.A. Frieman, H.E. Haber and K. Freese, Phys. Lett. B 200 (1988) 115.
[187] J.M. Soares and L. Wolfenstein, Phys. Rev. D 40 (1989) 3666.
[188] G. Raffelt and L. Stodolsky, Phys. Lett. B 119 (1982) 323.
[189] R. Cowsik, Phys. Rev. Lett. 39 (1977) 784.
[190] G.G. Raffelt, Phys. Rev. D 31 (1985) 3002.
[191] R. Cowsik, Phys. Rev. D 19 (1979) 2219.
[192] T. Goldman and G.J. Stephenson Jr, Phys. Rev. D 19 (1979) 2215.
[193] A.S. Goldhaber and M.M. Nieto, Rev. Mod. Phys. 43 (1971) 277.
[194] J.D. Barrow and R.R. Burman, Nature 307 (1984) 14.
[195] G. Cocconi, Phys. Lett. B 206 (1988) 705.
[196] R.W. Romani, Phys. Lett. B 215 (1988) 477.
[197] L.F. Abbott, A. de Rújula and T.P. Walker, Nucl. Phys. B 299 (1988) 734.
[198] E.N. Adams, Phys. Rev. D 37 (1988) 2047.
[199] W.D. Arnett and J.L. Rosner, Phys. Rev. Lett. 58 (1987) 1906.
[200] J.N. Bahcall and S.L. Glashow, Nature 326 (1987) 476.
[201] A. Burrows and J.M. Lattimer, Astrophys. J. 318 (1987) L63.
[202] A. Burrows, Astrophys. J. 328 (1988) L51.
[203] H.-Y. Chiu, K.L. Chan and Y. Kondo, Astrophys. J. 329 (1988) 326.
[204] R. Cowsik, Phys. Rev. D 37 (1988) 1685.

[205] E.W. Kolb, A.J. Stebbins and M.S. Turner, Phys. Rev. D 35 (1987) 3598.
[206] E.W. Kolb, A.J. Stebbins and M.S. Turner, Phys. Rev. D 36 (1987) 3820.
[207] S. Midorikawa, H. Terazawa and K. Akama, Mod. Phys. Lett. A 2 (1987) 561.
[208] K. Sato and H. Suzuki, Phys. Rev. Lett. 58 (1987) 2722.
[209] K. Sato and H. Suzuki, Phys. Lett. B 196 (1987) 267.
[210] D.N. Spergel and J.N. Bahcall, Phys. Lett. B 200 (1988) 366.
[211] T.J. Loredo and D.Q. Lamb, Ann. NY Acad. Sci. 571 (1989) 601.
[212] G. Barbiellini and G. Cocconi, Nature 329 (1987) 21.
[213] J.A. Grifols, E. Massó and S. Peris, Phys. Lett. B 207 (1988) 493.
[214] G. Fiorentini and G. Mezzorani, Report, 1988.
[215] E.W. Kolb and M.S. Turner, Phys. Rev. D 36 (1987) 2895.
[216] M.J. Longo, Phys. Rev. D 36 (1987) 3276.
[217] L.D. Almeida, G.E.A. Matsas and A.A. Natale, Phys. Rev. D 39 (1989) 677.
[218] S. Pakvasa, W.A. Simmons and T.J. Weiler, Phys. Rev. D 39 (1989) 1761.
[219] L. Krauss and S. Tremaine, Phys. Rev. Lett. 60 (1988) 176.
[220] A.A. Coley and S. Tremaine, Phys. Rev. D 38 (1988) 2927.
[221] L. Stodolsky, Phys. Lett. B 201 (1988) 353.
[222] S. Weinberg, Gravitation and Cosmology (Wiley, New York, 1972).
[223] C.W. Misner, K.S. Thorne and J.A. Wheeler, Gravitation (Freeman, San Francisco, 1973).
[224] J.R. Oppenheimer and G.M. Volkoff, Phys. Rev. 55 (1939) 374.
[225] C.P. Burgess and J. Cloutier, Phys. Rev. D 38 (1988) 2944.
[226] E.N. Glass and G. Szamosi, Phys. Rev. D 35 (1987) 1205.
[227] E.N. Glass and G. Szamosi, Phys. Rev. D 39 (1989) 1054.
[228] R.L. Gilliland and W. Däppen, Astrophys. J. 313 (1987) 429.
[229] J.R. Kuhn, in: Proc. IAU-Symp. No. 123, Advances in Helio- and Asteroseismology, eds J. Christensen-Dalsgaard and S. Frandsen (Reidel, Dordrecht, 1988).
[230] J. Ellis, S. Kalara, K.A. Olive and C. Wetterich, Phys. Lett. B 228 (1989) 264.
[231] R. Boyd, R.E. Turner, M. Wiescher and L. Rybarcyk, Phys. Rev. Lett. 51 (1983) 609.
[232] M. Izawa, Prog. Theor. Phys. 75 (1986) 556.
[233] K. Freese, Astrophys. J. 286 (1984) 216.
[234] R.A. Carrigan Jr. Nature 288 (1980) 348.
[235] M.S. Turner, Nature 302 (1983) 804.
[236] J. Arafune, M. Fukugita and S. Yanagita, Phys. Rev. D 32 (1985) 2586.
[237] S. Dimopoulos, J. Preskill and F. Wilczek, Phys. Lett. B 119 (1982) 320.
[238] E.W. Kolb, S.A. Colgate and J.A. Harvey, Phys. Rev. Lett. 49 (1982) 1373.
[239] K. Freese, M.S. Turner and D.N. Schramm, Phys. Rev. Lett. 51 (1983) 1625.
[240] V.A. Kuzmin and V.A. Rubakov, Phys. Lett. B 125 (1983) 372.
[241] K.A. Olive and D.N. Schramm, Phys. Lett. B 130 (1983) 267.
[242] V.A. Rubakov, Pisma Zh. Eksp. Teor. Fiz. 33 (1981) 658 [JETP Lett. 33 (1981) 644].
[243] J. Arafune and M. Fukugita, Phys. Lett. B 133 (1983) 380.
[244] L. Bracci, G. Fiorentini and G. Mezzorani, Nucl. Phys. B 258 (1985) 726.
[245] S. Dimopoulos, S.L. Glashow, E.M. Purcell and F. Wilczek, Nature 298 (1982) 824.
[246] A.K. Drukier, Astron. Astrophys. 33 (1983) 127.
[247] J.A. Harvey, Nucl. Phys. B 236 (1984) 255.
[248] J.A. Harvey, M.A. Ruderman and J. Shaham, Phys. Rev. D 33 (1986) 2084.
[249] G. Steigman, C.L. Sarazin, H. Quintana and J. Faulkner, Astrophys. J. 83 (1978) 1050.
[250] D.N. Spergel and W.H. Press, Astrophys. J. 294 (1985) 663.
[251] M. Nauenberg, Phys. Rev. D 36 (1987) 1080.
[252] A. Gould and G. Raffelt, Astrophys. J. 352 (1990) 654.
[253] A. Gould and G. Raffelt, Astrophys. J. 352 (1990) 669.
[254] K. Griest, Phys. Rev. D 37 (1988) 2703.
[255] W.H. Press and D.N. Spergel, Astrophys. J. 296 (1985) 679.
[256] A. Gould, Astrophys. J. 321 (1987) 560.
[257] A. Gould, Astrophys. J. 321 (1987) 571.
[258] A. Gould, Astrophys. J. 328 (1988) 919.
[259] A. Gould, J.A. Frieman and K. Freese, Phys. Rev. D 39 (1989) 1029.
[260] A. Gould, Astrophys. J. 356 (1990) 302.
[261] A. Bouquet and P. Salati, Astron. Astrophys. 217 (1989) 270.

[262] J. Faulkner and R.L. Gilliland, Astrophys. J. 299 (1985) 994.
[263] R.L. Gilliland, J. Faulkner, W.H. Press and D.N. Spergel, Astrophys. J. 306 (1986) 703.
[264] A. Bouquet, J. Kaplan and F. Martin, Astron. Astrophys. 222 (1989) 103.
[265] Y. Giraud-Héraud, J. Kaplan, F. Martin de Volnay, C. Tao and S. Turck-Chiéze, Report PAR-LPTHE 89-24, Solar Physics (1990), to be published.
[266] D. Dearborn, K. Griest and G. Raffelt, Report CfPA-TH-90-012 (1990), to be published in Astrophys. J.
[267] J. Faulkner, D.O. Gough and M.N. Vahia, Nature 321 (1986) 226.
[268] W. Däppen, R.L. Gilliland and J. Christensen-Dalsgaard, Nature 321 (1986) 229.
[269] A.N. Ellis and D.O. Gough, in: Proc. IAU-Symp. No. 123, Advances in Helio- and Asteroseismology, eds J. Christensen-Dalsgaard and S. Frandsen (Reidel, Dordrecht, 1988).
[270] S. Raby, Report (1989).
[271] P. Salati, Astrophys. J. 348 (1990) 738.
[272] J. Faulkner and F.J. Swenson, Astrophys. J. 329 (1988) L47.
[273] A. Renzini, Astron. Astrophys. 171 (1987) 121.
[274] M. Rees, in: Proc. IAU-Symp. No. 126, Globular Cluster Systems in Galaxies, eds J.E. Grindley and A.G.D. Philip (Kleuwer Academic Publishers, Dordrecht, 1986).
[275] D.N. Spergel and J. Faulkner, Astrophys. J. 331 (1988) L21.
[276] A. Bouquet, G. Raffelt, P. Salati and J. Silk, Report, LBL-TH-25215 (May 1988), unpublished.
[277] A. Bouquet and P. Salati, Astrophys. J. 346 (1989) 284.
[278] D. Dearborn, G. Raffelt, P. Salati, J. Silk and A. Bouquet, Nature 343 (1990) 347.
[279] D. Dearborn, G. Raffelt, P. Salati, J. Silk and A. Bouquet, Astrophys. J. 354 (1990) 568.
[280] P. Salati, G. Raffelt and D. Dearborn, Astrophys. J. 357 (1990) 566.
[281] I. Goldman and S. Nussinov, Phys. Rev. D 40 (1989) 3221.
[282] L.M. Krauss, K. Freese, D.N. Spergel and W.H. Press, Astrophys. J. 299 (1985) 1001.
[283] P. Salati and J. Silk, Report LBL-24797, Astrophys. J. 338 (1989) 24.
[284] J. Silk, K.A. Olive and M. Srednicki, Phys. Rev. Lett. 55 (1985) 257.
[285] B.A. Campbell, J. Ellis, K. Enqvist, D.V. Nanopoulos, J.S. Hagelin and K.A. Olive, Phys. Lett. B 173 (1986) 270.
[286] K. Freese, Phys. Lett. B 167 (1986) 295.
[287] T.K. Gaisser, G. Steigman and S. Tilav, Phys. Rev. D 34 (1986) 2006.
[288] L.M. Krauss, M. Srednicki and F. Wilczek, Phys. Rev. D 33 (1986) 2079.
[289] J. Ellis, R.A. Flores and S. Ritz, Phys. Lett. B 198 (1987) 393.
[290] K. Griest and D. Seckel, Nucl. Phys. B 283 (1987) 681, Nucl. Phys. B 296 (1988) 1034 (E).
[291] J.S. Hagelin, K. Ng and K. Olive, Phys. Lett. B 180 (1987) 375.
[292] K. Ng, K.A. Olive and M. Srednicki, Phys. Lett. B 188 (1987) 138.
[293] K.A. Olive and M. Srednicki, Report, UMN-TH-636/87, Univ. of Minnesota, 1987.
[294] S. Ritz and D. Seckel, Nucl. Phys. B 304 (1988) 877.
[295] M. Srednicki, K.A. Olive and J. Silk, Nucl. Phys. B 279 (1987) 804.
[296] A. Finzi and A. Harpaz, Astron. Astrophys. 211 (1989) 441.
[297] E. Chudnovsky and A. Vilenkin, Phys. Rev. Lett. 61 (1988) 1043.
[298] A. Gould, B.T. Draine, R. Romani and S. Nussinov, Phys. Lett. B 238 (1990) 337.
[299] G. Baym and C.J. Pethick, Annu. Rev. Nucl. Sci. 25 (1975) 27.
[300] G. Baym and C.J. Pethick, Annu. Rev. Astron. Astrophys. 17 (1979) 415.
[301] S.L. Shapiro and S.A. Teukolsky, Black Holes, White Dwarfs, and Neutron Stars (Wiley, New York, 1983).
[302] D. Pines, Lectures presented at the NATO Institute "High Energy Phenomena and Collapsed Stars", 1985.
[303] D.J. Helfand and J.-H. Huang, eds, The Origin and Evolution of Neutron Stars, IAU-Symp. No. 125 (Reidel, Dordrecht, 1987).
[304] G. 't Hooft, Phys. Rev. Lett. 37 (1976) 8.
[305] G. 't Hooft, Phys. Rev. D 14 (1976) 3432.
[306] S. Weinberg, Phys. Rev. D 11 (1975) 3583.
[307] C.G. Callan, R.F. Dashen and D.J. Gross, Phys. Lett. B 63 (1976) 334.
[308] R. Jackiw and C. Rebbi, Phys. Rev. Lett. 37 (1976) 177.
[309] V. Baluni, Phys. Rev. D 19 (1979) 2227.
[310] R. Crewther, P. diVecchia, G. Veneziano and E. Witten, Phys. Lett. B 88 (1979) 123.
[311] R. Crewther, P. diVecchia, G. Veneziano and E. Witten, Phys. Lett. B 91 (1980) 487 (E).
[312] I.S. Altarev et al., Phys. Lett. B 102 (1981) 13.
[313] J.M. Pendlebury et al., Phys. Lett. B 136 (1984) 327.
[314] L. Wolfenstein, Annu. Rev. Nucl. Part. Sci. 36 (1986) 137.
[315] D.B. Kaplan, Nucl. Phys. B 260 (1985) 215.
[316] P. Sikivie, in: Cosmology and Particle Physics, eds E. Alvarez et al. (World Scientific, Singapore, 1987).

[317] M. Srednicki, Nucl. Phys. B 260 (1985) 689.
[318] H. Georgi, D.B. Kaplan and L. Randall, Phys. Lett. B 169 (1986) 73.
[319] Y. Chikashige, R.N. Mohapatra and R.D. Peccei, Phys. Lett. B 98 (1981) 265.
[320] G.B. Gelmini and M. Roncadelli, Phys. Lett. B 99 (1981) 411.
[321] P.B. Pal, Phys. Lett. B 205 (1988) 65.
[322] W.A. Bardeen and S.H.H. Tye, Phys. Lett. B 74 (1978) 580.
[323] J. Kandaswamy, P. Salomonson and J. Schechter, Phys. Rev. D 17 (1978) 3051.
[324] W.A. Bardeen, R.D. Peccei and T. Yanagida, Nucl. Phys. B 279 (1987) 401.
[325] Particle Data Group, Phys. Lett. B 204 (1988) 1.
[326] J.E. Kim, Phys. Rev. Lett. 43 (1979) 103.
[327] M.A. Shifman, A.I. Vainshtein and V.I. Zakharov, Nucl. Phys. B 166 (1980) 493.
[328] C. Itzykson and J.-B. Zuber, Quantum Field Theory (McGraw-Hill, New York, 1980).
[329] R.D. Peccei, T.T. Wu and T. Yanagida, Phys. Lett. B 172 (1986) 435.
[330] L.M. Krauss and F. Wilczek, Phys. Lett. B 173 (1986) 189.
[331] M. Davier, in: The Standard Model, The Supernova 1987A (XXIInd Rencontre de Moriond, March 1987), ed. J. Tran Thanh Van (Editions Frontières, Gif sur Yvette, 1987).
[332] M. Dine, W. Fischler and M. Srednicki, Phys. Lett. B 104 (1981) 199.
[333] A.P. Zhitnitskii, Sov. J. Nucl. Phys. 31 (1980) 260.
[334] M.B. Wise, H. Georgi and S.L. Glashow, Phys. Rev. Lett. 47 (1981) 402.
[335] H.P. Nilles and S. Raby, Nucl. Phys. B 198 (1982) 102.
[336] J. Gasser and H. Leutwyler, Phys. Rep. 87 (1982) 77.
[337] D.J. Gross, R.D. Pisarski and L.G. Yaffe, Rev. Mod. Phys. 53 (1981) 43.
[338] J. Preskill, M.B. Wise and F. Wilczek, Phys. Lett. B 120 (1983) 127.
[339] L.F. Abbott and P. Sikivie, Phys. Lett. B 120 (1983) 133.
[340] M. Dine and W. Fischler, Phys. Lett. B 120 (1983) 137.
[341] J.J. Sakurai, Advanced Quantum Mechanics (Addison-Wesley, Reading, Ma., 1967).
[342] J.M. Flynn and L. Randall, Report LBL-25115 (April 1988), unpublished.
[343] EM Collaboration, J. Ashman, et al., Phys. Lett. B 206 (1988) 364.
[344] J. Ellis, R.A. Flores and S. Ritz, Phys. Lett. B 198 (1987) 393.
[345] D. Kaplan and A. Manohar, Harvard preprint HUTP-88/A021 (1988).
[346] J. Ellis and M. Karliner, Phys. Lett. B 213 (1988) 73.
[347] R.L. Davis, Phys. Lett. B 180 (1986) 225.
[348] R.L. Davis and E.P.S. Shellard, Nucl. Phys. B 324 (1989) 167.
[349] D. Harari and P. Sikivie, Phys. Lett. B 195 (1987) 361.
[350] A. Guth, Phys. Rev. D 23 (1981) 347.
[351] A.D. Linde, Phys. Lett. B 108 (1982) 389.
[352] A. Albrecht and P.J. Steinhardt, Phys. Rev. Lett. 48 (1982) 1220.
[353] A.D. Linde, Rep. Prog. Phys. 47 (1984) 925.
[354] R. Brandenberger, Phys. Rev. D 32 (1985) 501.
[355] G. Blumenthal, S. Faber, J. Primack and M. Rees, Nature 311 (1984) 517.
[356] M.S. Turner, Phys. Rev. D 33 (1986) 889.
[357] J.D. Barrow, Fundam. Cosmic Phys. 8 (1983) 83.
[358] S.-Y. Pi, Phys. Rev. Lett. 52 (1984) 1725.
[359] A.D. Linde, Phys. Lett. B 201 (1988) 437.
[360] N. Dowrick and N.A. McDougall, Phys. Rev. D 38 (1988) 3619.
[361] H. Goldberg, Report NUB-2977 (1989).
[362] A. Vilenkin and A.E. Everett, Phys. Rev. Lett. 48 (1982) 1867.
[363] P. Sikivie, Phys. Rev. Lett. 48 (1982) 1156.
[364] P. Sikivie, Phys. Rev. Lett. 61 (1988) 783.
[365] A. Dabholkar and J. Quashnock, Nucl. Phys. B 333 (1990) 815.
[366] C. Hagmann and P. Sikivie, in preparation (1990).
[367] M.S. Turner, Phys. Rev. Lett. 59 (1987) 2489.
[368] T.W. Kephart and T.J. Weiler, Phys. Rev. Lett. 58 (1987) 171.
[369] M.A. Bershady, M.T. Ressell and M.S. Turner, approved proposal to the Kitt Peak Observatory, unpublished (1989).
[370] P. Sikivie, Phys. Rev. Lett. 51 (1983) 1415; 52 (1984) 695 (E).
[371] P. Sikivie, Phys. Rev. D 32 (1985) 2988; 36 (1987) 974 (E).
[372] D.E. Morris, Report LBL-17915 (May 1984), unpublished.
[373] S.-I. Cho, C. Hagmann, P. Sikivie, N.S. Sullivan and D.B. Tanner, Japan. J. Appl. Phys., Suppl. 26 (1987) 1705.

[374] L. Krauss, J. Moody, F. Wilczek and D.E. Morris, Phys. Rev. Lett. 55 (1985) 1797.
[375] S. DePanfilis et al., Phys. Rev. Lett. 59 (1987) 839.
[376] W.U. Wuensch et al., Phys. Rev. D 40 (1989) 3153.
[377] P. Sikivie, N. Sullivan and D. Tanner, Experimental Proposal (April 1984) unpublished.
[378] C. Hagmann, P. Sikivie, N.S. Sulivan and D.B. Tanner, Phys Rev. D 42 (1990) 1297.
[379] S. Inagaki, M. Kobayashi, T. Shintomi, E. Ezura and I. Satoh, KEK-89-32 (1989).
[380] Sir R. Peierls, Proc. R. Soc. London A 347 (1976) 475.
[381] A. Ashkin and J.M. Dziedzic, Phys. Rev. Lett. 30 (1973) 139.
[382] V.N. Tsytovich, Zh. Eksp. Teor. Fiz. 40 (1961) 1775 [Sov. Phys. - JETP 13 (1961) 1249].
[383] S.A. Chin, Ann. Phys. (NY) 108 (1977) 301.
[384] A. Bechler, Ann. Phys. (NY) 135 (1981) 19.
[385] J.F. Donoghue, B.R. Holstein and R. Robinett, Ann. Phys. (NY) 164 (1985) 233.
[386] A.H. Weldon, Phys. Rev. D 26 (1982) 1394.
[387] A.G. Sitenko, Electromagnetic Fluctuations in Plasma (Academic Press, New York, 1967).
[388] E.J. Levinson and D.H. Boal, Phys. Rev. D 31 (1985) 3280.
[389] A.H. Weldon, Phys. Rev. D 26 (1982) 2789.
[390] D. Nötzold and G. Raffelt, Nucl. Phys. B 307 (1988) 924.
[391] B.D. Serot and J.D. Walecka, Adv. Nucl. Phys. 16 (1986) 1.
[392] C.J. Horowitz and B.D. Serot, Nucl. Phys. A 464 (1987) 613.
[393] S.L. Adler, Ann. Phys. (NY) 67 (1971) 599.
[394] W.-Y. Tsai and T. Erber, Phys. Rev. D 12 (1975) 1132.
[395] B. Jancovici, Nuovo Cimento 25 (1962) 428.
[396] P. Debye and E. Hückel, Phys. Z. 24 (1923) 185.
[397] S. Ichimaru, Plasma Physics - An Introduction to Statistical Physics of Charged Particles (Benjamin-Cummings, Menlo Park, 1986).
[398] D.B. Boercker, Astrophys. J. 316 (1987) L95.
[399] M. Baus and J.-P. Hansen, Phys. Rep. 59 (1980) 1.
[400] W.L. Slattery, G.D. Doolen and H.E. DeWitt, Phys. Rev. A 21 (1980) 2087.
[401] W.L. Slattery, G.D. Doolen and H.E. DeWitt, Phys. Rev. A 26 (1982) 2255.
[402] J.-P. Hansen, Phys. Rev. A 8 (1973) 3096.
[403] S. Galam and J.-P. Hansen, Phys. Rev. A 14 (1976) 816.
[404] E.E. Salpeter, Phys. Rev. 120 (1960) 1528.
[405] S.J. Brodsky, E. Mottola, I.J. Muzinich and M. Soldate, Phys. Rev. Lett. 56 (1986) 1763.
[406] F. Wilczek, Phys. Rev. Lett. 58 (1987) 1799.
[407] K. van Bibber, N.R. Dagdeviren, S.E. Koonin, A.K. Kerman and H.N. Nelson, Phys. Rev. Lett. 59 (1987) 759.
[408] A.A. Anselm, Phys. Rev. D 37 (1988) 2001.
[409] M. Gasperini, Phys. Rev. Lett. 59 (1987) 396.
[410] L. Maiani, R. Petronzio and E. Zavattini, Phys. Lett. B 175 (1986) 359.
[411] G. Raffelt and L. Stodolsky, Phys. Rev. D 37 (1988) 1237.
[412] T. Yanagida and M. Yoshimura, Phys. Lett. B 202 (1988) 301.
[413] M. Yoshimura, Phys. Rev. D 37 (1988) 2039.
[414] K. van Bibber, P.M. McIntyre, D.E. Morris and G.G. Raffelt, Phys. Rev. D 39 (1989) 2089.
[415] M.C. Huang and P. Sikivie, Phys. Rev. D 32 (1985) 1560.
[416] N. Ganoulis and M. Hatzis, Mod. Phys. Lett. A 1 (1986) 409.
[417] W.J. Marciano and A.I. Sanda, Phys. Lett. B 67 (1977) 303.
[418] H.A. Bethe, Proc. Cambridge Philos. Soc. 31 (1935) 108.
[419] A.V. Kyuldjiev, Nucl. Phys. B 243 (1984) 387.
[420] G. Raffelt, Phys. Rev. D 39 (1989) 2066.
[421] J.N. Bahcall, W.F. Huebner, S.L. Lubow, P.D. Parker and R.K. Ulrich, Rev. Mod. Phys. 54 (1982) 767.
[422] J.N. Bahcall and R.K. Ulrich, Rev. Mod. Phys. 60 (1988) 297.
[423] F.T. Avignone III, R.L. Brodzinski, S. Dimopoulos, G.D. Starkman, A.K. Drukier, D.N. Spergel, G. Gelmini and B.W. Lynn, Phys. Rev. D 35 (1987) 2752.
[424] A.A. Anselm, private communication (1990).
[425] W.E. Harris and R. Racine, Annu. Rev. Astron. Astrophys. 17 (1979) 241.
[426] F. Shu, The Physical Universe (University Science Books, Mill Valley, 1982).
[427] A. Renzini and F. Fusi Pecci, Annu. Rev. Astron. Astrophys. 26 (1988) 199.
[428] I. Iben Jr and A. Renzini, Phys. Rep. 105 (1984) 329.
[429] A.V. Sweigart and P.G. Gross, Astrophys. J. Suppl. 36 (1978) 405.
[430] R.D. Cannon, Mon. Not. R. Astron. Soc. 150 (1970) 111.

[431] B.M. Tinsley and J.E. Gunn, Astrophys. J. 206 (1976) 525.
[432] A.V. Sweigart and P.G. Gross, Astrophys. J. Suppl. 32 (1976) 367.
[433] A. Buzzoni, F. Fusi Pecci, R. Buonanno and C.E. Corsi, Astron. Astrophys. 128 (1983) 94.
[434] W.B. Hubbard, Fundam. Cosmic Phys. 3 (1978) 167.
[435] J. Liebert, Ann. Rev. Astron. Astrophys. 18 (1980) 363.
[436] V. Weidemann and D. Koester, Astron. Astrophys. 132 (1984) 195.
[437] J. Liebert, C.C. Dahn and D.G. Monet, Astrophys. J. 332 (1988) 891.
[438] I. Mazzitelli and F. D'Antona, Astrophys. J. 308 (1986) 706.
[439] T.A. Fleming, J. Liebert and R.F. Green, Astrophys. J. 308 (1986) 176.
[440] D.E. Winget, C.J. Hansen, J. Liebert, H.M. van Horn, G. Fontaine, R.E. Nather, S.O. Kepler and D.Q. Lamb, Astrophys. J. 315 (1987) L77.
[441] L. Mestel, Mon. Not. R. Astron. Soc. 112 (1952) 583.
[442] I. Iben Jr and A.V. Tutukov, Astrophys. J. 282 (1984) 615.
[443] H.M. van Horn, in: Proc. IAU-Symp. No. 42, White Dwarfs, ed. W.J. Luyten (Reidel, Dordrecht, 1971).
[444] D. Koester and D. Schönberner, Astron. Astrophys. 154 (1986) 125.
[445] G. Shaviv and A. Kovetz, Astron. Astrophys. 51 (1976) 383.
[446] D.Q. Lamb and H.M. van Horn, Astrophys. J. 200 (1975) 306.
[447] I. Iben Jr. and G. Laughlin, Astrophys. J. 341 (1989) 312.
[448] S.E. Woosley and T.A. Weaver, Annu. Rev. Astron. Astrophys. 24 (1986) 205.
[449] Mark II Collab., Phys. Rev. Lett. 63 (1989) 2173.
[450] L3 Collab., Phys. Lett. B 231 (1989) 509.
[451] ALEPH Collab., Phys. Lett. B 231 (1989) 519.
[452] OPAL Collab., Phys. Lett. B 231 (1989) 530.
[453] DELPHI Collab., Phys. Lett. B 231 (1989) 539.
[454] K. Nomoto and S. Tsuruta, Astrophys. J. 312 (1987) 711.
[455] S. Tsuruta, Report MPA-183 (1985).
[456] K. Nomoto and S. Tsuruta, Astrophys. J. 305 (1986) L19.
[457] K. Sato and M. Kobayashi, Prog. Theor. Phys. 58 (1977) 1775.
[458] M. Takahara and K. Sato, Phys. Lett. B 174 (1986) 373.
[459] D.N. Schramm and J.R. Wilson, Astrophys. J. 260 (1982) 868.
[460] R. Buonanno, A. Buzzoni, C.E. Corsi, F. Fusi Pecci and A. Sandage, Mem. Soc. Astron. Ital. 57 (1986) 391.

Note added in proof

After completion of the manuscript several recent works have come to my attention which ought to be mentioned in this report. Gould [461] has investigated the capture of solar system WIMPs by the Earth and found that one may essentially use the "free space" capture formula although the Earth is deep in the potential well of the Sun. Cox et al. [462] have investigated solar oscillations including cosmion energy transfer in their models. They found that they could not match the observed and calculated frequencies and claimed that cosmions could not solve the solar neutrino problem. Equally, Kaplan et al. [463] have numerically investigated the cosmion problem and found that the confrontation with helioseismological data disfavors cosmions in the Sun.

Burton and Carlson [464] have investigated Goldberg's claim that even in an inflationary scenario the cosmic axion density did not depend on an initial value for the axion field (ref. [361] and section 3.1). They disagree with Goldberg and reaffirm the standard axion scenario. According to these authors the cosmic axion density does depend on initial conditions as shown in the upper left panel of fig. 11.1.

As discussed in section 3.4, hadronic axions with a mass around a few eV could produce a decay line in the glow of the night sky. The decay photons could, indeed, stimulate further axion decay. It has been speculated that coherently enhanced decay of cosmic axions could provide the energy source for quasars [465] or even lead to the formation of the observed voids in the structure of the universe by the explosion of clustered axions [466]. Axions with such parameters, however, are probably excluded by the absence of axion induced signals in the SN 1987A neutrino observations [96].

It has been proposed [467] to upscale the University of Florida axion search experiment in order to conduct a realistic axion search. The main ingredient of this proposal is to use a large superconducting magnet (volume of magnetic field $\sim 2.8\,\mathrm{m}^3$ at $\sim 7\,\mathrm{T}$) owned by Lawrence Livermore National Laboratory (California) that could be made available for this purpose. Moreover, one would subdivide the field volume in anywhere from 1 to 1024 individual cavities in order to allow for search masses from 0.6 to 16 μeV. Over a search time of ~ 4 years one may be able to reach the "axion line" in fig. 3.2 over the range of search masses and thus would be able to find or exclude GUT axions in their role as the dark matter of our galaxy.

Goyal and Anand [468] have computed the neutrino emissivity of strange quark matter, while Anand et al. [469] have computed the emission of axions by bremsstrahlung processes involving quarks. They found that the emissivity of strange quark matter was a factor of 4–10 below that of nuclear matter at the same density and temperature so that bounds on DFSZ-type axions (which couple directly to light quarks) from SN 1987A would be diminished if the SN core consisted of strange quark matter. This work is complementary to refs. [55, 55a, 94] discussed in section 10.8.

Gandhi and Burrows [470] have considered the flipping of neutrinos into right-handed states in SN 1987A, assuming a Dirac mass term (section 10.3.2 and table 10.6). They included the corresponding energy loss rate in Burrows' supernova code and computed the duration of the neutrino signal in the IMB and Kamiokande detectors along the lines discussed in section 10.5. They found a mass bound $m_\nu < 14\,\mathrm{keV}$, in good agreement with the result given in table 10.6.

Several groups of authors [471–473] have considered particles with a small fractional electric charge (milli- or mini-charged particles). They have derived constraints in the mass–charge plane from various arguments, including the stellar energy loss argument applied to HB stars, white dwarfs, and SN 1987A.

References

[461] A. Gould, IAS preprint (1990).
[462] A. Cox, J.A. Guzik and S. Raby, Astrophys. J. 353 (1990) 698.
[463] J. Kaplan, F. Martin de Volnay, C. Tao and S. Turck-Chièze, report PAR-LPTHE 90-38 (September 1990).
[464] J.W. Burton and E.D. Carlson, Phys. Lett. B 247 (1990) 16.
[465] I.I. Tkachev, Phys. Lett. B 191 (1987) 41.
[466] T.W. Kephart and T.J. Weiler, report VAND-TH-90-2 (1990).
[467] P. Sikivie, N.S. Sullivan, D.B. Tanner, K. van Bibber, M.S. Turner and D.M. Moltz, Proposal to the U.S. Department of Energy and to the Lawrence Livermore National Laboratory (1990), unpublished.
[468] A. Goyal and J.D. Anand, Phys. Rev. D 42 (1990) 992.
[469] J.D. Anand, A. Goyal and R.N. Jha, Phys. Rev. D 42 (1990) 996.
[470] R. Gandhi and A. Burrows, Phys. Lett. B 246 (1990) 149.
[471] M.I. Dobroliubov and A. Yu. Ignatiev, Phys. Rev. Lett. 65 (1990) 679.
[472] R.N. Mohapatra and I.Z. Rothstein, Phys. Lett. B 247 (1990) 593.
[473] S. Davidson, B. Campbell and D. Bailey, report (1990), to be published in Phys. Rev. D.